AXIAL VARIATIONS AND ENTRY EFFECTS IN A PRESSURE SCREEN

THE UNIVERSITY OF
WAIKATO
Te Whare Wānanga o Waikato

A thesis submitted for the
requirements of the degree of

Doctor of Philosophy

at

The Department of Engineering

The University of Waikato

Martin John Atkins

2007

Abstract

Pressure screens are used for contaminant removal and fibre length fractionation in the production of pulp and paper products. Axial variations and entry effects in the screen are known to occur and these variations have not been adequately quantified. This thesis describes a fundamental study of the axial variations of several factors that occur within an industrial pressure screen; namely, pulp consistency, fibre length distribution, rotor pressure pulse, and feed annulus tangential velocity.

Axial variations of pulp consistency in the screen annulus and the accept chamber of the screen were studied using an internal radial sampling method. Localised pulp samples were taken and evaluated and common measures of screen performance such as fibre passage ratio and fractionation efficiency were calculated along the screen. Consistency generally increased along the length of the screen although under certain conditions the consistency toward the front of the screen was lower than the feed consistency. A two passage ratio model that incorporated forward and reverse passage ratio was derived to elucidate the flow of both fibre and fluid through the screen and their effects on overall screen performance. The passage of fibre through the screen decreased with screen length which generally had a positive effect on the fractionation efficiency toward the back of the screen. The passage of individual fibre length fractions was also studied and it was found that long fibre had a much lower passage than short fibre which caused the average fibre length in the annulus to increase.

Rotor induced pressure pulse variations along the screen length were also investigated. The magnitude of the pressure pulse was significantly lower (up to 40 %) at the rear of the screen. The variation in pressure caused by the rotor is due to a Venturi effect and the shape of the rotor. The relative velocity of the fluid and the rotor, called the slip factor, also directly affects the size of the pressure pulse in the annulus. The slip factor decreases along the length of the screen due to the increase in tangential velocity of the fluid. Pressure pulse data was also used to estimate the instantaneous aperture velocity and back-flush ratio. The instantaneous aperture velocity was calculated to vary considerably from the superficial aperture velocity by up to 5 m/s in the forward direction and 10 m/s in the reverse direction.

Computational Fluid Dynamics (CFD) was used to model tangential velocity changes in simplified screen annuli with axial through flow. For a smooth screen rotor the mean tangential velocity increased over the entire length of the annulus without reaching a maximum value. A step and bump rotor were modelled and the shape of the pressure pulses showed good agreement with experimentally measured pulses. The mean tangential velocity and the entrance length were found to be heavily dependant on the screen rotor used.

Acknowledgements

I wish to express my humble thanks and appreciation to all of the many people who have helped, encouraged, and supported me throughout the course of this research.

Firstly, my supervisor, Dr. Michael Walmsley, for his continued guidance, support, and advice through the duration of this project. His encouragement and direction has been invaluable in completing this project and finding the right direction to take. His critical evaluation of the work and valuable insights have taught me a lot and made the process a fruitful and enjoyable one.

Dr. Zuben Weeds for his help and advice and for sharing some of his insights into screening that have helped me to find fruitful areas of investigation. I have enjoyed our long discussions regarding screening and life in general.

Dr. James Neale for all his help, guidance, and support in reviewing sections of the thesis and for keeping a watchful eye over the CFD work that I undertook for part of this thesis.

Members of the Energy Research Group for many interesting discussions, the encouragement, and support. Chris Burrell for his help fixing computer related issues that tend to make life difficult. All of the academic, technical, and workshop staff at the university who have helped me throughout the years in getting this project finished.

The University of Waikato for financial support throughout the duration of the project.

Finally, but most of all, I wish to express my thanks to my wife, Yvette, for all her encouragement, support, and patience, especially during the writing of the manuscript, and for looking after our two young boys, Mason and Samuel, while I've been finishing.

Table of Contents

List of Figures

List of Tables

Notation

A	Aspect ratio
$A_{annulus}$	Area of the annulus (m^2)
A_{open}	Open area of the screen (m^2)
$A_{open.z}$	Localised open area of the screen (m^2)
A_{pipe}	Area of a pipe (m^2)
C	Pulp consistency (%)
C_a	Accept consistency (%)
C_{av}	Average pulp consistency (%)
C_{az}	Local accept consistency (%)
C_{crit}	Critical consistency for formation of stable flocs (%)
C_{exit}	Exit layer consistency (%)
C_f	Feed consistency (%)
C_{for}	Consistency of pulp in the forward direction (%)
C_{in}	Consistency of pulp fed into a narrow section (%)
$C_{L.a}$	Consistency of the long fibre fraction in the accepts (%)
$C_{L.z}$	Consistency of the long fibre fraction in the annulus (%)
C_m	Mass concentration (%)
$C_{n.ax}$	Local number consistency of fraction x in the accepts
$C_{n.x}$	Local number consistency of fraction x in the annulus
C_{out}	Consistency of pulp out a narrow section (%)
C_p	Non-dimensional pressure coefficient
C_r	Reject consistency (%)
C_{rev}	Consistency of pulp in the reverse direction (%)
C_s	Aperture consistency (%)
$C_{S.a}$	Consistency of the short fibre fraction in the accepts (%)
$C_{S.z}$	Consistency of the short fibre fraction in the annulus (%)
C_{sed}	Sedimentation consistency (%)
$C_{sed(3)}$	Sedimentation consistency for three fibre contacts (%)
$C_{sed(4)}$	Sedimentation consistency for four fibre contacts (%)
C_u	Upstream consistency (%)
C_{vol}	Volumetric concentration (%)
$C_{x.az}$	Local accept consistency of fraction x (%)

$C_{x.f}$	Mass fraction of debris x in the feed (%)
$C_{x.r}$	Mass fraction of debris x in the rejects (%)
$C_{x.z}$	Local annulus consistency of fraction x (%)
C_z	Local annulus consistency (%)
D	Normalised consistency drop
D_f	Fibre diameter (m)
D_s	Diameter of the screen (m)
E	Modulus of elasticity or Young's modulus (Pa)
E_r	Removal efficiency
F	Fibre flexibility
H_{exit}	Height of exit layer (m)
I	Moment of inertia (kgm^2)
k	Back-flush ratio
K^*	Apparent pressure loss coefficient
K_{for}	Forward pressure loss coefficient
K_L	Pressure or hydraulic loss coefficient
K_{rev}	Reverse pressure loss coefficient
L	Screen length (m)
L_f	Fibre length (mm)
L_L	Length-weighted fibre length average (mm)
L_N	Arithmetic or numerical average fibre length (mm)
L_r	Length of recirculation zone (m)
L_s	Slot length (m)
L_W	Weight-weighted fibre length average (mm)
M_d	Mass of dry fibre (kg)
m_f	Feed mass flow rate of fibre (kg/s)
M_f	Mass of the fibre (mg)
$m_{particles}$	Net flow of particles through the screen (kg/s)
m_r	Reject mass flow rate of fibre (kg/s)
M_w	Mass of wet pulp sample (kg)
N	Crowding number
n	Fibre length frequency
$N_{contact}$	Contact number
P	Passage ratio

p	Permeability index
P_{acc}	Accept pressure (kPa)
P_{ann}	Annulus pressure (kPa)
P_{bulk}	Bulk passage ratio
P_c	Instantaneous capture probability
P_{con}	Contaminant passage ratio
P_{for}	Forward passage ratio
p_{for}	Probability of passage in the forward direction
P_i	Instantaneous passage probability
P_L	Long fibre fraction passage ratio
$P_{L.bulk}$	Bulk long fibre fraction passage ratio
P_{Lz}	Local long fibre fraction passage ratio
$P_{n.x}$	Number passage ratio of fraction x
P_p	Pulp passage ratio
P_{plug}	Plug flow passage ratio
P_r	Instantaneous recirculation probability
p_{rev}	Probability of passage in the reverse direction
P_{rev}	Reverse passage ratio
P_s	Instantaneous passing probability
P_S	Short fibre fraction passage ratio
$P_{S.bulk}$	Bulk short fibre fraction passage ratio
P_{Sz}	Local short fibre fraction passage ratio
P_t	Turning effect passage ratio
P_w	Wall effect passage ratio
$P_{x.z}$	Local passage ratio of fraction x
P_z	Local passage ratio
Q	Screening quotient
Q_a	Accept flow rate (m^3/s)
Q_{az}	Local accept flow rate (m^3/s)
$Q_{az.for}$	Local accept forward flow rate (m^3/s)
$Q_{az.rev}$	Local accept reverse flow rate (m^3/s)
Q_f	Feed flow rate (m^3/s)
Q_{for}	Forward volumetric flow rate (m^3/s)
Q_{in}	Flow rate into a narrow screen section (m^3/s)

Q_{int}	Instantaneous volumetric aperture flow rate (m^3/s)
Q_{max}	Maximum volumetric capacity (m^3/s)
Q_{out}	Flow rate out a narrow screen section (m^3/s)
Q_r	Reject flow rate (m^3/s)
Q_{rev}	Forward volumetric flow rate (m^3/s)
Q_z	Local annulus flow rate
r	Aperture radius (m)
r_i	Radius of inner cylinder (m)
R_m	Mass reject ratio
r_o	Radius of outer cylinder (m)
R_v	Volumetric reject rate
R_{vz}	Local volumetric reject rate
r_x	Radial position (m)
S	Fibre stiffness (Nm^2)
T	Reject thickening factor
T_s	Slot depth (m)
T_z	Local reject thickening factor
U^+	Dimensionless velocity quotient
u_{ax}	Axial velocity (m/s)
$\bar{u}_{ax}$	Mean axial velocity (m/s)
u_n	Normalised velocity
$\bar{u}_s$	Average or superficial aperture velocity (m/s)
u_s	Instantaneous aperture velocity (m/s)
$\bar{u}_{s.for}$	Average or effective forward aperture velocity (m/s)
$u_{s.for}$	Instantaneous forward aperture velocity (m/s)
$\bar{u}_{s.rev}$	Average or effective reverse aperture velocity (m/s)
$u_{s.rev}$	Instantaneous reverse aperture velocity (m/s)
$\bar{u}_{tan}$	Mean tangential velocity (m/s)
u_{tan}	Tangential velocity (m/s)
$u_{tan.ini}$	Initial tangential velocity (m/s)
u_{tip}	Rotor or tip speed (m/s)
$\bar{u}_u$	Upstream velocity (m/s)
u_x	Fluid velocity (m/s)
w	Slot width (m)

w_f	Fibre wall thickness (m)
y^+	Dimensionless distance from the wall
z	Screen position (m)
Z_N	Normalised screen length
α	Separation ratio
α_z	Local separation ratio
β	Fibre length passage curve parameter
γ	Slip factor
δ	Annular gap (m)
ΔP	Pressure drop (kPa)
ζ	Annular lengths or non-dimensional axial length
K	Apparent von Kármán constant
κ	Debris removal parameter
λ	Fibre length passage coefficient
μ	Static coefficient of friction
ξ	Normalised annular gap or non-dimensional radial location
ρ	Density (kg/m^3)
σ	Compressive stress of a floc (Pa)
Φ	Fractionation index
ψ	Dimensionless penetration parameter
ω	Fibre coarseness (mg/m)
Ω_i	Annular velocity of the inner cylinder (rad/s)

1 Introduction

Screening, or more specifically solid-solid separation, is an important operation in many processing and manufacturing industries. Screens are used for both the sizing of material (fractionation) and for contaminant removal. All screens operate on one or both of two fundamental principles: barrier or probability screening (Kelly & Spottiswood, 1982). Barrier screening, or positive size separation, occurs when the rejected material is greater in all dimensions than the screen apertures, and cannot physically pass through the aperture. Probability screening occurs when the material being screened is less than the size of the screen apertures in at least one dimension and there remains the possibility that the particle will pass through the aperture, conditional on a number of factors such as the orientation of the particle as it is presented to the aperture. The feed material is often suspended in liquid, usually water, and may be processed under full line pressure. This is known as pressurised processing and allows a marked increase in throughput over atmospheric processing methods.

The removal of contaminants is vital in the production of pulp and paper products. The nature of contaminants range from dirt, sand, shives (bundles of fibres which have not been separated during the pulping process), and staples through to fragments of plastic. The physical properties such as the size, shape, buoyancy, and density of these contaminants vary widely. There are two main types of equipment employed to remove contaminants at various stages of the pulping and papermaking process namely hydrocyclones and pressure screens. Both exploit differences in the physical properties of the contaminants and valuable fibre. Hydrocyclones separate on the basis of specific surface area (Franko, 1987) whereas pressure screens separate principally on length (Karnis, 1997) and secondly on flexibility (Sloane, 1993; Atkins, 2003). Screens have the advantage over hydrocyclones because of their higher capacity and lower specific energy consumption.

Wood fibre is a natural material and as with most natural materials there is a high degree of variability in the physical properties of the fibre. There can be very large differences in properties such as fibre length, diameter, and coarseness (mass of fibre per unit length) even within the tree itself. Such variation can have a substantial

effect on both the operation of equipment such as paper machines and also the quality of the finished product. One method to overcome this natural variation is to fractionate the fibre in order to reduce variation of a certain property such as fibre length.

There are a number of different methods of fibre fractionation however most methods are not practical in a mill situation or are not economic due to small throughput, high capital costs, and high operational costs. It is well accepted that pressure screens and hydrocyclones exhibit the greatest practical potential for viable and cost effective fractionation of wood fibre (Duffy, 1999; Wakelin et al., 1999). Although pressure screens have been used for many decades for contaminant removal their role has expanded in the past few decades to include fractionation.

A modern pressure screen consists of a rotor, a screen plate or basket and housing, feed, accept and reject streams. A typical pressure screen is shown in Figure 1-1. A number of configurations are possible with a considerable range of different rotor types and screen plates available from several equipment suppliers. The pulp suspension enters the feed chamber and then enters the screen annulus. Fluid and some of the pulp will pass through the screen apertures and into the accept chamber and then exit the screen via the accept outlet. If the pulp does not pass through the apertures and is rejected it travels through the entire length of the screen before exiting via the reject outlet.

An understanding of the rheology and screening behaviour of the pulp suspension is fundamental to both the operation and design of effective and efficient pressure screens. The screening and fractionation of pulp is much more complex than the screening of particulates. The rheological behaviour of pulp suspensions is complex and as such classical models of particle-fluid interaction are not valid. The rheology of fibre suspensions is complex for a number of reasons. Wood fibre has a high aspect ratio (length - diameter ratio) usually in the order of 50 to 100 and is flexible. By contrast most particulate slurries contain particles which are roughly cubic or spherical and fairly rigid. Furthermore fibre suspensions are not homogenous, except under unique conditions, due to the tendency of fibres to flocculate. A fibre suspension can only be considered homogenous at very low concentrations and/or

under fully developed turbulence. Different flow conditions, fibre consistencies, and pulp types will all strongly influence the rheological behaviour of the pulp suspension. An understanding of fibre suspension flow is helpful to understanding the mechanisms of screening that occur in a pressure screen for both contaminant removal and fractionation.

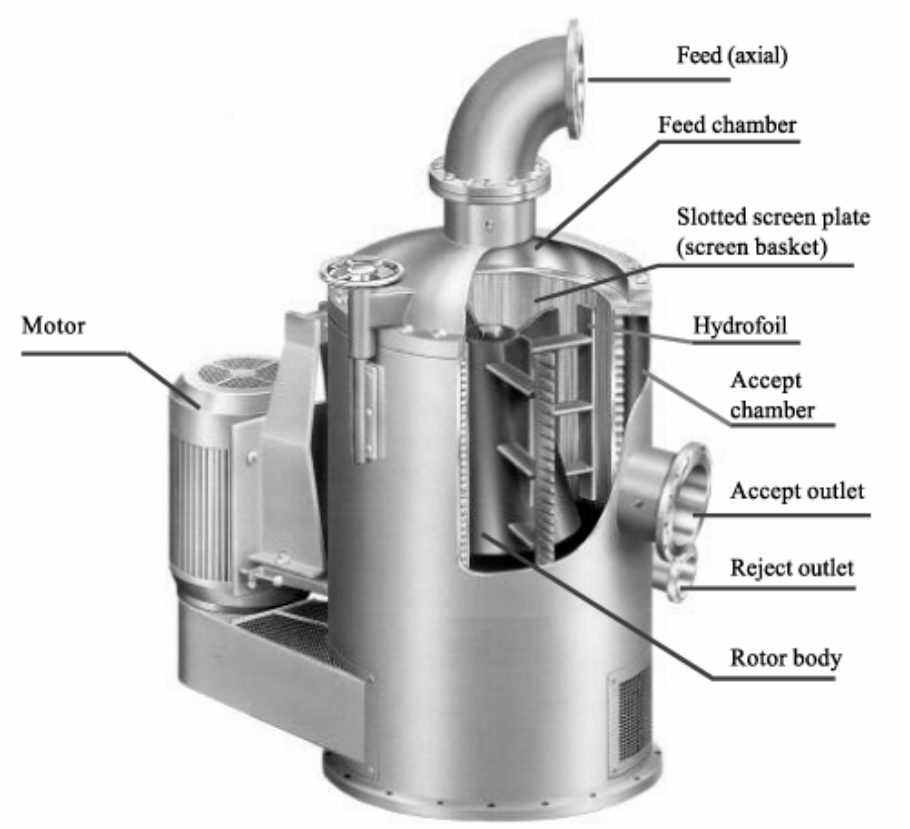

Figure 1-1 A modern pressure screen (Hautala et al., 1999)

Despite the use of pressure screens by the industry for many decades and the large amount of research that has been conducted into fibre suspension flow, the specific mechanisms of screening and fractionation are not well understood. Combinations of different screen baskets, rotor types, feed configurations and operational conditions create unique, highly turbulent flow fields that even without the presence of pulp, are extremely complex. When the complicating factor of pulp rheology is also considered the complexity of the system is multiplied. This complexity has restricted the use of Computational Fluid Dynamics (CFD) to simplified and specific aspects of pressure screening.

The overall performance of a pressure screen is contingent on the localised screen performance. The consistency of the pulp in the screen is known to change along the axial length of the screen, although the rate of change and the affect this has on screening performance has not been adequately quantified. It has been postulated that flow conditions including the local accept flow rate and tangential velocity of the suspension in the screen annulus will also vary with screen length (Rienecker, 1997; Weeds, 2006). Any variation in accept flow and tangential velocity is expected to be primarily due to the action of the rotor and will affect localised screen performance. Furthermore screening theory fails to accurately explain the role of forward flow (feed to accepts) and reverse flow (accepts to feed), of both fluid and fibre, under the action of the rotor pressure pulse, on the overall performance of the screen.

This thesis aims to present a fundamental study of the variations that occur axially within a pressure screen. Specifically, axial variations in consistency and rotor pressure pulse signature were measured on a laboratory pressure screen for a number of flow configurations and operating conditions. This data is useful in elucidating changes in flow fields within the screen, the separation mechanisms whereby screens remove contaminants and fractionate fibre suspensions. Furthermore, forward and reverse flow can be accounted for and quantified by using internal consistency sampling and pressure pulse measurement. Computational Fluid Dynamics has also been employed to supplement the findings of the experimental portion of this research.

A review of the relevant literature regarding fibre properties, flocculation, rheology, and pressure screening is presented in Chapter Two. Relevant aspects and concepts of fibre properties, flocculation phenomena, and fibre suspension rheology are introduced and discussed. Screening equipment and configurations are reviewed before a detailed analysis of screening mechanisms is presented. Finally a discussion of the modelling of pressure screening operations, including consistency changes, contaminant removal, and fractionation efficiency is offered.

The experimental equipment and procedure used throughout the research is described in Chapter Three. The Beloit MR-8 pressure screen is illustrated and described as well as the various screen baskets and rotors that were used. The details and

validation of the internal sampling technique is presented as well as a discussion regarding the merits and limitations of internal sampling. Other analysis techniques such as fibre length and pressure pulse measurement are discussed.

Chapter Four presents the results of the study of variations of localised consistency changes that occur along the axial screen length. These internal consistency profiles are then used to calculate performance parameters such as fibre passage ratio, and fractionation efficiency. Descriptions of the flow mechanisms that occur internally, which account for the measured disparity in performance between sections of the screen, are offered. Explanations of the mechanisms of actual screening process, based on the experimental data are also presented.

Chapter Five presents results from the experimental programme concerning the pressure pulse and its affects on forward and reverse flow of fibre and fluid. Disparities in the pressure pulse magnitude from the front to the rear of the screen were established and the causes of this disparity are discussed. The forward and reverse pressure loss coefficients of the screen were also measured for use in analysis of the pulse data. By combining the pressure pulse data and loss coefficients, predictions of the instantaneous and effective aperture velocity as well as forward and reverse flows can be obtained.

The results of CFD studies are presented in Chapter Six. Several three-dimensional flow domains representing a simplified screen annulus with a smooth rotor were solved. Two common screen rotors, the step and bump rotors were also modelled using a sliding mesh approach. The aim of this study was to examine changes in flow velocities along the screen length and relate these changes to experimentally measured phenomena presented in previous chapters.

The major findings and conclusions of this work is summarised in Chapter Seven. Finally, potential future areas of investigation that may be productive if pursued are discussed in Chapter Eight.

2 Fibre Flocculation, Rheology, & Pressure Screening – A Review

This chapter will critically review the published technical literature on a number of areas related to and including pressure screening. Basic pulping processes and general fibre properties, such as fibre length and coarseness, are reviewed in order to help understand the influence these properties have on fibre flocculation, pulp rheology, and ultimately screening. A good comprehension of fibre flocculation and pulp rheology is essential for understanding the screening process and the complexity that occurs within a pressure screen. General pressure screening equipment and configurations are discussed including the role of the rotor and pressure pulse. Screening mechanisms, including barrier and probability screening, and the fibre alignment and fibre mat theories of fibre passage, are examined and critiqued. Finally the modelling of pressure screens, internal variations, reject thickening are discussed.

2.1 Pulping and Fibre Properties

Natural fibres have been used in papermaking for centuries and it has long been known that both the pulping process and the properties of the fibres directly affect the properties of the paper produced (Hunter, 1947). This section will briefly describe the major mechanical and chemical pulping processes before examining the physical properties of fibres such as fibre structure, flexibility, collapsibility, coarseness, and earlywood and latewood fibres. Only wood fibre will be considered because it constitutes by far the major feed stock for modern papermaking. As fibre properties affect the screening of the suspension the overview presented will provide good background for later sections.

2.1.1 Pulping

Before fibres can be used for papermaking they first need to be reduced to single fibres or cells. Pulping involves rupturing the bonds that bind the fibres together. This is achieved through means of mechanical, thermal, or chemical action, or a

combination of these. Thus pulping processes can be divided into three generic categories: mechanical, chemical, and semi-chemical pulping.

Mechanical Pulping

The groundwood process involves pressing logs against a large, roughened grinding stone, which rotates at high peripheral speeds. Heat is produced as a result of the friction which in turn softens the lignin that binds the fibres together. As fibres are removed from the wood they are washed from the stone surface and then processed. Stone Groundwood (SGW) has been important in the production of newsprint as SGW can be added to the furnish to improve formation and print quality.

The most common method of mechanical pulp can best be described as Refiner Mechanical Pulp (RMP) and is produced by breaking up wood chips between two rotating disks of a refiner. The refiner subjects the chips to repeated compression - decompression cycles that generate heat which then liberates the fibres. Thermomechanical Pulp (TMP) is produced using the same process except the chips are preheated to around 130°C using steam. TMP produces pulp that is significantly stronger than RMP and can also have very little reject material. RMP may be carried out at atmospheric pressure or can be pressurised (Richardson et al., 1999).

Chemical pre-treatment of the chips or chemical additions during refining can reduce the amount of energy needed to mechanically pulp the chips; however the pulp properties can also be significantly altered by the addition of chemicals. Chemithermomechanical pulp (CTMP) and Chemimechanical pulp (CMP) are examples of semi-chemical pulping.

Chemical Pulping

The major chemical pulping process is the sulphate or kraft process. Wood chips are cooked in an alkaline mixture of sodium hydroxide and sodium sulphide at elevated temperatures and pressures. The “liquor” dissolves the lignin that bind the fibres together and after cooking, which can be a batch or continuous process, the chips and the liquor are blown into a blow tank which breaks up the chips into fibres. These fibres are then screened and washed. The cooking time and conditions can be varied depending on the desired properties and end use of the pulp. The kraft process has a

number of advantages over other chemical processes because of its efficient chemical recovery and production of strong pulps that are easily bleached.

2.1.2 Wood Fibre Structure

Fibres are generally defined as natural or synthetic filaments with a high aspect ratio (i.e. length to diameter ratio). Wood fibre is a natural, tubular, elongated cell which is made primarily from cellulose. Wood fibres are hollow and generally have an aspect ratio in the order of 50 to 100. The void through the centre of the fibre is called the lumen and is used for fluid transport to various parts of the tree. The fibres in a tree comprise a large volume of the total tree and are bound together by a substance called lignin.

Woods are classified into one of two categories, softwoods (gymnosperms) or hardwoods (angiosperms), depending on the structure of the wood. Softwood fibres are called tracheids and several layers make up an individual fibre wall as shown in Figure 2-1. Hardwood fibres or vessels are generally shorter than softwood fibres and the structure of a hardwood is more complex than that of softwood.

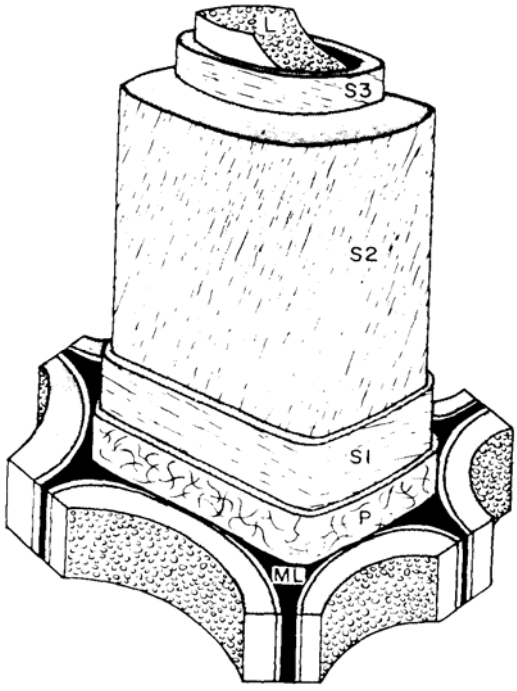

Figure 2-1 Softwood fibre structure (Smook, 1992)

The cell contains chains of cellulose molecules called microfibrils which constitute a major portion of the fibre structure. The layers are distinguished by the alignment of the microfibrils and physical properties of the fibre, such as stiffness, are dependant of the orientation of the microfibrils in each layer especially the S_2 layer which is the thickest layer. Furthermore the several layers also differ slightly in chemical composition. The middle lamella (ML) is the section that binds the fibres together and contains mostly lignin. The primary wall (P) is typically between 0.05 and 0.1 μm thick. Three layers (S_1, S_2, S_3) make up the secondary wall and each have a different microfibril angle. The microfibrils in the S_1 layer are arranged in a crossed-hatched pattern and the layer is 0.1 – 0.3 μm thick. The microfibrils in the S_2 layer are aligned nearly parallel to the cell axis and are the most influential factor to the mechanical properties of the fibre. The bulk of the cell wall is made up of the S_2 layer which is typically from 1 to 5 μm in thickness. Small changes in the microfibril angle of the S_2 layer will greatly affect the mechanical properties of the fibre (Claudio-da-silva, 1983; Anagnost et al., 2002) and this angle will vary within a tree and between trees of the same species. The greater the microfibril angle of the cell wall the greater the modulus of elasticity of the fibre (Paavilainen, 1993).

2.1.3 Fibre Length

The fibre length L_f is a significant fibre property as it affects the rheology of the suspension, how the pulp flows through pipes and apertures (Duffy, 1995; Olson, 1996; Duffy & Abdullah, 2003), the tendency of the fibres to flocculate (Kerekes & Schell, 1995), and also many paper properties (Watson & Dadswell, 1961; Dinwoodie, 1965). As wood fibre is a natural product there is natural variation in the fibre length produced during pulping process. An example fibre length distribution is given in Figure 2-2.

There are three common ways of expressing the mean fibre length: the arithmetic or numerical average L_N (Equation 2-1), the length-weighted average L_L (Equation 2-2), and the weight-weighted average L_W (Equation 2-3), where L_f is the fibre length and n is the number of fibres in that length fraction or the fibre length frequency.

$$L_N = \frac{\sum nL_f}{n} \qquad \textbf{2-1}$$

$$L_L = \frac{\sum nL_f^2}{nL_f} \qquad \textbf{2-2}$$

$$L_W = \frac{\sum nL_f^3}{nL_f^2} \qquad \textbf{2-3}$$

For mechanical pulps, fibre length is usually measured using a Bauer-McNett classifier. For chemical pulps, automated fibre analysers, such as the Kajanni Fibre Lab, Kajanni FS-200 or Fibre Quality Analyser (FQA), are used. These analysers typically report the fibre length distribution, fibre length averages, fibre coarseness, fibre width, and the number of fibres measured.

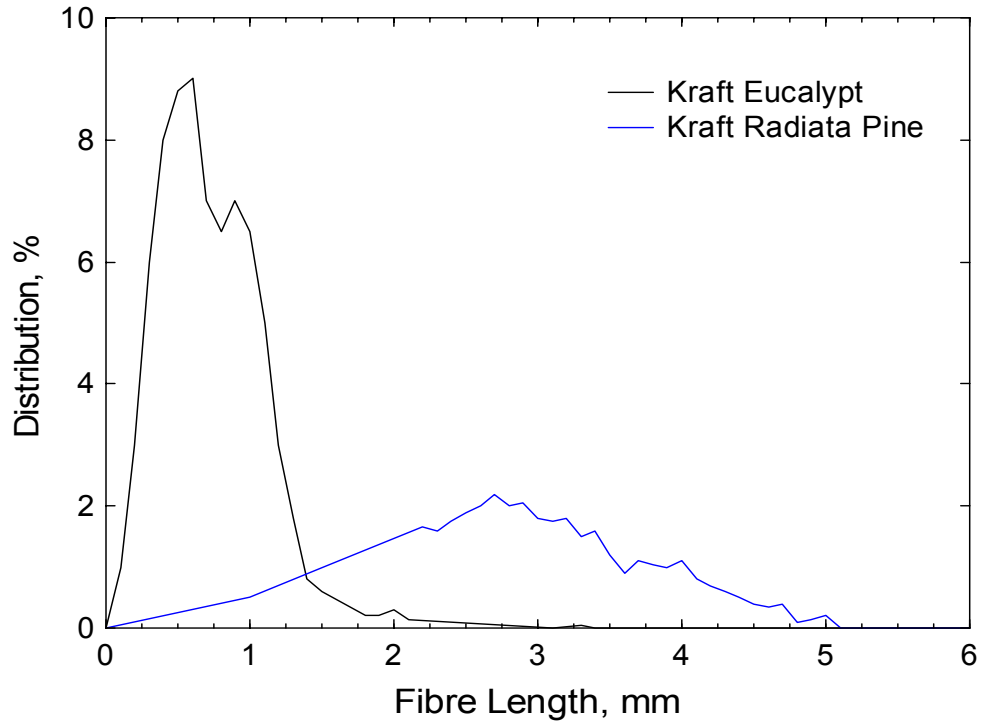

Figure 2-2 Fibre length distribution for a kraft hardwood pulp (Eucalypt) and a kraft softwood pulp (Radiata Pine)

2.1.4 Fibre Coarseness, Flexibility & Collapsibility

Fibre coarseness ω is an important property in that it affects a wide range of paper properties such as smoothness, density, tear resistance, and printing qualities (Clark, 1985). Coarseness is defined as the mass of fibre per unit length (Equation 2-4) where M_f is the mass of the fibre and L_f is the length of the fibre. It has been well established that coarseness increases with fibre length (Sastry & Wellwood, 1972; Clark, 1985).

$$\omega = \frac{M_f}{L_f} \qquad \textbf{2-4}$$

Collapsibility or lateral compression of a fibre is a measure of the tendency of the lumen of the fibre to collapse. Collapse is dependant on geometrical considerations as shown in Figure 2-3, which illustrates two fibres with the same cross sectional area or coarseness but different collapsibility and flexibility. Collapsed fibres increase the effective fibre-to-fibre contact or bond area and this produces a denser sheet with higher tensile and burst strength and low opacity. Uncollapsed fibres produce lower strength papers with higher bulk, stiffness, and opacity due to the lower contact area between fibres (Claudio-da-silva, 1983).

Fibre coarseness however is not always a good indication of fibre flexibility or collapsibility. It is possible to have two fibres of equal coarseness or cross sectional area but quite different fibre collapsibility or flexibility. Thin walled or earlywood fibres will tend to collapse to form thin ribbons upon drying while thick walled or latewood fibres tend to retain their shape and resist collapse (Walmsley et al., 2005).

The longitudinal flexibility of a fibre is an important fibre property in both papermaking and screening. Paper properties such as strength, compressibility, and surface smoothness are all affected by the flexibility of the fibre. The more flexible a fibre is, the greater the number of bonds that fibre will form in the network, which will in turn increase the tensile strength of the paper.

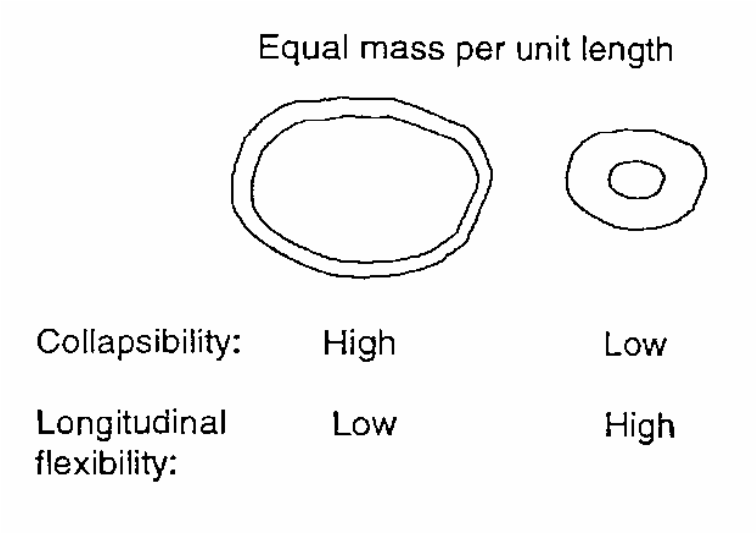

Figure 2-3 Effect of cell wall area on flexibility (Wakelin, 1997)

Fibre flexibility F can be calculated theoretically using the bending theory of a beam. The stiffness of a beam is equal to the product of the modulus of elasticity (or Young's modulus) E and the moment of inertia I. Flexibility is the inverse of fibre stiffness S (Equation 2-5).

$$F = \frac{1}{EI} = \frac{1}{S} \qquad \textbf{2-5}$$

Numerous methods have been proposed and employed to measure fibre flexibility however all have their short comings. Several methods involve measuring the deflection of a supported fibre whilst a known force is being applied (Samuelsson, 1963; Tam Doo & Kerekes, 1981; Kuhn et al., 1990; Lawryshyn & Kuhn, 1996; 1998). Kuhn et al. (1990) developed a flow channel that employed a T-junction which caused the fibre to staple and stiffness could be estimated from the deflection. Forgacs & Mason (1958) studied the rotational orbits of fibres in a laminar shear flow and observed five different orbits and the distribution of fibres in each orbit type could be used to characterise the flexibility of the sample.

A major shortcoming of all flexibility measurement methods is that it is assumed that an "ideal" fibre is being measured. As with other fibre properties there is a high degree of variation in the flexibility of a pulp sample. Factors such as fibre pitting,

location of the fibre in the tree, fibre damage, the pulping process, and whether the fibre is dried or never dried all affect the flexibility. If the fibre is damaged during pulping, refining or screening the damaged section of the fibre will act as a hinge. Table 2-1 lists the stiffness of different natural and synthetic fibres reported in the literature, and demonstrates the variability in the measured stiffness of the natural fibres but also the large difference in stiffness between the natural fibres and the synthetic fibre Nylon.

Table 2-1 Stiffness of certain natural and synthetic fibres

Pulp Type	Stiffness ($\times 10^{-12}$ Nm^2)
Abies concolor (kraft pulp)[a]	
Earlywood (unbeaten)	9.3
Latewood (unbeaten)	26.0
Earlywood (beaten)	3.2
Latewood (beaten)	19.4
Picea exceisa (sulphate pulp)[b]	
Earlywood (unbeaten)	2.9 - 4.9
Latewood (unbeaten)	3.9 - 4.9
Picea exceisa (sulphite pulp)[b]	
Earlywood (unbeaten)	1.6 - 2.1
Latewood (unbeaten)	1.6 - 2.6
Spruce (semi-bleached kraft pulp)[c]	2.7
Nylon[d]	350 - 290 000
Rayon[d]	0.50 - 4

[a] Schniewind et al. (1966) [b] Samuelsson (1964)

[c] Tam Doo & Kerekes (1981) [d] Synthetic fibres used by Gooding (1986)

2.1.5 Freeness

Freeness is commonly defined as an index of the drainability of a pulp suspension. There are numerous measures of freeness although a common method is the Canadian

Standard Freeness test. Many papermaking properties have been correlated to the freeness of the pulp although the correctness and reproducibility of these correlations has been challenged (Clark, 1985). In the production of mechanical pulps, freeness is a useful indicator of the development of the pulp properties because the freeness is related to the extent of fibre fibrillation and fines generation.

2.1.6 Earlywood and Latewood

Natural differences in fibres also occur due to the seasonal variation of the growing season. Earlywood or springwood fibres are formed in the early part of the active growth season during times of favourable temperature and rainfall conditions. Their main purpose is water transportation and usually have large fibre diameters (30 - 50 μm) and thin cell walls (3 – 5 μm).

Latewood or summerwood fibres are formed during the later portion of the growth season when growth rates have declined. Their main function is primarily a mechanical reinforcement tissue. Latewood fibres have small diameters (20 – 30 μm) and thicker walls (4 – 10 μm) than earlywood fibres.

The properties of earlywood and latewood fibres can be markedly different especially for softwood pulps. Latewood fibres tend to be longer than earlywood fibres (Kibblewhite, 1973; Cown, 1975), tend to be stiffer than earlywood fibres (Alexander et al., 1968), earlywood fibres are inclined to collapse into ribbons on drying whereas latewood fibres tend to resist collapse (Kibblewhite & Bailey, 1988; Walmsley et al., 2005), and surface charge differences have been reported (Walmsley et al., 2005). The difference in the fibre dimensions also result in a difference in basic wood density of between 30 – 50 % (Smook, 1992; Walmsley et al., 2005).

2.2 Flocculation

Pulp fibres have an inherent tendency to flocculate and form transient, semi-coherent, and coherent structures called flocs. This tendency has a number of consequences for the transportation and processing of pulp during the manufacture of paper. The degree of flocculation is dependant on a number of factors including fibre type,

suspension consistency, and flow conditions. This section will discuss and review the flocculation of pulp with specific reference to mechanical flocculation. This will provide an important background for the discussion of the flow behaviour of fibre suspensions or pulp rheology and its affect on flocculation.

2.2.1 Mechanical Flocculation

Wood fibres have an inherent tendency to form flocs or agglomerates. Flocs are local mass concentrations of fibres which are bound together to form a collection of entangled fibres. It has been shown that flocs will form at very low consistencies although they will be very weak and therefore transient in nature. These flocs may consist of only a few fibres and under most conditions will be very small. Above a critical consistency C_{crit} flocs will readily form and be stable entities. These flocs will possess mechanical strength, density, and elasticity. Floc size and strength have been shown to increase with consistency (Kerekes, 1983b; Jokinen & Ebeling, 1985; Kerekes et al., 1985; Kerekes & Schell, 1992) and average fibre length (Kerekes & Schell, 1995; Dodson, 1996).

There are four mechanisms that have been identified which mechanically secure fibres in a floc or fibre network: a) elastic fibre bending, b) physical surface properties, c) surface tension forces, and d) electrochemical and colloidal forces. Figure 2-4 illustrates the first two of these mechanisms. By far the most important factor in mechanical flocculation is elastic fibre bending (Kerekes, 2006).

Elastic Fibre Bending

Frictional forces are created due to normal forces between fibre-fibre contacts which arise due to elastic fibre bending. This action holds fibres in place in the floc and helps to resist fibre movement. Duffy (1995) points out that this is a result of repulsive forces at points of fibre contact rather than fibre surface attractive forces. A number of factors will influence this mechanism; these include the number of fibre-fibre contact points, fibre flexibility, and the coefficient of friction between the fibres.

Physical Surface Properties

Fibres can become hooked and entangled by other fibres and the forces created will then oppose relative movement between the fibres. Increased fibre fibrillation or surface roughness, fibre stiffness, and the degree of fibre contouring will affect the tendency of fibres to be held in place.

Surface Tension Forces

At consistencies above 8 % surface tension forces produced by small entrapped air bubbles generate cohesive forces, otherwise this effect has minimal affect on mechanical flocculation.

Electrochemical and Colloidal Forces

While not a mechanical force by nature, electrostatic and electrokinetic forces exist between small particles. This is especially important a low fibre consistency and when chemical additives are present.

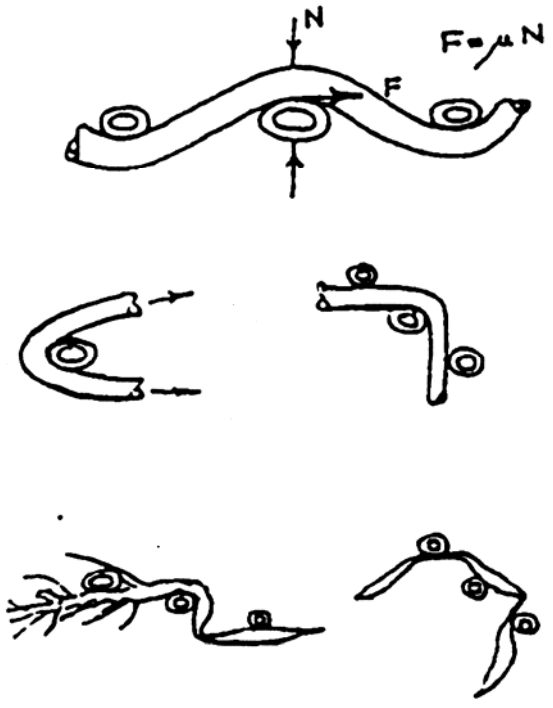

Figure 2-4 Flocculation mechanisms (Paul, 1999)

2.2.2 Crowding Number

Mason (1950; 1954) conducted early investigations into the motion of fibres in a shear flow and derived an expression to estimate the critical consistency at which flocs will form. This expression was based on the rotational motion of fibres and the spherical volume or orbits produced due to this motion. In a suspension, fibres will tend to contact other fibres as they rotate only if their orbits overlap. As the consistency increases there will be a greater probability of fibres contacting and subsequently becoming entangled to form flocs. Equation 2-6 shows the expression developed by Mason for the critical consistency where L_f is the fibre length, D_f is the fibre diameter and w_f is the fibre wall thickness.

$$C_{crit} = \frac{2}{3}\left(\frac{L_f \pi}{2 D_f w_f}\right)^2 \qquad \textbf{2-6}$$

Above a second critical consistency, called the sedimentation consistency C_{sed}, flocs will also contact other flocs, become entangled and form a continuous fibre network. A fibre network is a cohesive structure which also has mechanical strength, density, and elasticity. The sedimentation consistency can be predicted theortically for three fibre contacts $C_{sed(3)}$ (Equation 2-7) and for four fibre contacts $C_{sed(4)}$ (Equation 2-8). The sedimentation consistency can also be established using settling tests in a column (Thalen & Warhen, 1964), and $C_{sed(4)}$ more closely predicts the experimentally determined C_{sed}.

$$C_{sed(3)} \approx 339\left(\frac{w_f}{L_L}\right)^2 \qquad \textbf{2-7}$$

$$C_{sed(4)} \approx 536\left(\frac{w_f}{L_L}\right)^2 \qquad \textbf{2-8}$$

2.2.3 Crowding Number

A convenient means of expressing the degree of flocculation is the crowding number N, which is based on the work of Mason (1950; 1954) and Kerekes & Schell (1992; 1995). Consider a spherical volume where the diameter is the average fibre length, the crowding number is the number of fibres expected in that volume and is expressed in Equations 2-9 and 2-10, where A is the aspect ratio, C_{vol} the volumetric concentration, C_m the mass concentration, and ω the mean fibre coarseness.

$$N = \frac{2}{3} A^2 C_{vol} \qquad \textbf{2-9}$$

$$N = \frac{5 C_m L_f^{\,2}}{\omega} \qquad \textbf{2-10}$$

The crowding number is related to both the critical consistency and sedimentation consistency. The critical consistency is considered to occur when fibres will contact one other fibre whereas the sedimentation consistency is considered to be when three or four fibre contacts are made. When the critical consistency is reached the crowding number is equal to one and flocs will form. When the sedimentation consistency is reached the crowding number is equal to 60 and a network is considered to have formed.

Meyer & Wharen (1964) developed a contact number $N_{contact}$ which expresses the number of fibre contacts per fibre although their formulation has subsequently been modified by Ringner (1995) (Equation 2-11). The contact number is similar to the crowding number and the critical and sedimentation consistencies. The critical consistency occurs when there is one contact per fibre and the sedimentation consistency occurs when there are three or four contacts per fibre. A value of four contacts per fibre for the sedimentation consistency corresponds better to experimental findings (Thalen & Warhen, 1964) although three contacts is regarded as the minimum to form a coherent network (Dodson, 1996).

$$N_{contact} = \frac{4AC_{vol}}{(2 + \pi C_{vol})} \qquad \textbf{2-11}$$

Kropholler & Sampson (2001) further developed the crowding number to incorporate a lognormal fibre length distribution in place of the mean fibre length. They found that the calculated crowding number was between 1.8 to 7 times higher than when using the mean fibre length in the calculation. Although this approach may be more realistic it is nevertheless a more laborious method as the coefficient of variation of the fibre length distribution has to be calculated. However the model can be used to calculate the percentage of fibres that have a crowding number of greater or less than a desired value. This is advantageous as it allows the "free fibre fraction" (i.e. the percentage of fibres with a crowding number less than four) to be calculated. This "free" fraction is then the fibres which do not make up the network as they have less than four contacts and are therefore considered to be "free". For a nominal TMP and a chemical pulp used by Kropholler & Sampson a crowding number of 60 occurred at a consistency of 0.29 % and 0.15 % respectively. The "free fibre fraction" was calculated to be approximately 35 % for the TMP and 11 % for the chemical pulp.

Using the concept of the fibre crowding number three flocculation regimes can be described namely the dilute, semi-concentrated, and concentrated regimes.

Dilute Regime (N < 1)

The dilute regime occurs when the crowding number is less than one, which will also be below the critical consistency. In this regime there is considered to be only chance collisions or contacts between fibres. The flocs formed will be very small, weak, and transient in nature. In this regime the elastic fibre mechanism is unlikely to occur and the strength of the contact will be dependant on weak chemical, electrostatic, and physical surface properties of the fibres.

Semi-concentrated Regime (1 < N < 60)

When the crowding number exceeds one and is lower than 60 the suspension is in the semi-concentrated regime. In this regime fibre to fibre collisions or contacts will more readily occur and collisions are said to be forced. The fibres are much more

likely to contact more than one other fibre and form transient and coherent flocs. Elastic fibre bending will increasingly become the predominant mechanism for floc formation.

Concentrated Regime (N > 60)

The concentrated regime occurs when the crowding number is greater than 60. Fibres are considered to be in continuous contact and a fibre network is formed. However a fibre network is not to be considered as a single continuous floc but rather as an entanglement of individual flocs which form the network. At elevated concentrations electrochemical forces will become an important factor in the flocculation mechanism. Moreover at consistencies greater than about 8 %, surface tension forces created by entrapped air will also contribute to flocculation.

While the crowding number is usually greater than 60 for most processing operations including screening, a network may not be formed if there is a sufficiently strong flow field or enough turbulence present to disrupt the network and flocs. Despite this the crowding number is still an important parameter in that it describes the likelihood of collisions and contacts between fibres in the suspension.

2.3 Rheology of Fibre Suspensions

The rheology of a fibre suspension is dependant on the properties of the fluid the fibres are suspended in, the properties of the fibres, and also the network or flocs the fibres form (Kerekes, 2006). Extensive studies of the rheology of fibre suspensions for pipe flow have been carried out and to a lesser extent for flow in rotary shear devices.

Flow in Pipes

Extensive research has been conducted into the flow of wood fibre suspensions in pipes. Duffy and co-workers have produced the most comprehensive body of work into the flow of pulp in pipes (Duffy et al., 1974; Duffy, 1976a; 1976b; Duffy et al., 1976; Duffy & Lee, 1978; Duffy, 1979; 1995; Duffy & Abdullah, 2002; 2003). Figure 2-5 illustrates a typical friction loss curve for a pulp suspension and the water curve and demonstrates the several regimes that occur in pipe flow.

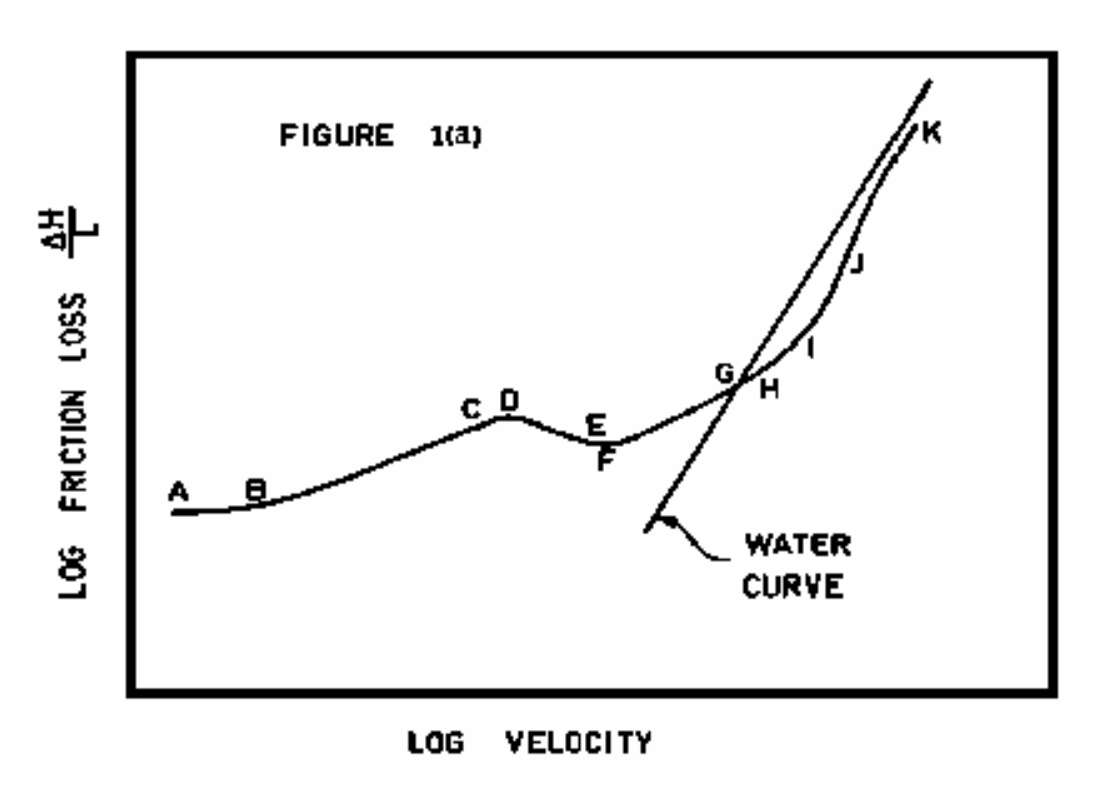

Figure 2-5 Typical friction loss curve for a pulp suspension (Duffy et al., 1976)

The flow mechanisms that occur during the several regimes shown in Figure 2-5 are:

AB Plug flow where plug-wall interactions dominate and increasing velocity does not affect the pressure drop greatly due to boundary friction between the wall and the plug.

BC Plug flow with plug-wall interactions and also hydrodynamic shear. Single flocs break off from the main plug and roll along the pipe surface at a lower velocity than the plug. This is caused by interactions between the wall and the outer surface of the plug. Moreover pockets of water occur between the flocs which partially cause the hydrodynamic shear.

C Interactions between the plug and the wall cease.

DE Plug flow and a thin water annulus which is in laminar shear. Fibres and flocs which protrude from the plug are deflected and the fibre network is deformed

by the flow stresses. The thickness of the water annulus increases with increased velocity.

E Turbulence begins in the water annulus.

FH Plug flow with turbulent water annulus although the plug surface remains intact.

GH The plug is permanently disrupted and drag reduction begins. Flocs are torn from the surface of the plug however the bulk of the plug is undisturbed.

HJ The transition between plug flow with turbulent annulus to fully developed turbulence. Measured velocity profiles reveal that the plug size decreases as velocity increases although still exists when drag reduction is the greatest (point I).

I Maximum drag reduction occurs and is due to two competing mechanisms: a) at lower velocities large flocs behave as solids which link to aid momentum transfer, and b) at higher velocities smaller flocs and individual fibres dampen turbulent fluctuations.

JK Fully developed turbulence, decrease in drag reduction gradually and damping of turbulence.

Figure 2-6 illustrates schematically the several flow regimes that can occur during pipe flow. Although the mechanisms of pipe flow of pulp suspensions do not directly apply to pressure screens, because the flow structures and geometry occurring are significantly different, there is value in examining pipe flow as a starting point for understanding pulp rheology.

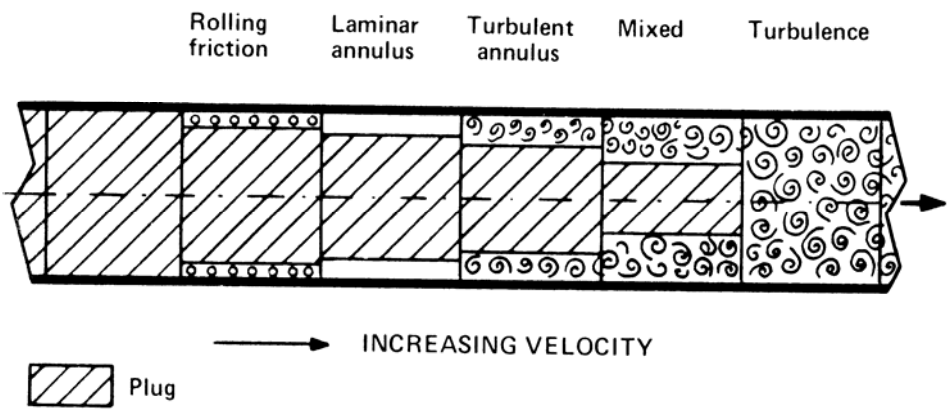

Figure 2-6 Various pipe regimes (Gullichsen & Härkönen, 1981)

Duffy & Abdullah (2003) also studied the flow of pulp in small diameter pipes and found that different mechanisms occur when the pipe diameter is less than about 7.5 mm. The friction loss curve for pulp flow in small diameter pipes follows or is close to the water curve for a large variation in bulk velocities. The change in mechanism is due to the fact that the mean floc size is of the same order as the pipe diameter for small diameter pipes and a different floc structure exists. A turbulent water layer is formed but cannot develop as shear increases due to the dense structure of the floc in the small diameter pipe. Fibres are generally aligned in the same direction as the flow.

Flow in Rotary Shear Devices

Rotary shear devices have been used to study the rheology of pulp suspension (Gullichsen & Härkönen, 1981; Bennington, 1988). Gullichen & Härkönen (1981) measured an increase in torque as rotational speed was increased for medium consistency pulp as illustrated in Figure 2-7. They found a sharp increase in torque close to the water curve and described the flow in the device at this point as being in a vigorous state of turbulence or complete turbulence. They equate this point with the point in pipe flow where there is fully developed turbulence (region JK in Figure 2-5) and state that at this point the suspension is fluid like or behaves as a fluid. Duffy (1995) is critical of this interpretation because, for pipe flow, at the point where the pulp curve intersects the water curve (point G in Figure 2-5), there still exists a large plug (the plug occupies ≈ 95 % of the pipe diameter) and therefore this cannot be called a "fluid like" suspension. It is not until point J in Figure 2-5 that the plug

ceases to exist and fully developed turbulence is considered to exist. It is only after this point that the suspension could be referred to as behaving in a "fluid like" manner. It appears the reason for the misinterpretation is that Gullichen & Härkönen compared their data from a rotary shear device at medium consistency with extrapolated low consistency data from pipe flow experiments.

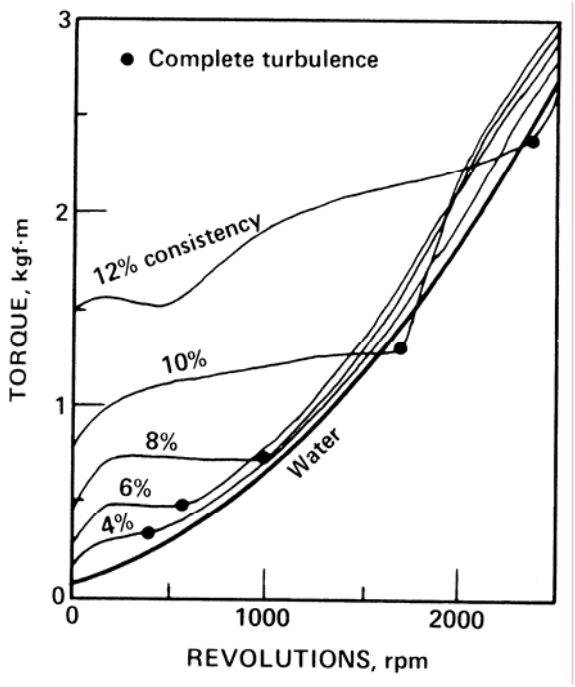

Figure 2-7 Torque versus rotational speed for several consistencies of kraft pulp (Gullichsen & Härkönen, 1981)

Bennington (1988) also studied the rheology of several pulps using a device similar to that used by Gullichen & Härkönen (1981) and the device is illustrated in Figure 2-8. The effect of annular gap and rotational speed was studied which led to the description of several flow regimes or flow patterns observed which are illustrated in Figure 2-9.

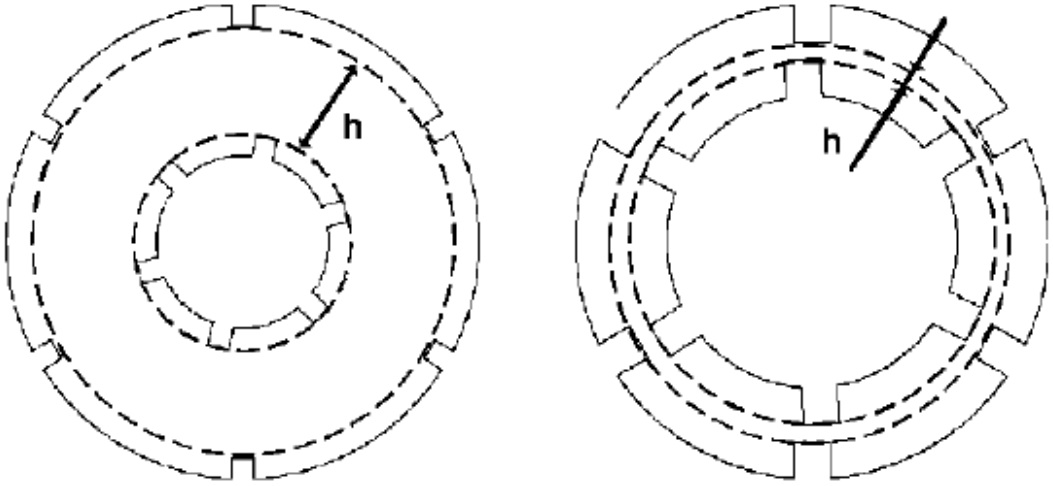

Figure 2-8 Rotary shear device used by Bennington (1988)

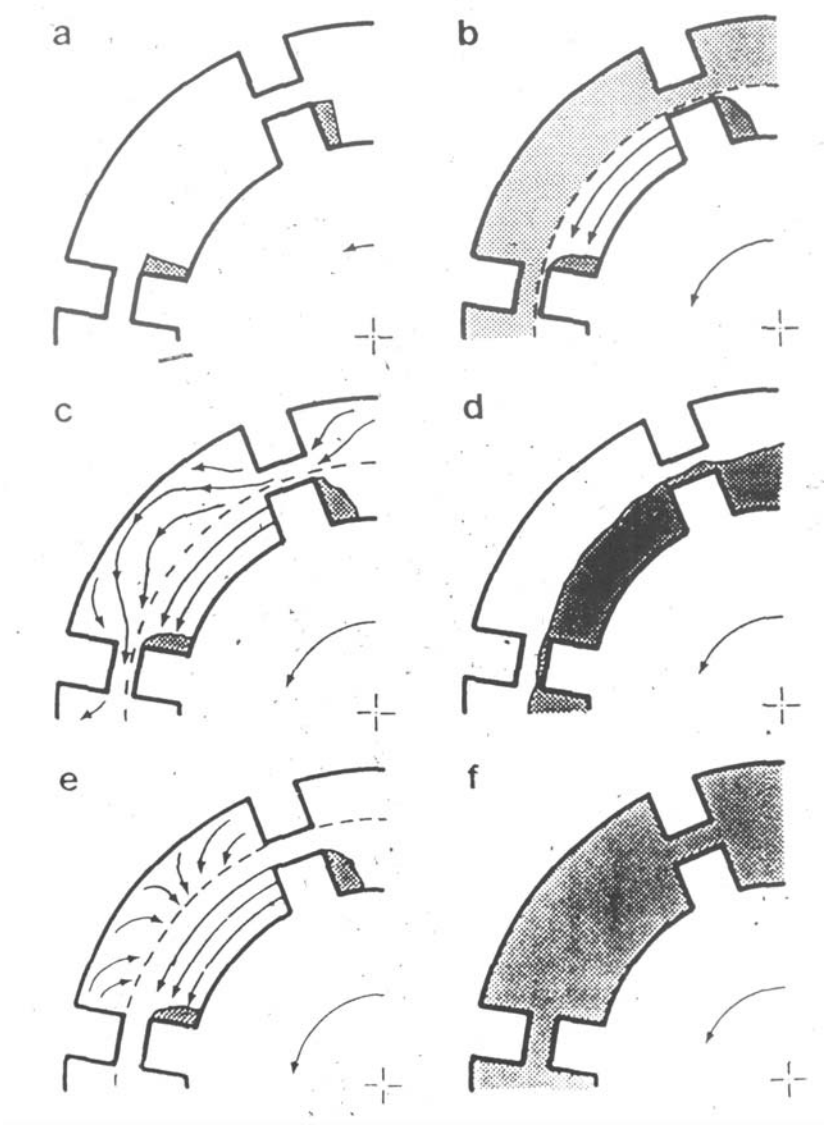

Figure 2-9 Pulp flow regimes in a rotary shear device (Bennington, 1988)

a. Yield – The network begins to yield and void spaces appear at the back of the rotor lugs.
b. Shear plane formation – A shear plane is created around the rotor and intense fibre motion occurs between the rotor and the housing baffles. The suspension is stagnant in the remaining zone adjacent to the outer wall and baffles (shaded area).
c. Tangential-cavity flow – The suspension flows tangentially and flocs are squeezed between the rotor lugs and baffles.
d. Phase separation occurs – Phase separation may occur which leads to a slight reduction in the suspension density adjacent to the rotor. Flow pattern may cease at b or c.
e. Inward radial flow – Radial flow from the outer wall begins.
f. Post-transition flow – Intense flow fills the chamber. Unknown flow patterns exist, which are most likely to have axial, radial and tangential flow components.

"Fluidisation"

The validity of the use of the term "fluidisation" to pulp suspension flow has been the subject of some debate for a number of years. Gullichen & Härkönen (1981) first used the term in relation to their work using a rotary shear device. Since then it has been used by several authors referring to several different flow regimes or states and is usually not defined in each instance, or if it is defined, it is poorly described. This ambiguity has led to inconsistencies and misunderstanding. Duffy (1995) questions the validity of using the term at all in reference to pulp suspension flow (or transport processes in general) and points out that the term is not used at all in reference to slurry flows.

The crux of the matter is the meaning intended when the term is used. It appears that most researchers have used the term in reference to relative motion between flocs implying the point of complete network disruption (Gullichsen & Härkönen, 1981; Kerekes et al., 1985; Bennington et al., 1989; 1991; Kerekes, 2006). However some have also used the term in discussing relative motion between individual fibres implying no flocs are present in the suspension (Gullichsen & Härkönen, 1981; Kerekes et al., 1985; Bennington et al., 1989; 1991). Bennington et al. (1989) note

that the term fluidisation could equally be applied to fibre – fibre or floc – floc relative motion (fibre-level and floc-level fluidisation respectively). The term fluidisation has been used in the screening literature numerous times, although once again no clarification of the precise meaning is given. It is apparent however that when it has been used in the screening literature it has been in reference to relative fibre – fibre motion, implying a condition where no coherent flocs are present and fibres move independent of each other (see Section 2.5.3). Several researchers have reported the presence of flocs in the flow even at high shear rates (Norman et al., 1986; Bennington, 1988).

2.3.1 Flocculation - Formation, Dispersion and Turbulence

The behaviour of pulp in turbulence is a fundamental consideration in the formation of the wet paper web but also has application to pressure screening. Mason (1948; 1954) proposed the concept of a "dynamic equilibrium" where flocs are continually being formed and dispersed. This dynamic equilibrium process was observed by Mason, however the consistency at which it was observed was very low (< 0.05 %). The existence of these transient flocs was also postulated by Hubley et al. (1950) although the measurement technique used in that study did not allow the observation of any dynamic equilibrium.

It has been shown that when flocs flow through a contraction they will tend to elongate and deform rather than rupture (Kerekes, 1983a; 1983b; James et al., 2003), although this may be pulp specific (Norman et al., 1977). Kerekes (1983b) found that typically softwood flocs ruptured only if they were elongated to five times their original length. Salmela & Kataja (2005) reported that the floc size in decaying turbulence was more dependant on the largest scale of turbulence than the overall turbulence intensity immediately after a sudden expansion. The motion of fibre in turbulent flow has also been considered theoretically (Olson & Kerekes, 1998b; Olson, 2001b).

Kerekes (1983b) reviews the literature dealing with flocculation in decaying turbulence and concludes that there still remains large deficiencies in the knowledge about the structure of the suspension, the types of flocs present, and the rate of

formation and dispersion in decaying turbulence. He proposes a mechanism for floc formation as a result of decaying turbulence. Three regimes are proposed and schematically illustrated in Figure 2-10. Coherent flocs are ruptured and dispersed in the immediate wake of a disturbance where turbulence intensity is greatest. A fully turbulent region exists which will cause fibres to entangle and form transient flocs which are in turn disrupted or dispersed. Coherent flocs will only form from transient flocs when the fluid shear is inadequate to rupture the transient floc. This occurs during an intermediate flow regime where small coherent flocs and transient flocs exist concurrently. In support of the idea of an intermediate or transition regime, Andersson (1966) has shown that stable and coherent flocs will exist among transient flocs and fibres, and will exhibit a random turbulent motion. As the turbulence energy reduces further and is insufficient to continually rupture transient flocs, larger coherent stable flocs will be formed. This final stage was called a plug flow regime and is not to be confused with the plug flow regime described previously for pipe flow.

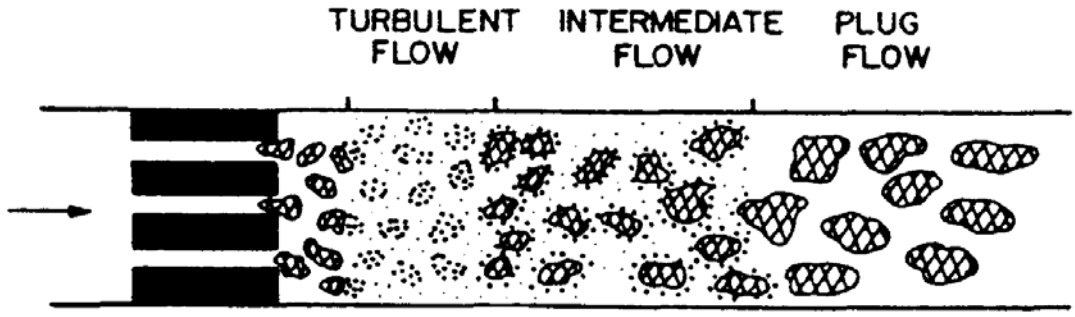

Figure 2-10 Mechanisms for floc dispersion and formation in decaying turbulence (Kerekes, 1983b)

This mechanistic explanation is supported by a number of experimental observations. The size of the floc has been found to be closely dependant on the local turbulence structure and intensity, with floc size increasing as turbulence intensity decreased (Parker, 1961). Reflocculation will occur very rapidly as the turbulence intensity decreases. Reflocculation times increase markedly with increased consistency and the reflocculation time for pulp at 4 % consistency has been measured to be 1 millisecond (Grundström et al., 1973; Kallmes, 1977). A summary of reported reflocculation times is given in Table 2-2.

Björkman (2005) proposed a discrete floc splitting mechanism as well a continuous floc sizing mechanism based on experimental work using a Couette instrument. Yan & Norman (2006) found that the majority of flocs (≈80 %) in a softwood kraft suspension tended to elongate and deform rather than rupture during flow through a contraction. The contraction was from an initial channel of 40 mm to a final section of 20 mm with flow velocities increasing from 8 to 16 m/s before and in the contraction. Flocs readily deformed and a dewatering mechanism was proposed similar in concept to that of Björkman's floc sizing concept. It should be noted that the floc size travelling through the contraction was much less than the contraction itself and therefore the deformation was only due to fluid forces.

Table 2-2 Reported reflocculation times under decaying turbulence (Arola et al., 1998)

Researcher	Consistency (wt. %)	Flow Velocity (m/s)	Reflocculation Time (ms)
Parker (1961)	0.155	0.76 – 1.04	<2000
Kallmes (1977)	0.5	Not provided	500
	1.0		1000
	2.0		40
	3.0		20
	4.0		1
Grundström et al. (1973)	3.0	Not provided	2 – 10
	4.0		1
d'Incau (1983)	0.45	0.013 – 2	160
Takeuchi et al. (1983)	0.14 – 0.86	0.83	500 – 1500
Bonano (1984)	1.0	7.6	7
		9.1	14
		10.2	12
	2.0	9.1	14
		10.2	12
Kerekes et al. (1985)	0.3	1.3	840
Arola et al. (1998)	0.5	0.13 – 0.9	510 ±140

2.3.2 Momentum Transfer

Momentum transfer is an important consideration in the transport and processing of fluids and suspensions. Momentum transfer can be defined as the process where momentum is transferred from one fluid region to an adjacent fluid region and depending on the scale considered, this may occur via the interchange of molecules between fluid layers or larger fluid particles. If fluid particle A with velocity u_x is considered as it moves to position B it will cause the velocity in that fluid layer to decrease. Similarly if fluid particle C moves to position D then it will increase the velocity of that layer of fluid. This interchange is illustrated in Figure 2-11. Effective transfer occurs when there is a small difference between the velocities of the two fluid regions. As a result of the unique rheological properties of pulp suspensions the process of momentum transfer is somewhat more complicated than that described above. Norman et al. (1977) discuss three distinct mechanisms whereby momentum is transferred in a flowing fibre suspension: a) viscous stress, b) turbulent or Reynolds stress, and c) fibre interlocking stress.

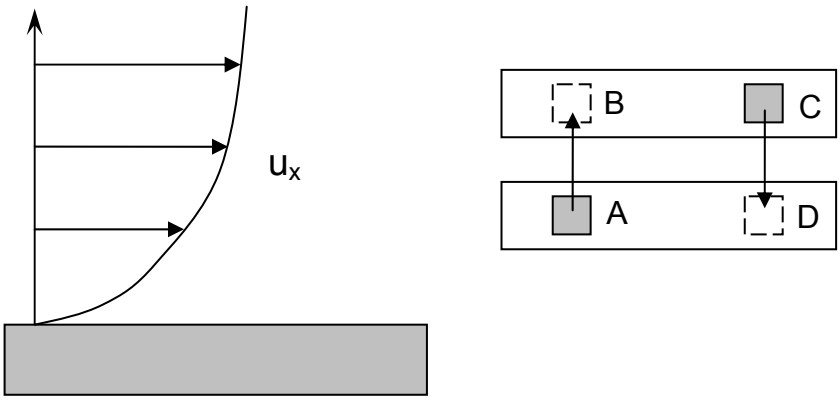

Figure 2-11 Mixing layer concept (Davidson, 2004)

Viscous Stress

Momentum is transferred as a result of molecular interactions as discussed in the previous paragraph and illustrated in Figure 2-11. Molecular transport is a random process in both magnitude and direction and is based on the kinetic theory of gases. This type of momentum transfer will only occur in the fluid phase of the suspension and will be dependant on the viscosity of the fluid.

Turbulent or Reynolds Stress

In turbulent flows fluid particles may travel from one region of the fluid to an adjacent region which will then transfer momentum from one region to another. This is analogous to momentum transfer by viscous stress or molecular transport. This macroscopic movement of turbulent eddies leads to Prandtl's mixing length hypothesis which is analogous to the mean free path of a gas molecule. The more intense the turbulent eddies the more efficient the momentum transfer.

The presence of fibres in the suspension complicates the transfer of momentum as the presence of fibres alters the turbulence of the fluid. Small eddies decay very rapidly in a pure fluid and the rate of decay increases for pulp suspensions (Wahlström, 1981). Bennington & Mmbaga (2001) found that turbulence in the liquid phase decreased exponentially as fibre consistency was increased. Fibres act as a force-bearing linkage between adjacent fluid regions with different velocities and as a result the turbulence is dampened or suppressed, which minimises the transfer of momentum due to eddy transport. The consistency, fibre length, and flexibility will all affect the level of effectiveness of the fibre in suppressing the turbulence.

Fibre Interlocking Stress

Fibre interlocking stress occurs due to the frictional forces at contact points between fibres in the suspension and flocs. This stress will be greater in a fibre floc and the strength of a floc has been shown to be dependant on consistency, fibre length, fibre flexibility, and the fibre surface. Momentum transfer will be improved due to fibre interlocking by providing a physical means whereby force is transferred from one region to another without transport of material. Lundell et al. (2005) note that usually turbulent energy is dissipated as heat in a pure fluid such as water, however in a pulp suspension turbulent energy is dissipated due to fibre interactions.

Norman et al. (1977) presented hypothetical distributions of the viscous, Reynolds stress and interlocking stress over the radius of a pipe at the point of maximum drag reduction, which is reproduced in Figure 2-12. Near the wall the viscous stress is important and dominates. These viscous stresses are only important in the viscous sublayer and buffer region ($y^+ < 30$). Reynolds stresses then become important in the turbulent core region ($y^+ > 30$) with interlocking stress making a moderate

contribution. The interlocking stress becomes increasingly dominant toward the centre of the pipe with a decrease in the Reynolds stress. Finally when the solid plug is reached (S_p/R on the figure) the interlocking stress dominates. Interlocking stresses therefore make a sizeable contribution to the momentum transfer in most regimes in pipe flow.

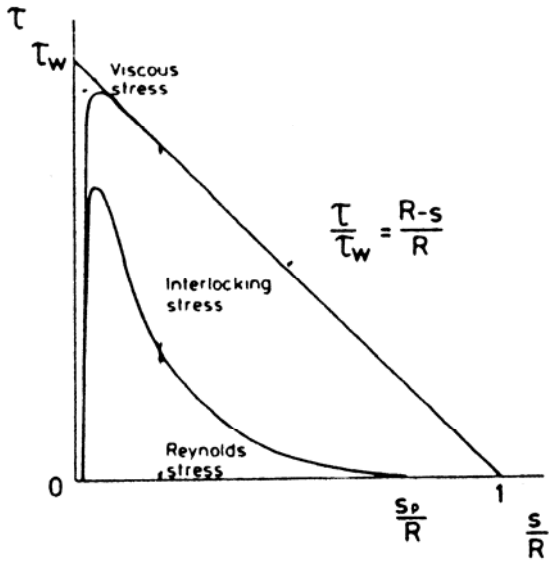

Figure 2-12 Hypothetical distributions of the viscous, interlocking and Reynolds stress components of the total mean shear stress in a pipe for a flow rate near the point of maximum drag reduction (Norman et al., 1977)

Lee & Duffy (1976a; 1976b) found the velocity profile in a pipe was modified due to the presence of pulp and used an apparent von Kármán constant *K* to quantify the effect of pulp on the velocity profile. Increased pulp consistency lowered the apparent von Kármán constant which will in affect cause the velocity profile in the turbulent core region to increase as illustrated in Figure 2-13 where U^+ is the dimensionless velocity quotient and y^+ is the dimensionless distance from the wall. Lee & Duffy suggest that the presence of fibre does not modify the velocity profile in the viscous sublayer or buffer layer. This apparent von Kármán constant approach was found to predict well local average velocities and also the pipe flow resistance in the fully developed turbulence regime (region JK in Figure 2-5). It was suggested that measured values of the apparent von Kármán constant could be used to describe the turbulent flow in other applications or systems such as head boxes or refiners.

Different mechanisms will dominate in different physical regions of the flow and will become more significant at different flow conditions (i.e. increased velocities). For pipe flow the viscous stress is important only in the small viscous sublayer of the boundary layer directly next to the pipe wall. This region is relatively free of fibre and therefore viscous stress dominates. When a fibre plug region is present the interlocking forces will dominate which will increase the efficiency of momentum transfer. In regimes where a turbulent water annulus is present it is expected that Reynolds stresses will dominate that region.

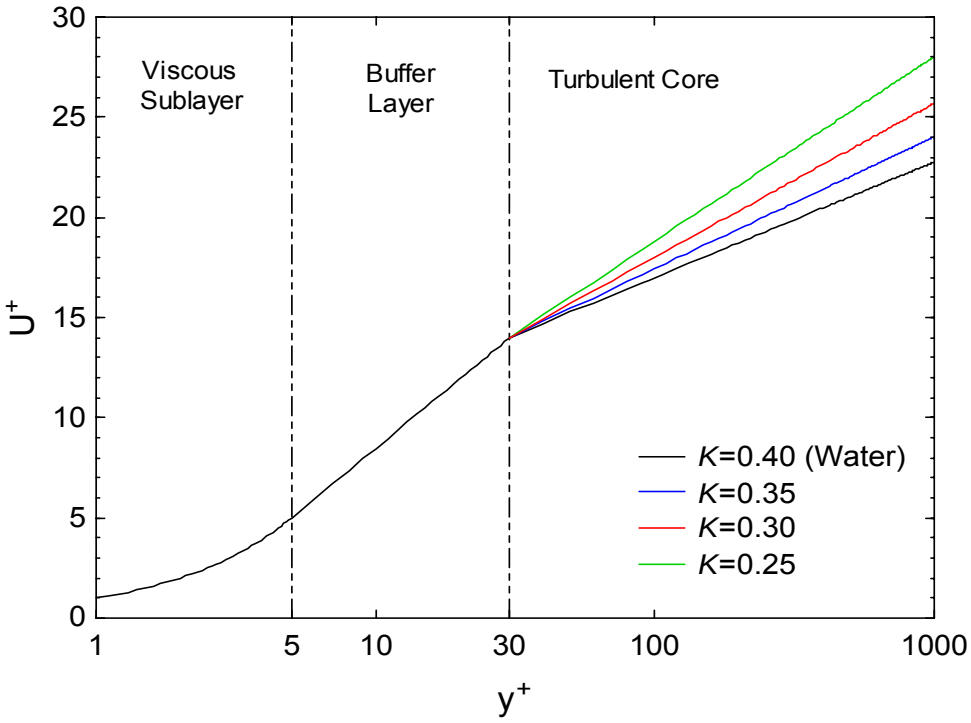

Figure 2-13 The effect of apparent von Kármán constant on the normalised velocity U^+ as a function of normalised wall coordinates

In summary the presence of fibres affects the transfer of momentum in two ways. Firstly, turbulence is suppressed or dampened due to the presence of fibres which reduces the transfer of momentum. Fibres are very efficient at dampening turbulence even at very low consistencies. Secondly, flocculated fibres will increase momentum transfer as a result of mechanical entanglement and interlocking. These two mechanisms are competing and opposing in their effect on momentum transfer and both will be dependant on the consistency of the suspension and the fibre properties (mainly length and stiffness). The consistency and fibre length will increase the

likelihood that fibres will contact and form flocs or a fibre network and also mean floc size. Fibre stiffness on the other hand will affect the degree of turbulence suppression and momentum transfer between the flocs and the fluid.

Summary

Flocculation and rheological phenomena are important considerations in screening as both the consistency and suspension properties change along the length of the screen. Moreover it is highly probable that the flow conditions and degree of turbulence are also changing along the screen length. These numerous factors will impact the degree and propensity of the suspension to flocculate. As will be shown, flocculation has not been sufficiently accounted for in the contemporary theory and explanation of pressure screening.

2.4 Pressure Screening

Pressure screens play a vital part in the manufacture of pulp and paper. They are utilized predominately to remove contaminants from the pulp furnish during the stock preparation stages of production and also as a final guard to the paper machine in the approach flow system. Pressure screens are also employed to improve furnish properties via fibre fractionation. Pressure screens are complex and a multiplicity of factors and variables affect their operation and performance. This section examines the current level of understanding and discusses some deficiencies in the mechanistic understanding and explanation of how pressure screens function, separate contaminants, and fractionate long and short fibre.

2.4.1 Screen Design, Equipment, and Configuration

Screening has become an increasingly important unit operation in the production of pulp and paper products. Pressure screens are used in a variety of ways at a number of different stages in the manufacturing process. They are used to remove contaminants such as shives and dirt from the pulp furnish, or stickies from recycled pulp. Furthermore pressure screens are used to protect the headbox of the paper machine from unwanted particles.

There are a multitude of different commercial pressure screens and screening equipment used and available, produced by a number of manufacturers, at the present time. A detailed assessment of the merits and limitations of all the available screens is not the intent of this section. A general overview of the generic types of equipment and configurations will be given.

A pressure screen consists of a rotor, screen basket and housing. The pulp suspension enters the feed chamber and then enters the screen annulus. Fluid and some of the pulp will pass through the screen apertures and into the accept chamber and then exit the screen via the accept outlet. If the pulp does not pass through the apertures and is rejected it travels through the entire length of the screen before exiting via the reject outlet. Screens can be fed axially or tangentially as in Figure 2-2-14. The screen may or may not have a feed chamber which the pulp passes through before entering the screen annulus. Furthermore stock may flow centrifugally or centripetally through the screen. Figure 2-15 illustrates four typical flow configurations with tangential feeds. The more common configuration is a centrifugal screen in which the rotor is located concentrically inside the feed annulus with accepted pulp flowing centrifugally in a radial direction.

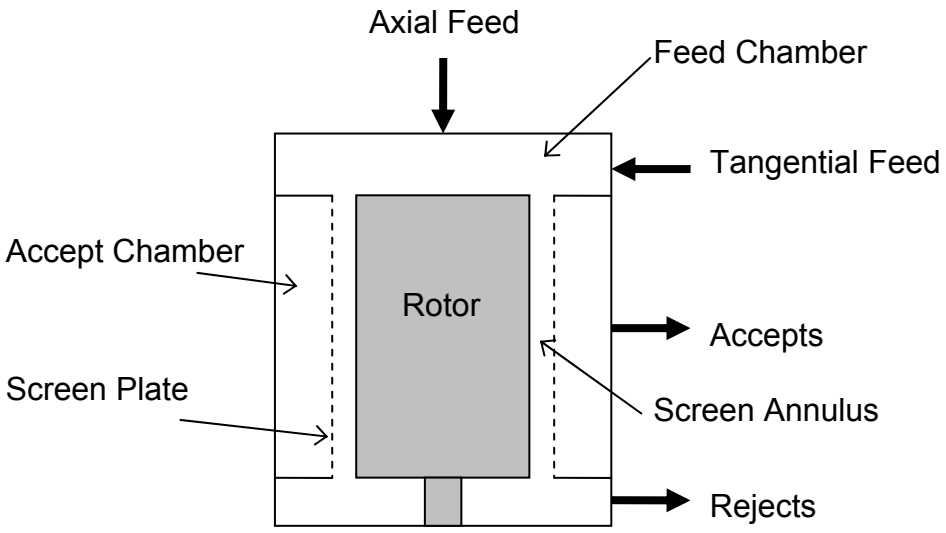

Figure 2-2-14 Axially and tangentially fed pressure screens

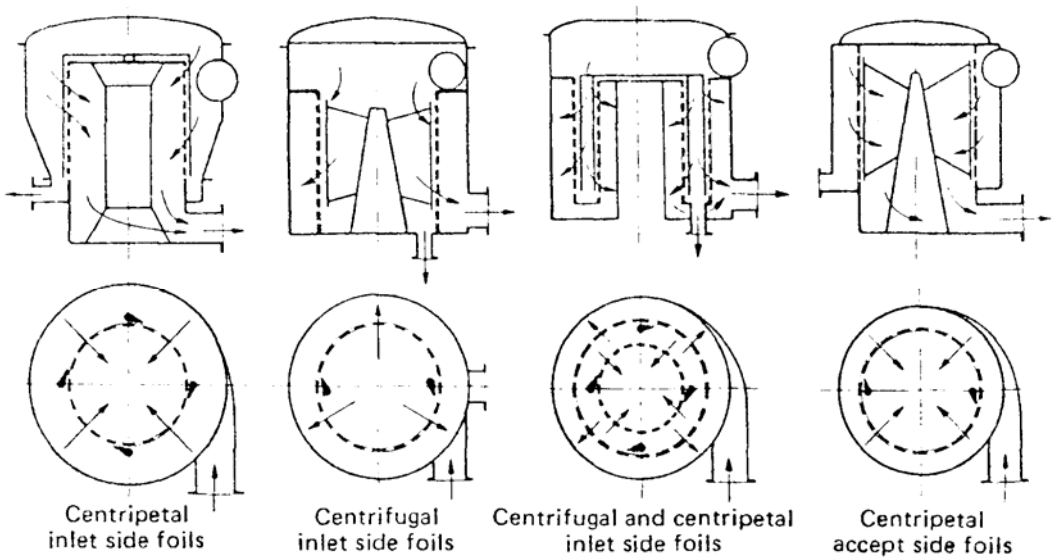

Figure 2-15 Four typical pressure screen flow configurations (Smook, 1992)

More recently some screens are being partitioned such that there are multiple accept chambers and the feed annulus contains so called "deflocculation" and dilution devices (Serres & Rees, 2002). These screens, although novel, are simply two screens in series with the reject of the first section becoming the feed of the second section. Although it has been claimed that these screens increase capacity and fractionation efficiency, these claims have yet to be independently verified and data that has been published to date is far from comprehensive or convincing. Alternatively there have also been novel screen configurations that have arranged short screens in parallel as illustrated in Figure 2-16 (Pimley & Rees, 1998). The design of the housing of the screen has come under increased attention in recent years in an attempt to alter the internal flow characteristics of the screen. For example, Schweiss (2000) used computational fluid dynamics to optimise the flow through the screen by tapering the accept chamber and locating the screen basket eccentrically instead of concentrically inside the housing.

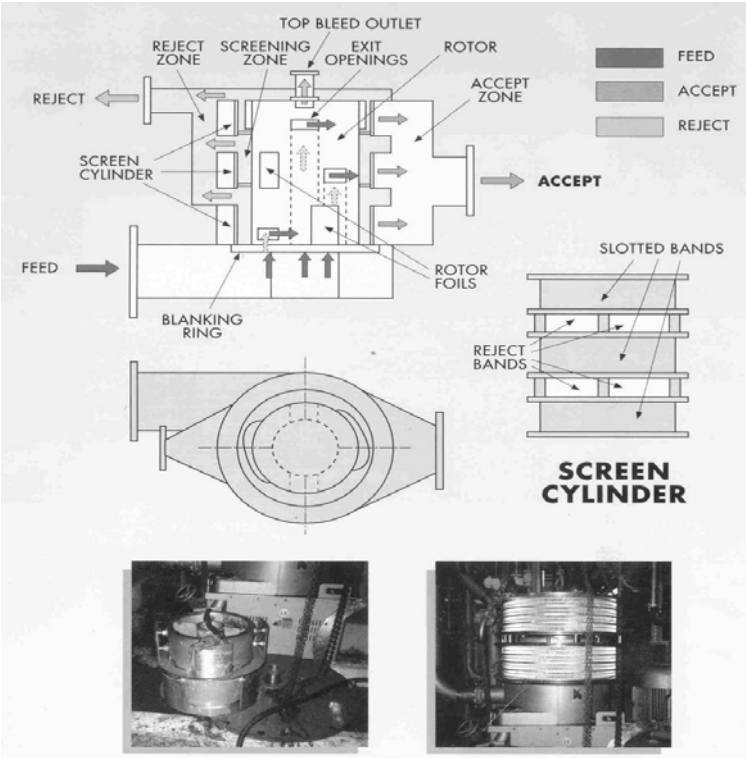

Figure 2-16 A novel screen design with multiple short screens sections in parallel within one screen housing (Pimley & Rees, 1998)

There are three velocity components in a pressure screen as shown in Figure 2-17. The axial component is due to the flow from the feed to the rejects end and decreases as flow occurs to the accept chamber through the screen. The tangential velocity is induced by the rotor although there may also be an initial tangential velocity component due to the feed configuration. The radial velocity component is a function of accept flow rate and it has been suggested that it is four times greater than the axial velocity (Niinimäki, 1998) although this will be dependant on the reject rate and mean aperture velocity. The direction and velocity of the flow over the apertures will be a function of the axial and tangential velocity components. Usually the tangential velocity component is much greater than the axial component and therefore it is assumed that the flow is approaching normal to the aperture. However as it is apparent that both the tangential and axial velocity components are changing along the axial length of the screen it seems likely that the angle of incidence will also change. Several authors have estimated these velocities from first principles although only bulk flows were used in these calculations. For example, the radial velocity is taken to be the average aperture velocity and therefore dependant only on the accept

flow rate and open area of the screen basket. The instantaneous aperture velocity will be constantly changing due to the dynamic nature of the flow although this has not been quantified as yet.

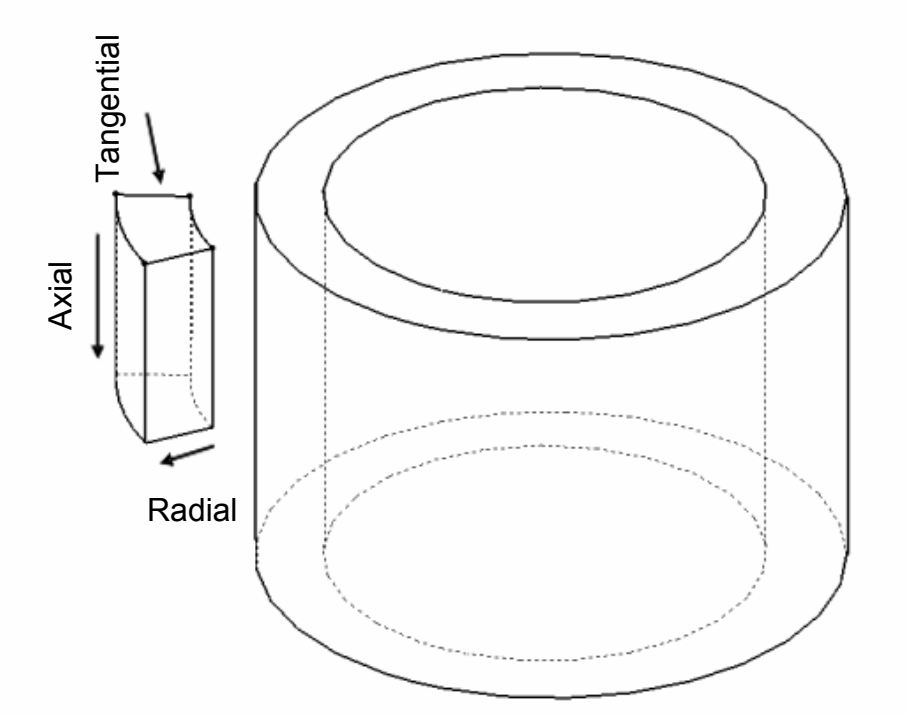

Figure 2-17 Velocity components in a pressure screen

2.4.2 Screen Baskets

Screen baskets, also known as screen plates, are generally holed or slotted and may be smooth or contoured. Holed screens are generally smooth and range in hole diameter from 6 to 20 mm for screens used for knot removal (called knotters) and 0.8 to 3 mm for screening and fractionation. Holed screens are generally preferred for fractionation and have a much larger open area than slotted screens. The accept side is often recessed to reduce the pressure drop over the screen plate and it has been speculated that as a result the reverse passage ratio for holed screens may be higher than the forward passage ratio (Atkins, 2003).

Holed screens have inherently high strength, low screen wear, good removal efficiency for long thin material, poor removal efficiency for cubical debris, and a high capacity per unit area. The spacing between the holes (called pitch) is an

important design variable with holed screens. If the pitch is too small then fibres can become stapled or pinned between two adjacent holes and will increase the likelihood of blocking (Gooding & Craig, 1992; Yu & DeFoe, 1994).

Slotted screens are nearly always contoured and slot widths range from around 0.085 to 1 mm. A number of different contour profiles are available and the contour creates turbulent eddies on the feed side of the screen as in Figure 2-18. These eddies are thought to increase throughput by fluidising an exit layer and by aligning fibres, thus increasing the passage of fibre through the aperture. Slotted screens have much lower strength than holed screens, however recent advances in fabrication techniques have increased their strength considerably. They generally wear more quickly than holed screens and have low capacity per unit area. Slotted screens provide excellent removal efficiency for cubical debris and can be used to remove certain contaminants via barrier screening (Julien Saint Amand, 2001). Slotted screens are also exclusively used in the screening of stickies from recycled pulp. Contour height and profile are almost as important as slot width when selecting slotted screens (Jokinen, Ämmälä et al., 2007).

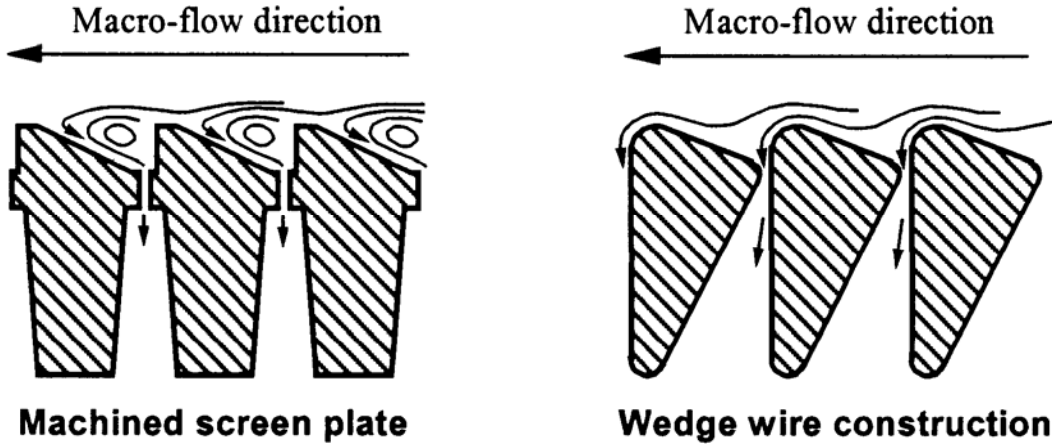

Figure 2-18 Turbulent eddies created by a screen aperture profile (Julien Saint Amand & Perrin, 1998)

There is evidence in the literature that screening mechanisms that occur in holed screens differ to that which occur in slotted screens (Olson & Kerekes, 1998a; Olson & Wherrett, 1998; Olson et al., 2000; Olson, 2001a) however this has yet to be established with any degree of certainty. While holed screens generally give superior

fibre length fractionation efficiency, slotted screens can produce a very clean short fraction (Siewert et al., 1989; Yu, DeFoe et al., 1994). Furthermore similar fibre length fractionation efficiencies can be obtained using a slotted basket if the correct slot width, contour profile and height, and optimum operating conditions are used. Wakelin & Corson (1997) note that contoured screen plates give greater operational flexibility than do smooth plates.

2.4.3 Screen Rotor

The screen rotor is a vital element in the operation of a pressure screen. The rotor produces a high tangential flow along the screen surface. Furthermore it creates large pressure variations across the screen plate. These pressure variations induce flow in the forward direction (feed to accept) and periodic reverse flow (accept to feed). Reverse flow unblocks the screen plate by removing or disrupting any fibre or contaminant accumulations over or in the aperture as illustrated in Figure 2-19. This process is commonly referred to as back-mixing.

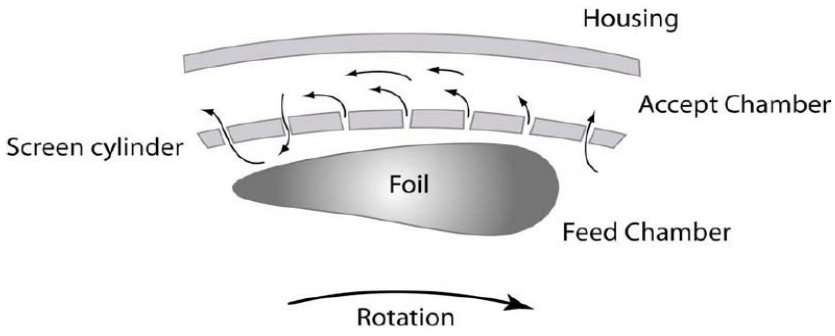

Figure 2-19 Rotor action for a foil rotor (Weckroth et al., 2001)

Numerous rotors are commercially available and these can be divided into three general types: open, semi-open, and closed rotors. Open rotors (as illustrated by rotor A in Figure 2-20) usually have hydro-foils that are held in place by supports which project radially from the centre. This creates a much larger annulus as pulp can flow between the rotor shaft and the foils. It is thought that the mixing in the annulus will be promoted by the foil supports. Closed rotors, also called drum rotors (as shown by rotors B, C, and D in Figure 2-20) are cylindrical with perturbations attached that will

produce a pressure pulse. Semi-open rotors are a mixture of the two and taper from the feed end to the reject end of the screen.

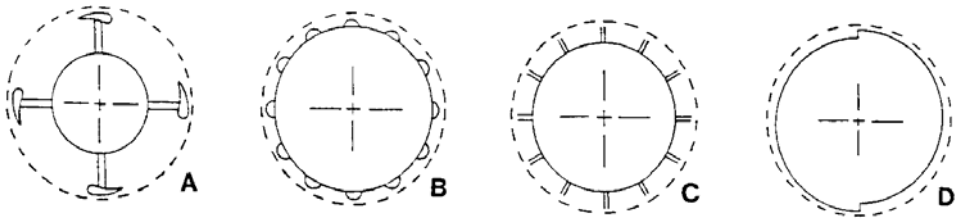

Figure 2-20 Types of rotors (Bliss, 1992)

2.4.4 Rotor Tip Speed

The rotor tip speed u_{tip} can vary and typically ranges from between 12 – 30 m/s. The tip speed is an important variable as it determines the intensity and frequency of the pressure pulse as well as the mean tangential velocity $\bar{u}_{tan}$ of the stock in the screen annulus. Different rotors produce different pressure pulse signatures. The frequency, shape and intensity will depend on the profile and settings of the rotor. The ability to alter the rotor speed can be a valuable advantage in the use of advanced control strategies for screen control. Unfortunately many screens do not have variable speed drives and therefore may not be operated at the optimal efficiency or capacity. Not running the screen at the optimal operating point will increase the specific energy consumption for the pulp and paper produced.

Despite the rotor tip speed being an important and easily manipulated variable, its affect on the performance and capacity of a screen is still poorly understood. It is accepted that the rotor speed will determine the mean tangential velocity of the stock in the feed annulus. Furthermore, flow channel experiments have found that the upstream velocity $\bar{u}_u$ (equivalent to the mean tangential velocity) has a major effect on the passage of fibre through the screen. In an attempt to relate the upstream velocity and the rotor tip speed, Gooding (1986) estimated that the mean tangential velocity in a screen annulus would be 15 % that of the tip speed. This can be expressed in the form of a slip factor γ (Equation 2-12). Gooding's estimation of the slip factor was based on a bump rotor and an analysis of the velocity profile in the wake of a cylinder taken from Schlichting (1960). Bennington et al. (1991) observed that the mean

velocity of flocs adjacent to the rotor in a rotary shear device ranged between 6 and 10 % of the rotor speed.

$$\bar{u}_{tan} = (1 - \gamma)u_{tip} \qquad \textbf{2-12}$$

While it is evident that the mean tangential velocity will be less than the tip speed, the actual slip factor will be different for different flow and operating conditions, rotors, and annulus sizes. Furthermore, as discussed previously, pulp has a complex rheology and therefore will not behave as a Newtonian fluid. The rheology of the suspension will change as it moves along the screen length due to consistency and average fibre length changes. This in turn will result in a variable slip factor along the screen length. Reinecker (1992), Niinimäki (1998), and Weeds (2006) have speculated that the slip factor will decrease along the screen length and as a consequence the mean tangential velocity in the annulus at the feed end of the screen will be lower than at the rear. A hypothetical illustration of the change in slip factor along the screen length, adapted from Reinecker (1992) is illustrated in Figure 2-21.

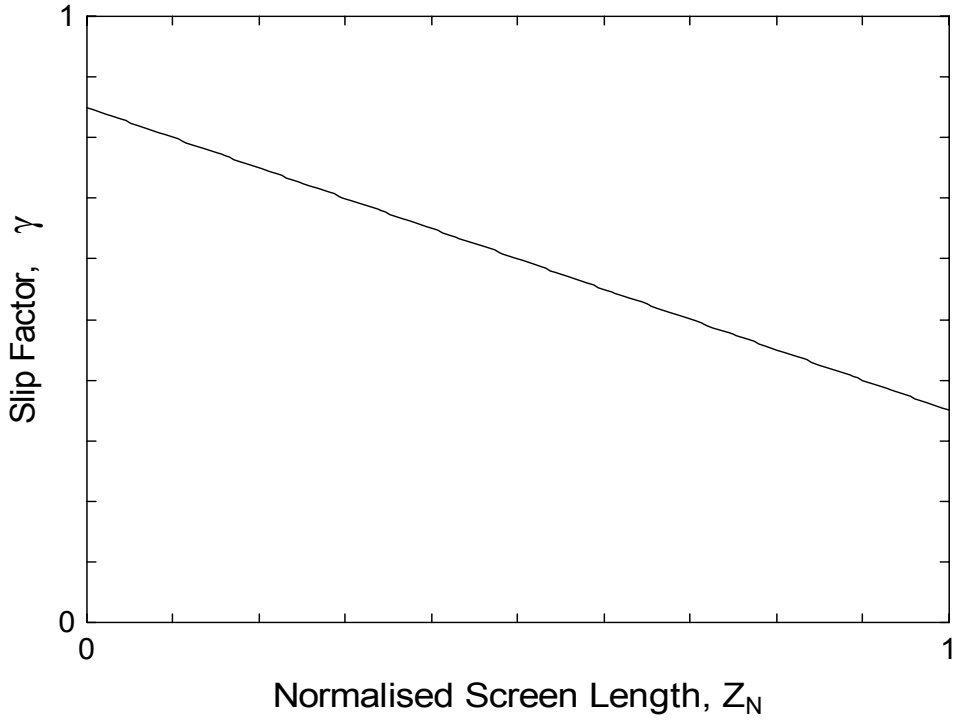

Figure 2-21 Schematic of the change in slip factor along the screen length adapted from Reinecker (1992)

Weeds (2006) measured the increase in the reject consistency over a narrow section near the front and at the rear of the screen and found that the thickening behaviour of the two sections was different. Furthermore, the thickening behaviour of the section toward the front of the screen was significantly altered when a pulp accelerator was used, while the behaviour of the section toward the rear was unaffected. The pulp accelerator is a novel device placed into the feed chamber of the screen to increase the tangential velocity of the pulp before it enters the screen annulus. He also found that the relative speed of the suspension and the rotor had a greater impact at superficial aperture velocities less than 2 m/s. This implies that the slip factor can be altered by means of novel rotor elements which in turn may alter the thickening behaviour along the screen length.

Elson (1979) showed that the velocity profile across an annular gap with a smooth rotating outside cylinder was dependant on the ratio of the length of the annulus to the size of the annular gap. Naser (1997) modelled using CFD the flow of Newtonian and non-Newtonian fluids through a concentric annulus with a smooth rotating inner wall. The predicted velocity profile for glucose at a Reynolds number of 7500 and an annular gap of 24.8 mm was compared with experimental data taken from Escudier & Gouldson (1995) and is shown in Figure 2-22. In the figure ξ is equal to the annular height and ξ=1 corresponds to the stationary wall, the ratio w/w_i is the normalised tangential velocity (w_i is equivalent to u_{tip}), and ζ is the axial distance along the annulus expressed as the number of annular lengths. As can be seen from the figure the mean tangential velocity profile is fully developed at around 245 annular lengths along the axial length. The experimental data is for ζ=245 and the disagreement between the predicted and measured values is attributed to the deficiencies of the k-ε turbulence model which was used in that study. Tangential velocity profiles measured across an annulus with a smooth rotating cylindrical rotor, illustrated in Figure 2-23 have shown that the average velocity over approximately 90 % of the annular gap to be about 50 % of the rotor tip speed (Antunes et al., 1996). The difference between the profiles shown in Figure 2-22 and Figure 2-23 may be due to the difference in annular gap used and the fact that there seems to be no axial flow through the annulus in the latter case. Antures et al. (1996) unfortunately do not give enough details to be certain as to the conditions and experimental set up that was used but it is likely that the profile in Figure 2-23 is for fully developed flow.

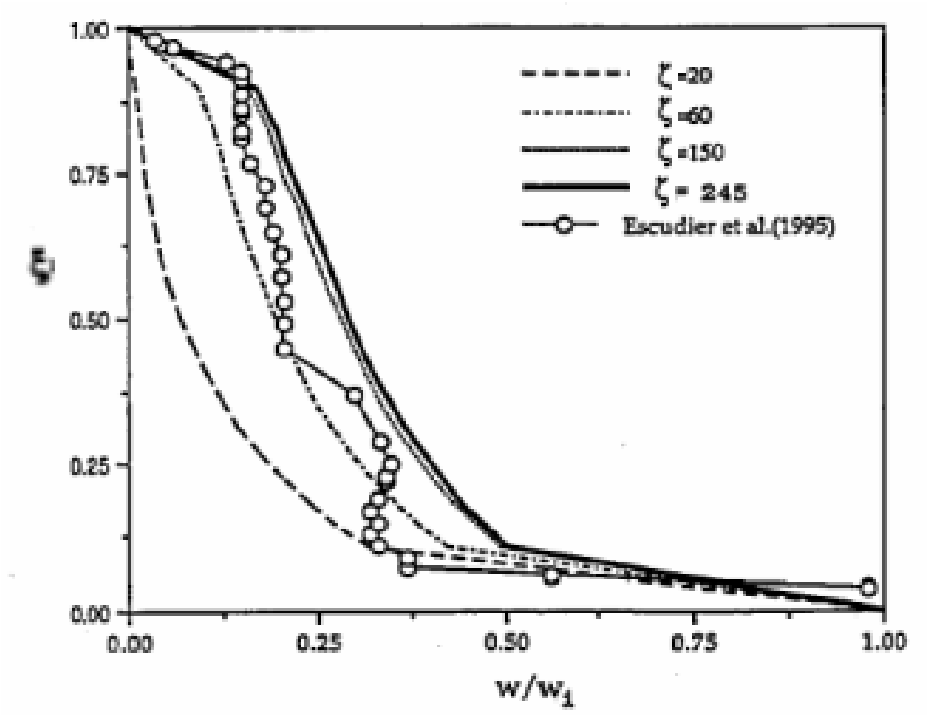

Figure 2-22 Tangential velocity profiles of Glucose, Re=7500 (Naser, 1997)

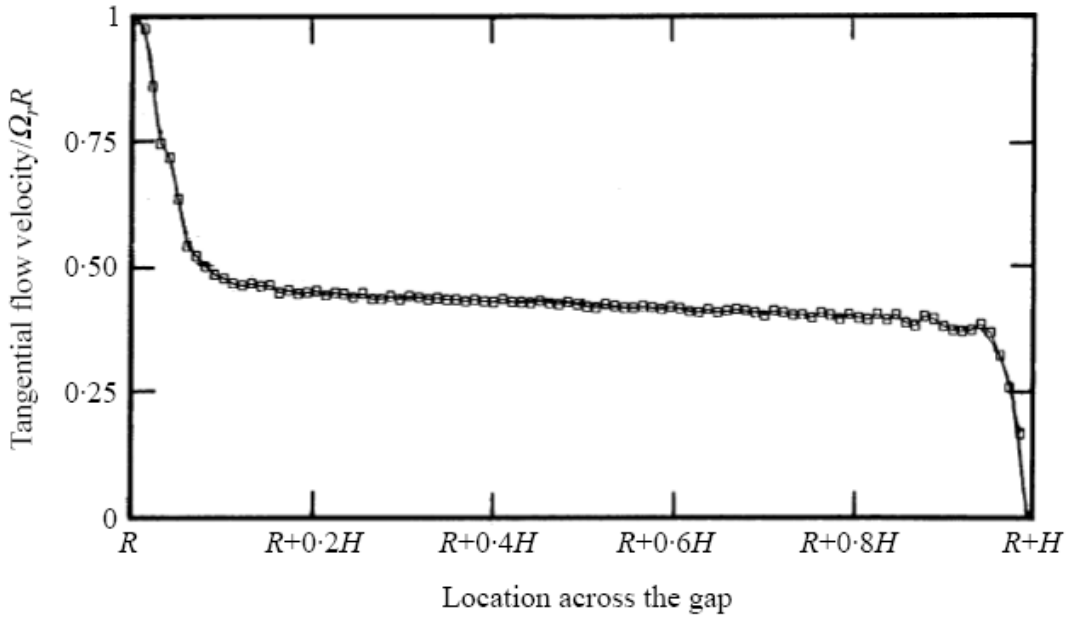

Figure 2-23 Tangential flow velocity profile across the annular gap (Antunes et al., 1996)

The effect of rotor tip speed on reject thickening and fractionation efficiency is ambiguous and often contradictory. The tip speed will affect the mixing conditions, turbulence intensity, pulse strength and frequency, and mean tangential velocity in the screen annulus. Some studies using industrial screens have shown that an increase in

rotor speed will not improve or reduce the screening and fractionation effect (Repo & Sundholm, 1996; Sloane, 1998; Walmsley & Weeds, 1998; Braaten & Wakelin, 1999; Sloane, 2000; Wakelin & Paul, 2001). McCarthy (1988) found that although a greater tip speed reduced screening efficiency the capacity of the screen was increased. By contrast, the flow channel experiments have shown that fractionation efficiency can be increased as the upstream velocity is increased (Kumar, 1991; Tangsaghasaksri & Göttsching, 1994; Tangsaghasaksri et al., 1994; Olson & Kerekes, 1998a; Julien Saint Amand, 2001). Still other studies have demonstrated that efficiency increases up to a critical tip speed and then decreases above this critical speed (Wakelin & Corson, 1997; Wakelin, 1998; Gooding, Olson et al., 2001; Ämmälä, 2004). It appears that the optimum rotor speed is dependent on the screen aperture geometry, furnish type, accept flow rate, and feed consistency.

It has been suggested that at very low tip speeds (below about 8 m/s) the conditions in the annulus approach an ideal disturbance free state, similar to those found in the flow channel experiments (Ämmälä, 2004). This suggestion is highly questionable because one of the limitations of the flow channel experiments is that there is no pulsation due to the absence of a rotor. In a screen even at low tip speeds, pulsation will still occur and produce an unstable flow field and a high degree of turbulence.

2.4.5 Pressure Pulse

As a consequence of the rotor, the pressure in the feed annulus is dynamic and is a combination of the static pressure from the pump and the variable pressure arising around the moving rotor. When the pressure in screen annulus is greater than the pressure in the accept chamber the flow will be in the forward direction (annulus to accepts). Likewise when the pressure in screen annulus drops below that of the accept chamber the flow will be in the reverse direction (accepts to annulus). Karvinen & Halonen (1984) found that the reverse flow during the negative part of the pressure pulse was caused by a drop in pressure due to the acceleration of the fluid. This acceleration is a result of the reduced section between the moving rotor element and the stationary screen and causes this Venturi effect. Yu et al. (1994) identified four forces that must be overcome during the reverse pulse in order for the aperture to be cleared of accumulated fibre: a) the pressure drop due to the forward

flow, b) the disruptive shear stress of the fibre network, c) inertial forces from the forward flow, and d) centrifugal forces.

Pressure pulse signatures have been experimentally measured or numerically modelled by numerous researchers (Javid, 1983; Karvinen & Halonen, 1984; Yu, 1994; Yu, Crossley et al., 1994; Gooding, 1996; Pietilä, 1996; Julien Saint Amand, 1997; Niinimäki, 1998; Julien Saint Amand & Perrin, 1999; Wikström & Fredriksson, 1999; Gonzalez, 2002; Wikström & Rasmuson, 2002; Pinon et al., 2003; Feng et al., 2005). Yu (1994) measured the pressure pulse for a generic foil, step, and bump rotor. The pressure pulse signature of the foil rotor is shown in Figure 2-24. The pressure pulse of a foil rotor has been widely studied using predominantly laboratory screen apparatus and modelled using CFD. The affect of variables such as rotor speed, pulp consistency, angle of attack, foil shape, chord length, and accept flow rate have been examined to various levels of detail.

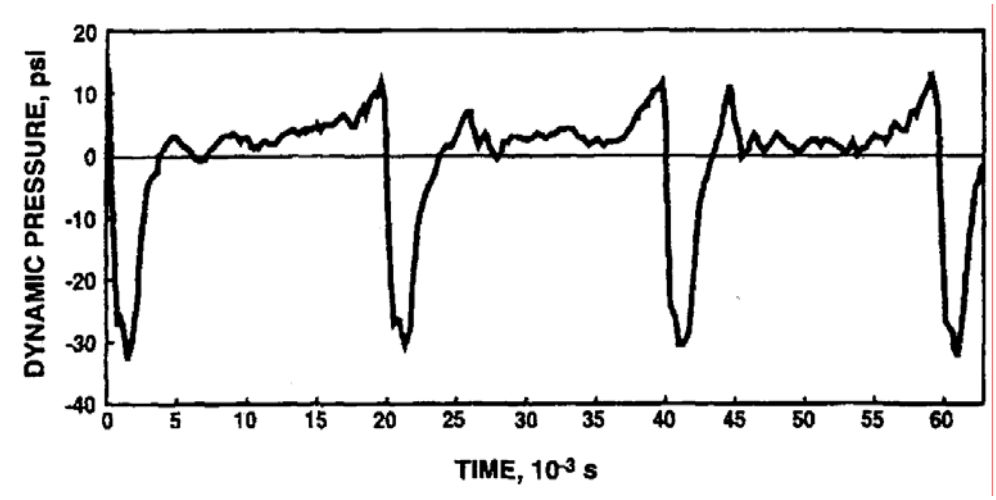

Figure 2-24 Pressure pulse signature of the foil rotor as measured by Yu (1994)

The shape of the pulse is not altered by changes in tip speed, however intensity or pulse magnitude and frequency are. Karvinen & Halonen (1984) and Yu (1994) found the pressure pulse was unaffected by changes in accept flow rate and feed consistency. However, Gonzalez (2002) and Pinon et al. (2003) reported that the magnitude of the pressure pulse of a foil rotor measured using a laboratory screen section, was reduced as consistency increased. Furthermore, Pinon demonstrated that the magnitude of the negative pulse was reduced more as consistency increased. It

has been shown that as the gap between the rotor and the screen surface is decreased the magnitude of the pressure pulse is increased (Gonzalez, 2002; Pinon et al., 2003; Feng et al., 2005).

The flow through an aperture is governed by the relationship expressed by Equation 2-13, which relates the average velocity through the aperture $\bar{u}_s$ to the pressure drop ΔP over the aperture by the parameter K_L, which is a non-dimensional pressure loss coefficient. K_L is a measure of the flow resistance and the value of K_L for a square edged entry is approximately 0.5. As K_L is dependant on the entry geometry of the aperture it is evident that K_L will usually be less for the reverse portion of the pressure pulse for holed apertures as the accept side of the apertures are often recessed, thereby reducing the flow resistance in the reverse direction (Gooding, Kerekes et al., 2001). Jokinen, Ämmälä et al. (2007) have demonstrated that the pressure drop in the reverse direction is greater than in the forward direction for slotted apertures. It has been shown that as the normalised velocity approaches zero that the loss coefficient rapidly increases from a steady value as illustrated in Figure 2-25.

$$\Delta P = K_L\left(\frac{1}{2}\rho\bar{u}_s^{\,2}\right) \qquad \textbf{2-13}$$

Jokinen, Ämmälä et al. (2007) recently published a study of the hydraulic resistance in the forward and reverse directions of several slotted screen plate geometries. The slot width, profile height, and wire height and width were varied and as expected the hydraulic resistance in the forward direction increased as the slot width decreased. Hydraulic resistance in the forward direction also increased as the wire height and width were increased. The resistance in the reverse direction was greater than in the forward direction which was expected due to the geometries of the slots. Slotted apertures tend to be very narrow and modern slotted screen baskets have much greater wire heights as the wires are embedded further into the supporting rings to increase basket integrity. The hydraulic resistance in the forward and reverse direction were related to the capacity of the screen.

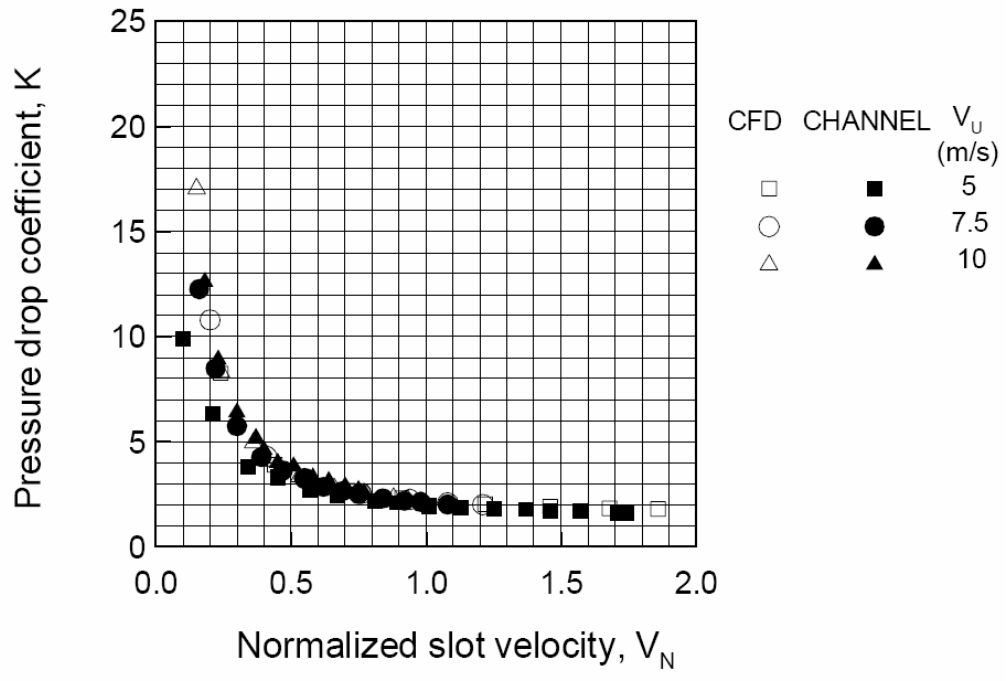

Figure 2-25 Pressure loss coefficient K_L as a function of normalised velocity

(Gooding, Kerekes et al., 2001)

The instantaneous volumetric flow rate through the screen aperture during the pressure pulse can be calculated by rearranging Equation 2-13, assuming that the loss coefficient remains constant. For screens with circular apertures this yields Equation 2-14, and for screens with slots Equation 2-15, where r is the radius of the aperture, w the width of the slot, and L_s is the length of the slot. The total volumetric flow rate during the positive and negative portions of the pressure pulse can be calculated using the pressure pulse signature data and by integrating Equation 2-14 or 2-15.

$$Q_{int} = \pi r^2 \left[\frac{2\Delta P}{\rho K_L} \right]^{\frac{1}{2}} \qquad \textbf{2-14}$$

$$Q_{int} = w L_s \left[\frac{2\Delta P}{\rho K_L} \right]^{\frac{1}{2}} \qquad \textbf{2-15}$$

The ratio of the volume of the forward flow to the reverse flow is known as the rotor back-flush ratio k (Equation 2-16). It has been estimated from the pressure pulse measured by Yu (1994) that for the step and bump rotor, k was equal to 0.5 and 0.125 respectively (Weeds, 2006; Walmsley & Weeds, 2007). These values are consistent with the characteristics of the two rotors in that the bump rotor is known as a high frequency, low pulse rotor. The step rotor on the other hand is a low frequency high pulse rotor which induces a much larger reverse flow than the bump rotor. The large amount of reverse flow was consistent with the fact that the step rotor is known to reduce reject thickening.

$$k = \frac{Q_{for}}{Q_{rev}} \qquad \textbf{2-16}$$

Yu (1994) showed that the magnitude of the positive pressure pulse for a step rotor was linearly proportional to the tip speed for all feed flow rates, however only a limited range of tip speeds were tested. Numerous researchers have found that the magnitude of the pressure pulse is roughly proportional to the square of the tip speed (Gonzalez, 2002; Pinon et al., 2003; Feng et al., 2005). Martinez et al. (1999) took a different approach and considered a force balance around a floc lodged in a screen aperture. From this starting point they derived an equation to predict the maximum volumetric capacity Q_{max} of the screen. Equation 2-17 shows that the maximum capacity of the screen is dependant on the open area of the screen A_{open}, the density of the suspension, the hydraulic resistance of the screen K_L, the magnitude of the pressure pulse ΔP, the static coefficient of friction μ between the floc and the aperture, the compressive stress of the floc σ, the slot depth T_s, and the slot width w.

$$Q_{max} = A_{open}\left[\frac{2(\Delta P - 2\mu\sigma\left(\frac{T_s}{w}\right)}{\rho K_L}\right]^{\frac{1}{2}} \qquad \textbf{2-17}$$

Weeds (2006) found that the maximum accept flow rate attainable before the screen blocked was about 40 % higher through a section at the front of the screen compared to a section at the rear of the screen. He applied Equation 2-17 from Martinez et al. (1999) to data and found that the predicted pressure pulse was about 33 % lower at the rear of the screen than at the front.

There seems to be some indication that the magnitude of the pressure pulse is also dependant on the relative speed, or slip factor, between the fluid in the feed annulus and the rotor tip. Julien Saint Amand (1997) has reported that the pressure pulse is amplified when a contoured screen is used as the contours exert a large braking force on the fluid in the annulus and therefore decrease the average velocity of the suspension. Furthermore, Yu (1994) found that the pressure pulse at the rejects end of the screen was less than that at the front of the screen. Although there was no explanation as to why this occured or any further investigation of this phenomenon, it is reasonable to suppose that the slip factor is reduced along the screen length, and therefore the strength of the pressure pulse will also be reduced toward the rear of the screen.

2.4.6 CFD Modelling of the Rotor

The foil rotor has been extensively modelled using CFD, although the quality of some of the modelling is difficult to determine in some of the literature as vital information is sometimes omitted. Although this may be for commercial reasons it places a certain amount of uncertainty over some of the results. For example Wikström & Fredriksson (1999) modelled the pressure pulse and assumed, with no explanation, that flow in the computational domain would be laminar (with the exception of the area directly adjacent to the foil and the screen). This assumption is highly questionable and in a later paper (Wikström & Rasmuson, 2002) they used a number of turbulence models and found good agreement with the experimentally measured pressure pulse, although there were slight variations between turbulence models.

Grégoire et al. (2000) have shown that the choice of turbulence model is important as the solution may be somewhat different if other turbulence models are used. As shown in Figure 2-26 the choice of turbulence model may introduce discrepancies

into the numerical solution. While an examination of the various turbulence models is beyond the scope of this discussion, there is need to exercise caution as the choice of an appropriate turbulence model is non-trivial and often the most suitable one is not the most popular. Two equation turbulence models, such as the widely used k-ε model, are poorly suited for rotating flows and call for ad hoc corrections in order make realistic predictions (Wilcox, 1998; Versteeg & Malalasekera, 2007).

Despite the intricacies and limitations of CFD, it is proving a valuable tool in understanding the relationship between a foil element and the pressure pulse. Furthermore this knowledge is being incorporated into improved rotor design. For example, Feng et al. (2005) modelled several different rotor foils in order to understand the effect of design and operating variables on the pressure pulse. Good agreement was found with the experimentally measured pulse. Furthermore the settings of the foil (e.g. angle of attack, clearance, etc) could be optimised using data obtained from the numerical solution.

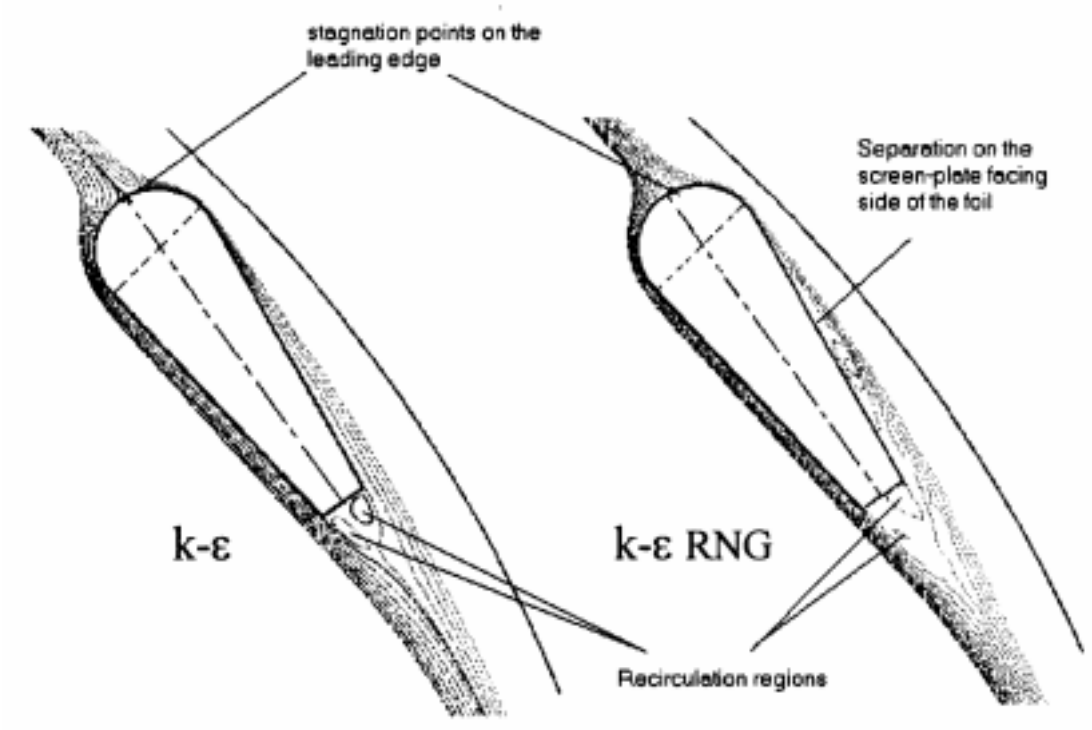

Figure 2-26 Discrepancies in the flow around a foil due to the use of different turbulence models: the standard k-ε and the k-ε RNG turbulence models (Grégoire et al., 2000)

2.5 Screening Mechanisms

The actual mechanisms of separation and fractionation that occur within a pressure screen are highly complex and not well understood. This is due to the complex interactions between the fibre and screen elements (i.e. rotor and screen aperture), fibre to fibre interactions (i.e. flocculation and consistency effects), the complex rheology of fibre suspensions, and hydrodynamic considerations (i.e. highly dynamic and complex flow fields). This section will discuss the work carried out on screening mechanisms and describe barrier and probability screening principles, and then the fibre alignment and fibre mat theories of pressure screening.

2.5.1 Barrier and Probability Screening

Solid-solid separations may occur in a screen due to one or a mix of two methods, barrier screening, also known as positive size separation, and probability screening. Pressure screens operate mainly on the probability mechanism of screening although barrier screening of larger contaminants may occur when fine slots are used (Rienecker, 1997; Julien Saint Amand & Perrin, 1998).

Barrier screening occurs when the particles to be separated are larger in all dimensions than the screen apertures as illustrated in Figure 2-27. It is physically impossible for the oversize particles to pass through the apertures and therefore they are rejected. However the flow field is still a factor in the rejection of particles capable of passing through the apertures. The accept stream will contain only undersize particles, however the rejects will still contain both undersize and oversized particles. Therefore the efficiency of the screen is still determined in part by the flow field or how many opportunities an undersize particle can approach an aperture and not exclusively by geometric considerations.

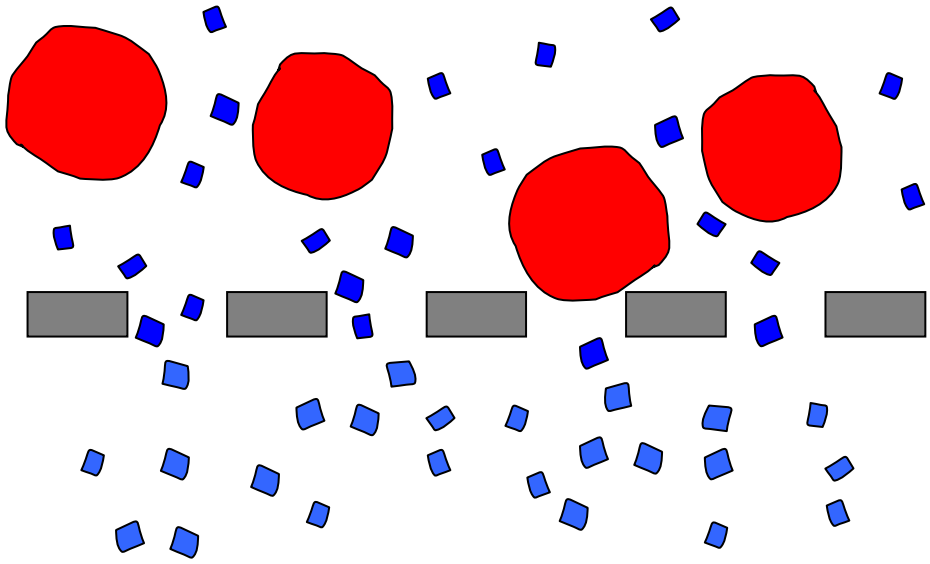

Figure 2-27 Barrier screening

Probability screening occurs when the particle is less than the aperture size in at least one dimension as shown in Figure 2-28. The particle may pass through the aperture but acceptance is dependant on the orientation of the particle in relation to the aperture. In screens that use a suspending medium, the flow field and hydrodynamics of the particle will play an important role in the screening of the particle. The flow field around the aperture will also be a factor influencing the orientation of the particle as it approaches and interacts with the aperture.

Probability screening by nature is more complex to both model and describe mechanistically than barrier screening. Factors such as particle geometry, particle behaviour, particle interactions with other particles and the screening apparatus, must all be considered when designing and operating a screen based on both barrier and probability screening mechanisms.

Pressure screens operate predominantly on probability screening. Wood fibres have a large aspect ratio and the width and height of the fibre are usually much less than the aperture size although the average length in usually larger. Barrier screening will occur if the contaminants (i.e. shives or stickies) are larger than the aperture size. The recent use of fine slots in the order of 0.1 mm in width for contaminant removal employs predominantly barrier screening. The removal of stickies by barrier

screening is somewhat problematic however because of their visco-elastic behaviour. Under some screening conditions, especially vigorous annular mixing conditions, stickies may be broken into smaller particles and therefore may no longer be screened under barrier conditions. Moreover they may also deform and be extruded through the aperture. This special case of particle extrusion will be discussed further in Section 2.5.3

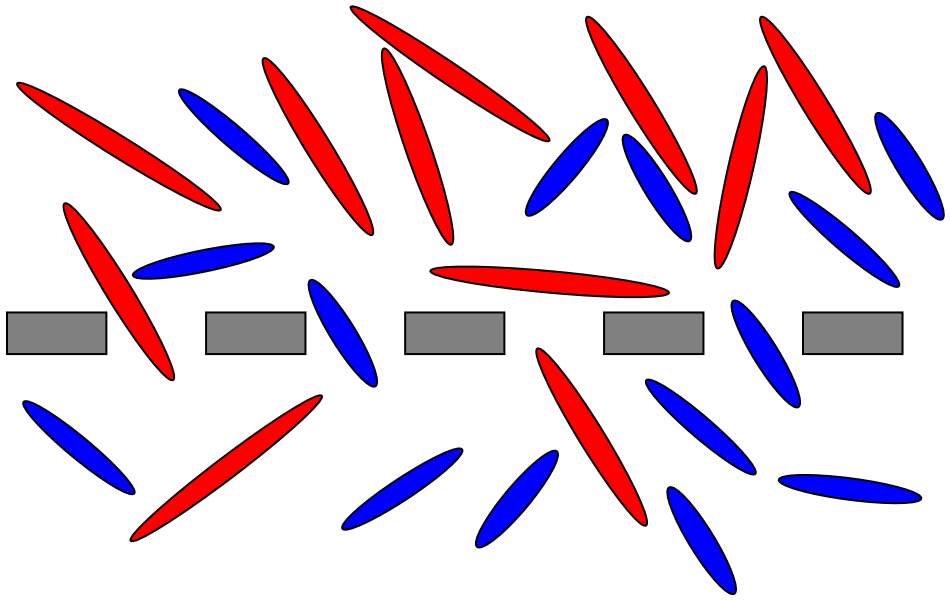

Figure 2-28 Probability screening

Kubát & Steenberg (Kubát & Steenberg, 1955; Kubát, 1956a; 1956b) developed the theory of probability screening by considering a screen fed with only one type of particle. The accept and feed/reject chambers where assumed to be well mixed, and the particles behaved as independent units (i.e. no particle interactions). A series of equations were developed based on these assumptions, which expressed the net flow of particles across the screen. These equations accounted for the pulsation effect of the screen and included probabilities of passage in both the forward p_{for} and reverse p_{rev} directions. The net flow of particles through the screen $m_{particles}$ is given by Equation 2-18 where Q_{for} and Q_{rev} is the amount of flow in the forward and reverse directions respectively, and C_r and C_a are the consistency of the reject and accept streams respectively.

$$m_{particles} = p_{for} Q_{for} C_r - p_{rev} Q_{rev} C_a \quad \textbf{2-18}$$

From Equation 2-18 a permeability index *p* (Equation 2-19) can be defined.

$$p = \frac{p_{for}\left(1 + \frac{Q_{rev}}{Q_a}\right)}{1 + p_{rev}\frac{Q_{rev}}{Q_a}} \quad \textbf{2-19}$$

Although numerous authors cite this early work, the principles of variable pressure or pulsation, and forward and reverse flow of particles and fluid, have rarely been applied to pressure screening theory or modelling.

During typical screening operations there is a consistency change between the feed, accept and reject streams. A normalised consistency drop factor D (Equation 2-20) can be used to express the consistency change over the screen from feed to accepts where C_f and C_a are the consistencies of the feed and accepts respectively.

$$D = \frac{C_f - C_a}{C_f} \quad \textbf{2-20}$$

Likewise a reject thickening factor T (Equation 2-21) describes the thickening of pulp from feed to rejects, where C_r is the consistency of the rejects.

$$T = \frac{C_r}{C_f} \quad \textbf{2-21}$$

The split between accepts and rejects is also an important factor and may be expressed by a volumetric reject rate R_v (Equation 2-22), or mass reject ratio R_m (Equation 2-23) where Q_f and Q_r are the feed and reject volumetric flow rates, and m_f and m_r are the mass flow rates of fibre for the feed and rejects.

$$R_v = \frac{Q_r}{Q_f} \qquad \textbf{2-22}$$

$$R_m = \frac{m_r}{m_f} = \frac{C_r Q_r}{C_f Q_f} \qquad \textbf{2-23}$$

Volumetric reject rate is a widely used operating variable and is commonly referred to simply as the reject rate and has found widespread use partly because it is much easier to measure volumetric flows than mass flows.

2.5.2 Fibre Alignment Theory

The behaviour of an individual pulp fibre as it approaches an aperture has been extensively studied by numerous researchers (Gooding, 1986; Kumar, 1991; Oosthuizen et al., 1992; Tangsaghasaksri & Göttsching, 1994; Tangsaghasaksri et al., 1994; Gooding, 1996; Olson, 1996; Atkins, 2003). These fundamental studies form the basis of the fibre alignment theory of screening which attempts to explain screening mechanisms by applying the fundamental behaviour of an individual fibre as it approaches an aperture to real industrial pressure screening applications. The vast majority of this fundamental research has been conducted using single apertures in a flow channel, screen sections, or novel screens. One advantage of this approach is that it simplifies the screening conditions and creates a steady uniform flow field. Researchers have attempted to relate the findings of these fundamental studies to industrial screening with some success (Gooding, 1996), although caution must be taken when applying the findings to industrial screening as the flow conditions can be markedly different (Walmsley & Atkins, 2003).

Early work on the screening of fibres in dilute suspensions was carried out by Riese et al. (1969). Retention of stiff nylon fibres in suspension, which flowed at normal incidence to a screen plate with circular holes, was examined in detail. All consistencies were at less than 3 mg/L in order to avoid any fibre-fibre interactions. Fibre ranged from 1.71 to 7.12 mm in length and from 93 to 255 μm in diameter. The screen plates ranged from 0.4 to 1 mm in thickness, 1, 2, and 4 mm holes were used

and numerous hole patterns used. Retention (or rejection) of fibre increased with increasing fibre length, fibre diameter and decreased with increasing flow rate, hole spacing and hole diameter. These basic findings apply to all fibre screening at low consistencies. Furthermore, the authors developed equations from theory to predict the retention of fibre and these compared well to the experimental findings over the range of conditions tested.

Gooding (1986) studied the motion of various synthetic and pulp fibres as they approached a single aperture and found that fibres which were accepted originated in a layer of fluid that was termed the "exit layer". This exit layer is the fluid below the stagnation line due to the bifurcation of the flow. The thickness of this layer H_{exit} is dependant on the flow conditions through the slot relative to the main bulk flow, with the thickness increasing as more of the flow passes through the slot. Thomas & Cornelius (1982) showed that in addition to this exit layer a recirculation zone formed on the upstream wall of the slot as illustrated in Figure 2-29. This recirculation zone is caused by a flow separation at the upstream edge of the slot and reattachment further along the upstream wall of the slot as shown in Figure 2-29.

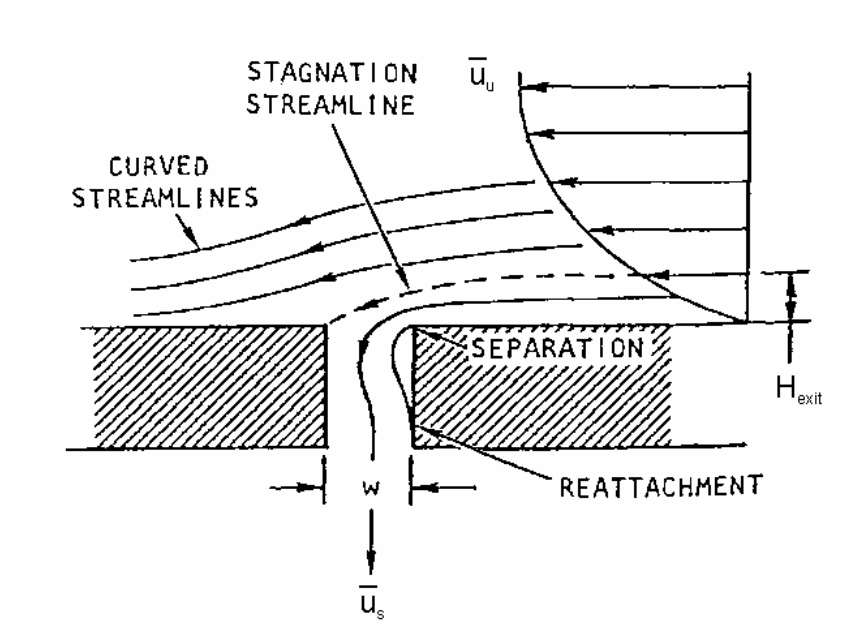

Figure 2-29 Exit layer H_{exit} and recirculation zone (Thomas & Cornelius, 1982)

The size of the recirculation zone is also dependant on the relative flow conditions or normalised velocity u_n (Equation 2-24). The normalised velocity is the ratio of the velocity of the fluid through the aperture $\bar{u}_s$ to the bulk velocity of the fluid directly upstream of the slot $\bar{u}_u$. The recirculation zone increases in size as the normalised velocity is decreased.

$$u_n = \frac{\bar{u}_s}{\bar{u}_u} \qquad \textbf{2-24}$$

The thickness or height of the exit layer H_{exit} can be calculated (Equation 2-25) if it is assumed that there is a constant velocity profile directly upstream of the slot, where w is the slot width (Olson & Wherrett, 1998).

$$H_{exit} = w\frac{\bar{u}_s}{\bar{u}_u} \qquad \textbf{2-25}$$

Gooding (1986) studied the probability of fibre passing through the aperture and defined the pulp passage ratio P (Equation 2-26) as the ratio of the consistency of fibre in the aperture C_s to the consistency upstream of the aperture C_u. The passage of a fibre has been shown to be dependant on a number of factors. The flow conditions, fibre properties, and aperture type and dimensions, all contribute, albeit sometimes competing roles, in determining if a fibre will be accepted or rejected by the aperture. The passage ratio is analogous to Kubát & Steenberg's permeability index.

$$P = \frac{C_s}{C_u} \qquad \textbf{2-26}$$

Gooding also reported five main trajectories that a fibre could follow in a single aperture channel. These five fibre motion types were:

1. The fibre travels past the aperture without entering or contacting the aperture wall;
2. One end of the fibre enters the aperture and comes into contact with one of the aperture walls and is subsequently swept back into the bulk flow;
3. One end of the fibre enters the aperture and is balanced over the downstream edge of the aperture (referred to as "stapling");
4. One end of the fibre enters the aperture and comes into contact with one or two of the aperture wall and subsequently passes through the aperture;
5. The fibre passes through the aperture without coming into contact with the aperture wall.

Wall & Turning Effects

The passage of a fibre through the aperture was found to be dependant on the orientation and position of the fibre relative to the exit layer. Gooding (1986) proposed two factors that were thought to affect the passage of a fibre: the wall effect (i.e. the interaction of the fibre with the upstream wall of the screen) and the turning effect (i.e. hydrodynamic forces applied to the fibre as it approaches and enters the aperture).

Gooding observed that the fibre consistency in the exit layer was less than 25 % of the bulk flow. He postulated that fibre interactions with the wall, migration away from the wall due to the fluid velocity gradient, surface induced turbulence, or fibre rotation might all contribute to this fibre depletion of the exit layer. Kumar (1991) suggests that fibre rotation is the dominant factor in the depletion, however more work is needed to determine the relative contributions of the causes of depletion. If fibre rotation is the dominant effect then fibre properties such as fibre length and stiffness will be important factors.

Olson (1996) measured the point fibre consistency (C/C_{av}) from the wall to the bulk flow using optical techniques and found the consistency was roughly equal to zero directly at the channel wall and increased linearly to a height of approximately one third the average fibre length at which point the consistency remained constant. Figure 2-30 shows the point fibre consistency normalised by the feed consistency as a function of height above the channel wall as reported by Olson (1996).

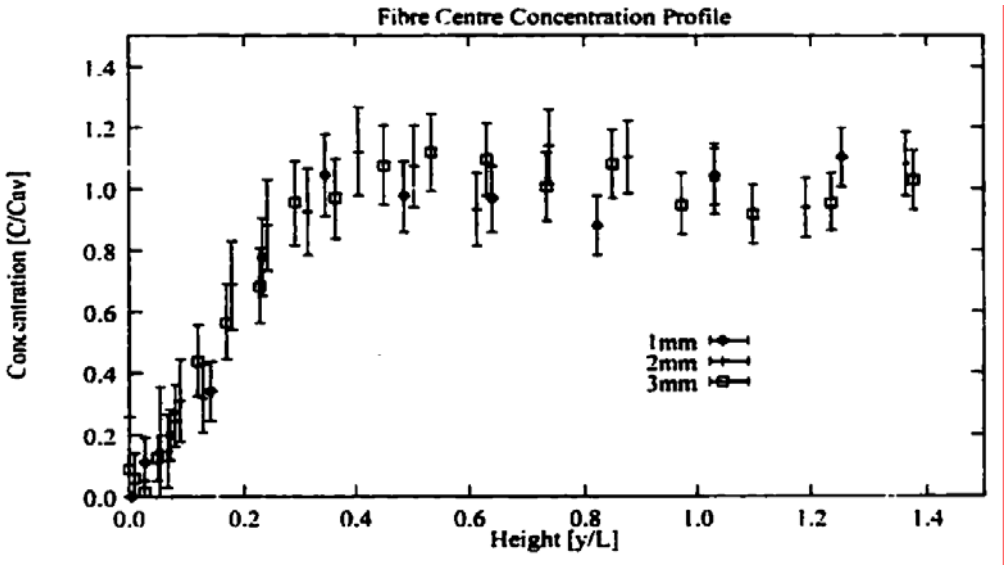

Figure 2-30 Fibre consistency as function of height above the channel wall (Olson, 1996)

Pulp fibres are much more flexible than synthetic fibres. This allows them to bend and rotate as they are subject to hydrodynamic forces. Oosthuizen et al. (1992) have shown that typical pulp fibres will tend to follow the streamlines even when the flow field is highly curved. The more flexible the fibre the more closely it will follow the streamlines. Two fibres of the same dimensions but differing flexibility will therefore have a different probability of passing the aperture (Kumar, 1991). Under the same flow conditions, the more flexible fibre will exhibit a higher probability of passage due to the ability to more closely follow the streamlines.

In order for fibres to pass through the aperture they must make a 90-degree turn from their orientation in the bulk flow. While in the bulk flow, fibres are aligned almost parallel to the streamlines of the flow. As discussed previously, typical pulp fibres are much more flexible than synthetic fibres and tend to align with and follow the streamlines, even in highly curved flow field such as that found directly adjacent to an aperture. This allows flexible fibres to bend and follow the streamlines through the aperture. However a stiff fibre will have to rotate in order to pass through the aperture. As the fibre rotates the trailing end of the fibre moves into streamlines with greater velocity which assists the rotation. The fibre may then contact the aperture wall and be swept either through the aperture or back into the main flow. This rotation of fibres near the aperture is known as the turning effect.

Theoretically an infinitesimally short fibre will follow the streamlines perfectly and therefore have a passage ratio equal to one. As a consequence fines (fibres less than 0.2 mm in length) are usually considered to have followed the fluid and are treated as having a passage ratio equal to approximately one. In a flow channel at low consistencies this will be the case. In a pressure screen this implies that the amount of fines rejected will be proportional to the volumetric reject rate. Olson et al. (2000) found that in a pressure screen there was no significant change in the consistency of the fines fraction between the feed, accept, and reject streams. This yields a passage of one and therefore the fines follow the flow of fluid. Ämmälä (2001) has shown that the amount of fines in the rejects is not wholly proportional to the volumetric reject rate. It is believed to be because the fibre mat acts as a secondary screen to block the passage of fines through the screen.

Particulate or denser contaminants may not follow the streamlines in the same way as small and flexible fibres do. High upstream velocities may increase the contaminant removal efficiency by causing high density contaminants to slip over or overshoot the apertures due to their greater momentum as shown in Figure 2-31 (Julien Saint Amand, 1997; 2001).

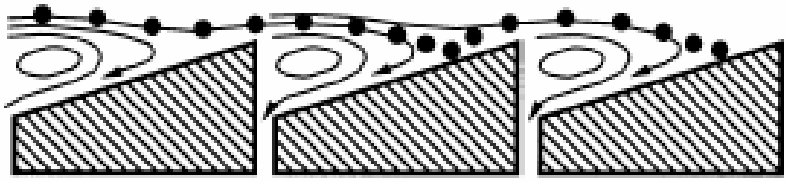

Figure 2-31 Particle slip or overshoot of high-density contaminant due to greater momentum (Julien Saint Amand, 2001)

Kumar (1991) also investigated the passage of fibre using a single aperture flow channel and specifically examined the effect of fibre length, slot width, upstream velocity, and aperture velocity. Three factors were identified that needed to be considered when determining whether a fibre would pass through an aperture: a) the extent of penetration of the fibre into the aperture, b) the degree and rate of rotation of the fibre as it enters the aperture, and c) the amount of bending of the fibre while in the aperture due to the penetration and rotation. Furthermore he proposed a

dimensionless penetration parameter ψ which was based on kinematic considerations (Equation 2-27). This parameter can be interpreted as the degree of physical fibre penetration in the aperture or alternatively the amount of the main flow relative to the fibre length taken into the aperture.

$$\psi = \frac{\bar{u}_s w}{\bar{u}_u L_f} \qquad \textbf{2-27}$$

Olson & Wherrett (1998) went on to demonstrate that ψ can be expressed as Equation 2-28 by substituting Equation 2-25 (exit layer height) into Equation 2-27. The penetration number can now be considered as the average exit layer height relative to the fibre length. Furthermore they suggest that ψ relates well to both the wall and turning effects and therefore passage will be well characterised by ψ.

$$\psi = \frac{H_{exit}}{L_f} \qquad \textbf{2-28}$$

The recirculation zone that occurs on the upstream wall of the aperture may hinder the turning of a fibre and therefore promote rejection of stiff fibres by decreasing the fibre penetration. This is consistent with Equation 2-28 because as the height of the exit layer decreases the size of the recirculation zone increases, therefore less of the fibre enters the aperture and the chance of rejection is increased. The recirculation zone may also hinder fibre motion and also promote stapling on the aperture edges or pinning of fibres between two adjacent apertures.

Lawryshyn & Kuhn (1998) utilised CFD to simulate the motion of a fibre as it approaches an aperture. Theoretical passage ratios were compared with those determined experimentally. They found that each of the five fibre motions as observed by Gooding (1986) occurred with the exception of fibre stapling. The simulation of fibre behaviour has potential to help elucidate the mechanisms that occur as a single fibre approaches an aperture. However due to computational

resources and lack of appropriate models, simulation of realistic consistencies is far beyond current computational and modelling capability.

The relative contributions of the wall and turning effects on fibre passage have been suggested by Gooding, who defined a wall effect passage ratio P_w (Equation 2-29) and a turning effect passage ratio P_t (Equation 2-30) where C_{exit} is the exit layer consistency.

$$P_w = \frac{C_{exit}}{C_u} \qquad \textbf{2-29}$$

$$P_t = \frac{C_s}{C_{exit}} \qquad \textbf{2-30}$$

The overall passage ratio will be equal to the product of these two passage ratios (Equation 2-31).

$$P_p = P_w P_t \qquad \textbf{2-31}$$

Julien Saint Amand & Perrin (1998) define analogous passage ratios to the wall and turning effect passage ratios (which they call passing probabilities) in order to calculate the instantaneous passage probability P_i. The instantaneous passage probability is defined as the product of the instantaneous probability for a particle to be captured in the exit layer P_c and the subsequent instantaneous probability of the particle passing through the aperture P_s (Equation 2-32).

$$P_i = P_c P_s \qquad \textbf{2-32}$$

Furthermore, they include an additional factor, an instantaneous recirculation probability P_r which is to account for particles that do not pass the aperture and are captured in the recirculation zone, and may subsequently be rejected back into the

main flow. Incorporating the recirculation probability into the previous equation yields Equation 2-33.

$$P_i = P_c\left(P_s + P_r\left(1 - P_s\right)\right) \qquad \textbf{2-33}$$

Fibre Properties and Fibre Passage

Fibre length is the dominant fibre property which affects fibre passage (Kumar, 1991; Tangsaghasaksri & Göttsching, 1994; Tangsaghasaksri et al., 1994; Kumar et al., 1996; Olson, 1996; Lawryshyn & Kuhn, 1998; Atkins, 2003). Numerous researchers working with different fibre types, pulping methods, furnishes, wood species, different equipment and under different flow conditions all agree that fibre passage decreases as fibre length increases (Gooding, 1986; Kumar, 1991; Olson, 1996; Olson & Kerekes, 1998a; Olson et al., 2000; Olson, 2001a; Atkins, 2003). The disparity in passage ratio of the different fractions causes a fractionation effect during screening. Longer fibre has a lower passage than shorter fibre and therefore is more readily rejected and becomes concentrated in the reject stream.

Synthetic fibres have been used to examine the effect of fibre flexibility on fibre passage using single aperture flow channels. As mentioned previously more flexible fibres follow the streamlines more closely and therefore for the same fibre length the more flexible the fibre the greater the passage. However, notwithstanding this, measuring the flexibility of real pulp fibres is not a trivial task and because of the large degree of variation in the fibre furnish a large number of fibres must be tested.

Some researchers have suggested that screens fractionate firstly on the basis of length and secondly on fibre flexibility, although there is no convincing evidence of fractionation on the basis of flexibility from industrial screening trials. Changes observed in furnishes that are attributed to flexibility changes are more likely due to changes in other properties which affect stiffness. For example, changes in furnish properties such as flexibility that occur during screening may be due to coarseness changes, which can also be explained by changes in fibre length. It is well known that a direct correlation exists between fibre length and fibre coarseness (Sastry & Wellwood, 1972; Clark, 1985). In short the length effect is a much more dominant

effect than other considerations such as fibre flexibility and coarseness, which are of secondary and minor importance. Factors such as flexibility may be more important in fibre-fibre interactions or flocculation effects which will be discussed in greater detail when considering the fibre mat theory (Section 2.5.5). The screening behaviour of earlywood and latewood fibre has also been studied with the goal of exploiting any differences in order to fractionate the two fractions (Atkins, 2003). However once again there was little difference in the screening behaviour of the two pulps and the fibre length effect was dominant.

2.5.3 Application to Industrial Screening

It has been maintained that there exists a region adjacent to the screen surface where the pulp is "fluidised" or completely deflocculated (LeBlanc, 1986; Goldenberg, 1987; Bliss, 1990; Julien Saint Amand, 1997; Niinimäki, 1998; Wikström & Rasmuson, 2002). The fluidised layer is free of flocs which enable particles and fibres to move independently (Wikström & Rasmuson, 2002). As a consequence, fibre alignment mechanisms are thought to occur during the screening phase of the pressure pulse before the aperture plugs. It is argued that pulp is fluidised due to turbulence created at the surface of the screen by the rotor and the aperture contour. If this is correct the tangential velocity caused by the rotor, as well as the geometry of the aperture, are critical in the passage of fibre through the screen. If the velocity is too low, sufficient turbulence will not be produced in order to disrupt the flocs and "fluidise" the suspension. The concept of a fluidised layer is illustrated schematically in Figure 2-32.

The concept of a fluidised layer completely free from flocs and fibre-fibre and fibre-particle interactions is problematic for several reasons. First, there exists no actual evidence from real screening studies that a fluidised layer exists. Existence of a fluidised layer is always inferred and there is visual evidence that flocs exists even in pressure screens and other devices with high rotary shear rates (Norman et al., 1986; Bennington, 1988). Furthermore the consistency at which most industrial screening takes place is high enough that the crowding number of the suspension in the annulus is well above 60 (Weeds, 2006). A crowding number greater than 60 suggests that fibre collisions will occur frequently and there maybe continuous

contact between fibres. Fibre-fibre interactions are expected to be significant at normal screening consistencies.

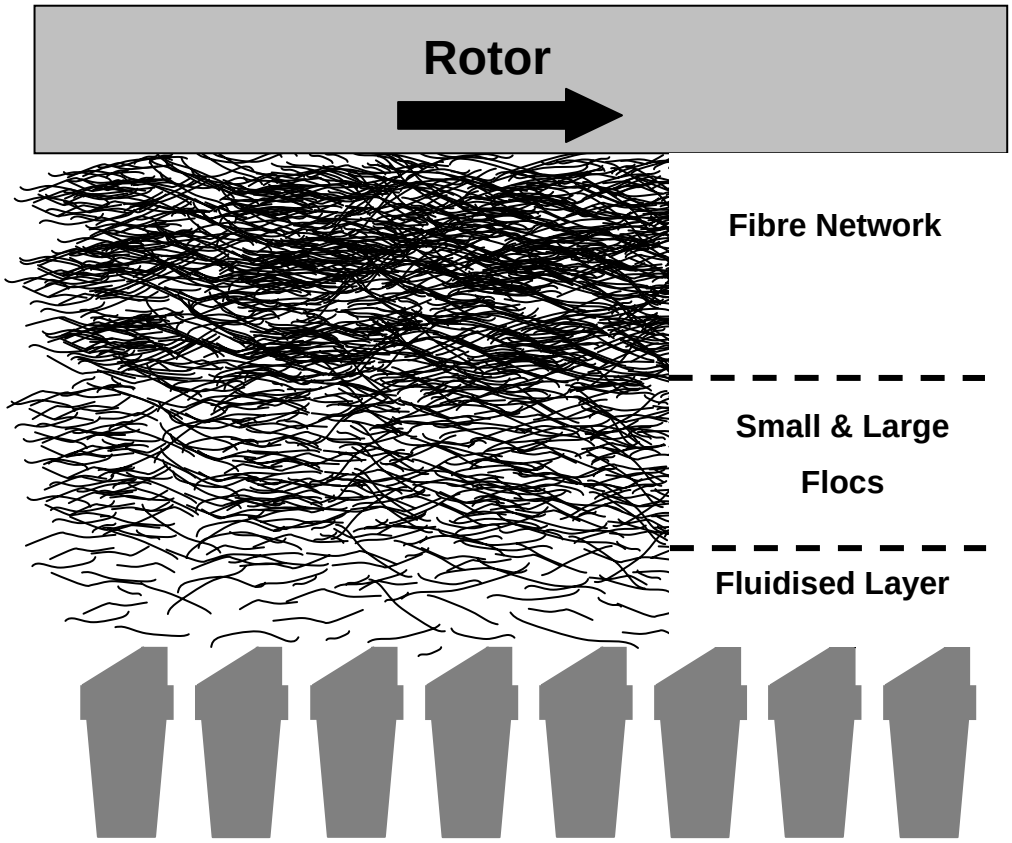

Figure 2-32 Fluidisation layer concept

A recent report into the passage of stickies has demonstrated by direct methods that stickies can, under certain conditions, be extruded through very fine slots (Julien Saint Amand et al., 2005). Numerical modelling involving CFD and Finite Element Analysis (FEA), as well as experimental visual studies, demonstrated that under certain conditions, viscoelastic contaminants or stickies that were larger than the aperture could pass through the aperture via an extrusion mechanism. This extrusion mechanism is illustrated in Figure 2-33 and Figure 2-34. This important finding has implications for the understanding of the passage of pulp. It seems logical that flocs may also be extruded through screen apertures if the conditions are correct. Kerekes (1983a) studied the behaviour of flocs in the entrance to constrictions and found that flocs could elongate without rupturing as they entered the constriction. Yu (1994)

contends that due to the pressure difference between the accept and feed, deformable contaminants cannot be extruded through the screen.

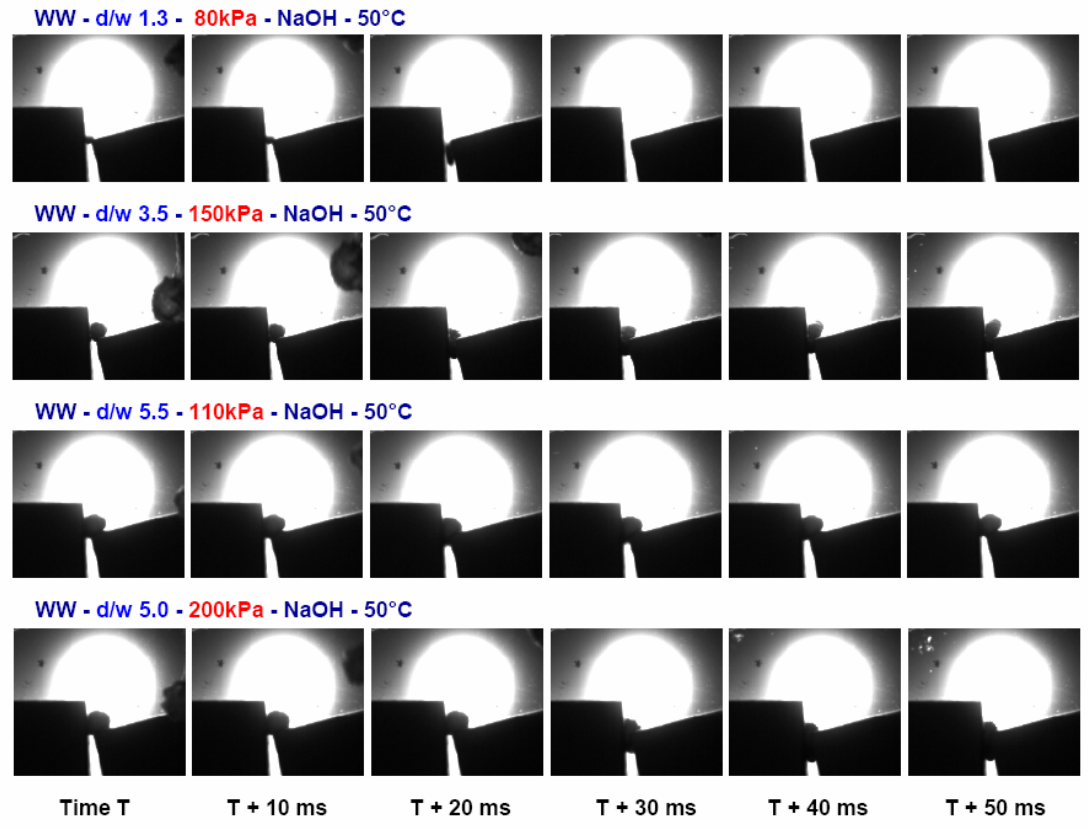

Figure 2-33 Stickie extrusion under various conditions (Julien Saint Amand et al., 2005)

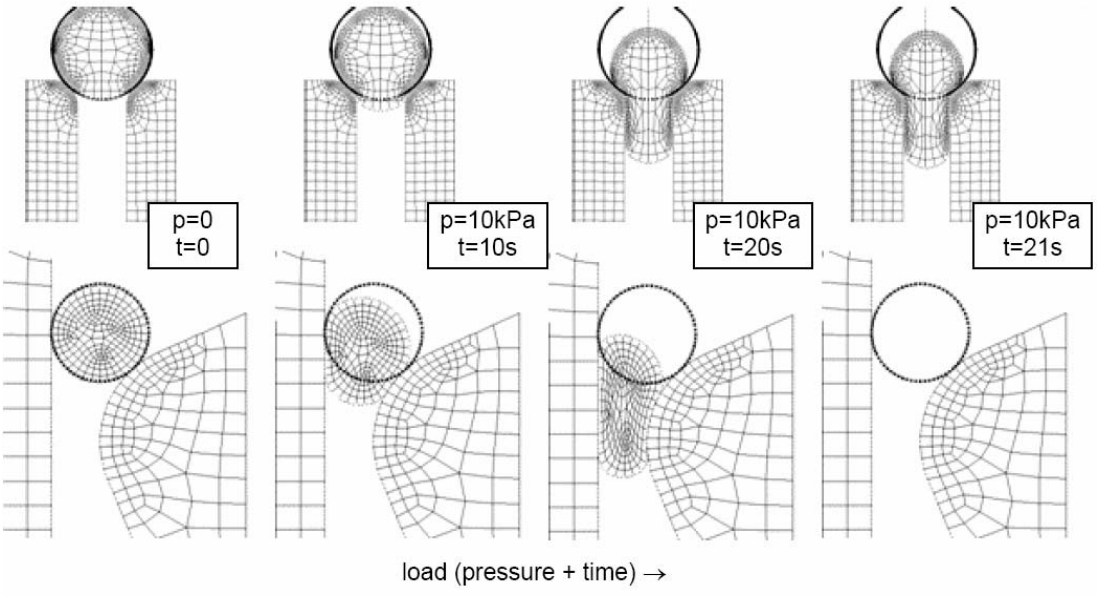

Figure 2-34 Finite element analysis of stickie extrusion through two different profiled apertures (Julien Saint Amand et al., 2005)

2.5.4 Limitations and Critique of the Fibre Alignment Theory

While the fibre alignment theory provides valuable insight into the fundamental behaviour of wood fibre in a flow field as it approaches and interacts with an aperture there are some fundamental problems applying these findings to a real industrial screen under typical operating conditions. The application to practical screening is problematic for several reasons.

The vast majority of the single aperture flow channel studies, by necessity, have been conducted at extremely low consistencies. There are three main reasons for this: a) to avoid plugging or blocking the apertures, b) rheological considerations at elevated consistencies are not a concern, and c) the mechanism of single fibre passage can be studied visually. Even at these very low consistencies fibres do accumulate at the aperture and may block or partially block the aperture and therefore in order to avoid this, the consistency used in the flow channel must be below this critical consistency so as to avoid plugging of the aperture (Atkins, 2003). Ensuring that there is no blocking of the aperture is crucial as there is no means whereby to unblock the apertures during the operation of the channel.

At the low consistency used in flow channel investigations, fibre-fibre interactions are minimal and the rheology of the suspension is essentially the same as water or the suspending fluid. At elevated consistencies, pulp suspensions have a unique rheology and fibre-fibre and fibre-suspension interactions become significant. As has been discussed previously the velocity profile in a pipe can be significantly affected by pulp especially at elevated consistencies. The fibre alignment theory does not consider possible effects on fibre passage due to fibre-fibre interactions or rheological properties that occur at normal screening consistencies.

One benefit from operating at low consistencies is that it enables visualisation studies to be conducted and the interaction of fibre, suspension, and the aperture can be investigated. High speed photography has been utilised to full advantage and a detailed picture exists of how single fibres are accepted or rejected by screen apertures. This visual approach has not been extended to real screens or normal screening consistencies with any degree of success.

"Low consistency" screening in industry is conducted at much higher consistencies than those used in flow channel experiments and as will be shown in the next section on the fibre mat theory fibre – fibre interactions play a more central part in the mechanism of screening. The fibre alignment theory neglects and does not incorporate fibre – fibre interactions in the explanation of screening.

Another limitation of applying findings from fundamental single aperture studies to industrial screens is that by their very nature the flow field in the channel is steady uniform flow. Caution must be taken when relating findings based on flow conditions found in a channel to that of a screen. The flow field in a pressure screen is highly dynamic and unsteady. The pressure pulse of the screen rotor creates this highly complex and unsteady flow field that is affected by variations in pressure and hydraulic resistance caused by the housing and screen plate. Actual flow conditions occurring in a screen have not been sufficiently measured or solved as there are many complicating factors. This has limited the use of CFD in modelling the macro flows within the screen and micro flow fields around individual apertures subjected to a pressure pulse (Grégoire et al., 1998; Schweiss, 2000).

In short, although the fibre alignment theory provides valuable insight into the behaviour of individual fibres in bifurcation flow fields it is an over simplification of the mechanisms that actually occur under typical screening conditions. The actual conditions are much more complex mainly due to fibre – fibre interactions and complex flow fields due to the pulsation of the rotor and unsteady nature of the flows that occur in a real screen.

2.5.5 Fibre Mat Theory

In contrast to the fibre alignment theory the fibre mat theory or fibre accumulation theory attempts to describe screening mechanisms by accounting for the interactions of fibre or flocs with a fibre mat at the surface of the screen. The existence of a fibre mat that forms on the feed side of the screen has been proposed by many researchers (Steenberg, 1953; Cowan, 1969; Beaulieu et al., 1977; Hooper, 1987; 1989; Niinimäki et al., 1996a; 1996b; Repo & Sundholm, 1996; Ämmälä et al., 1999b; Wakelin & Paul, 2001). Concepts of barrier screening were retained by using the explanation of

a fibre mat, which helped account for unanticipated results reported by early researchers. Despite widespread speculation as to the existence of a fibre mat and the appeal to it to explain certain results, very little specific work has been carried out verifying the existence of a fibre mat and any effect on screening and fractionation.

Cowan (1969) proposed that fibres and shives accumulated at the screen surface and this "fibre mat" caused a greater than expected increase in shive removal efficiency as hole size decreased. It was thought that as this large increase in removal efficiency could not be solely due to the reduction in hole diameter and another physical barrier such as a fibre mat or fibre accumulations must be the responsible factor. In contrast, Beaulieu et al. (1977) found no change in shive removal efficiency occurred when hole size was decreased from 2.4 mm to 1.3 mm. They proposed that a region of high debris concentration at the screen surface (or fibre mat) was acting as a barrier to the passage of shives through the screen. This physical barrier did not allow shives to pass but no mention was made of fibre passage being restricted by the fibre mat.

In support of the findings of Cowan, Wakelin & Paul (2001) also found a large increase in shive removal efficiency as hole size decreased and speculated that a fibre mat could be the cause. However they also point out that the same phenomenon could also be explained using the fibre alignment theory as a water annulus or low consistency zone may occur next to the screen similar to that which occurs in pipe flow. They concluded that the mechanisms that actually occur may be a combination of both theories as real screening involves fibre-fibre and fibre-shive interactions.

Norman et al. (1986) carried out a visual study of pulp passage at high consistency in a novel model screen with a plexiglass front. They found that at a feed consistency of 2.2 % of bleached hardwood kraft pulp and low rotational speeds, little fluidisation of the accumulated pulp occurred. The pulse generated by the cleaning pipe was not strong enough to dislodge accumulated fibre from the screen apertures. Fibre flocs plugged the apertures and the screen could not be operated. At higher rotational speeds, small fibre flocs accumulated on the downstream wall of the aperture before the pulse occurred and the aperture was cleared of the accumulated pulp. The pulp was also observed to be well dispersed in the feed annulus. When TMP at 2.9 % was screened the holes completely plugged with large fibre flocs after a very short period

of through flow. These flocs were then broken up and removed by the suction pulse after which the process would begin again with through flow and then plugging. Although the screen used by Norman et al. was a centripetal screen and did not have a conventional rotor (the suction pulse was generated by the reject pipe which rotated around the screen basket) it is probable that a similar process of fibre accumulation will occur in a conventional screen. At low rotor speeds the pulse was not strong or frequent enough to prevent screen blocking and operation was extremely difficult. Fibre and flocs were expected to accumulate to a certain extent and then be cleared by the pressure pulse generated by the rotor. The uniqueness of this particular study is that it was conducted at typical operating consistencies and was a visual study. Unfortunately the actual mechanisms of fibre accumulation and fibre disruption were not examined in detail.

Yu & De Foe (1994) used a flow channel with several typical screen apertures to investigate the formation of a fibre mat. They studied different pulp furnishes, screen apertures, and feed consistencies. As a result of their experimental work they proposed a mechanism of mat formation based on observation. A fibre mat formed at the aperture extremely quickly although a seeding material such as a stapled fibre or contaminant was needed to initiate mat formation. The mat also reached a critical height of between 2 - 3 mm before shear forces broke up the mat and swept it into the main flow. Steenberg (1953) notes that the rate at which the screen will plug is determined by the consistency of pulp in the screen and the flow rate through the aperture. Furthermore the pores between the fibres over the aperture will be large enough for water molecules and perhaps fines to flow through.

Pimley & Rees (1998) suggest a dewatering mechanism over the last 50 % of the screen length. They claim that no fibre and only water passed through the screen over the last half of the screen in their trials. They speculated that a mat must form over the screen which would be at higher consistency than the local annulus consistency and therefore block the passage of fibre over that portion of the screen. This suggests that effective screening only occurred over the first half of the screen and only reject thickening occurred over the remainder.

2.5.6 Limitations and Critique of the Fibre Mat Theory

The fibre mat theory attempts to offer a plausible alternative explanation to the fibre alignment theory by incorporating fibre – fibre interactions. However the explanation of the actual screening mechanisms is not extensive or adequate. Although it has been claimed that the formation of a fibre mat in a screen has been observed, the details of such observations are more often than not vague and not adequately reported or explained.

The claim that the fibre mat will act as a secondary screen surface and that short fibres will still pass through this fibre mat is unlikely. Yu & De Foe (1994) found that the fibre mat to be approximately 2 to 3 mm thick and the crowding number of this mat will be much greater than the average crowding number of the bulk suspension. Fibres will be in such close proximity to each other that it will be impossible for fibres of any length (with perhaps the exception of fines) to make their way through the mat structure and pass through the aperture. The mat is in essence a localised fibre network of high consistency that may cover multiple apertures and even restrict the flow of water through that section of the screen by increasing the localised hydraulic resistance (Gooding, 1996). When reverse flow occurs, during the negative section of the pressure pulse, the fibre mat formed will be disrupted and remixed back into the bulk suspension if the amount and velocity of the reverse flow is sufficient to accomplish the mat disruption.

Although the investigation by Yu & De Foe (1994) provided valuable insight into how a fibre mat may form in a pressure screen, no study has been conducted using an industrial pressure screen. Despite the high probability of a fibre mat forming sometime during the screening phase there remains a number of unanswered questions. Where does the fibre mat form and during which portion of the pressure pulse does it form? The flow conditions are extremely complex and it is reasonable to infer that as the flow through the screen varies, depending on the position of the rotor, a fibre mat would block some portions of the screen, while others would not be blocked. This dynamic formation and disintegration of the fibre mat needs to be investigated more fully and comprehensively and not left up to mere speculation as to its affects on screening and fractionation. Moreover, does a fibre mat form on the

accept side of the screen plate during the reverse pulse? The flow conditions on the accept side, especially directly after the aperture, will be much different than during the screening phase of the pressure pulse. The turbulence will be decaying and as discussed previously decaying turbulence promotes a high level of reflocculation. As the pulp passes through the aperture and moves into this decaying turbulence it will reflocculate and this may retard the reverse passage of the fibre. However the accept side profile may also have an affect on the reverse passage of fibre. Most holed screens have a relieved aperture on the accept side so as to reduce the pressure drop across the screen. This kind of profile may promote reverse passage of fibre and also possible passage of small flocs. James et al. (2003) demonstrated that flocs may rupture in this type of extensional flow. In contrast the accept profile of many fine slots may promote the formation of a fibre mat due to their contour and therefore reduce reverse passage.

There still exists a deficiency in the knowledge. The fibre mat model as it stands at present is really only a qualitative description of a possible screening mechanism whereas the fibre alignment theory attempts rather successfully for a quantitative description of screening mechanisms.

2.6 Modelling Pressure Screens

Modelling various changes that occur during screening is important for the optimal and efficient operation of pressure screens. For example, the accurate prediction of the reject thickening behaviour of a pressure screen is vital in order to operate the screen as close to the optimal reject rate as possible without plugging the screen. Screens should be run as close to the optimum as possible to maximise throughput, efficiency, and energy efficiency. Modelling work has been carried out for predicting reject thickening (Gooding & Kerekes, 1989), contaminant removal efficiencies (Kubát & Steenberg, 1955; Nelson, 1981), and fibre length fractionation (Olson & Kerekes, 1998a; Olson et al., 2000; Olson, 2001a). Most modelling assumes probability screening occurs however some researchers have also combined barrier screening into the models (Gooding & Kerekes, 1989). All models that assume probability screening can be modified to fit barrier screening or the combined barrier

and probability case if the passing probability is set equal to zero or one depending if the particle is oversize or undersize.

2.6.1 Reject Thickening

A number of models have been derived which attempt to relate the reject thickening behaviour of a screen and screening efficiency to the volumetric reject rate and the probability of passage of the various components in the suspension (e.g. pulp fibre, contaminants, stickies, etc). Two ideal flow configurations exist, where the degree of mixing in the screen is considered either perfectly mixed like a well mixed tank (mixed flow) or poorly mixed like a pipe (plug flow) (Levenspiel, 1999). The screening models that are derived based on these two premises and are referred to as the mixed flow and plug flow models respectively. The derivations of the models are presented here as well as a discussion of the application of the models.

Plug Flow

Gooding & Kerekes (1989) derived the plug flow model using a bump rotor and the model assumes: a) passage ratio is constant along the length of the screen and independent of local consistency C_z and local flow rate Q_z, b) there is no axial mixing, and c) mixing is perfect in the radial direction. Consider a fluid element in the annulus with thickness *dz* as in Figure 2-35.

A material balance across the screen can be expressed as Equation 2-34.

$$Q_z C_z = (Q_z - d\,Q_z)(C_z - d\,C_z) + P C_z\, d\,Q_z \qquad \textbf{2-34}$$

Equation 2-34 may be rewritten as Equation 2-35.

$$\frac{d\,C_z}{C_z} = (P - 1)\frac{d\,Q_z}{Q_z} \qquad \textbf{2-35}$$

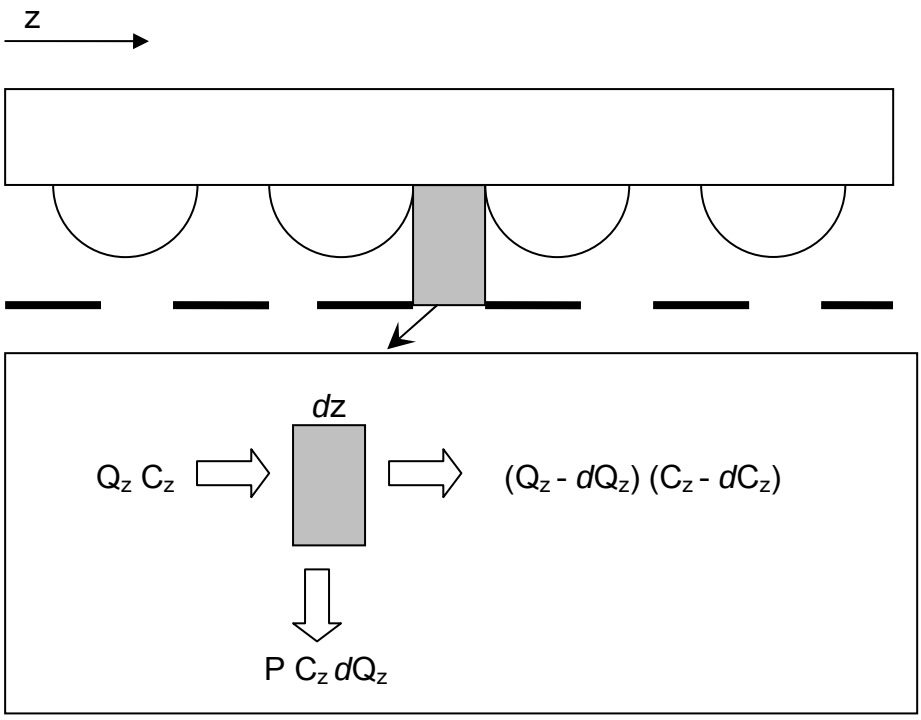

Figure 2-35 Material balance around an infinitesimally narrow fluid element of width *dz* adapted from Gooding & Kerekes (1989)

Passage ratio is assumed to be constant along the length of the screen and independent of C_z and Q_z, therefore Equation 2-35 can be integrated directly to give Equation 2-36.

$$\frac{C_r}{C_f} = \left(\frac{Q_r}{Q_f}\right)^{(P-1)} \qquad \textbf{2-36}$$

Substituting Equations 2-21 and 2-22 for T and R_v respectively into the previous equation gives Equation 2-37.

$$T = R_v^{(P-1)} \qquad \textbf{2-37}$$

Although some of the assumptions of the plug flow model, such as constant passage ratio and accept flow rate, have been questioned (Weeds, 2006) the model has been successfully utilised for long screens. Furthermore, despite the fact that other rotors

create distinctly different mixing conditions than the bump rotor, the plug flow model has been found to predict satisfactory the thickening behaviour of a foil type rotor (Wakelin & Corson, 1997; Olson & Wherrett, 1998; Walmsley & Weeds, 1998; Julien Saint Amand & Perrin, 1999; Walmsley & Weeds, 2004).

Mixed Flow Model

The mixed flow model assumes: a) perfect mixing in the radial and axial directions, b) a well mixed screening zone, and c) the flow field at every aperture is the same. Consider a screen of length L as in Figure 2-36. As the annulus is assumed to be well mixed in both the radial and axial directions the annulus can be considered analogous to a stirred tank. As a result the consistency of the pulp that is fed into the screen annulus will immediately, upon entering the annulus, become C_z. As the annulus is assumed to be well mixed the consistency of the rejects will be equal to C_z.

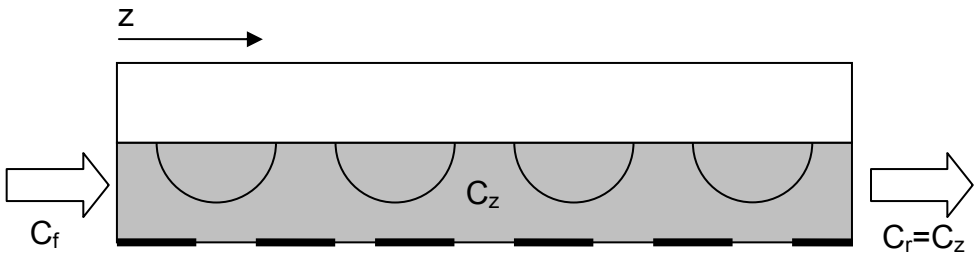

Figure 2-36 Mixed flow model

A material balance for the entire screen length is equal to Equation 2-38.

$$T = \frac{1}{P - R_v P + R_v} = \frac{C_r}{C_f} \qquad \textbf{2-38}$$

Passage is therefore equal to Equation 2-39.

$$P = \frac{C_a}{C_r} \qquad \textbf{2-39}$$

A modified mixed flow model has also been derived where the consistency of the annulus is estimated to be the linear average of the feed and reject consistency. For short screens Weeds (2006) has shown that an accurate method of calculating passage that is independent of R_v is by dividing the accept consistency by the average consistency in the feed annulus (Equation 2-40).

$$P = \frac{C_a}{\frac{C_f + C_r}{2}} = \frac{2C_a}{C_f + C_r} \qquad \textbf{2-40}$$

As the width of the screen approaches zero the average consistency in the feed annulus becomes equal to C_z and therefore the passage ratio is equal to Equation 2-41.

$$P = \frac{C_a}{C_z} \qquad \textbf{2-41}$$

The localised bulk passage ratio is then expressed as Equation 2-42.

$$P_z = \frac{C_{az}}{C_z} \qquad \textbf{2-42}$$

If the passage ratio as defined by Equation 2-41 is substituted into the mass balance equation, the thickening curve for the modified mixed flow model is found (Equation 2-43).

$$T = \frac{2 - P(1 - R_v)}{2R_v - PR_v + P} \qquad \textbf{2-43}$$

For a fraction x (e.g. a fibre length fraction or contaminant fraction) the localised passage ratio of that fraction becomes Equation 2-44 .

$$P_{x.z} = \frac{C_{x.az}}{C_{x.z}} \qquad \textbf{2-44}$$

Equation 2-44 can be used to calculate the localised passage ratio of pulp for a given fibre length at any position along the screen length as long as the localised consistency in the annulus is known.

The mixed flow and modified mixed flow models are useful for analysis of shorter screens whereas the plug flow model is more suited for longer screens.

In summary the reject thickening factor can be predicted using the plug flow, mixed flow, or modified mixed flow models if the passage ratio and volumetric reject rate are known. The predicted thickening curves for these three models are illustrated in Figure 2-37 for a passage ratio of 0.8 and 0.5.

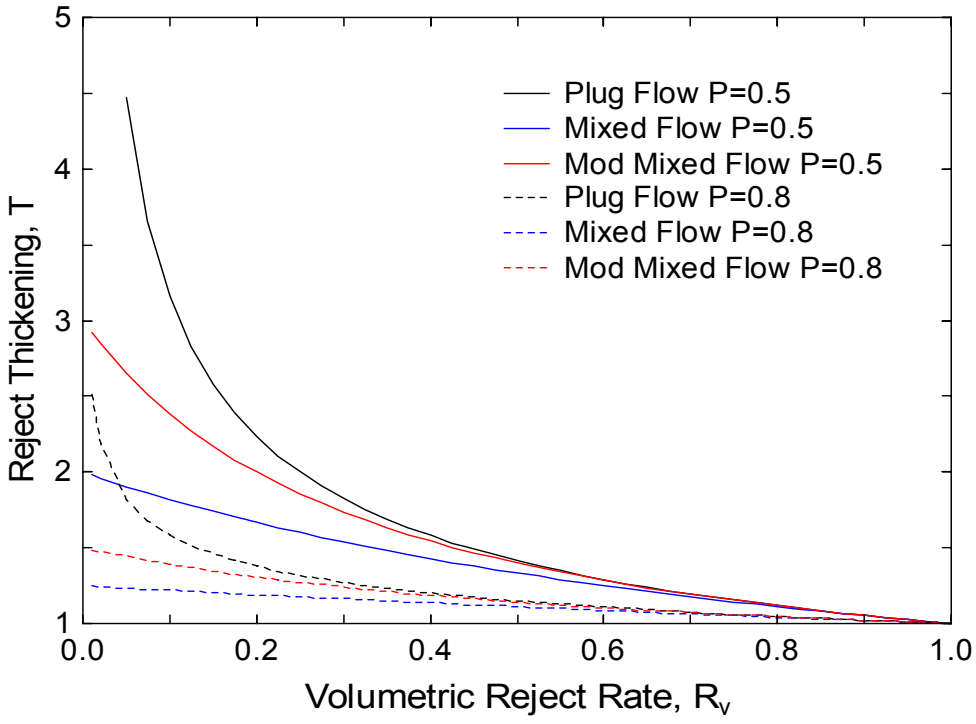

Figure 2-37 Predicted reject thickening as a function of reject rate for several passage ratios

2.6.2 Contaminant Removal

As contaminant removal is a common function of pressure screens it is important to be able to model the removal efficiency in order to run the screen under optimal operating conditions. Moreover, understanding how efficiency changes with alterations in operating conditions is also an important consideration.

Generally, screening efficiency is defined by the debris removal efficiency E_r and is defined in the TAPPI information sheet TIS 0605-04 by Equation 2-45 or alternatively by Equation 2-46 where $C_{x.r}$ and $C_{x.f}$ denote the mass fraction of debris x in the rejects and feed respectively.

$$E_r = \frac{\text{amount of debris removed}}{\text{amount of debris feed}} \times 100\% \qquad \textbf{2-45}$$

$$E_r = \frac{Q_r C_{x.r}}{Q_f C_{x.f}} \qquad \textbf{2-46}$$

Nelson (1981) proposed a different measure of screening performance based on a screening quotient Q as defined in Equation 2-47 or by Equation 2-48. The screening quotient has since found widespread use in the industry. The removal efficiency as a function of mass reject rate for several screening quotients is shown in Figure 2-38. Equation 2-48 can also be derived using the mixed flow model (Gooding & Kerekes, 1989).

$$Q = \frac{E_r - R_m}{E_r(1 - R_m)} \qquad \textbf{2-47}$$

$$E_r = \frac{R_m}{1 - Q + QR_m} \qquad \textbf{2-48}$$

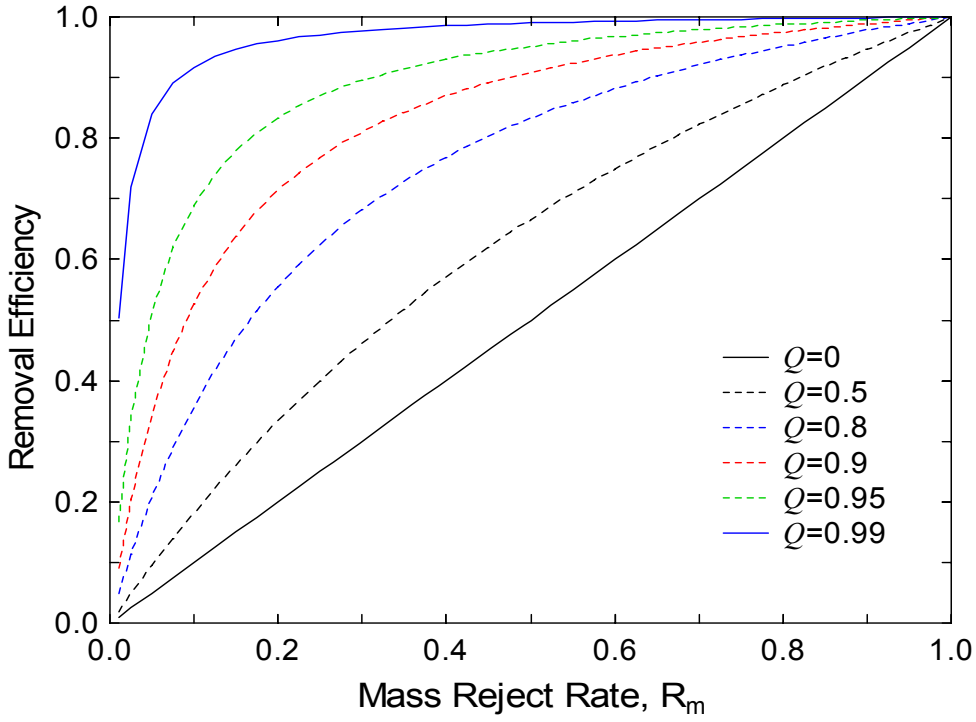

Figure 2-38 Removal efficiency as a function of mass reject rate for several values of the screening quotient *Q*

The screening quotient describes the fraction of debris directed to the accept and reject streams. As Q increases the efficiency increases and when Q is equal to zero the flows are simply split and no separation occurs. Moreover, Q is also convenient to use as it is equal to Equation 2-49 where $C_{x.a}$ is the mass fraction of the debris in the accepts. It has also been shown that Q is related to the passage ratio of pulp and the contaminants P_{con} (Equation 2-50).

$$Q = \frac{C_{x.r} - C_{x.a}}{C_{x.r}} \qquad \textbf{2-49}$$

$$Q = 1 - \frac{P_{con}}{P_p} \qquad \textbf{2-50}$$

Gooding & Kerekes (1989) extended the work of Kubát & Steenberg (1955) and found that the contaminant removal efficiency can be expressed as a function of R_m

and an independent parameter κ with efficiency increasing as κ decreases (Equation 2-51). Similarly, Equation 2-51 can also be derived from the plug flow model (Gooding & Kerekes, 1989).

$$E_r = R_m^{\kappa} \qquad \textbf{2-51}$$

2.6.3 Fractionation

Olson & Wherrett (1998) developed a model of fibre fractionation based on the penetration number of Kumar (1991) as discuss in Section 2.5.2. The findings from single aperture flow channel studies were applied in the derivation of the model and then the model was tested using a laboratory screen section. A linear concentration gradient, proportional to the fibre length, was defined based on the experimental findings of Olson (1996). A fibre was considered to have a passage of one (i.e. the fibre *will* pass through the aperture) if the centre of the fibre originates in the exit layer and a passage of zero if the centre of the fibre originates outside the exit layer. Their analysis found that passage ratio was dependant alone on penetration with two regimes corresponding to the two cases where the exit layer was greater than and less than the height of the concentration gradient. It was argued that the penetration number was a useful parameter in that it combines the crucial screening variables.

It is well established that screens fractionate primarily by fibre length with passage decreasing as fibre length increases. It has been found that passage decreases following a negative exponential curve with increasing fibre length as in Figure 2-39.

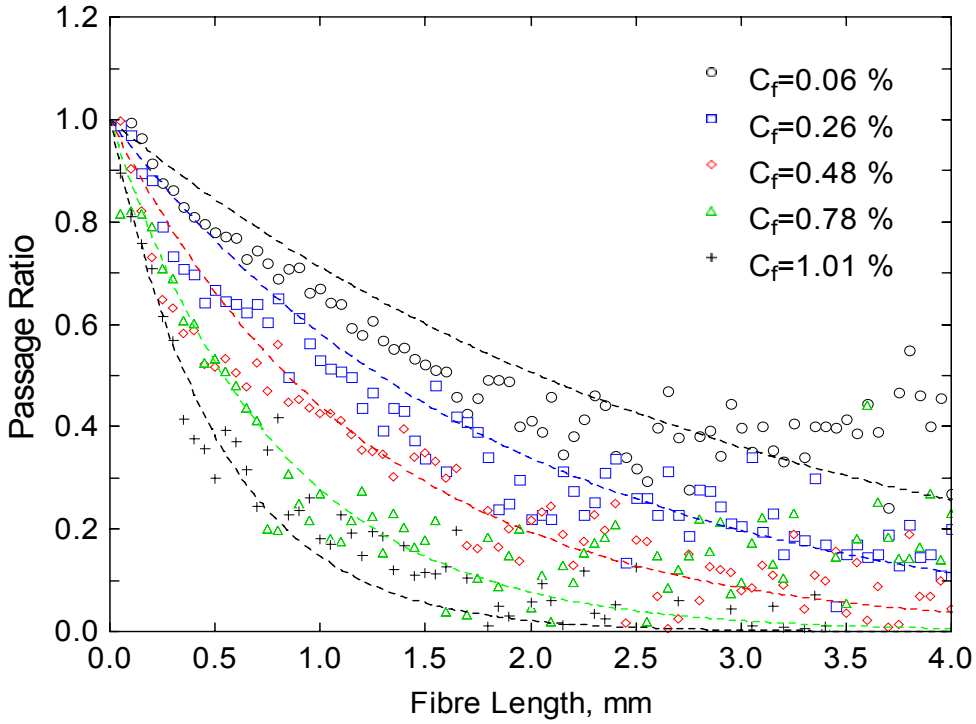

Figure 2-39 Fibre passage as a function of fibre length for several feed consistencies (Weeds, 2006)

This curve has been modelled by Olson et al. (2000) and Olson (2001a) for both smooth holes and slotted screen plates (Equation 2-52). The coefficients β and λ are found by fitting the function to experimentally determined passage versus fibre length data. It has been found that the coefficient β was found to be equal to 1 and 0.5 for holed and slotted screens respectively. The coefficient λ has a physical interpretation being that fibres with a length 0.61λ will have a passage of 0.5. The affect of λ and β on the passage ratio of different fibre lengths is demonstrated in Figure 2-40. The greatest difference between the passage of the short and long fibre fractions occurs when λ is equal to one.

$$P(L_f) = e^{-\left(\frac{L_f}{\lambda}\right)^{\beta}} \qquad \textbf{2-52}$$

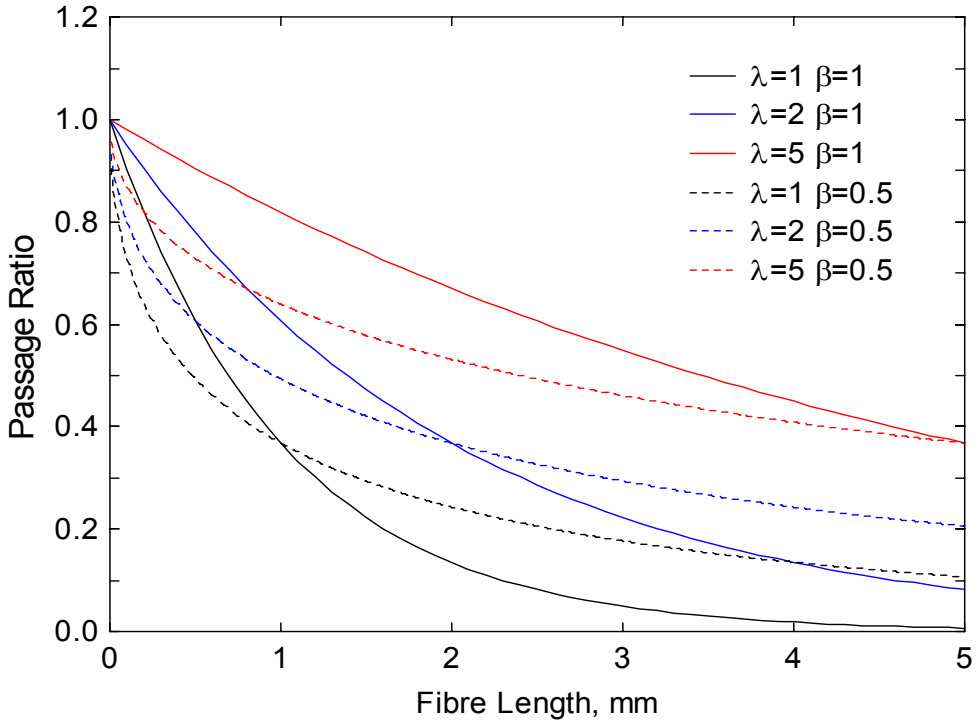

Figure 2-40 Theoretical prediction of passage using Equation 2-52 for a range of λ and β

Weeds (2006) extended this approach and related λ to the fractionation index Φ which in turn is related to the passage of short and long fibre by Equation 2-53.

$$\Phi = R_v^{P_L} - R_v^{P_S} \qquad \textbf{2-53}$$

The fractionation index attempts to incorporate the mass flow of short and long fibre to the accept and reject streams. It aims to penalise the rejection of short fibre to the reject stream and the acceptance of long fibre into the accept stream Olson (2001a). Therefore a "perfect" fractionation device would separate all the short fibre from the long fibre and would have a fractionation index equal to one. The optimum fractionation occurred when λ was between 1 and 2 for all volumetric reject rates. The fractionation index increased considerably in this range for lower reject rates as in Figure 2-41. The fractionation index was also related to reject thickening and it was shown that for a given reject rate there is an optimum fractionation index as illustrated in Figure 2-42.

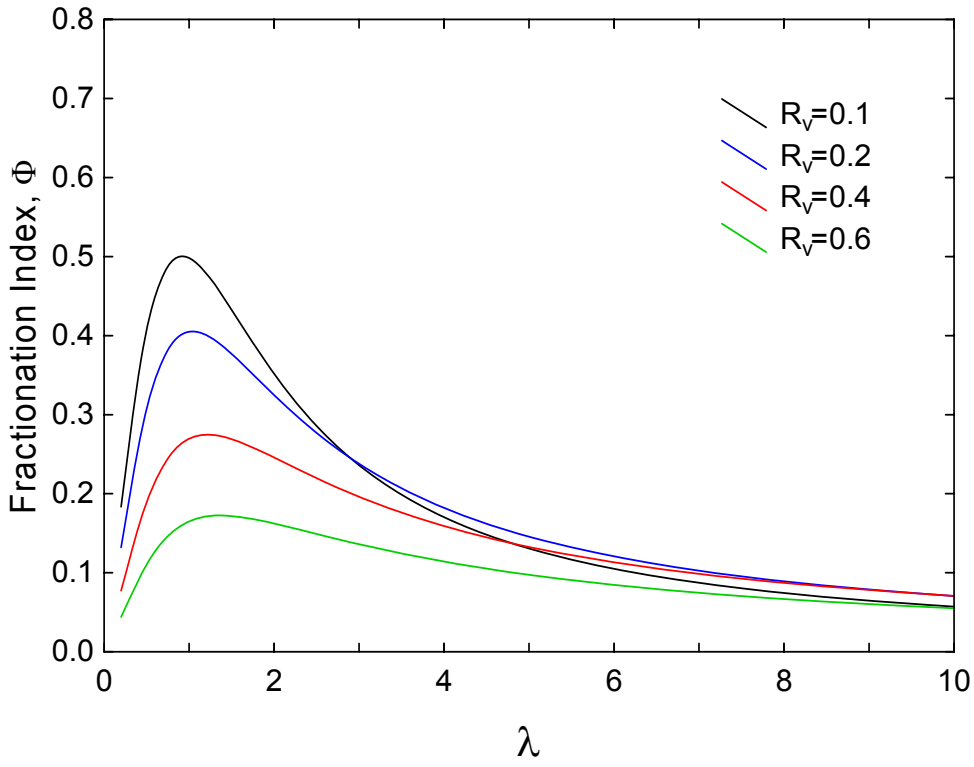

Figure 2-41 Predicted fractionation index Φ as a function of λ at various volumetric reject rates (Weeds, 2006)

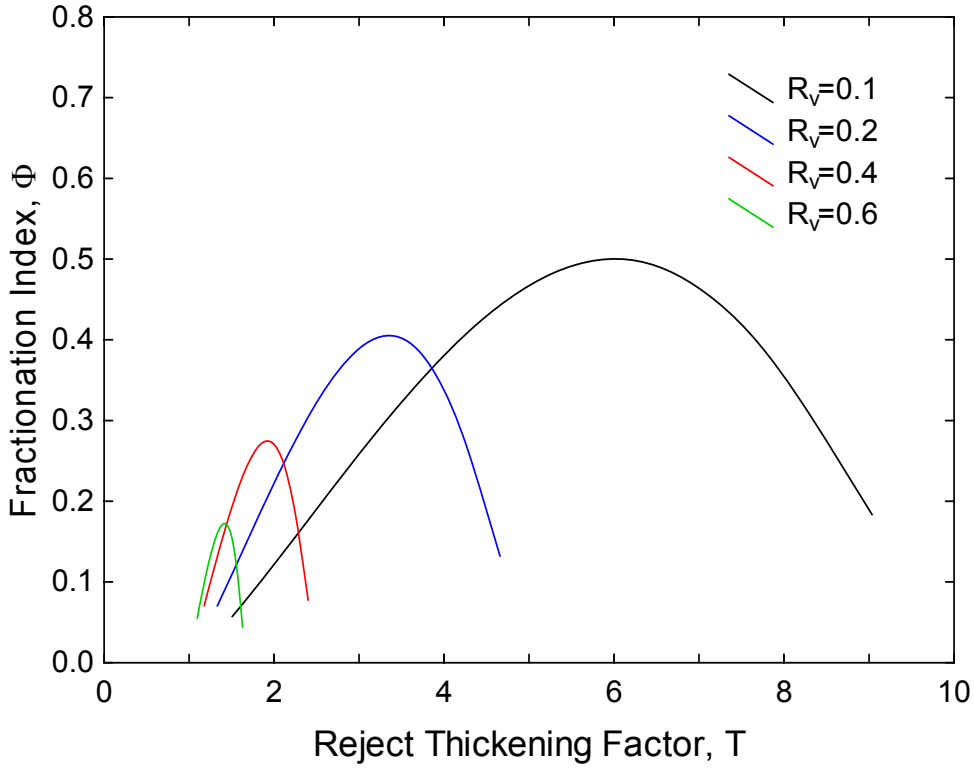

Figure 2-42 Predicted fractionation index Φ as a function of predicted reject thickening factor (Weeds, 2006)

2.6.4 Critique of Screen Modelling

There is increasing evidence that some of the assumptions the screen models are based on are not completely valid and better accounting for the actual mixing and flow conditions that occur in the screen is warranted. It is still unclear which of the plug flow or mixed flow models best represents the internal behaviour of the screen. Reject thickening data is predicted best by the plug flow model whereas contaminant removal data are better predicted by the mixed flow model (Gooding & Kerekes, 1989; Wakelin et al., 1994; Paul, 1999; Olson, 2001a; Weeds, 2006).

Although the models can give satisfactory prediction of screen performance in some situations their general use as predictive design tools is still limited. Ämmälä (1999a) and Niinimäki et al. (1996a; 1996b) sampled pulp internally from a screen and found that pulp consistency and freeness varied considerably in both the axial and radial directions. This suggests that complete radial mixing may not occur especially for open type rotors such as those used by Ämmälä and Niinimäki.

Schweiss (2000) used computational fluid dynamics to model the flow of water through an industrial screen and found considerable flow variations with a concentrically located screen. The flow was then optimised by mounting the screen basket eccentrically within the housing and tapering the accept chamber. Caution must be taken when using results from CFD because usually only water is modelled and the addition of pulp will alter the rheology of the fluid.

Rienecker (1992; 1997) speculates that the relative speed (slip factor) between the rotor and suspension, and the specific throughput of the screen decreases along the screen length, although no experimental data is provided. If this is the case then the local accept flow, passage ratio, and pressure pulse strength are likely to be affected, which in turn will alter the screening conditions and performance of the screen both locally and globally. Some researchers have tacitly acknowledged variations along the screen length by using only small sections of their pressure screen in an attempt to minimise axial variations in flow conditions (Julien Saint Amand & Perrin, 1998).

Application of existing models to new novel screens may also be problematic in that many new screens are relatively short and have novel flow arrangements such as parallel or series configurations. Currently there has been no comparison of the performance of these screens to the predictions made by the screen models.

In reality the plug flow and mixed flow models characterise two extreme mixing conditions in a continuous reactor or separator but it is extremely likely that the actual mixing conditions that occur will lie somewhere in between these two extremes. In order to determine the actual mixing characteristics more work needs to be carried out. The theoretical framework and experimental techniques exist (Levenspiel, 1999) but as yet these have not been applied to pressure screens.

2.7 Internal Variations in the Screen

While the plug and mixed flow models assume constant passage and flow conditions along the screen length, the actual conditions which occur within the screen are difficult to determine. While generalised statements have been made regarding internal variations of a screen very little experimental data has been presented to support these statements.

If a screen of length L is considered there will be changes in numerous factors along the screen length. Generally the consistency, average fibre length and mean tangential velocity will increase with position along the screen length (Rienecker, 1992; 1997; Niinimäki, 1998; Weeds, 2006). If a constant accept flow rate along the screen length is assumed it has been calculated that the axial velocity will decrease linearly (Equation 2-54) where u_{ax} is the axial velocity, $A_{annulus}$ is the area of the annulus, z is the axial position along the screen, and L is the total length of the screen (Gooding, 1986).

$$u_{ax} = \frac{1}{A_{annulus}}\left(Q_f - \frac{z}{L}Q_a\right) \qquad \textbf{2-54}$$

Ämmälä et al. (1999a; 1999b) conducted internal sampling of a screen equipped with a foil rotor. Movable sampling tubes that were both axially and radial mounted were used to sample pulp from within the screen annulus, reject, and feed chambers. They reported a sudden increase in consistency at the front of the screen which then decreased along the screen length as in Figure 2-43. There was also considerable variation of consistency in the radial direction with pulp being more highly concentrated toward the screen surface. They attributed the sudden increase in consistency at the front of the screen to a backflow mechanism as illustrated in Figure 2-44, where fibre is dewatered in the feed chamber and over the very first section of the screen. Although the screen they used was axially fed, they conclude that the trends would be the same for a screen with a tangential feed.

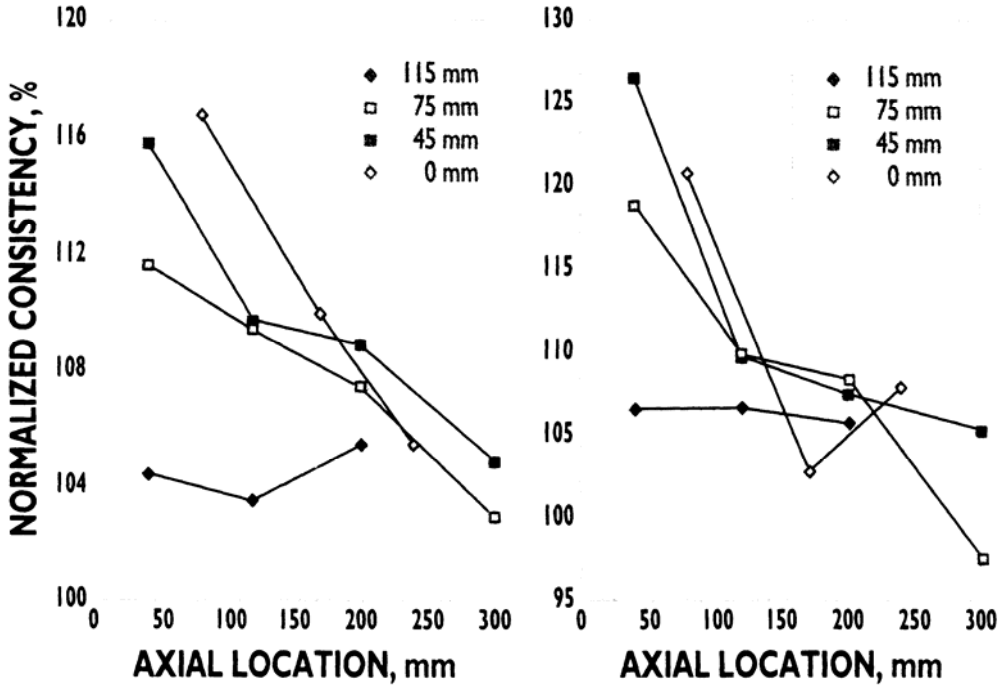

Figure 2-43 Normalised consistency distributions in the screen basket for groundwood pulp (left) and bleached kraft pulp (right) (Ämmälä et al., 1999a)

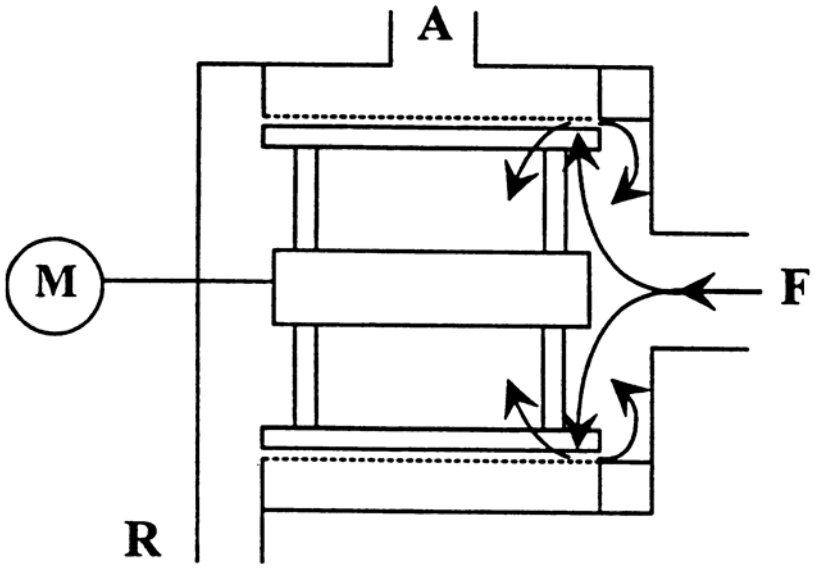

Figure 2-44 Backflow mechanism at the feed end of the screen (Ämmälä et al., 1999b)

Weeds (2006) found that the passage ratio for a narrow section decreased as the section was moved toward the rejects end of a screen as illustrated in Figure 2-45. The change in the passage ratio was greater at lower superficial aperture velocities and he postulated that relative speed between the rotor and suspension as well as a change in pressure pulse magnitude were responsible and had a greater impact at lower aperture velocities.

2.8 Reject Thickening

Recent work has shown that the relationships between reject thickening, fibre passage and feed consistency are more complex than first thought (Weeds, 2006; Walmsley & Weeds, 2007). The effect of feed consistency on reject thickening and fibre passage has been unclear as some researchers have reported that reject thickening was unaffected by changes in feed consistency (Julien Saint Amand & Perrin, 1998; 1999; Paul, 1999; Wakelin & Paul, 2001) while others have reported a direct relationship (Kumar, 1991; Gooding & Kerekes, 1992; Weeds, 2006; Walmsley & Weeds, 2007).

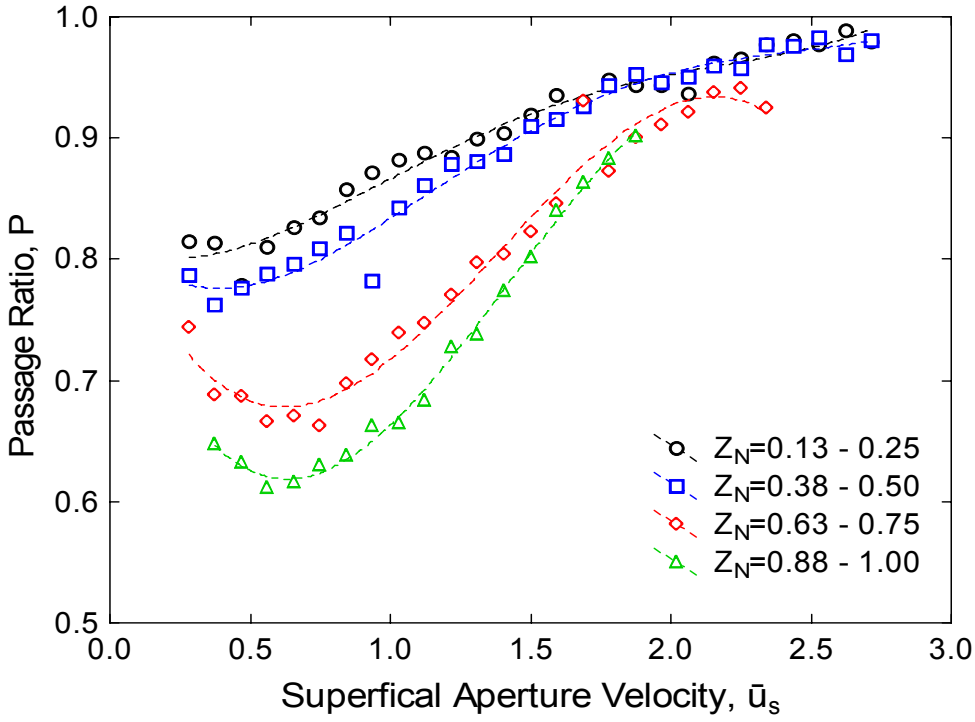

Figure 2-45 Effect of superficial aperture velocity on fibre passage for a narrow screen section at several screen positions Z_N (1 mm holes, bump rotor, R_v=0.2, C_f~0.5 %) (Weeds, 2006)

As illustrated in Figure 2-46 and Figure 2-47 Weeds (2006) has shown that there is a strong relationship between feed consistency, reject thickening, and passage ratio. Several regions exist and rotor type has a strong effect on their correlation. Mechanisms were proposed that explained the different regions and the dependence on rotor type. At low consistencies (region 1) a fibre alignment mechanism is thought to occur with minimal fibre – fibre interactions or very little influence on passage and thickening due to fibre – fibre interactions. Above a critical consistency (region 2) fibre – fibre interactions in the screen annulus become increasingly important and have a detrimental affect on fibre passage in the forward direction. Above a second critical consistency (region 3) fibre – fibre interactions on the accept side adversely affect fibre passage in the reverse direction which leads to an increase in reject thickening. It was postulated that the difference in the thickening and passage ratio behaviour for the two rotors with a feed consistency greater than 1 % was due to the disparity of fibre flux across the screen which was dependant on the forward and reverse passage ratios as well as the value of the back-flush ratio *k* although *k* was estimated solely on the pressure pulse data without consideration of the effect of the forward and reverse loss coefficients.

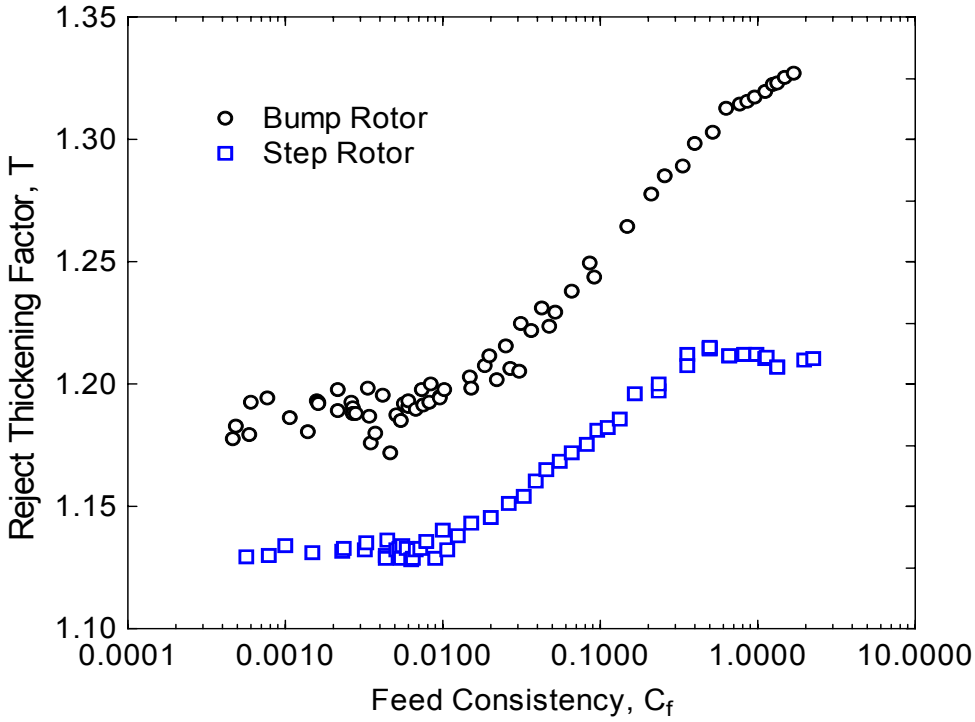

Figure 2-46 Effect of feed consistency on the reject thickening factor for different rotor types in a 55 mm length screen with smooth 1 mm holes ($\bar{u}_s$=0.6 m/s, u_{tip}=22 m/s, step - R_v=0.77, bump - R_v=0.73) (Weeds, 2006)

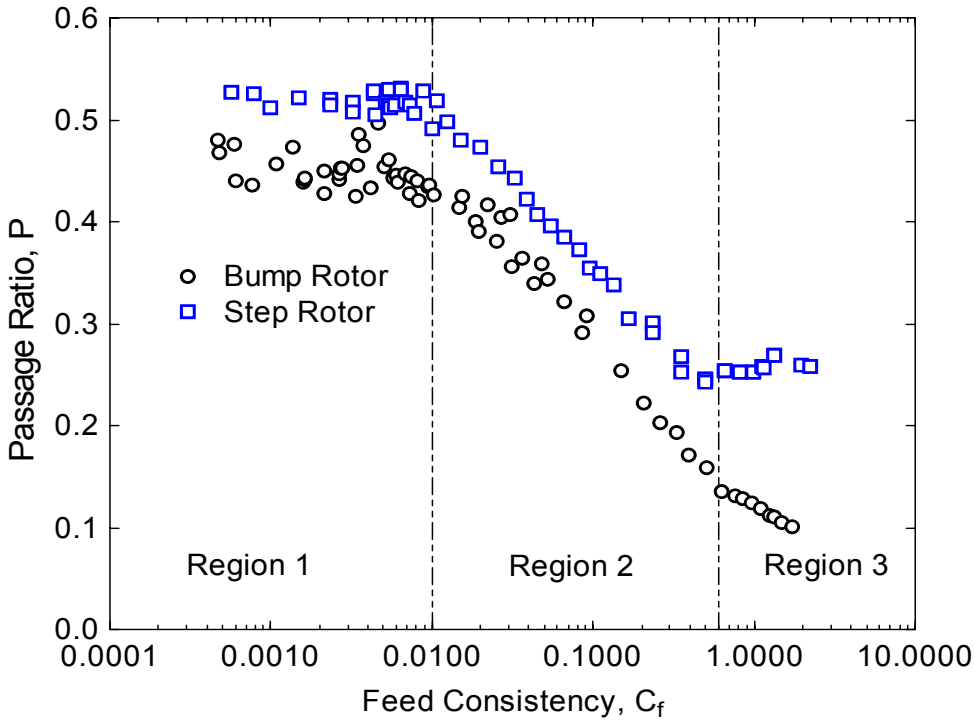

Figure 2-47 Effect of feed consistency on the passage ratio for different rotor types in a 55 mm length screen with smooth 1 mm holes ($\bar{u}_s$=0.6 m/s, u_{tip}=22 m/s, step - R_v=0.77, bump - R_v=0.73) (Weeds, 2006)

Paul (1999) studied the effect of suspension viscosity on reject thickening and found that thickening could almost be eliminated and capacity increased when the viscosity was increased. The fractionation effect was also reduced and it was proposed that the reduction in thickening due to increased viscosity was because of improved flow fields inside the screen, increased fibre passage due to increased drag, decreased flocculation, and a minor contribution from a change in the slip factor.

2.9 Summary

Pressure screening is a complex process which involves a multiplicity of factors that affect the performance of the screen. Pressure pulsations caused by the screen rotor can have a significant affect on the flow field and performance of the screen. There are two broad theories that attempt to explain screening mechanisms that occur during pressure screening, the fibre alignment theory, and the fibre mat theory. Due to the complex nature of the screening process and the interactions of the screen, suspension and rotor there still exists deficiencies in the understanding and explanation of the mechanisms that occur during screening. This is especially true of the internal mechanisms and variations that occur within a pressure screen. It is evident that axial changes in the screen need to be further examined and related to variations in consistency, suspension rheology, and flow and rotor conditions.

3 Equipment and Methods

This chapter describes the details of the pressure screen and other equipment used throughout the course of this research. A detailed explanation and analysis of the internal sampling method is also presented. Furthermore the particulars of the pulps used during the trials are given as well as description of the several experimental procedures used for each experimental programme.

3.1 Experimental Equipment

3.1.1 Beloit MR8 Pressure Screen

A Beloit MR8 pressure screen, as pictured in Figure 3-1, was used for the duration of this investigation. The MR8 is a centrifugal pressure screen which was specifically designed by Beloit for research purposes. As illustrated in Figure 3-1 the screen is mounted horizontally, which is an unconventional configuration for a pressure screen. Usually screens are mounted vertically; however the horizontal configuration has a number of advantages. The system height is reduced and the bearings are protected from water leaking onto them. The Beloit MR (Multi Rotor) range of screens was available in a number of screen diameters and the MR8 is the smallest size available.

The screen basket is located concentrically in the screen housing and has a diameter of 8 inches (203 mm). The screen basket has an axial length of 10 inches (220 mm) which gives an aspect ratio of 1.1. The feed enters a 125 mm feed chamber tangentially via an 80 mm nominal diameter pipe. The accepts exit the screen from the centre of the housing in a vertical and radial direction through a pipe with a nominal diameter of 80 mm. The rejects exit the screen tangentially from the rear of the screen through a 50 mm nominal diameter pipe. There is also an attachment that allows the screen to be axially fed instead of the standard tangential feed and is illustrated in Figure 3-2. A schematic diagram of the entire screening system is shown in Figure 3-3.

Figure 3-1 Beloit MR8 pressure screen – tangential feed

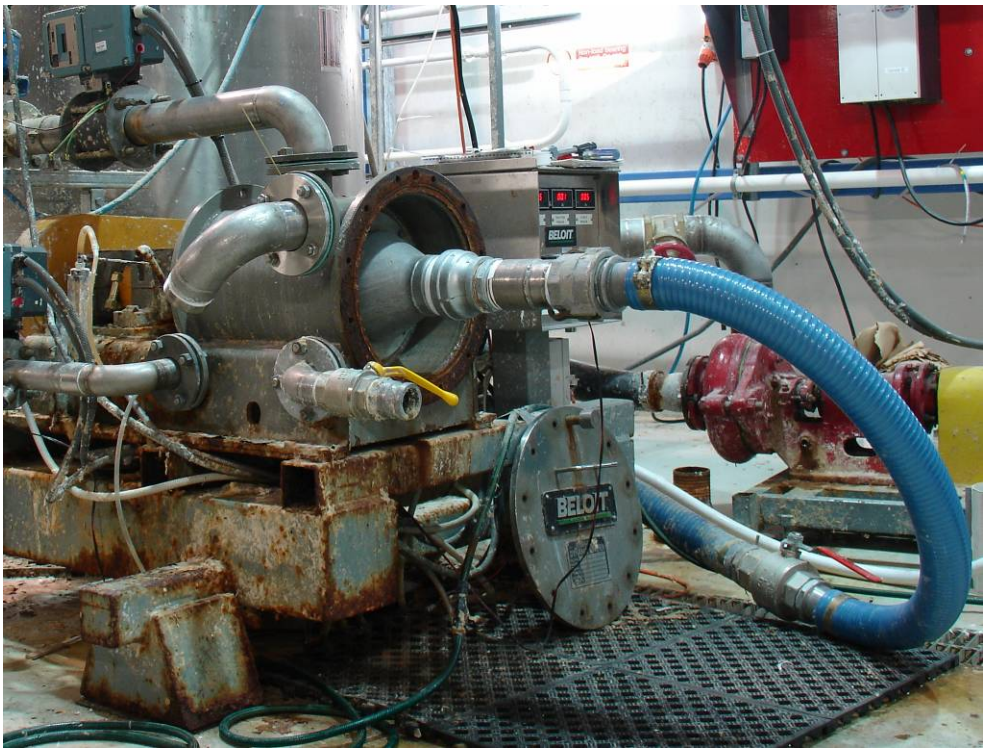

Figure 3-2 Axial feed attachment

A 3 m^3 tank supplies the screen and for most of the trials the accept and reject streams were returned immediately to the tank. The tank is equipped with a top entry stirrer which used a marine impellor to mix the contents of the tank. A suspension of 2 % softwood kraft pulp could be mixed comfortably without using baffles. A 147.5 mm open impellor centrifugal pump (KL-ISO model 80 x 65-160) supplies the screen with stock from the tank. The pump was powered by a 20 kW AC motor which was controlled by a variable speed drive (Model UD31) supplied by PDL Electronics Ltd.

The flow rate of the accept and reject streams was controlled by means of two Neles-Jamesbury electro-pneumatic segment valves, Models R21CA03CCJA/B6/NE7 (80 mm model) & R21CA02CCJA/B6/NE7 (50 mm) respectively. These valves use a pneumatic double acting cylinder actuator to move a V-ported segment ball valve. The position of the valve is set by a 4 – 20 mA electro-positioner which is manually controlled via a remote panel. The flow rate of the accept and reject streams was measured using two, 2 inch magnetic flow meters supplied by the Foxboro Company (Model IMTZO-TC10FGZ). The feed flow rate was calculated from the sum of the accept and the reject flow rates. The static pressure of the feed, accept, and reject lines are measured using WIKA electronic pressure transducers (Model 891.13.520) which have an operating range of 0 to 400 kPa.

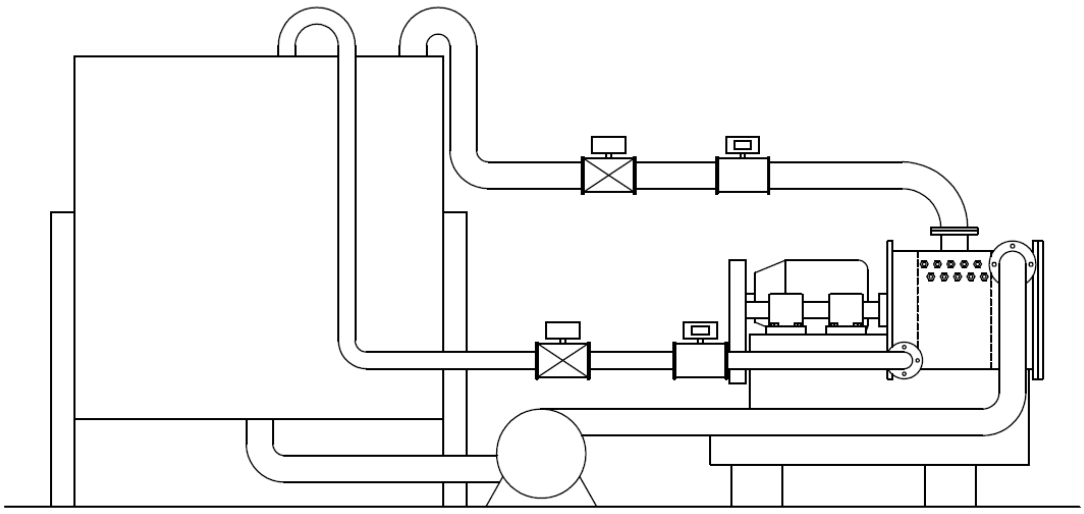

Figure 3-3 Schematic of the entire screening system

Screen Rotors

Four different screen rotors were used during this investigation. Three of the rotors were solid-core or closed rotors, namely the Beloit S-rotor (hereafter referred to as the step rotor), a bump rotor and a locally manufactured smooth rotor. An open type foil rotor was used during some of the trials. The properties of the three rotors are summarised in Table 3-1.

Table 3-1 Rotor properties

	Step	Bump	Smooth	Foil
Pulse Frequency	Low	High	-	Low
Pulse Intensity	Med – High	Low	-	High
Rotor Type	Closed	Closed	Closed	Open
Clearance	12.5 mm	6 mm	16.5 mm	3 mm

The step rotor is considered a low frequency, high pulsation rotor and was designed for use in high consistency screening applications. The face of the step is 20 mm and has a rotor tip to screen clearance of 12.5 mm. The step rotor is pictured in Figure 3-4.

The bump rotor is considered as a high frequency low pulsation rotor and was designed for fractionation applications. The bump rotor has 12 mm high hemispherical lobes positioned radially around a solid core as pictured in Figure 3-5. There is a rotor tip to screen clearance of 6 mm.

The foil rotor has two hydrofoils located directly opposite each other and run the length of the screen. The foil rotor employed here can be considered as a low frequency, high but brief pulsation rotor. Foil rotors are used in numerous screening applications; especially in contaminant removal applications and when using fine slotted screen baskets. The foils are 38 mm long and 10 mm thick and there is a rotor tip to screen clearance of 3 mm.

Figure 3-4 Step rotor

Figure 3-5 Bump rotor

Figure 3-6 Foil rotor

A smooth rotor was specifically manufactured for use in fundamental studies such as the pressure loss measurement in the forward and reverse directions through the screen. No pulsations occur due to the absence of any rotor elements or perturbations on the rotor. A "steady flow" in the annulus is obtained by using the smooth rotor. The annular gap when using this rotor is 16.5 mm. The smooth rotor is illustrated in Figure 3-7.

Figure 3-7 Smooth rotor

Screen Baskets

The screen was equipped with a 1 mm holed screen basket. The holes were smooth and recessed on the accept side of the screen as shown in Figure 3-8. This basket is made from 316s stainless steel and had an inside diameter of 8 inches (203 mm) and a length of 10 inches (220 mm). The holes were set in a 3 mm triangular pitch pattern and had an open area of 13.1 %. The dimensions of the apertures and the aperture pitch pattern are illustrated in Figure 3-8. The screen basket is pictured in Figure 3-9.

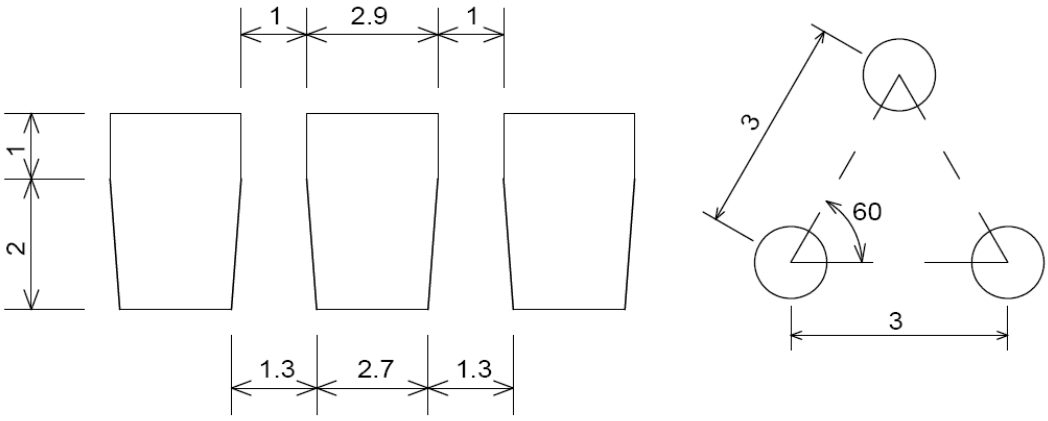

Figure 3-8 Dimensions of the screen apertures and aperture pitch (all dimensions in mm)

Figure 3-9 The 1 mm holed screen basket

3.1.2 High Speed Pressure Transducers

The pressure pulse of various rotors was measured using two high frequency, sub miniature, model S type, flush diaphragm pressure transducers supplied by Sensotec Ltd. The pressure range was from 0 – 690 kPa and the diameter of the sensor face was 7.6 mm. An inline amplifier (model UV) was also used to amplify the signal from the transducer before the data logger. The transducers were mounted so that the face of the transducers was flush with the screen surface.

3.2 Internal Sampling Method

Localised consistency of the feed annulus and accept chamber was measured using a radial sampling method as illustrated in Figure 3-10. Localised consistency of the feed annulus was measured by sampling pulp in the annulus using 8 mm nominal diameter tubes as shown in Figure 3-11. The screen basket was modified so that the sampling tubes could be mounted radially and set flush with the feed side of the screen surface as shown in Figure 3-12. A total of ten positions spaced at 20 mm intervals along the axial length of the screen were sampled. This allowed a detailed consistency profile in the feed annulus to be measured. A sample was taken by simply fully opening the ball valve at the end of the sampling tube and allowing the suspension to flow out into the sampling container. No sampling pump was needed or used as the pressure in the screen is greater than the atmosphere.

Niinimäki (1996b) used a similar method to measure internal consistency however only one axial position at the centre of the screen was measured. Ämmälä et al. (1999a; 1999b) and Weeds (2006) used both radially mounted tubes as well as an axial method of sampling to measure localised consistency. Weeds found a significant difference in measured consistency between the two methods, however a comprehensive comparison was outside the scope of that study. In order to validate the radial sampling method used in this study a comparison of the two methods was conducted and the results are presented in Section 3.3.4.

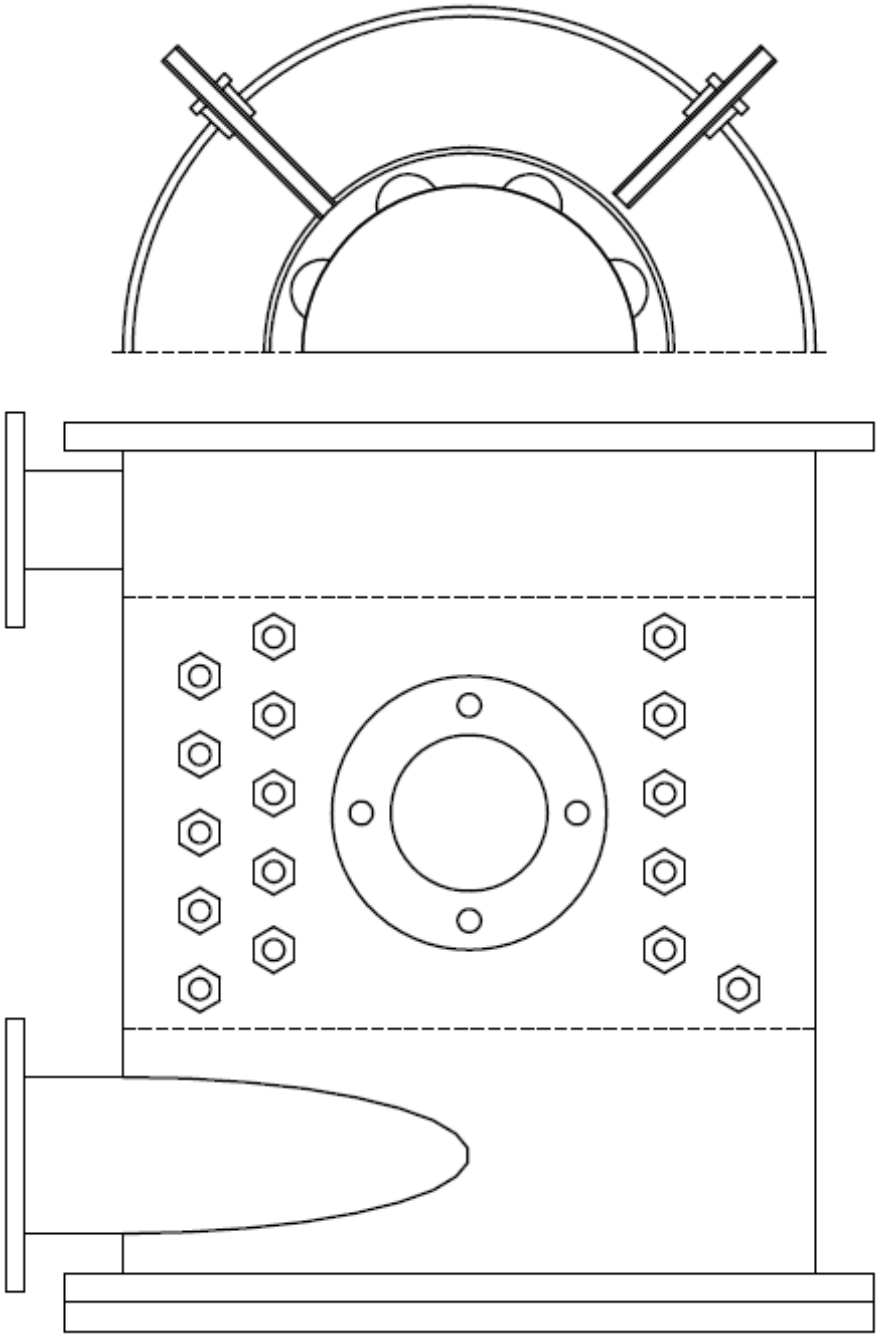

Figure 3-10 Schematic illustrating radial sampling method of the feed annulus and accept chamber

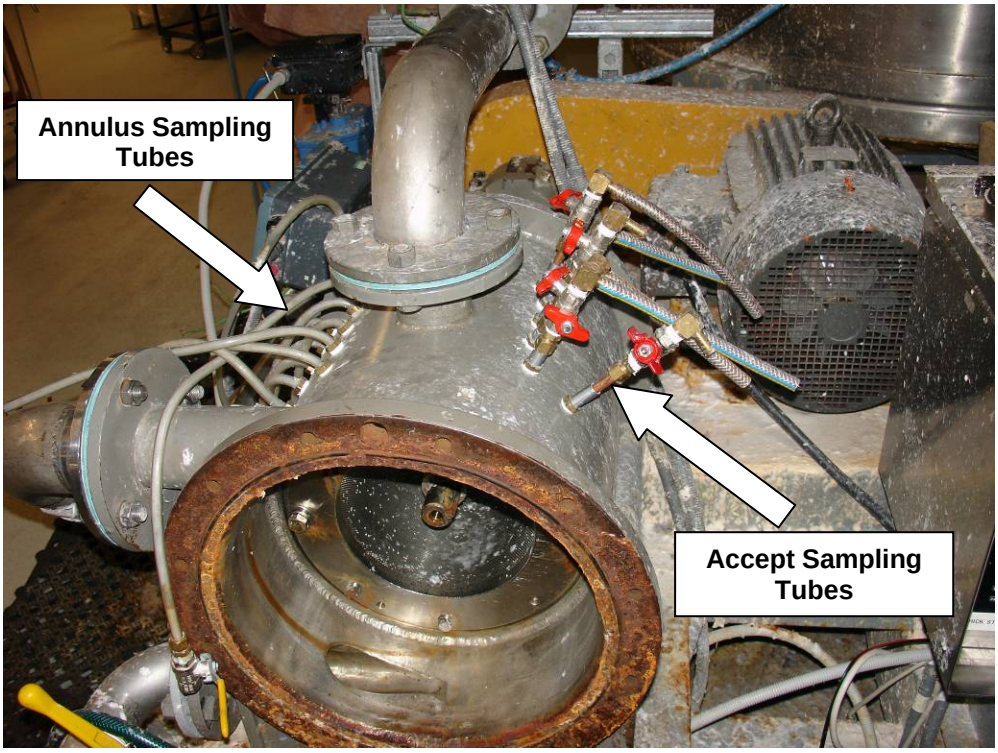

Figure 3-11 Picture of sampling method for the annulus and accept chamber

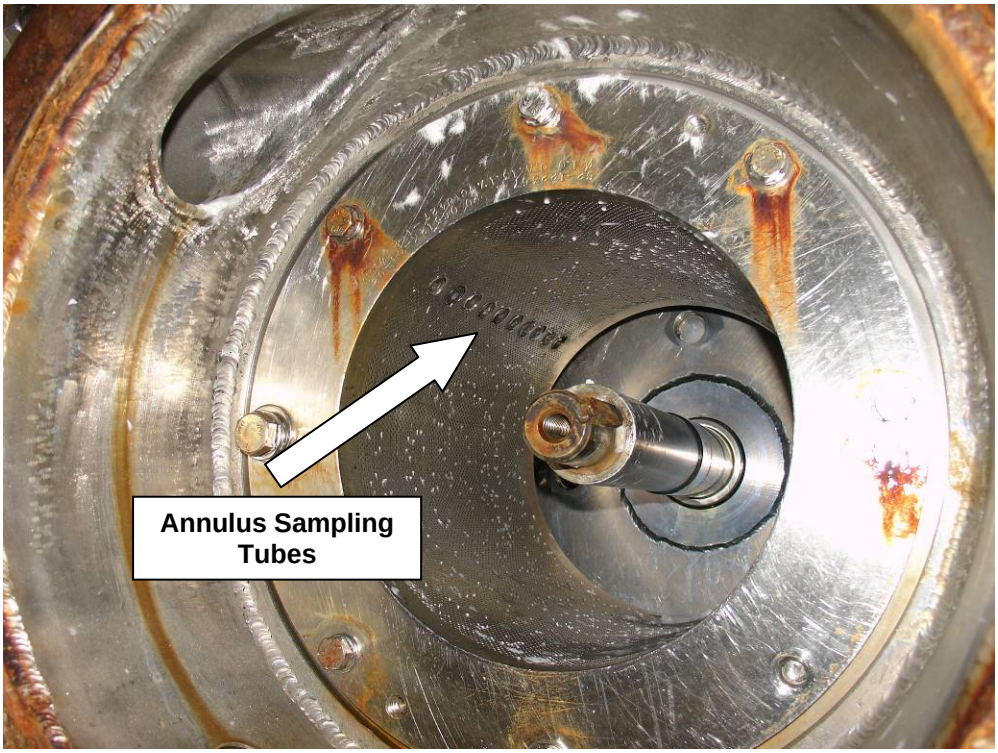

Figure 3-12 Annulus sampling tubes mounted flush with the inside surface of the screen

The localised consistency of the accept chamber was measured by sampling pulp approximately 5 mm from the accept side of the screen surface using 8 mm nominal diameter tubes as shown in Figure 3-13. These tubes were also mounted radially and a total of six positions, located at 20, 40, 80, 120, 160 and 180 mm along the axial length of the screen, were sampled.

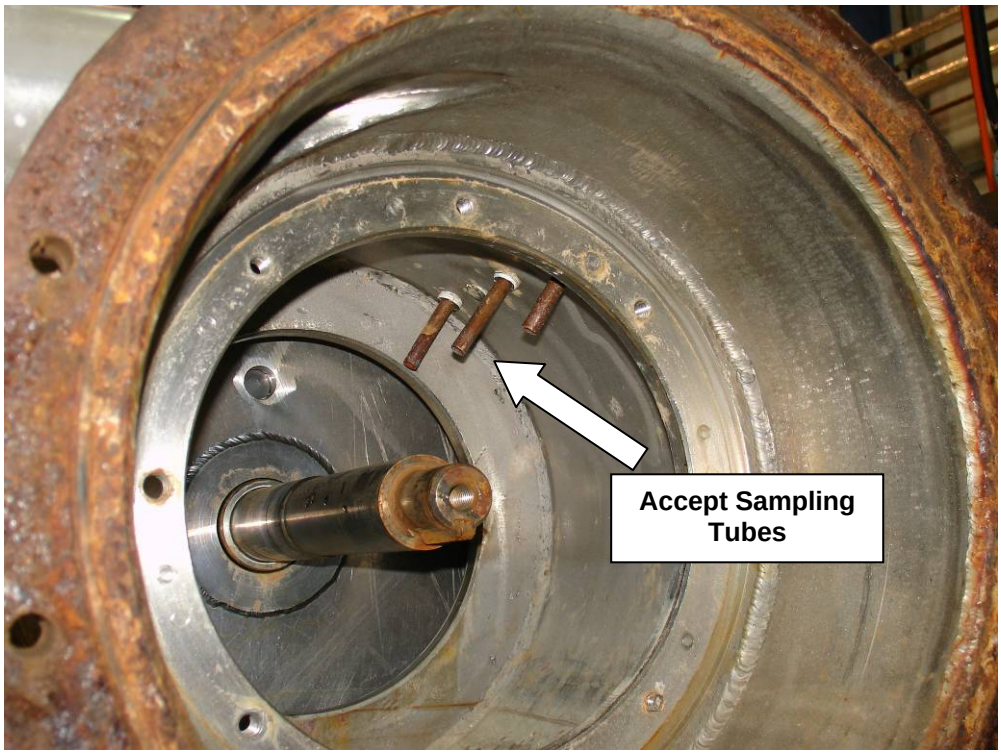

Figure 3-13 Accept sampling tubes (only 3 of 6 shown)

3.3 Experimental Procedure & Analysis

3.3.1 Pulps

A bleached and unbleached *Pinus Radiata* kraft pulp was used during this research. The market pulp was supplied in lap sheets from Carter Holt Harvey Kinleith Mill. The lap sheets were re-pulped by softening the sheets in water and afterwards torn into pieces about 50 mm x 50 mm and then added to the tank and pumped around the system in order to completely disintegrate the sheets. The two pulps had very similar properties however there was a slight difference in the average fibre length. A bleached Eucalypt kraft pulp was used in the internal sampling method validation trials. The properties of the pulps are summarised in Table 3-2.

Table 3-2 Pulp properties

	Bleached Pine	Unbleached Pine	Eucalypt
Arithmetic Fibre Length Average (mm)	1.13	1.08	0.66
Length-Weighted Fibre Length Average (mm)	2.31	2.44	1.11
Coarseness (mg/m)	0.249	0.253	0.080

3.3.2 Consistency Measurement

Pulp consistency was calculated throughout this study using Equation 3-1 where M_d is the mass of the oven dry pulp and M_w is the mass of the wet pulp sample. The Tappi standard for consistency measurement (T 240 om-88) was followed throughout this study where possible. The consistency was calculated to three decimal places, averaged, and reported to two decimal places. The average of two samples was used to determine the consistency, value although at low consistencies (< 0.001 %) the average of three samples was used. Each pulp sample was weighed and then filtered on a tared filter paper using a Buchner vacuum. These samples were dried for at least 24 hours in a forced-draught oven before the dried mass of pulp was determined.

$$C = \frac{M_d}{M_w} \times 100 \qquad \textbf{3-1}$$

The feed consistency was calculated indirectly from the mass balance of the bulk flow through the screen as in Equation 3-2. This approach was used to eliminate any mass balance error. The mass balance error has been previously checked for this equipment and found that mass balance errors were less than 2 % (Weeds, 1998; Paul, 1999; Atkins, 2003; Weeds, 2006). The feed flow rate was calculated as the sum of the accept and reject flow rate as only two flow meters were used.

$$C_f = \frac{Q_a C_a + Q_r C_r}{Q_a + Q_r} \qquad \textbf{3-2}$$

3.3.3 Axial Sampling Studies

Axial sampling was conducted for the 1 mm holed screen basket. The storage tank was filled with water and then enough fibre was added to give the desired consistency. Only bleached kraft pulp was used during the axial consistency trials. The volumetric accept and reject flow rate was set to give the appropriate aperture velocity and volumetric reject rate. The rotor speed was set to the desired tip speed. Once the screen had been running under steady conditions for over 2 minutes, two, 2 litre samples were taken of the accept and reject streams and the consistency of the samples determined. A single 2 litre sample was taken at each feed annulus and accept chamber axial sampling point and the consistency determined. This localised consistency was normalised by the feed consistency and plotted on a log axis against normalised screen length Z_N. The normalised screen length (Equation 3-3) where L_z is the axial position of the sampling point and L is the total length of the screen. This allows consistency profiles measured at different feed consistencies and screen lengths to be compared.

$$Z_N = \frac{L_z}{L} \qquad \textbf{3-3}$$

As discussed in the previous chapter, a complex relationship exists between fibre passage ratio and consistency. A consistency in Region 2 was chosen for the first set of experiments ($C_f \approx 0.15$ %) and axial consistency was measured at a number of different reject rates varying from 0.1 to 0.6 at two aperture velocities, 0.3 and 0.6 m/s. The trials were then repeated using the different rotors at similar operating conditions. In some cases the rotor speed was altered to determine the effect on axial consistency. Axial consistency profiles were also measured for a feed consistency in Region 3 ($C_f \approx 1$ %) with operating parameters set to match those used for trials in Region 2.

For selected conditions, an additional 2 litre sample was taken from the accept and reject streams and each axial sampling point for fibre length analysis using the Kajaani FS-200. The fibre length distribution data was then used to calculate the fibre concentration for each length fraction expressed as the number of fibres per unit volume of suspension. This fibre concentration was then used to calculate parameters such as local fibre length passage ratio, fibre length passage coefficient λ, and separation ratio.

3.3.4 Method Validation

As discussed previously, several authors have employed internal sampling methods in order to measure localised consistency inside various screens (Niinimäki et al., 1996b; Ämmälä et al., 1999a; 1999b; Weeds, 2006). Weeds found that under similar conditions the axially and radially mounted tube methods of sampling yielded quite different measurements as shown in Figure 3-14. As a large portion of this research involved internal sampling a preliminary study was conducted in order to verify which method was suitable. Moreover, comparisons of the measured localised consistency with the predicted consistency from various flow models was unfeasible, as the assumptions of these models are known to be inadequate for internal thickening predictions (Weeds, 2006).

The screen was operated at a moderate rotor speed and fed with bleached kraft eucalyptus pulp in order to minimise any adverse affect from softwood pulp. The accept valve was shut to ensure no accept flow and to eliminate reject thickening. In this case the screen acts as a pump and no consistency change should occur and the internal consistency should equal the feed for the entire length of the screen. The internal consistency was measured at various positions along the screen length using both sampling methods. The axial tube is fixed in place along the screen basket, as shown in Figure 3-15, and is drawn out a set distance along the screen, a sample taken and then this process is repeated along the entire screen length. The measured consistency was then normalised by the feed consistency and results are shown in Figure 3-16 for the step rotor.

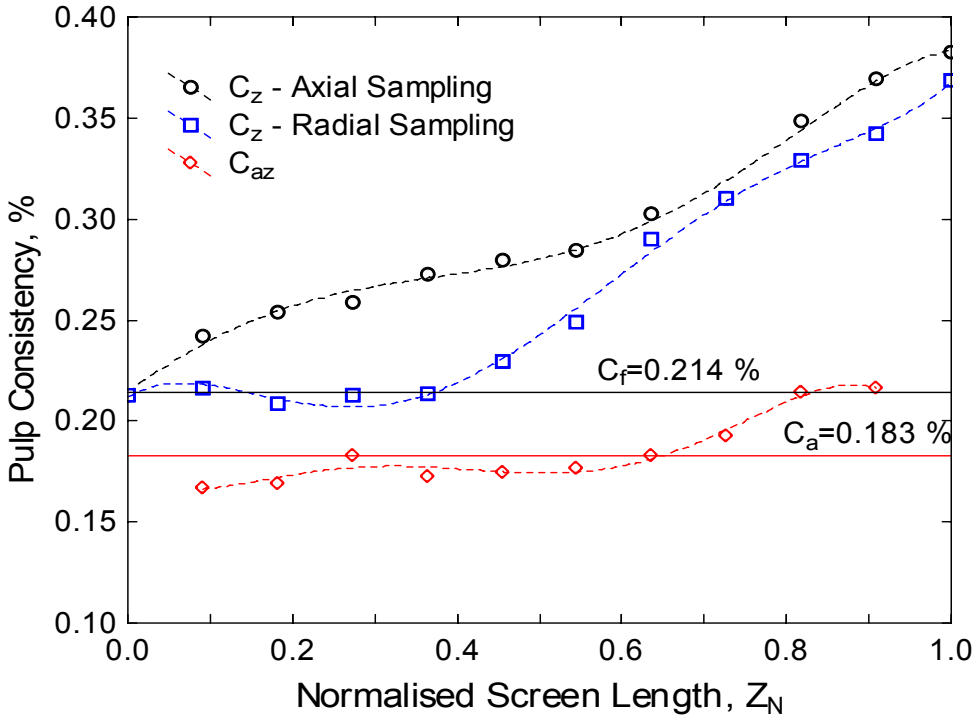

Figure 3-14 Internal consistency variations using two methods of internal sampling (Weeds, 2006)

Figure 3-15 Axial sampling tube

With both sampling methods there was a substantial difference from what was expected. The radial method yielded values lower than unity while the axial method gave values greater than unity. After the experiment it was observed that the end of the radial tubes where not exactly flush with the screen and extended in the annulus slightly which may have influenced the results slightly. The radial tubes were set flush for the next trials. Also it was thought that although there was no accept flow there is likely to be forward and reverse flow through the screen due to the rotor which may have changed the consistency in the screen annulus.

In order to understand these affects better and confirm which method is most reliable the entire screen was blanked off using "duct" tape and thin stainless steel sheet secured in place with straps. This is the same method used for blanking off portions of the screen when studying narrow screen sections and would completely eliminate any possibility of internal secondary flows that could influence the consistency measurement. The experiment was then repeated under the same conditions and the results from this modified test are shown in Figure 3-17. The measured consistency was much closer to unity for the radial method for both the step and the bump rotor. The axial method however still produced consistency measurements 10 % above unity for most of the screen.

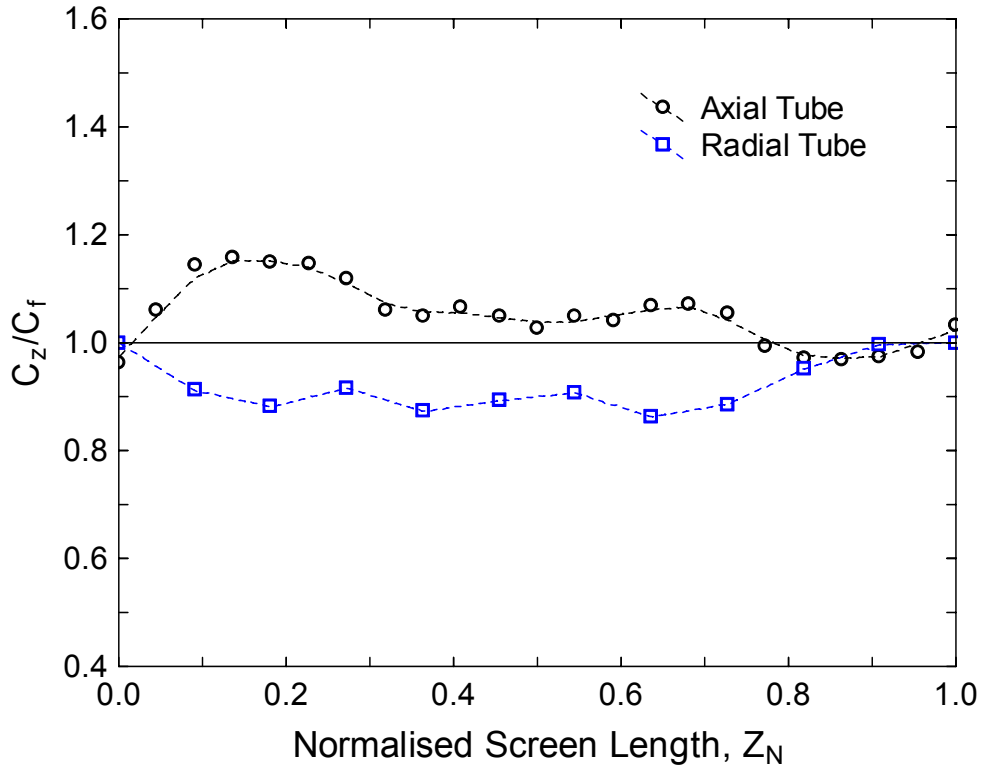

Figure 3-16 Effect of sampling method for the step rotor (C_f=0.041 %, Q_f=640 L/min, u_{tip}=17 m/s)

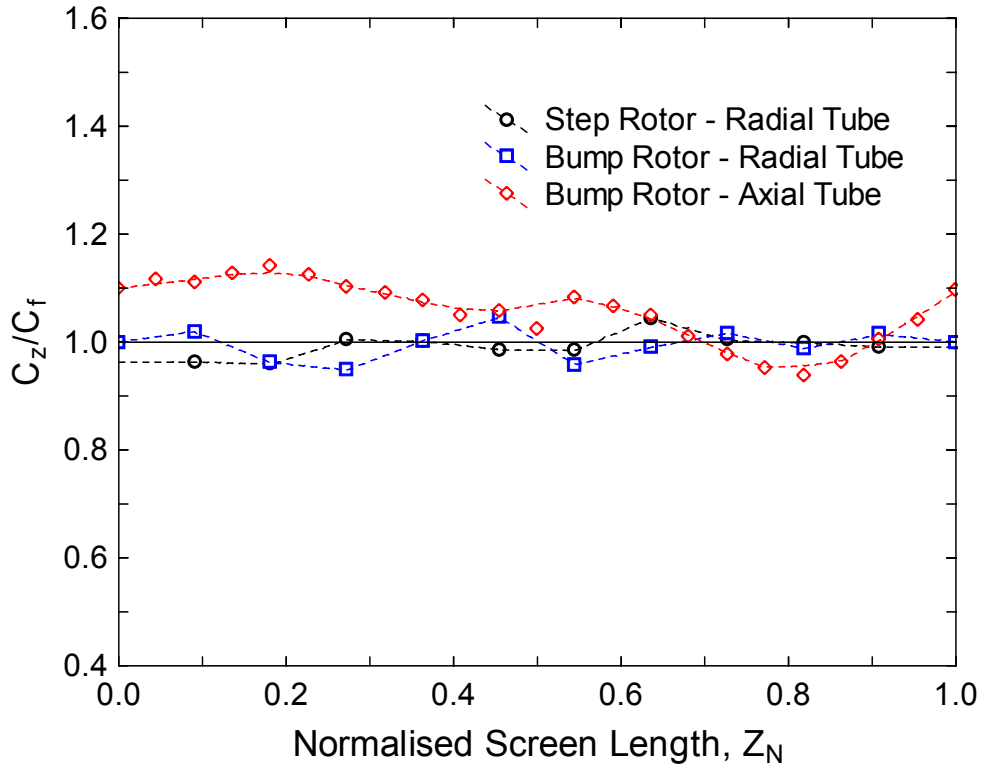

Figure 3-17 Effect of blanked screen and sampling method for the two rotors (C_f=0.041 %, Q_f=640 L/min, u_{tip}=17 m/s)

It was suspected with the axial method that the presence of the axial tube affected the consistency and the flow in the annulus by acting as a "turbulence bar" which would aid in disrupting the flocs in the suspension. The turbulence bars were also found to significantly alter the thickening behaviour of the screen for tangential aligned slots (unpublished results).

In order to understand the affect of a turbulence bar further the screen was arranged so there was some accept flow (R_v=0.16) and internal consistency experiments were done with the axial method and the radial method while the axial tube was present for both, and again with the radial method with the axial tube removed. The consistency profiles obtained for all three cases are shown in Figure 3-18.

Similar profiles were obtained for both the axial and radial methods when the axial tube was present and the profile altered significantly when the axial tube was removed. The change was even more pronounced over the first portion of the screen which gives support to the hypothesis that the axial tube interferes with the flow by acting as a turbulence generator. The actual mechanism that is occurring to yield an increase in the measured consistency is uncertain and this is an area for future investigation. This effect of an axial sampling tube is likely to be more significant when using a closed rotor such as this, compared to an open rotor case such as the one conducted by Niinimäki et al. (1996b) and Ämmälä et al. (1999a; 1999b).

The reproducibility of the radial method was also investigated to ensure that data could be reliably replicated. Two trials for each rotor were conducted and the consistency profile measured and good agreement between the two trials was obtained. A typical normalised annulus consistency profile for two trials for the foil rotor is shown in Figure 3-19.

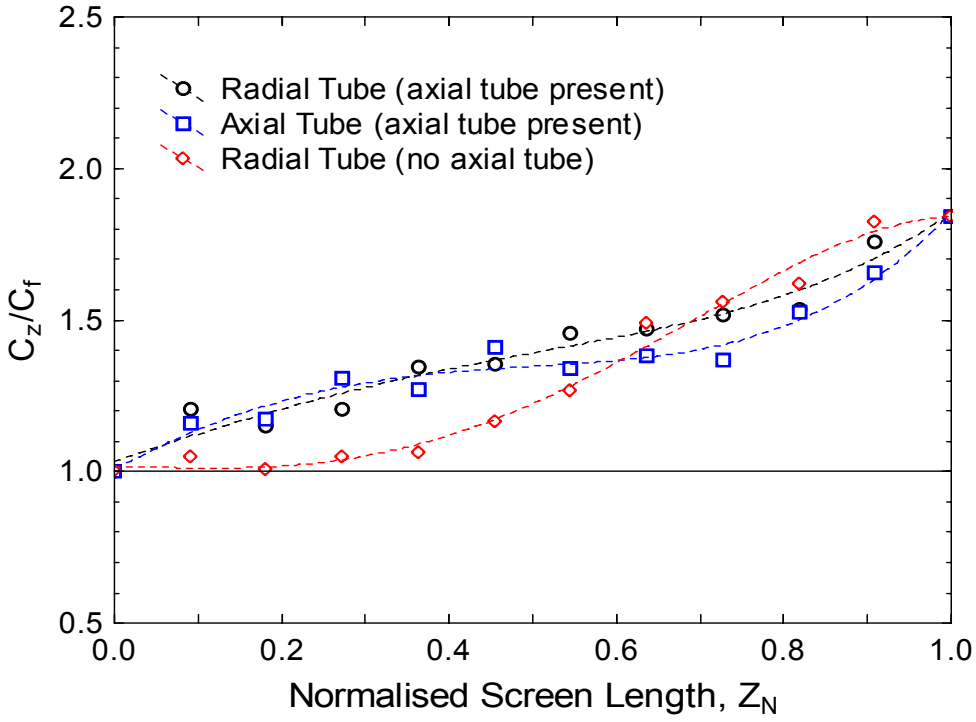

Figure 3-18 Effect of axial sampling tube present and removed for the step rotor (C_f=0.5 %, Q_a=640 L/min, R_v=0.16, u_{tip}=17 m/s)

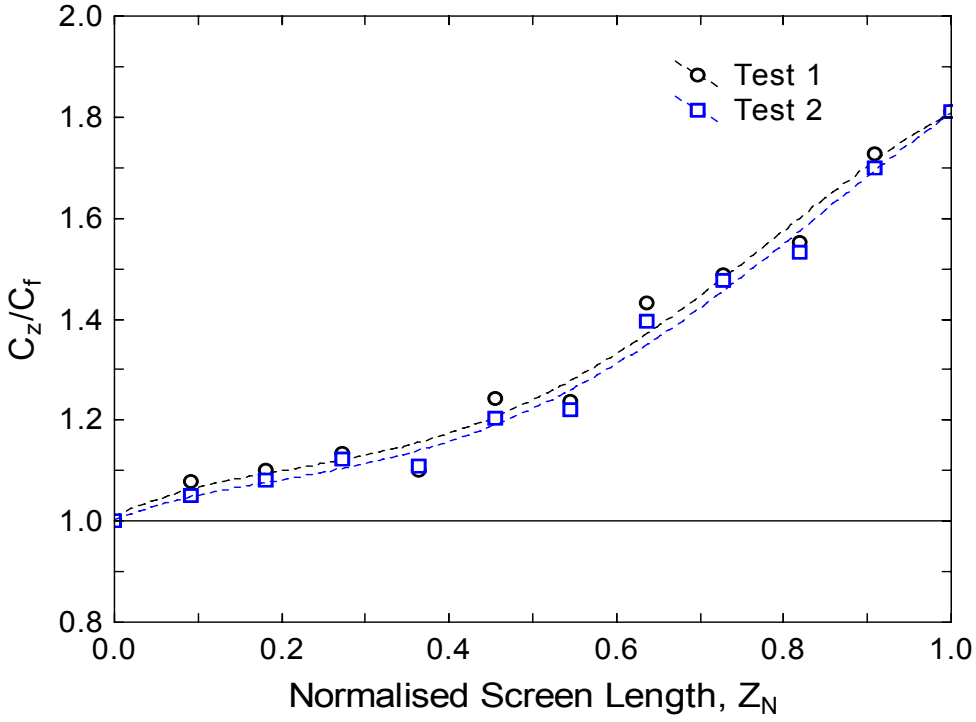

Figure 3-19 Reproducibility of the radial sampling method (C_f=0.5 %, Q_a=640 L/min, R_v=0.16, u_{tip}=17 m/s)

The change in passage ratio with hole diameter was also considered and values from the literature were examined to determine if the diameter of the sampling tube needed to exceed a minimum hole diameter. Passage ratio data was correlated from several published experimental studies (Sloane, 1998; Olson et al., 2000; Gooding, Olson et al., 2001; Wakelin & Paul, 2001; Weeds, 2006) to determine if an 8 mm sampling tube would affect the measured consistency of the sampled suspension. The change in passage ratio as the hole diameter is increased is shown in Figure 3-20 for several different pulps (softwood TMP, softwood and hardwood kraft pulps, recycled blend) over a range of reject rates (0.1 - 0.7) and feed consistencies (0.7 % - 2.5 %). As illustrated in the figure the passage ratio approaches one as the hole diameter is increased and it appears as though as long as the hole diameter is greater than about 3 mm the passage ratio should be equal to one. If the passage raito is equal to one then there is no change in the consistency of the suspension that is entering the aperture or tube. The radial sampling tube that was used was 8 mm in diameter and therefore the consistency of the sampled suspension should be representative of the consistency at that particular sampling point.

In light of this investigation it was concluded that the radial method was the best method to use and was sufficiently accurate for conducting the internal sampling. Furthermore the radial method held significant other advantages over the axial method. The radial method was more efficient in that once the tubes had been mounted and the screen basket set in place consistency profiles could be obtained for multiple conditions without having to remove the screen basket from the housing. As the axial tube needed to be drawn out for each sampling point, the tube then needed to be reattached to the screen after each test. This was a tedious and time consuming process which was a major disadvantage to the method.

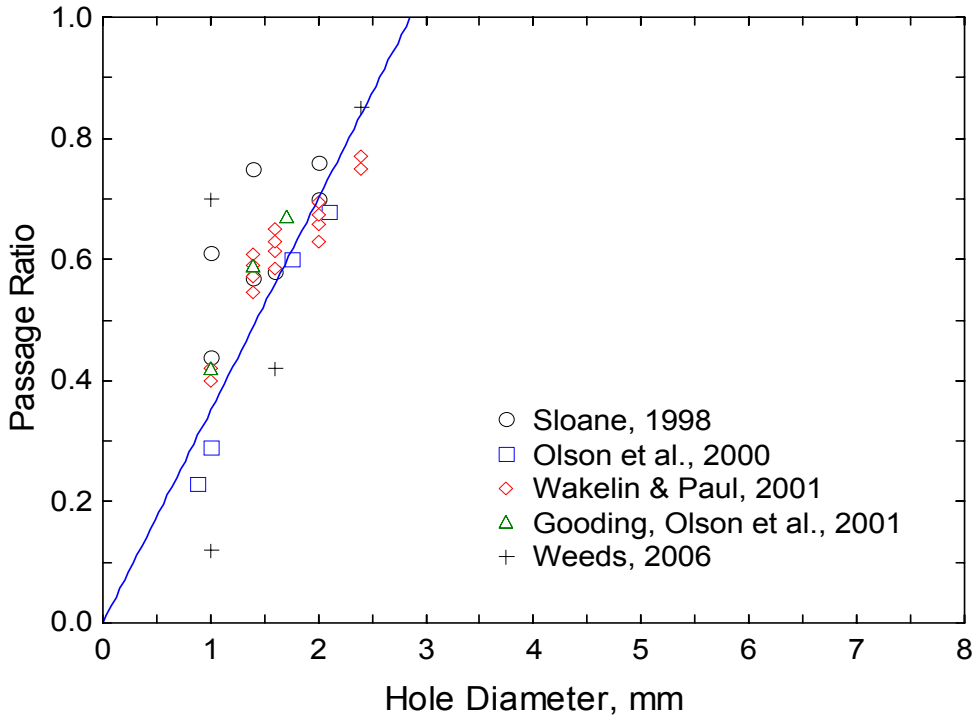

Figure 3-20 Effect of hole diameter on passage ratio for numerous different pulps at several reject rates and over a range of feed consistencies

As mentioned previously, the accept sampling tube was set at a distance of 5 mm away from the screen basket. A narrow screen section was used to compare the measured localised accept consistency to the overall accept consistency. A narrow section was used to minimise the accept consistency variation along the screen length. It was expected that slight variations in consistency would occur in the radial direction of the accept chamber. The normalised accept consistency for several distances away from the screen basket is shown in Figure 3-21. The normalised consistency was close to unity when the sampling tube was around 5 mm away from the screen basket and therefore this distance was used for all the accept sampling tubes throughout this research.

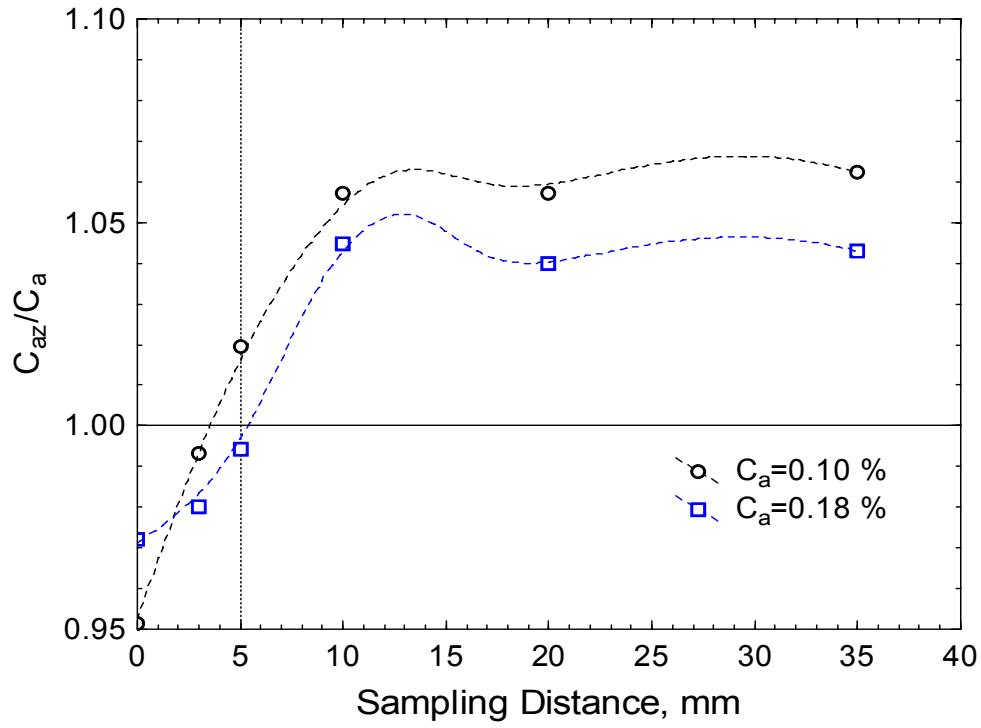

Figure 3-21 Effect of accept sampling tube on the normalised accept consistency for a narrow screen section (Q_a=330 L/min, R_v=0.5)

3.3.5 Fibre Length Analysis

The fibre length distribution of selected samples was measured using a Kajaani FS-200 fibre analyser. The FS-200 provides fibre length distribution and coarseness measurement by analysing a representative pulp sample. The sample is placed into a beaker and placed in the analyser. The sample is then diluted by the analyser and the fibres are sucked through a 0.4 mm capillary tube. The sample is continuously stirred by the analyser throughout duration of the testing. As the fibres travel up the capillary tube they enter the optics section where they are passed through a laser beam. An image of the fibre is projected onto a detector and the fibre length is measured. The measuring principle is illustrated in Figure 3-22. The FS-200 measures fibres from below 0.05 up to 7.2 mm in length in 0.05 mm intervals. The number of fibres in each length class is recorded and this file is then transferred to a computer where the file is stored. This file was then transferred to a Microsoft Excel spreadsheet to be used for further analysis.

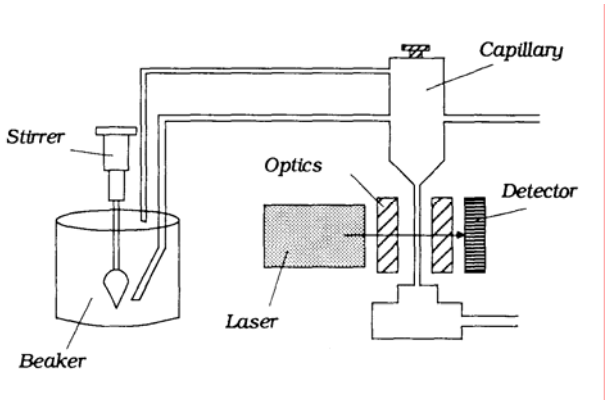

Figure 3-22 Kajaani FS-200 measuring principle (Kajaani User Manual)

A minimum of two samples for every test run was averaged and used in the analysis. Samples are only valid if the fibre count is greater than 11,000 fibres and the arithmetic and length-weighted averages for each test were within 0.03 mm of each other. To aid in the analysis these length classes were then grouped into six length fractions based on a modified particle size model. The length classes are grouped together into the fractions listed in Table 3-3.

Table 3-3 Grouped fibre length fractions

Fraction Range (mm)	Fraction Mid Point (mm)
0 – 0.2	0.1
0.2 – 0.5	0.35
0.5 – 1.2	0.85
1.2 – 2.0	1.6
2.0 – 3.2	2.6
3.2 – 7.2	5.2

These length fractions are based on a particle size model that was modified to accommodate the 0.05 mm measurement intervals of the FS-200. The concentration of fibres decreases as the fibre length increases. The longer fractions encompass a larger range of fibre lengths to account for the decrease in concentration with increased fibre length. The fines are defined as fibres with a fibre length less than 0.2 mm or the first length class. For the purposes of length fractionation calculations the

short fibre fraction is defined as fibres less than 2 mm in length and the long fibre fraction fibre greater than 2 mm in length.

3.3.6 Pressure Pulse Measurement

The pressure pulse of the step and foil rotors was measured at two axial positions along the screen length. The first transducer was mounted toward the front of the screen at axial position 2 which was located 40 mm from the feed end of the screen. The second transducer was mounted toward the rear of the screen at position 9 which was 40 mm from the reject end of the screen. The signal was run through a 200 MHz oscilloscope and the data was then transferred to a computer for further processing. Several trials were run using water only to determine the effect of reject rate and rotor speed on the pressure pulse. The feed consistency was also slowly increased to just below 3 % in order to study the affect of consistency. Unbleached pine kraft pulp was used exclusively during the pressure pulse trials.

3.3.7 Pressure Loss Coefficient Measurement

To determine the loss coefficients in the forward and reverse direction a smooth rotor and a narrow screen section was used. The narrow screen section was 55 mm in length and positioned approximately half way along the screen as illustrated in Figure 3-23. The narrow section was used to minimise flow variations in the annulus. A smooth rotor was used to remove the pulsation effect and create a steady flow where the approach flow velocity to the apertures could be estimated with more certainty. The annular gap of the smooth rotor was 16.5 mm. The pressure in the feed annulus was measured using a fluid leg mounted directly into the annulus, and the attachment nipple can be seen in Figure 3-23. The pressure in the accept chamber was measured either using a fluid leg for reverse direction measurements or a pressure transducer on the accept pipe for forward direction measurements. For determining the forward loss coefficient the screen was operated with the reject valve shut so all the flow went through the screen and out the accept pipe and the flow rate was measured using a magnetic flow meter. For determining the reverse loss coefficient, flow was reversed and fluid was pumped through the accept port and out the reject end of the screen (feed valve shut). For both cases the flow rate and the rotor speed was varied, and the

pressure drop across the screen was measured. The apparent loss coefficient for the step and foil rotors was measured using the same method as the forward direction measurements but with the step and foil rotors instead of the smooth rotor.

Figure 3-23 Narrow screen section and annulus pressure tap

3.4 Summary

This chapter has described the pressure screen and the experimental equipment used throughout this study. A detail comparison of radial and axially mounted sampling tubes for internal sampling of pulp from the screen has also been presented. The radially mounted tubes were found to be the more suitable of the two methods. Pressure pulse studies and loss coefficient measurements are also described. The next two chapters present and discuss the main body of the experimental programme of this thesis. Internal variations in the consistency, pressure pulse, and velocities within the screen are examined in detail.

4 Axial Variations in Consistency and Screen Performance

Pulp screening models assume the average local fibre passage ratio and local accept flow rate are constant along the length of the screen. Even under dynamic flow and passage conditions one may expect the average flows and passage ratio not to change significantly along the screen. However it is well established from fluid mechanics theory that flow entrance effects give rise to non-uniform flow conditions that take a certain distance into the flow to steady. It is postulated that fluid entrance effects give rise to large variations in screening behaviour in the first part of the screen. Several authors have suggested that there is variation in conditions along the screen length although very little data has been published (see Section 2.7). Experimental data presented by a number of authors all support the hypothesis that conditions are non-uniform along the screen length (Niinimäki et al., 1996a; 1996b; Niinimäki, 1998; Ämmälä et al., 1999a; 1999b; Walmsley & Weeds, 2002; 2004; Weeds, 2006).

This chapter reports internal consistency measurements taken within a pressure screen using a radial sampling method. Localised consistency measurements have been taken at several positions along the axial length from within the feed annulus and also from the accept side of the screen. Consistency measurement profiles are useful for inferring the flow and fibre passage characteristics along the screen length. Pulp consistency profiles in the pressure screen feed annulus were measured under numerous operating conditions and for three different screen rotors. Measuring localised consistencies in the accept chamber allowed important performance parameters, such as fibre passage ratio and fractionation efficiency, to be calculated.

4.1 Internal Axial Consistency Profiles

A typical consistency profile for the step rotor at a volumetric reject rate of 0.1 and a feed consistency of 0.14 % is shown in Figure 4-1. Two related data sets are shown, C_z which is the local internal feed annulus consistency, and C_{az} which is the local internal accept chamber consistency. The measured localised consistency in the feed annulus and the accept chamber are normalised by the feed consistency and plotted on a log axis against normalised screen length Z_N. This allows consistency profiles measured at different feed consistencies to be compared. The overall thickening

factor T is the last datum for C_z on the axial consistency profile at Z_N=1 and for this case T=5.14. The term C_z/C_f can also be considered to be the overall reject thickening factor up to that location in the screen. This is not to be confused with the localised reject thickening factor T_z (Equation 4-1).

$$T_z = \frac{C_{z-1}}{C_z} \qquad \textbf{4-1}$$

The annulus consistency dropped below the feed consistency (i.e. $C_z/C_f < 1$) over the front portion of the screen length. This yields a localised thickening factor T_z of less than unity. This "annular dilution" in this case caused the consistency of the stock in the annulus to be as low as 80 % of the feed. The phenomenon of annulus dilution has not previously been reported in the literature. The cause of annular dilution and its implications will be discussed later in Section 4.2. At about one third along the screen length the pulp in the annulus begins thickening rapidly until it reaches the final overall thickening factor of 5.14.

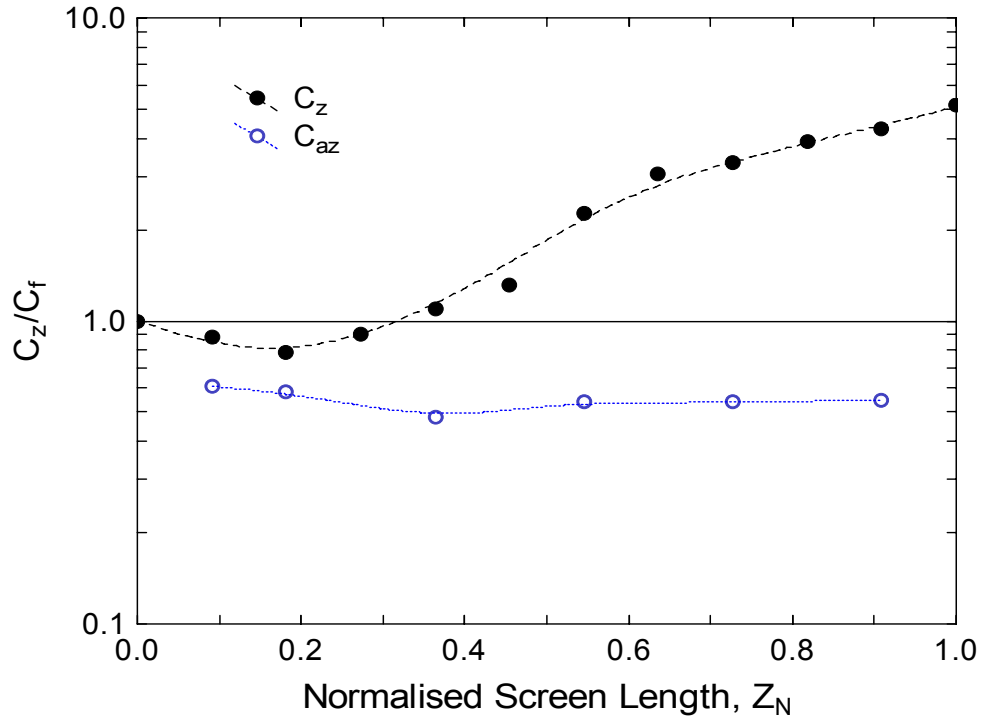

Figure 4-1 Normalised axial consistency profiles for the step rotor at R_v=0.1 and $\bar{u}_s$=0.6 m/s (C_f=0.14 %, u_{tip}=28 m/s)

The reason pulp thickens as it moves through the annulus can be explained by considering the plug flow model mass balance around a narrow screen element as depicted in Figure 2-35. The mass balance equations are for steady state and neglect the dynamic nature of the flows and fibre flux forward and reverse through the screen. Under normal screening conditions there is bulk forward flow from the feed annulus to the accept chamber (i.e. $Q_{az.for} > Q_{az.rev}$) and pulp is likely to be of lower consistency in the accept chamber thus giving a passage ratio of less than one. By applying the mass balance equations the pulp remaining in the annulus will thicken (i.e. $T_z > 1$) if and only if both the local passage ratio P_z and the local reject rate R_{vz} are less than one. When either of these is greater than unity the rejected pulp from that section will be of lower consistency than the pulp fed to that section. The rate of thickening will therefore depend on the passage ratio and local reject rate. A detailed analysis of the thickening and flows around and through a narrow screen element will be presented in Section 4.2.1.

The local accept consistency is less than the feed consistency as expected because in most circumstances the bulk accept consistency is lower than the feed. This yields an overall passage ratio for the bulk accepts of less than one. Local accept consistency is fairly uniform along the screen length.

The axial consistency profiles for the step and bump rotor are shown in Figure 4-2 and Figure 4-3 respectively for a range of volumetric reject rates at a feed consistency of 0.14 %. As illustrated in the figures the overall thickening factor increased as the reject rate was decreased, as predicted from the thickening models. The axial consistency profiles of the two different rotors were of similar shape although of different magnitude. The level of dilution in the annulus increased and occurred over a larger section of the screen as reject rate was increased. The amount of annular dilution that occurred was greater for the step rotor and was more affected by reject rate than the bump rotor. The axial dilution occurred despite changing the reject rate and appears to be more severe as the reject rate is increased. The local accept consistency, although fairly uniform along the screen length, decreased as reject rate was increased and occurred for both rotors.

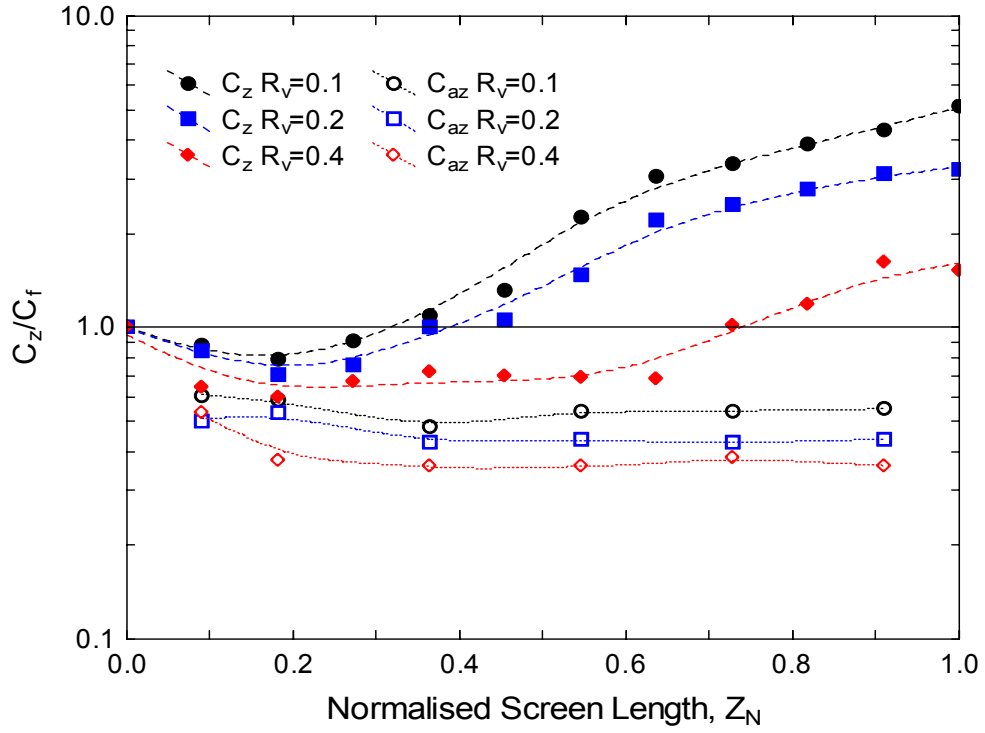

Figure 4-2 Normalised axial consistency profiles for the step rotor at a range of reject rates ($\bar{u}_s$=0.6 m/s, C_f=0.14 %, u_{tip}=28 m/s)

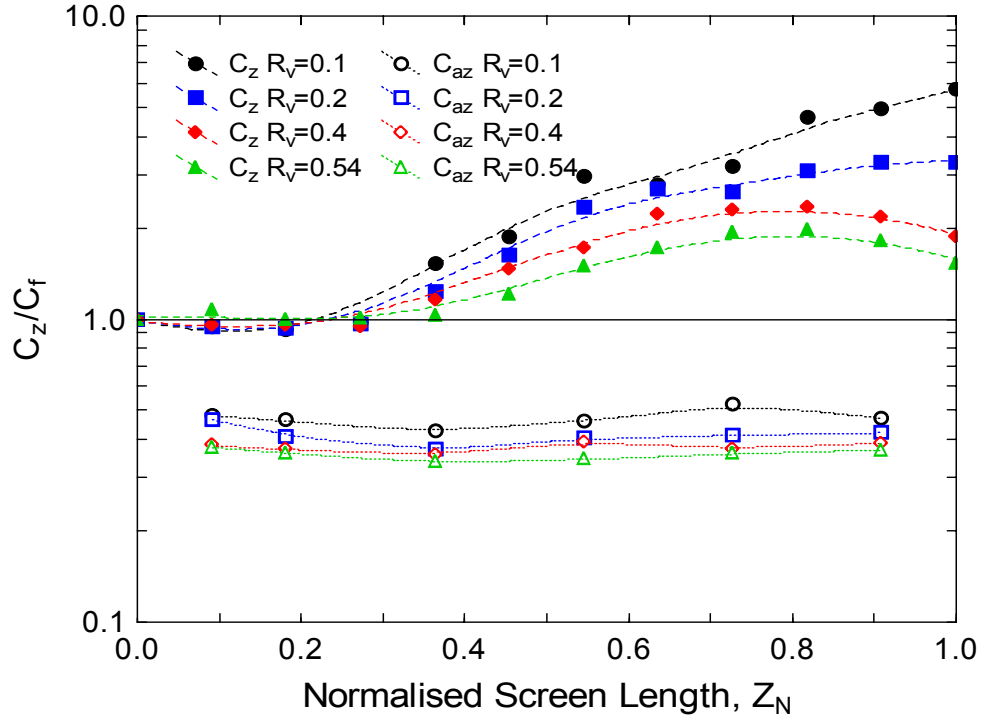

Figure 4-3 Normalised axial consistency profiles for the bump rotor at a range of reject rates ($\bar{u}_s$=0.6 m/s, C_f=0.14 %, u_{tip}=28 m/s)

The consistency profile of the foil rotor, run at half the tip speed of the closed rotors, at different reject rates is shown in Figure 4-4. The reason for the lower tip speed is that the foil rotor is a high intensity rotor with a much stronger reverse pulse than either the step or bump rotors. The rule of thumb is to run the foil at half that of the closed rotors to give a comparable reject thickening rate at similar reject rates. Furthermore the clearance between the foil element and the screen (≈3 mm) is much less than the closed rotors (≈10 mm) and the clearance has been shown to heavily influence the strength of the reverse pressure pulse (Gonzalez, 2002; Pinon et al., 2003; Feng et al., 2005).

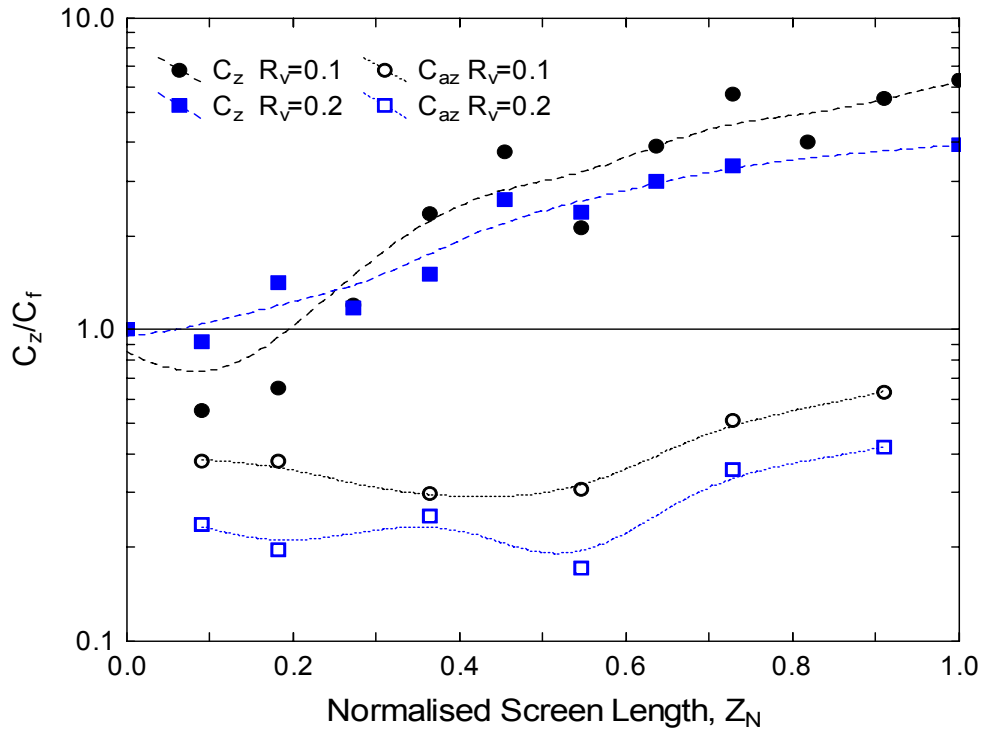

Figure 4-4 Normalised axial consistency profiles for the foil rotor at a range of reject rates ($\bar{u}_s$=0.6 m/s, C_f=0.15 %, u_{tip}=14 m/s)

Less annular dilution occurred when using the foil rotor at the higher reject rate than compared to the bump and step rotors. However a substantial amount of annular dilution still occurred at the lower reject rate for the foil rotor. This is most likely due to the foil rotor being an open type rotor with substantially different macro flow patterns in the feed annulus than a closed type rotor. The difference in mixing characteristics is also suspected to be the reason for the increased scatter in the measured consistencies. It is expected that open rotors will have much different

velocity profiles across the annulus in the radial direction than for the closed rotors due to the increased axial and radial mixing that will occur. The local accept consistency was more variable along the screen length for the foil rotor than the other rotors but also decreased as reject rate was increased.

A comparison of the consistency profiles of the three rotors at a reject rate of 0.2 is shown in Figure 4-5. The consistency of the accepts for the foil rotor is much lower than for the other two rotors especially over the first portion of the screen. The cause of this is partly due to the different flow patterns in the annulus and also the difference in the tip speed that the foil rotor is operated at. As mentioned previously the foil rotor was run at half the speed of the other two rotors and therefore the suspension will not be as "fluidised" which will decrease the passage of fibre through the screen and the accept consistency. A radial consistency profile as well as an axial consistency profile will develop (Ämmälä et al., 1999a; 1999b) and centrifugal force will contribute to the development of this radial consistency profile. A high consistency zone will occur near the screen and this will restrict fibre and floc movement and therefore lower passage.

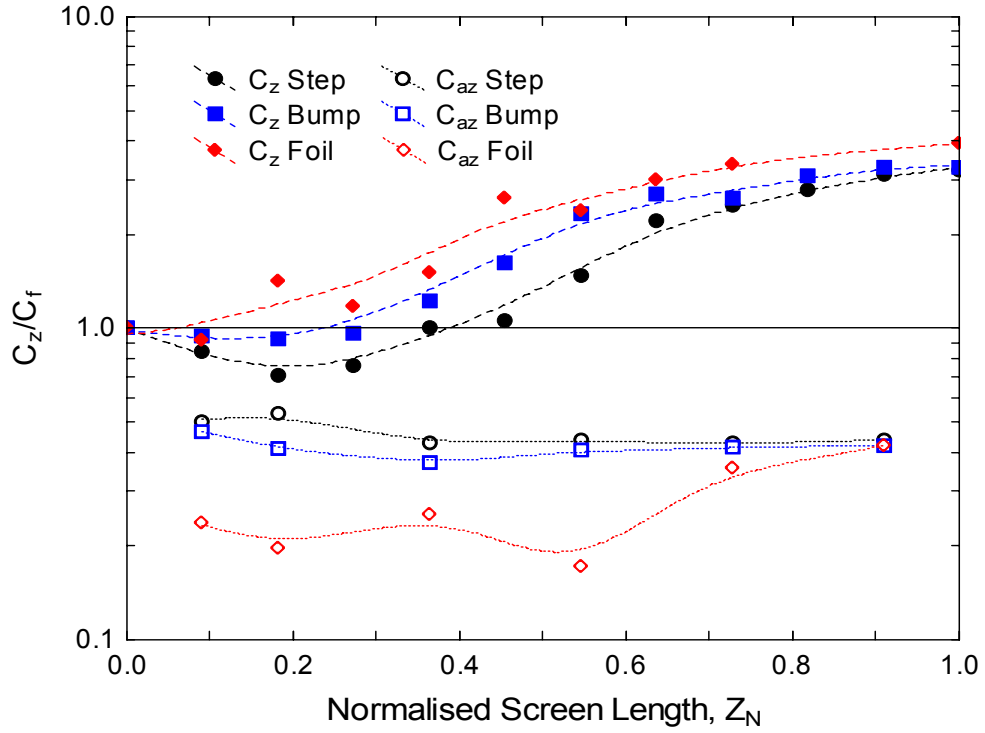

Figure 4-5 Comparison of the normalised axial consistency profiles for the three rotors at R_v=0.2 (Step & bump: $\bar{u}_s$=0.6 m/s, C_f=0.14 %, u_{tip}=28 m/s) (Foil: $\bar{u}_s$=0.6 m/s, C_f=0.15 %, u_{tip}=14 m/s)

4.1.1 Feed Consistency

Consistency profiles were also measured for a higher feed consistency (i.e. C_f = 1 %) under similar operating conditions as the lower consistency cases. The consistency profiles for the step and bump rotors are shown in Figure 4-6 and Figure 4-7 respectively at the higher feed consistency for two reject rates. The profiles show that much less annular dilution occurred than for the lower feed consistency situation (Figure 4-2 and Figure 4-3) and the thickening rate was fairly even over the length of the screen. The overall thickening factor increased in both cases for the higher feed consistency which is expected as overall fibre passage decreases with increased consistency, although any further increase in feed consistency will not increase the thickening for the step rotor, as discussed in Section 2.8 (Weeds, 2006). The localised accept consistency however remained about the same for the step rotor but decreased for the bump rotor at the higher consistency case. A decrease in passage ratio was expected for the bump rotor because passage has been shown to be more readily affected by feed consistency when using the bump rotor (Weeds, 2006).

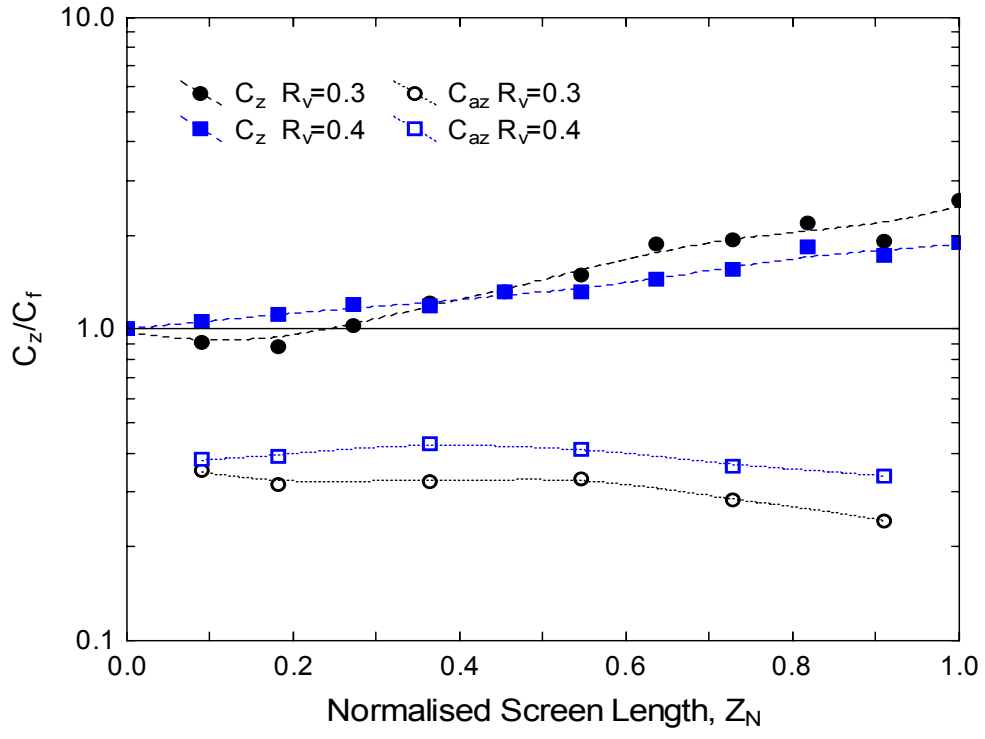

Figure 4-6 Normalised axial consistency profiles for the step rotor at a range of reject rates ($\bar{u}_s$=0.6 m/s, C_f=1.0 %, u_{tip}=28 m/s)

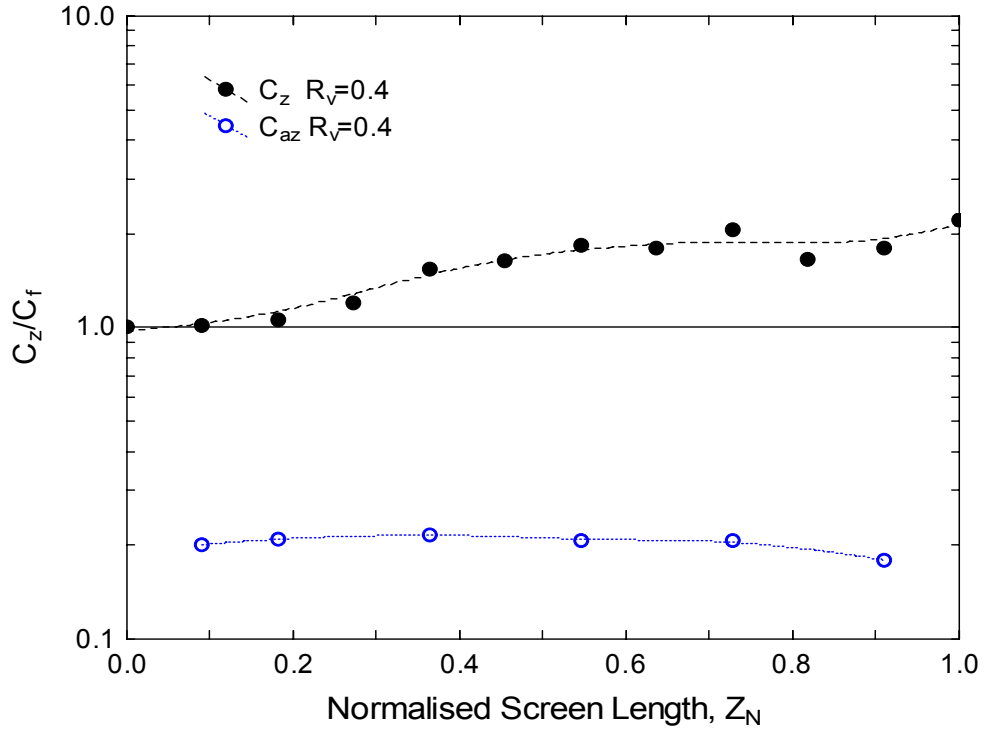

Figure 4-7 Normalised axial consistency profiles for the bump rotor ($\bar{u}_s$=0.6 m/s, C_f=1.0 %, u_{tip}=28 m/s)

4.1.2 Rotor Speed

The rotor tip speed u_{tip} was varied to determine the effect on the axial consistency profile for the three rotors. The axial consistency profiles for the step, bump, and foil rotors at two different tip speeds are shown in Figure 4-8, Figure 4-9 and Figure 4-10 respectively. A decrease in tip speed of approximately 40 % caused a 10 - 20 % increase in the final thickening factor, a 30 - 50 % decrease in overall passage ratio and the axial consistency profile to shift up slightly, resulting in less axial dilution for all of the rotors. However localised accept consistency decreased on average by approximately 6 % for the foil rotor and 45 – 55 % for the closed rotors when the tip speed was lowered. The decrease in local accept consistency for the closed rotors is comparable to the large decrease in overall passage ratio noted above. Such a large change is due to the difference in the amount and duration of the reverse flow induced by the different rotors. The differences and consequences of this disparity in reverse flow will be discussed later in this chapter and in greater detail in Chapter 5.

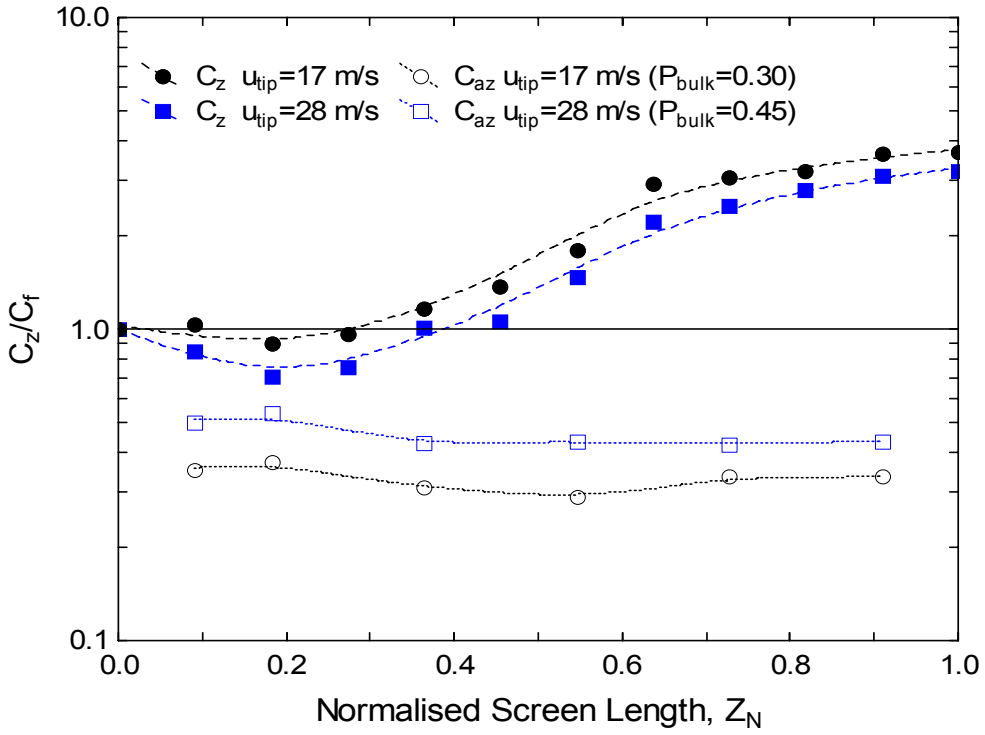

Figure 4-8 Normalised axial consistency profiles for the step rotor at R_v=0.2 for two different rotor speeds ($\bar{u}_s$=0.3 m/s, C_f=0.16 %)

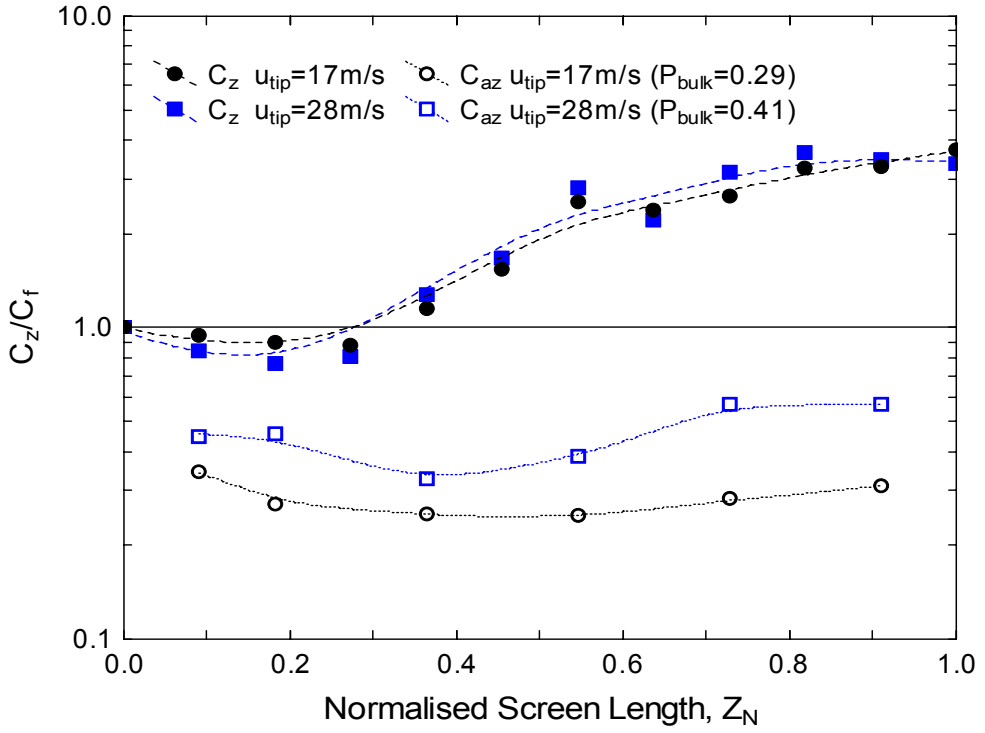

Figure 4-9 Normalised axial consistency profiles for the bump rotor at R_v=0.2 for two different rotor speeds ($\bar{u}_s$=0.3 m/s, C_f=0.12 %)

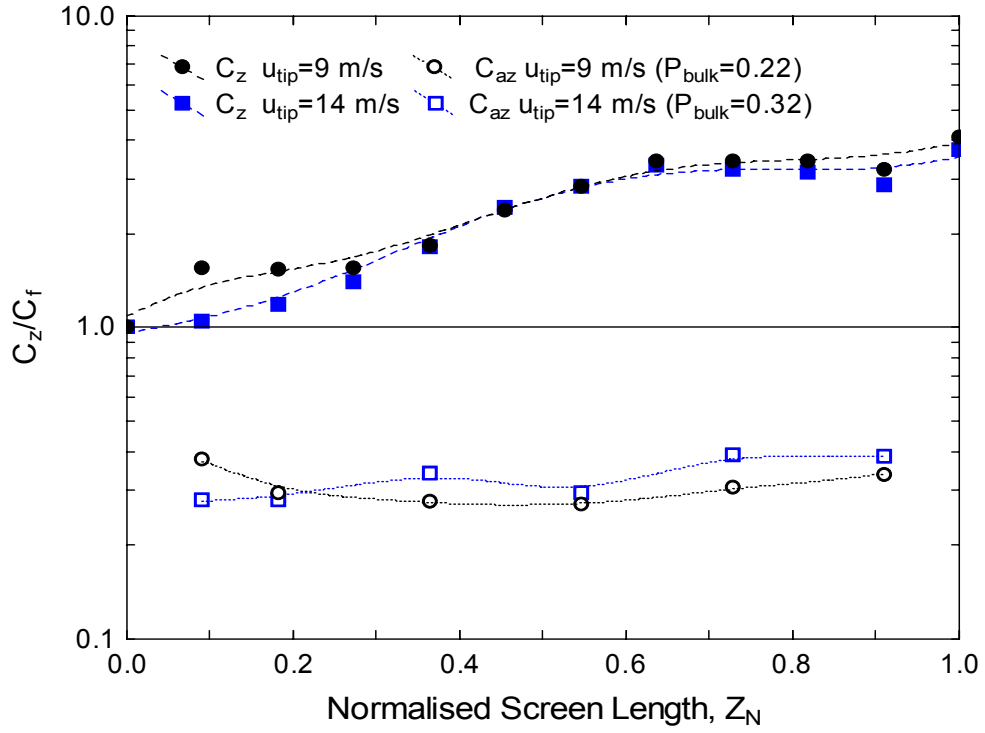

Figure 4-10 Normalised axial consistency profiles for the foil rotor at R_v=0.2 for two different rotor speeds ($\bar{u}_s$=0.3 m/s, C_f=0.12 %)

Although it may appear as though mass is not conserved for the closed rotors due to the large change in the accept consistency, when an overall mass balance is performed mass is conserved because the overall passage ratio is sensitive to small changes in the reject thickening factor especially at high reject rates. It should also be remembered that the vertical axis on the consistency profile figures is a logarithmic scale and therefore can be slightly deceptive as to the relative values of the reject thickening factors.

The effect of tip speed on both the reject thickening factor and passage ratio is complex and conclusions have been difficult of make due to the ambiguous and contradictory nature of data reported in the literature (see Section 2.4.4). Some authors have shown that an increased tip speed will yield no change or a decrease in fractionation efficiency, thus implying a decreased level of reject thickening (Repo & Sundholm, 1996; Sloane, 1998; Walmsley & Weeds, 1998; Braaten & Wakelin, 1999; Sloane, 2000; Wakelin & Paul, 2001). However Wakelin & Corson (1997), Gooding, Olson et al. (2001), and Ämmälä (2004) have shown an increase in fractionation up to a critical tip speed and then a decrease above this critical speed. Results from flow

channel investigations suggest that reject thickening should increase when the normalised velocity is decreased. At the same superficial aperture velocity, if the upstream velocity (analogous to tip speed) is increased the normalised velocity will decrease and therefore the passage will also decrease. From the literature it is easy to conclude that a complex relationship exists between reject thickening, passage ratio and rotor speed and that governing factors and mechanisms have yet to be clearly articulated.

Tip speed is an important operating variable as it determines the mean tangential velocity of the stock in the feed annulus, the intensity and frequency of the pressure pulse, and the amount of forward and reverse flow through the screen apertures. Decreased mean tangential velocity and turbulence may promote flocculation of the suspension which is expected to decrease fibre passage and therefore increase reject thickening. Furthermore, the pressure loss coefficient K_L of the screen has shown to be dependant on the normalised velocity and therefore is also a function of rotor speed (Gooding, Kerekes et al., 2001). Increasing the loss coefficient causes less flow through the aperture thereby reducing the aperture velocity and fibre passage. The effect of the rotor on the mean tangential velocity will be examined in more detail in Chapter 6.

Work by Weeds (2006) also suggests that the feed consistency will also affect the relationship between reject thickening and rotor speed. He postulated that at consistencies less than about 0.01 % fibres act independently of each other and fibre alignment mechanisms dominate. Experimental data in this region demonstrates that an increase in rotor speed leads to a decrease in passage, an increase in thickening and therefore confirms the findings of the flow channel experiments. However, at feed consistencies above about 0.01 % Weeds found that the opposite was true, as rotor speed increased, passage ratio increased and reject thickening decreased. It was proposed that above a critical consistency (≈0.01 %) clearing the apertures of accumulated fibre becomes increasingly important due to crowding and flocculation effects. Aperture cleaning is improved as the rotor speed is increased due to greater levels of reverse flow and the inability of fibres to accumulate. As a result the ability of the aperture to pass pulp is increased and passage ratio is increased. Data presented here supports the findings and explanation given by Weeds.

4.1.3 Effect of Accept Flow Rate

The accept flow rate was varied in order to study the affect of aperture velocity on axial consistency. It must be pointed out that the aperture velocity is the superficial or average aperture velocity $\bar{u}_s$ (Equation 4-2) where Q_a is the bulk accept flow rate and A_{open} is the open area of the screen, and not the instantaneous aperture velocity u_s. The instantaneous aperture velocity will be constantly changing due to the rotor and will be positive or negative depending on the position of the rotor. The average local aperture velocity $\bar{u}_{sz}$ (Equation 4-3) is also likely to change along the screen but even this is a superficial velocity and not an instantaneous one.

$$\bar{u}_s = \frac{Q_a}{A_{open}} \qquad \textbf{4-2}$$

$$\bar{u}_{sz} = \frac{Q_{az}}{A_{open.z}} \qquad \textbf{4-3}$$

The axial consistency profiles for two aperture velocities for the step and bump rotors are shown in Figure 4-11 and Figure 4-12 respectively, and at the higher feed consistency for the step rotor in Figure 4-13. There were only slight variations in the consistency profiles for both rotors at the different aperture velocity although the variation was somewhat less for the bump rotor. The reject thickening factor and passage ratio were more or less unchanged by the increase in aperture velocity although the range of aperture velocities tested was very small. If much higher aperture velocities were tested it would be expected that the passage ratio would increase up to a maximum value and this would result in a decrease in the thickening factor. The reason why elevated aperture velocities were not tested is because the screen becomes difficult to operate and the maximum capacity of the pump is reached. Holed apertures generally are operated at much lower aperture velocities than slotted apertures because of the increased open area and size of the aperture. The effect of increased aperture velocity on passage of fibre through an aperture has been thoroughly examined during the numerous single aperture investigations (Gooding, 1986; Kumar, 1991; Kumar et al., 1996; Olson, 1996; Atkins, 2003).

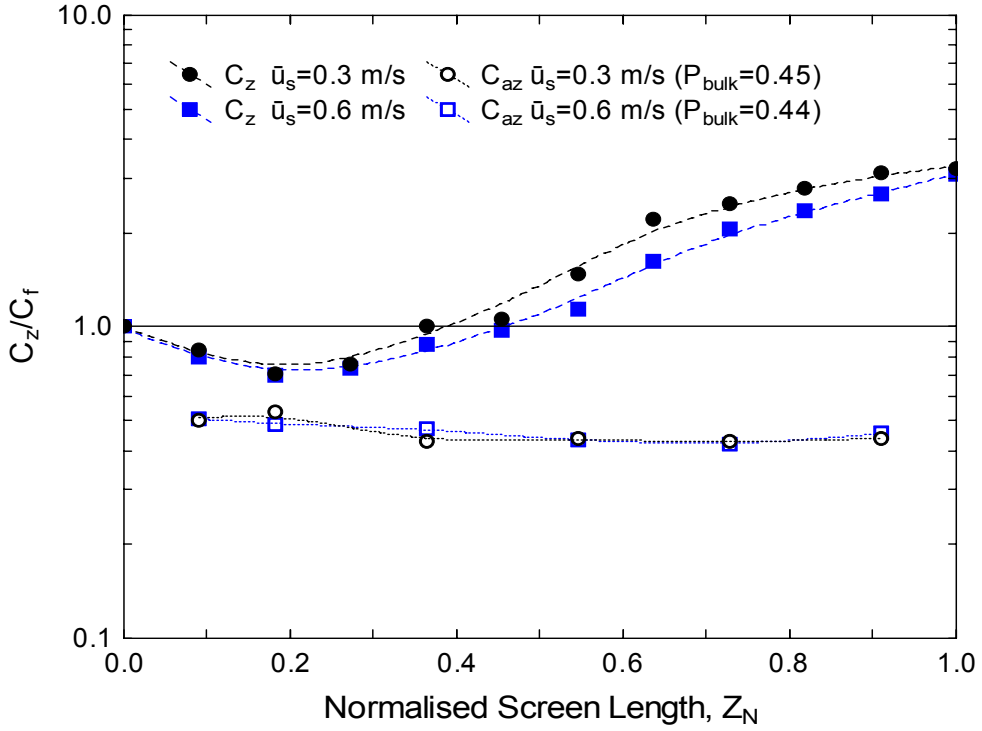

Figure 4-11 Normalised axial consistency profiles for the step rotor at R_v=0.2 for two different aperture velocities (u_{tip}=28 m/s, $\bar{u}_s$=0.3 m/s - C_f=0.16 %, $\bar{u}_s$=0.6 m/s - C_f=0.14 %)

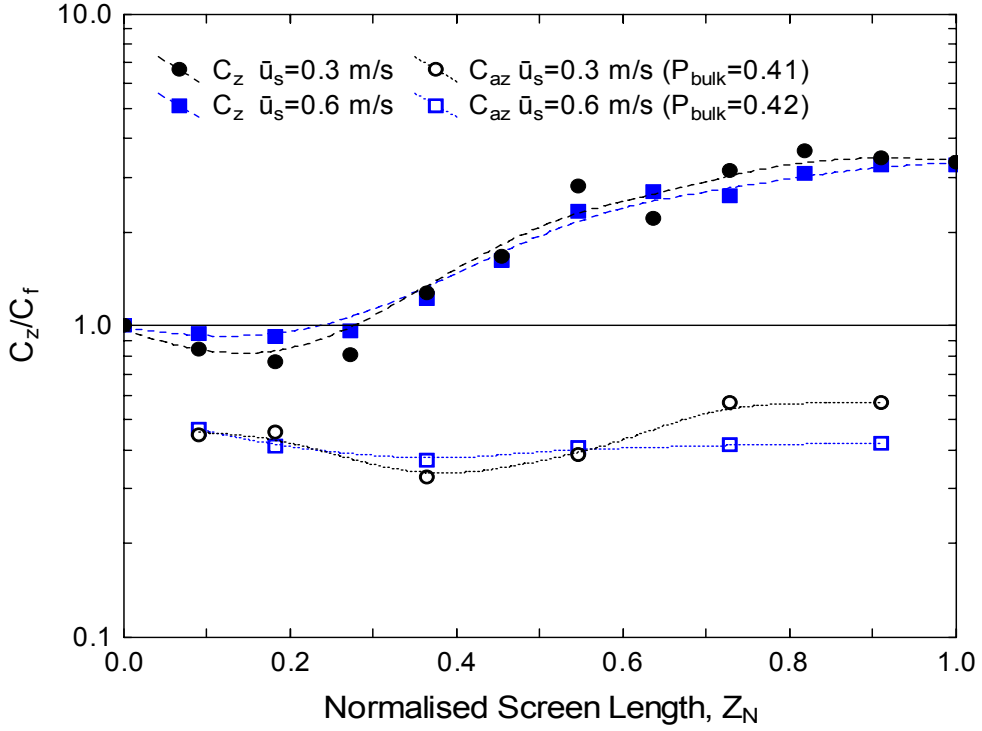

Figure 4-12 Normalised axial consistency profiles for the bump rotor at R_v=0.2 for two different aperture velocities (u_{tip}=28 m/s, C_f=0.13 %)

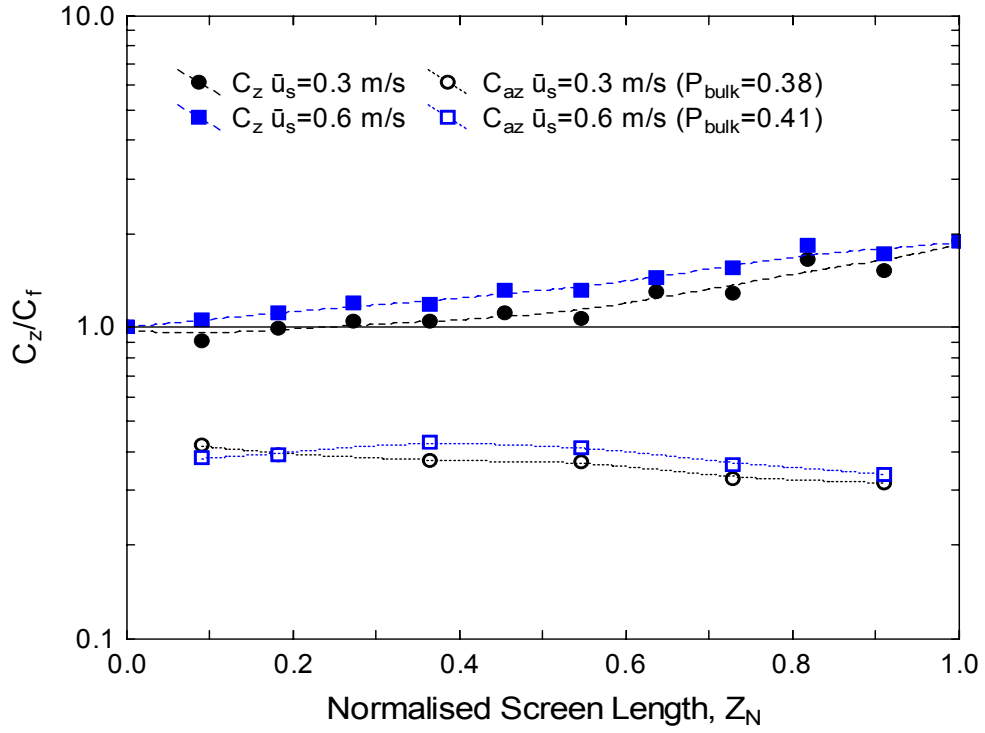

Figure 4-13 Normalised axial consistency profiles for the step rotor at R_v=0.4 for two different aperture velocities (u_{tip}=28 m/s, C_f=1.0 %)

4.1.4 Comparison with the Plug Flow Model

The plug flow model has previously been shown to predict the performance behaviour of a closed rotor (Walmsley & Weeds, 2004). The plug flow model can be used to predict the internal consistency profile for a given overall volumetric reject rate and reject thickening factor. From these two factors the plug flow passage ratio P_{plug} can be calculated (Equation 4-4). The plug flow model assumes that both the localised accept flow and fibre passage ratio are constant along the screen length and therefore the localised volumetric reject rate R_{vz} will decrease along the screen length (Equation 4-5). The plug flow passage ratio and the localised reject rate can be used to calculate the local reject thickening factor which can then be used to determine the overall consistency profile. Equations 4-4 and 4-5 are rearrangements of Equation 2-37.

$$P_{plug} = \frac{\log T}{\log R_v} + 1 \qquad \textbf{4-4}$$

$$R_{vz} = \sqrt[(P_{plug}-1)]{T_z} \qquad \textbf{4-5}$$

The predicted consistency profile using the plug flow is compared to the axial consistency profile data from Figure 4-2 for the step rotor and a reject rate of 0.2 is shown in Figure 4-14. The model substantially over predicts the thickening over the first half of the screen and then under predicts the thickening over the remaining half.

When the feed consistency is increased to 1.0 %, as illustrated in Figure 4-15, the plug flow model gives a slightly better prediction of internal consistency along the screen length. The prediction improves further as the reject rate increases with all other variables remaining the same as shown in Figure 4-16.

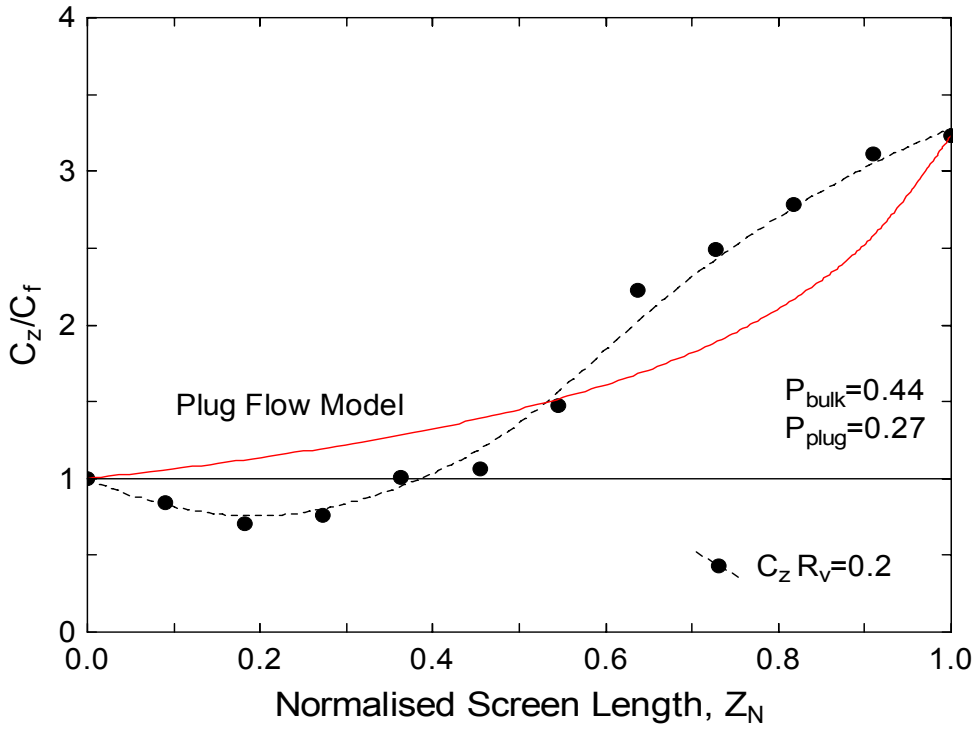

Figure 4-14 Comparison of the predicted and measured consistency profiles for step rotor R_v=0.2 ($\bar{u}_s$=0.6 m/s, C_f=0.14 %, u_{tip}=28 m/s)

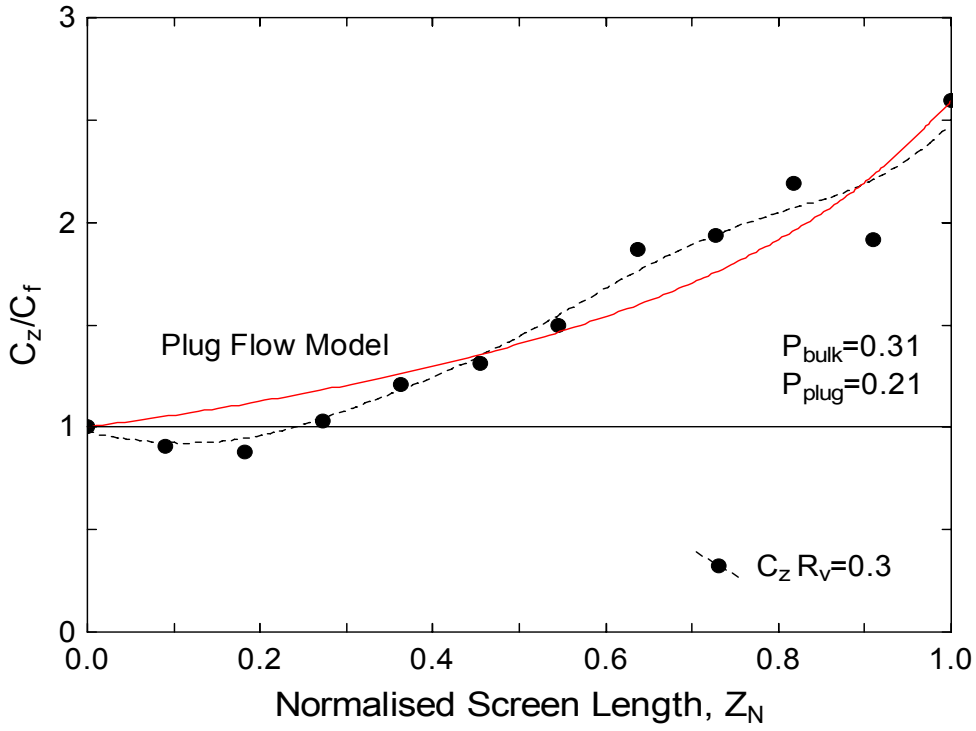

Figure 4-15 Comparison of the predicted and measured consistency profiles for step rotor R_v=0.3 ($\bar{u}_s$=0.6 m/s, C_f=1.0 %, u_{tip}=28 m/s)

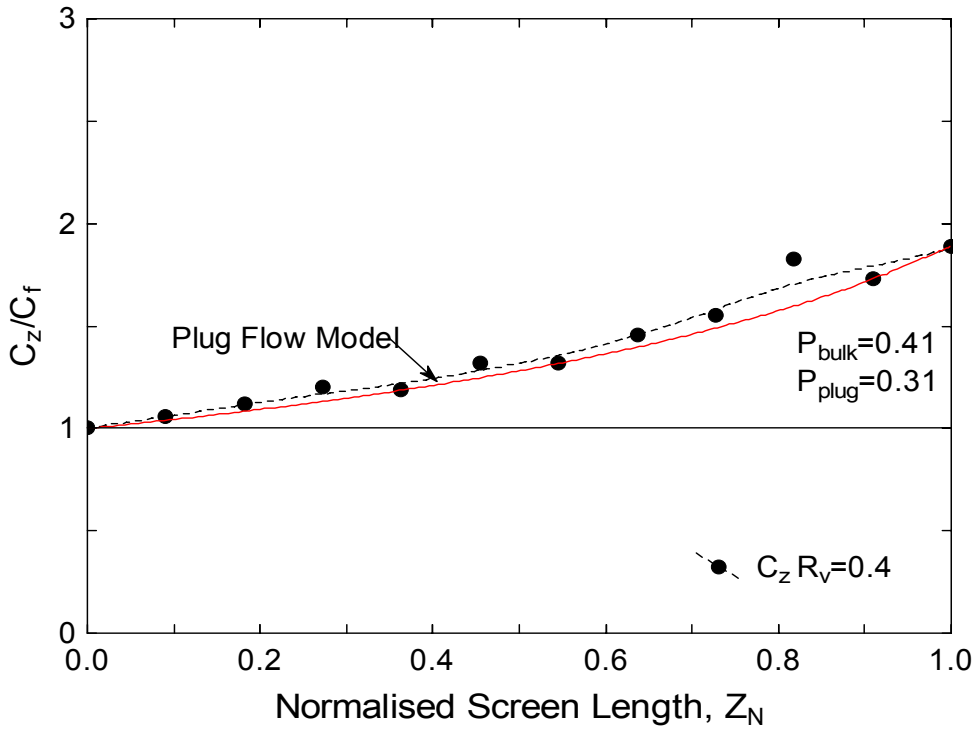

Figure 4-16 Comparison of the predicted and measured consistency profiles for step rotor R_v=0.4 ($\bar{u}_s$=0.6 m/s, C_f=1.0 %, u_{tip}=28 m/s)

A limited number of studies have been published examining the internal variations of consistency and furnish properties in a pressure screen. Niinimäki, Ämmälä, and co-workers have published several papers, using the same experimental apparatus and sampling techniques for each study, investigating furnish property variations in a pressure screen with an open style foil rotor (Niinimäki et al., 1996a; 1996b; Niinimäki, 1998; Ämmälä et al., 1999a; 1999b). Consistency was found to increase suddenly at the feed end of the screen and then decrease to the reject consistency along the screen basket. The increase in consistency at the beginning of the screen was attributed to a back-flow mechanism and fibre mat formation at the start of the screen which caused the pulp in the feed chamber to increase to well above the incoming feed consistency (Ämmälä et al., 1999a; 1999b). The authors also found considerable variation in consistency in the radial direction with pulp becoming more concentrated toward the screen surface. The back-flow mechanism described was found to occur for an axially feed screen and the authors supposed that it would also occur for a tangentially fed screen although this was not tested.

Weeds (2006) also measured internal consistency variations in a screen using both a radial and axial sampling method and found significant differences in the measured consistency profiles using the two methods. Although Weeds did not carry out a comprehensive comparison of the two methods he cautioned the use of either method without first conducting a comprehensive study to validate the technique of internal sampling. Lack of confidence in the sampling method casts doubt on the accuracy of some of the results reported by Niinimäki, Ämmälä, and co-workers because both radially and axially mounted tubes were used in those studies and no mention of sampling technique validation is made. Subsequent to Weeds' study, an evaluation of the two methods was conducted and it was found that the radial mounted tubes were more accurate than a axially mounted tube. The comparative study of the two methods is reported in Chapter 3.

The decrease in the consistency in the feed annulus found in this study does not agree with the result reported by Niinimäki & Ämmälä. The disparity could be due to a number of different factors including, differences in the sampling technique, screen configuration, and pulp furnish used. It is difficult to identify possible causes for the difference because not all of the relevant information is included. For example in

their paper (Ämmälä et al., 1999b) the feed consistency and reject rates are reported for different trials, as well as internal consistency and freeness measurements for selected cases, however no overall reject thickening factors are reported. An examination of their internal consistency data suggests that very little reject thickening occurred (estimated to be approximately 1.05 from the presented data) even though the volumetric reject rate was 0.25. The thickening of the pulp only occurred at the very front of the screen and in the feed chamber and then was diluted to almost the feed consistency over the remainder of the screen. It is highly unlikely that at that reject rate the reject thickening would have been so low. A slotted 0.15 mm screen basket was used in their study and for the pulps used, a thickening factor of approximately 1.5 would be expected based on similar pulps and screens used by this author (Atkins, 2003). Furthermore specific statements regarding the formation of a fibre mat on the screen surface are purely speculative and are not based on experimental evidence as no sampling was taken from the screen surface at the feed end of the screen, where it is alleged that the fibre mat is formed.

4.2 Explanation of Annular Dilution

As illustrated in the previous sections, the consistency in the annulus was lower than the feed consistency over the front portion of the screen under certain conditions. Weeds (2006) presented axial consistency profiles measured using both axially and radially mounted sampling tubes and found the radially mounted tubes gave a small amount of annular dilution. A flow model was used to predict the local volumetric aperture flow Q_{az} using axial consistency profile data. The flow prediction using consistency data from the radial method showed that there was a net negative flow over the first 20 % of the screen length. A detailed investigation of the two sampling methods was not conducted, and no discussion regarding the consequences of having a section of bulk reverse flow or explanations as to why negative flow was predicted were offered.

The phenomenon of feed annulus dilution is an interesting discovery and a number of feasible explanations are possible. If the entire screen is considered, pulp is thicker in the rejects because the accept consistency is lower than the feed consistency. The forward flow across the entire screen is much greater than the reverse flow and yields

a positive net flow that is equal to the accept flow rate. There are limited cases where accept thickening has been reported but this only occurs under very unique and isolated conditions (LeBlanc, 1986; Weeds, 2006). Accept thickening is where the accept consistency is greater than the feed, the reject consistency is lower than the feed, and a positive net flow across the screen still occurs. Possible causes of annular dilution are considered in the following section. A two passage ratio model will first be developed in order to examine what is occurring in the screen annulus more closely.

As discussed previously the plug flow model makes certain assumptions regarding the screening conditions and passage of fibre in the annulus. Flow of fibre and fluid through an aperture is complex due to the dynamic nature of the flow caused by the rotor. This is expected to cause flow of fibre in both the forward direction and reverse direction. Kubát & Steenberg (1955) considered a simple screen with pulsation and derived a permeability index that incorporated the probability of a particle being passed through the aperture in both the forward and reverse directions. Furthermore the permeability index included the effect of pulsation and the authors conclude that the permeability index should always increase as the amount of pulsation increases. By comparison the plug flow model does not account for pulsation and forward and reverse flow of fibre and uses bulk or average parameters such as the overall passage ratio. The terminology and definitions that were used by Kubát & Steenberg have been adapted and modified in modern screening literature and a two passage ratio model considering and incorporating the pulsation effect and forward and reverse passage ratios is derived below. The two passage ratio model presented below was developed at the same time as Weeds (2006) and the two models are estentially the same, however the dervivation presented here is much simplier and easier to follow than the one presented by Weeds.

4.2.1 Two Passage Ratio Model

Flow of pulp through a screen aperture involves flow of fluid and pulp in both the forward and reverse directions. If a single aperture is considered, as illustrated in Figure 4-17, the overall mass flow of pulp around the aperture is given by Equation 4-6.

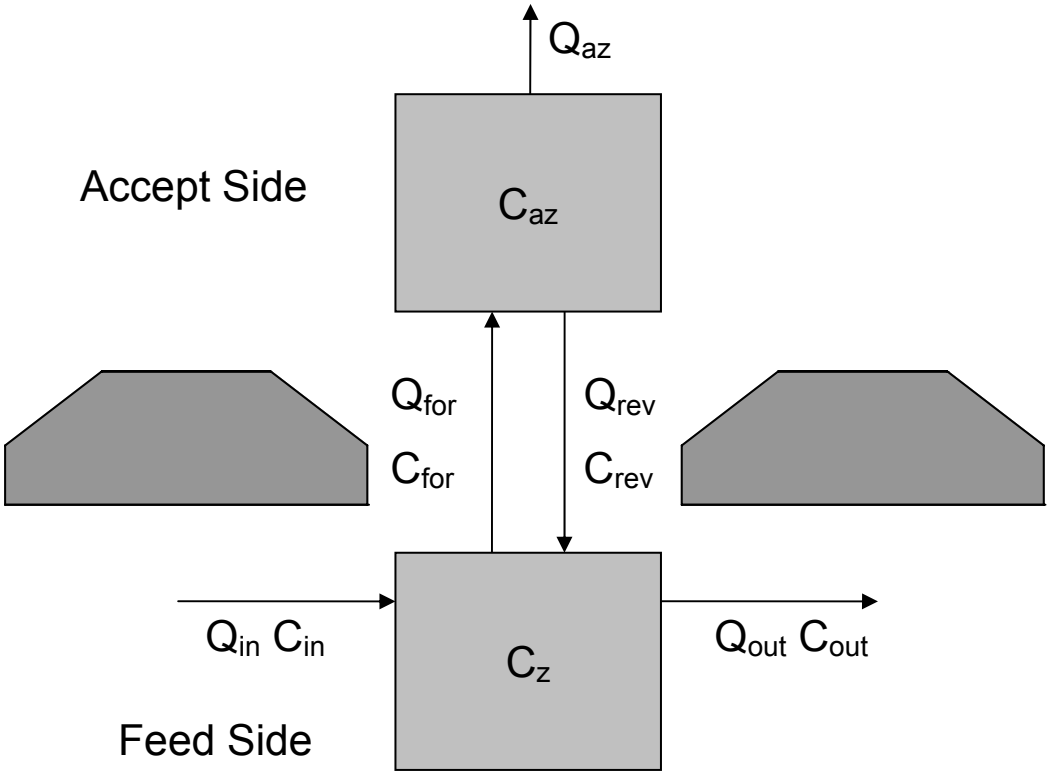

Figure 4-17 Schematic of flows through and around a single screen aperture

$$C_{in}Q_{in} = C_{az}Q_{az} + C_{out}Q_{out} \qquad \textbf{4-6}$$

If only the flow through the aperture is considered, the bulk flow is governed by Equation 4-7 using the local passage ratio P_z and local reject rate R_{vz}.

$$C_{az}Q_{az} = P_zC_zQ_{az} = P_zC_zQ_{in}(1-R_{vz}) \qquad \textbf{4-7}$$

When the forward and reverse flows through the aperture are used, instead of local passage ratio P_z, Equation 4-8 is derived.

$$C_{az}Q_{az} = C_{for}Q_{for} - C_{rev}Q_{rev} \qquad \textbf{4-8}$$

Alternatively Equation 4-8 can be expressed in terms of forward P_{for} and reverse P_{rev} passage ratios, as in Equation 4-9, where the forward and reverse passage ratios are defined in Equations 4-10 and 4-11 respectively.

$$C_{az}Q_{az} = P_{for}C_zQ_{for} - P_{rev}C_{az}Q_{rev} \quad \textbf{4-9}$$

$$P_{for} = \frac{C_{for}}{C_z} \quad \textbf{4-10}$$

$$P_{rev} = \frac{C_{rev}}{C_{az}} \quad \textbf{4-11}$$

The ratio of the reverse flow to the forward flow through the aperture can be expressed as a rotor back-flush ratio *k* (Equation 4-12). Usually Q_{rev} is much less than Q_{for} and therefore there exists bulk positive accept flow. The consistencies of the pulp flowing in the forward and reverse directions are not directly measurable and will be dependant on a number of factors including flow conditions and suspension properties.

$$k = \frac{Q_{rev}}{Q_{for}} \quad \textbf{4-12}$$

Further reworking can be made to Equation 4-7 by substituting Equations 4-9 and 4-12 and solving for P_z to give Equation 4-13. The effect of changes to the forward and reverse passage ratios on the overall local passage ratio as a function of the rotor back-flush ratio is illustrated in Figure 4-18. Equation 4-13 is similar to that derived by Kubát & Steenberg (1955) (Equation 2-19) although their forward and reverse passage probability terms are different to the forward and reverse passage ratio defined here.

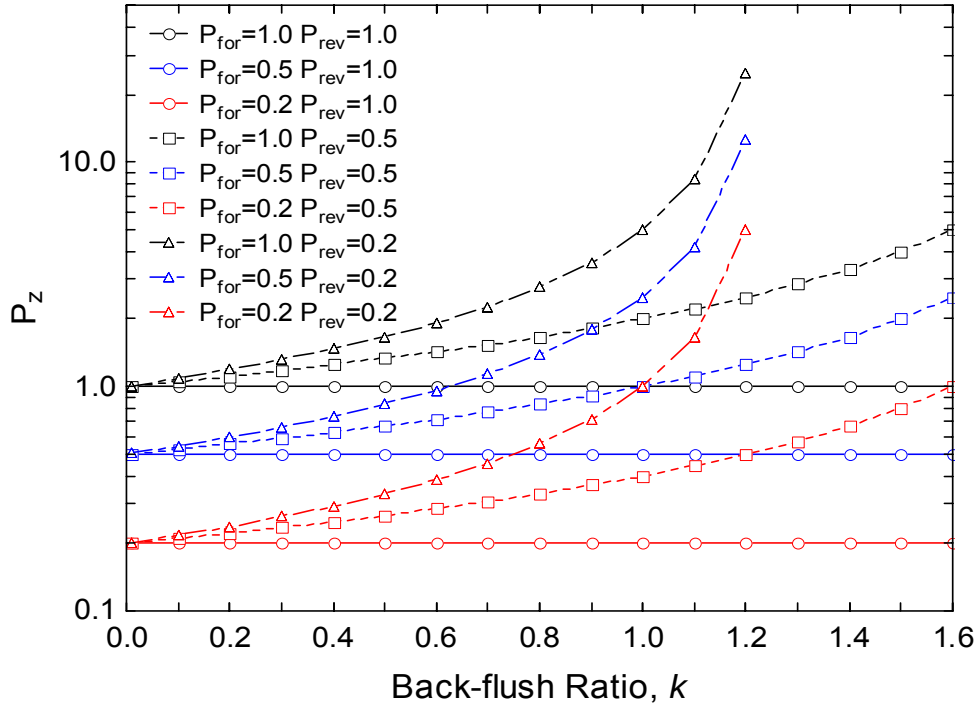

Figure 4-18 Overall local passage ratio as a function of back flushing ratio *k* for several forward and reverse passage ratios

$$P_z = \frac{P_{for}}{1-k+kP_{rev}} = \frac{P_{for}}{1+k(P_{rev}-1)} = \frac{C_{az}}{C_z} \qquad \textbf{4-13}$$

When the flow in the reverse direction is small, for example when using a low intensity rotor, *k* will be small because the forward flow dominates and the local passage ratio is approximated by the forward passage ratio only. Similarly if the reverse passage ratio is equal to one, the local passage ratio is approximated by the forward passage ratio as seen in the figure. As the reverse passage ratio decreases the local passage ratio becomes greater than the forward passage ratio. Accept thickening occurs if the local passage ratio is greater than one and will occur only under unique conditions. Firstly if the reverse passage ratio is much lower than forward passage ratio and *k* is less than one, or secondly if the forward and reverse passage ratios are similar and *k* is greater than one.

If a segment of the screen is considered, as in Figure 4-19, dilution of a section of the annulus (say z_1) may occur due to one of two reasons: a) a net positive flow across

that section of screen occurs and there is a localised passage ratio greater than one (localised accept thickening), or b) a net negative flow across the screen occurs and there is a localised passage ratio less than one (localised bulk reverse flow). These two situations will be discussed in further detail.

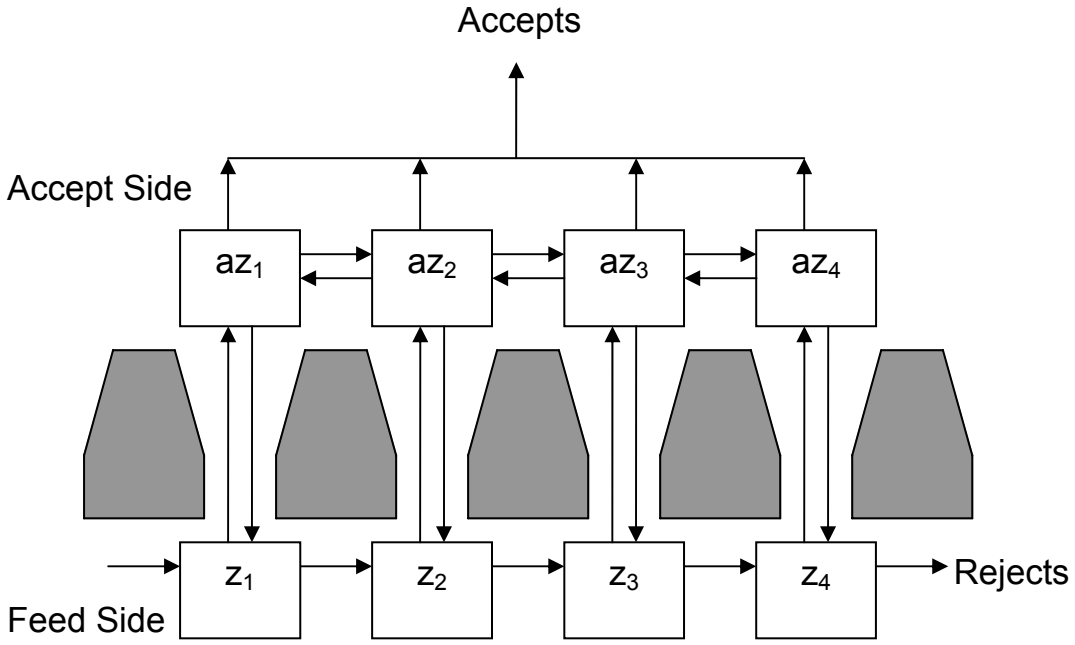

Figure 4-19 Schematic of a screen section

4.2.2 Localised Accept Thickening

Localised accept thickening is one possible explanation for the phenomenon of annular dilution. If the consistency in the region directly adjoining the aperture on the accept side of the screen (az_1) is greater than that of the feed annulus (z_1), the consistency of the pulp fed to the next aperture (z_2) will be less than that fed to the one prior. If localised accept thickening occurs it would yield a localised passage ratio greater than unity and a positive net flow across that section of screen would still occur. It is possible that over some sections of the screen localised accept thickening may have occurred. This would be extremely difficult to measure as the accept chamber is most likely to be chaotic and the localised consistency will constantly change due to the flow patterns and action of the rotor.

Accept thickening will occur if P_z is greater than unity and will only occur if P_{rev} is much less than P_{for} and the back-flush ratio is above a certain value as illustrated in Figure 4-18. It is expected that for screen baskets with recessed accept side profiles that P_{rev} will be greater than P_{for} and therefore accept thickening will not occur under typical operating conditions. For narrow slots however, P_{rev} is likely to be much less than P_{for} because of the geometry of the aperture, although this maybe negated if a foil rotor with a large negative pulse is used because it may extrude fibre accumulated on the accept side of the aperture back into the screen annulus.

No localised thickening was measured on the accept side of the screen during any of the trials. This may be obscured if lower consistency stock from the adjacent region of the accept chamber (az_2) mixed with the higher consistency stock (az_1) thus diluting the stock to the measured value. The sampling tube for the accept side consistency had a nominal diameter of 8 mm and was set 5 mm away from the screen surface. It would be sampling an "average" consistency in the region adjacent to several apertures (az_1-az_4).

4.2.3 Localised Bulk Reverse Flow

Another more likely explanation for annular dilution is that over the first section (z_1) of the screen the amount of reverse flow exceeds that of the forward flow thus giving a negative net flow over that section of the screen. It is expected that water and at least the fines would pass in the reverse direction. Therefore suspension coming back in the reverse direction would have a consistency many times less than the feed consistency and would therefore dilute the stock in the adjacent region of the feed annulus (z_1). At some point along the screen (say z_2) the amount of forward flow would become greater than the reverse flow and cause pulp to thicken. In order to compensate for this section of bulk reverse flow, the flow over the remainder of the screen would be much greater than the superficial average aperture velocity. Another important inference that follows on from this hypothesis is that in order to get the level of dilution in the feed chamber there must be substantially different flow patterns in the accept chamber than is currently envisaged.

Figure 4-18 can be reworked to illustrate the effect of local passage ratio P_z on the local thickening factor as a function of local volumetric reject rate as in Figure 4-20. This clearly shows the four regions where either annular dilution or annular thickening occur and local passage ratio is less than or greater than unity. If the local volumetric reject rate is less than one it denotes bulk forward flow (i.e. $k < 1$) and if it is greater than one bulk reverse flow occurs (i.e. $k > 1$). If the entire screen is considered (i.e. only the bulk flows and consistencies) the screen operates only in the top left region (i.e. $P_z < 1$ and $R_v < 1$) however the internal consistency data measured here suggests that on a local level there are regions of the screen that do not operate in this region but rather in the bottom right region (localised bulk reverse flow) or the bottom left region (localised accept thickening).

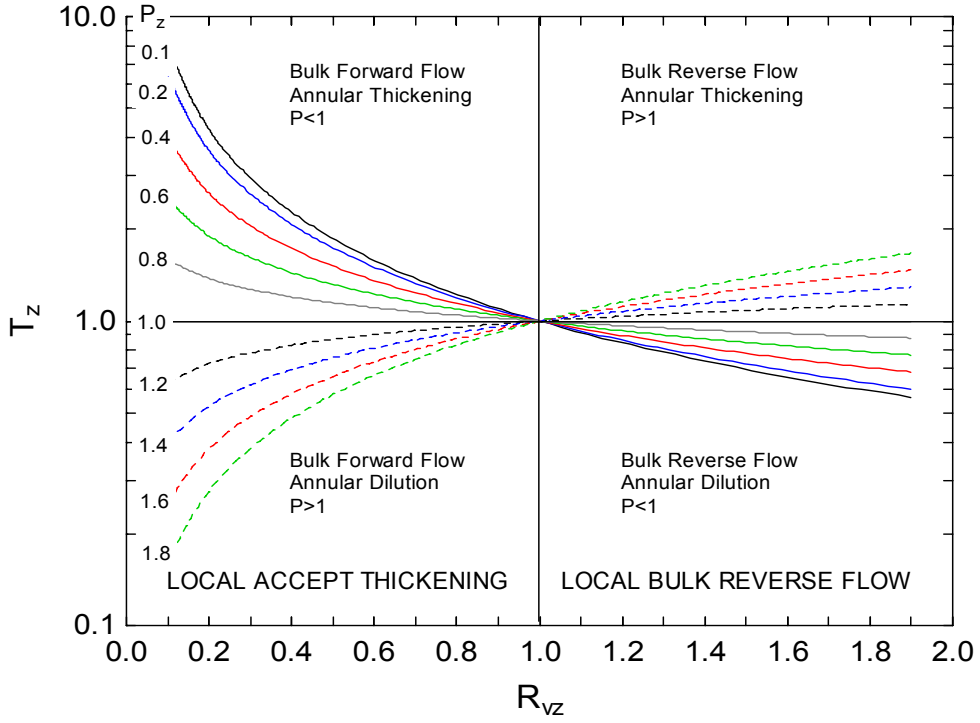

Figure 4-20 Local reject thickening curves as a function of local reject rate with the different regions shown

4.3 Passage Ratio

The local passage ratio P_z can be calculated using axial consistency data and Equation 4-14. The bulk passage ratio (Equation 4-15) is also indicated on the plot. Local passage ratio was calculated using data obtained for all rotors tested and is presented

in Figure 4-21, Figure 4-22, and Figure 4-23 for the step, bump, and foil rotors respectively.

$$P_z = \frac{C_{az}}{C_z} \qquad \textbf{4-14}$$

$$P_{bulk} = \frac{C_a}{C_f} \qquad \textbf{4-15}$$

Passage ratio decreased along the length of screen in all cases tested. This is consistent with the findings of Weeds (2006) who found that passage ratio decreased along the screen length as a narrow screen section was moved toward the rear of the screen (data shown in Figure 2-45). Although the situation of a narrow screen section is different to that of a full screen, it demonstrates that there is a position effect and that the passage ratio is affected by screen position.

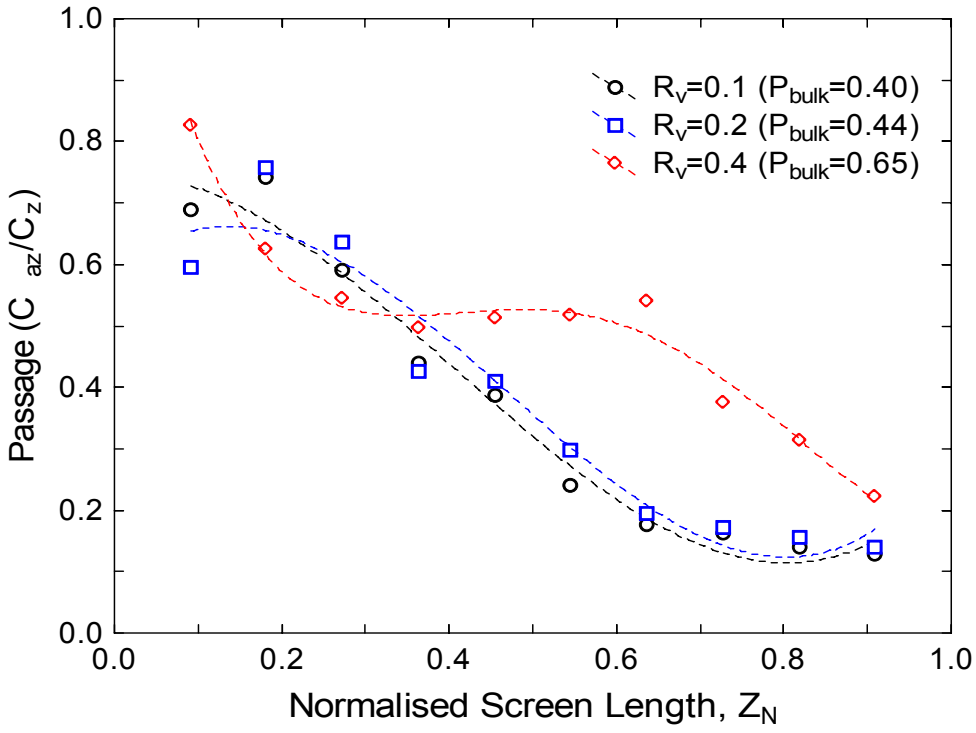

Figure 4-21 Localised passage ratio changes along the screen length for the step rotor at a range of reject rates ($\bar{u}_s$=0.6 m/s, C_f=0.14 %, u_{tip}=28 m/s)

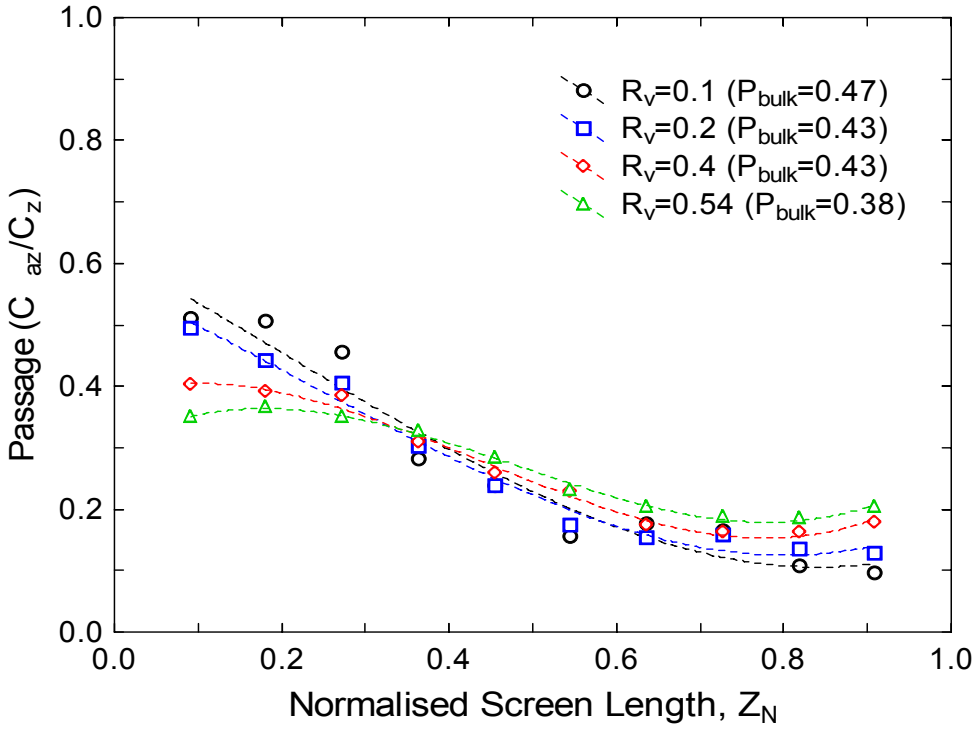

Figure 4-22 Localised passage ratio changes along the screen length for the bump rotor at a range of reject rates ($\bar{u}_s$=0.6 m/s, C_f=0.14 %, u_{tip}=28 m/s)

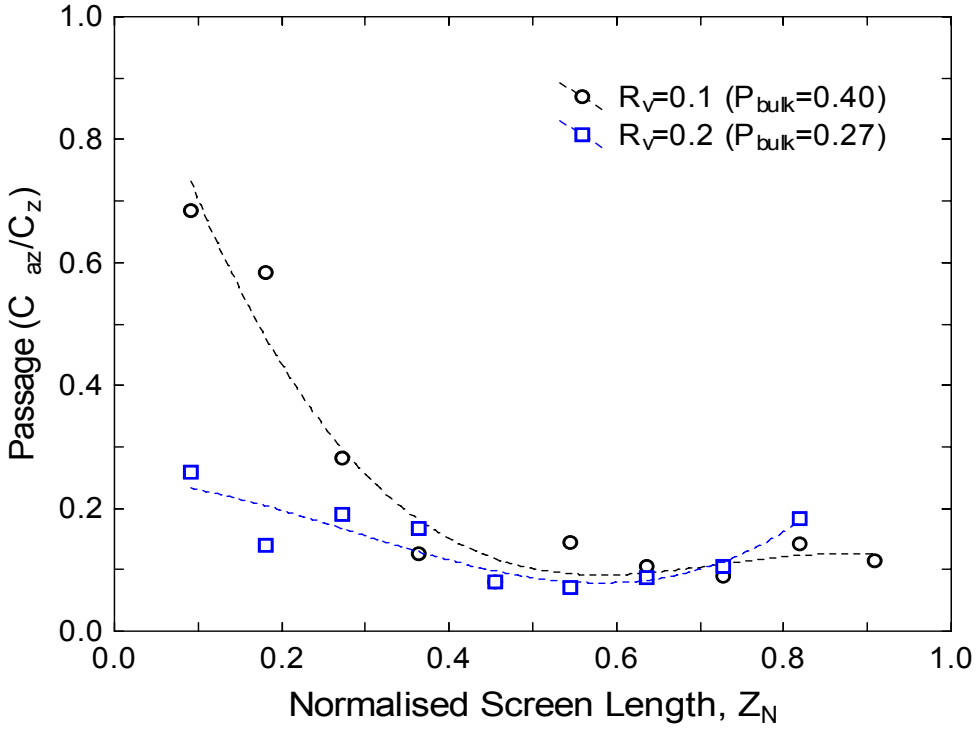

Figure 4-23 Localised passage ratio changes along the screen length for the foil rotor at a range of reject rates ($\bar{u}_s$=0.6 m/s, C_f=0.15 %, u_{tip}=14 m/s)

Passage data for each rotor at similar feed consistencies and aperture velocity is compared in Figure 4-24. Despite the bump and step rotors having similar bulk passage ratios the passage at the front of the screen was considerable lower for the bump rotor than the step. This may be because the step rotor has a much larger and longer reverse pulse, which in turn gives larger amounts of reverse flow, especially at the front of the screen. Larger amounts of reverse flow will alter the mixing in the annulus and encourage the passage of fibre by promoting floc and network disruption.

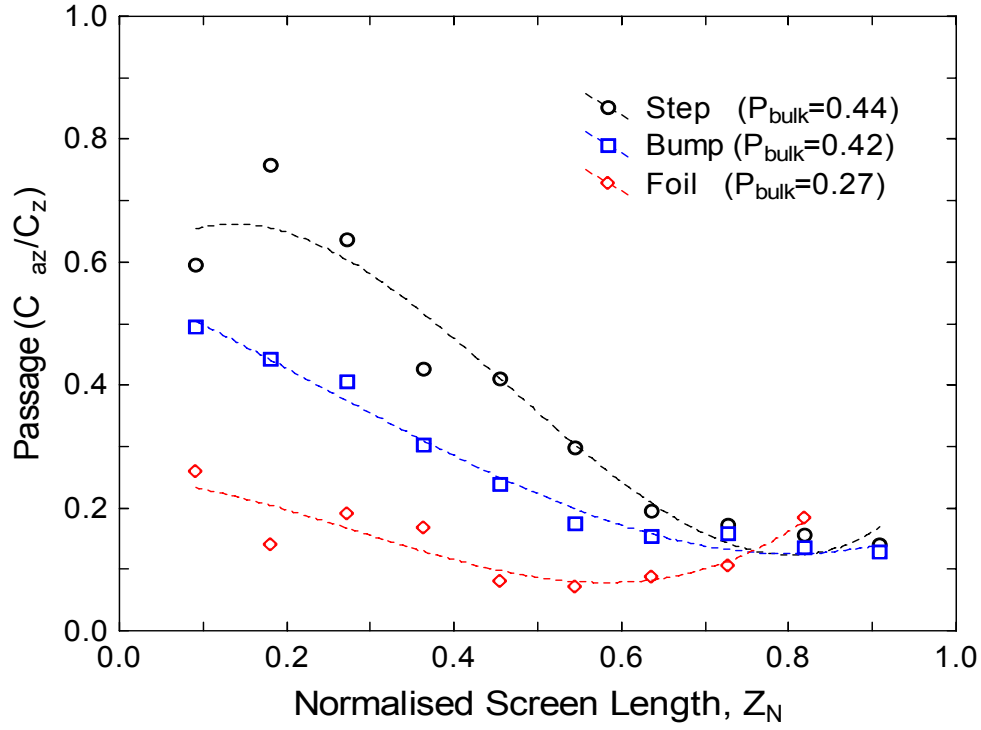

Figure 4-24 Localised passage ratio changes along the screen length for the step, bump & foil rotors at R_v=0.2 (Step & bump: $\bar{u}_s$=0.6 m/s, C_f=0.14 %, u_{tip}=28 m/s) (Foil: $\bar{u}_s$=0.6 m/s, C_f=0.15 %, u_{tip}=14 m/s)

At the higher feed consistency the passage ratio was much less variable along the screen length than at the lower consistency as illustrated in Figure 4-25 and Figure 4-26 for the step and bump rotors respectively. The passage ratio towards the end of the screen was similar to that at the lower feed consistency however the passage at the front of the screen was much lower. This lower passage at the beginning of the screen resulted in a lower bulk passage ratio for the two rotors. The bulk passage ratio of the bump rotor was much more affected by the increase in feed consistency than the step which compares well to the findings of Weeds (2006).

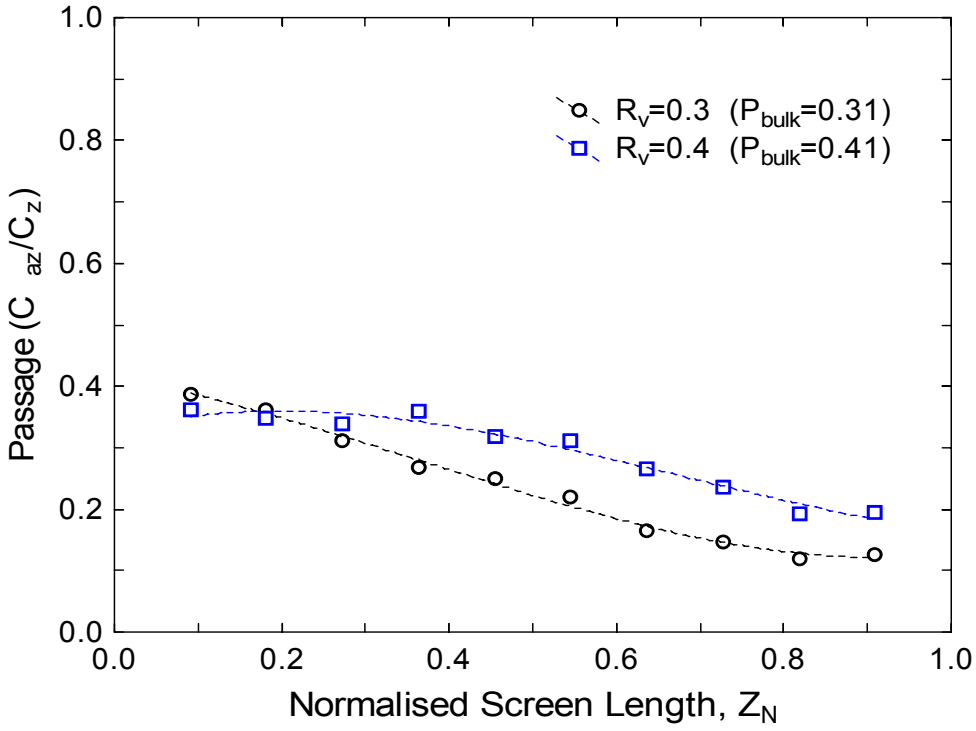

Figure 4-25 Localised passage ratio changes along the screen length for the step rotor at a range of reject rates ($\bar{u}_s$=0.6 m/s, C_f=1.0 %, u_{tip}=28 m/s)

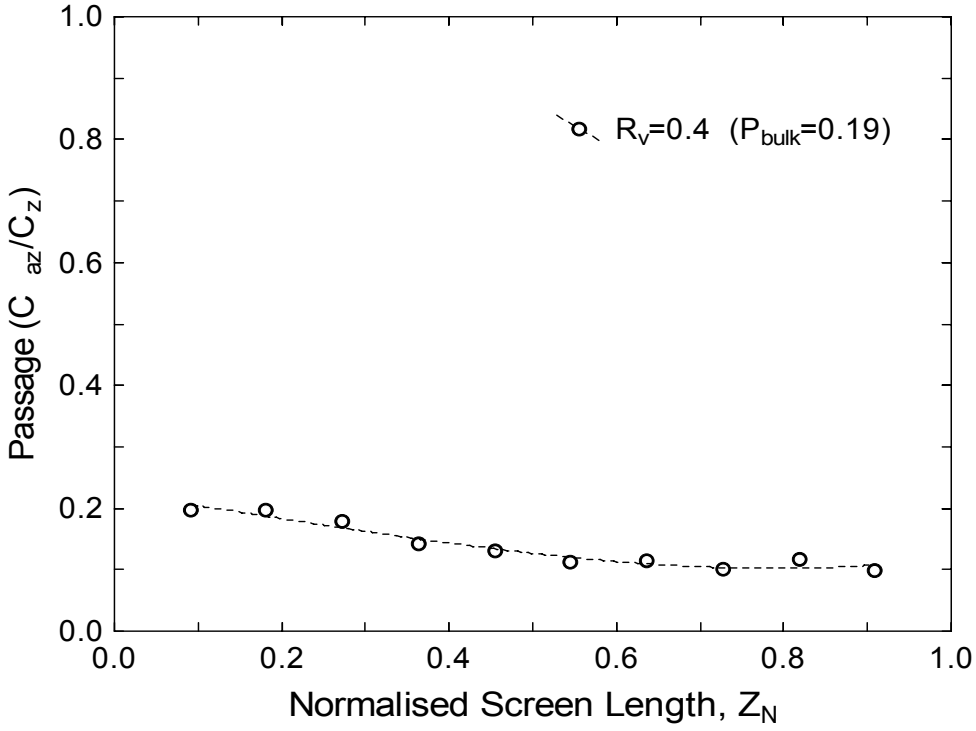

Figure 4-26 Localised passage ratio changes along the screen length for the bump rotor ($\bar{u}_s$=0.6 m/s, C_f=1.0 %, u_{tip}=28 m/s)

Local passage ratio also decreased at all positions along the screen length as the rotor speed was decreased from 28 to 17 m/s as shown in Figure 4-27, Figure 4-28, and Figure 4-29 for the step, bump and foil rotors respectively. For the step and bump rotors there was a large difference in the bulk passage between the two rotor speeds which was not surprising as there was approximately a 15 % difference in the overall thickening factor. The passage ratio also decreased along the screen length and the curve shifted down as the rotor speed decreased. There was much less variation between the two rotor speeds for the foil rotor. It is postulated that the decrease in variation is due to the fact that the foil is an open rotor and the mean tangential velocity and mixing in the annulus will be markedly different for an open style rotor such as the foil. Moreover increased rotor speed for an open style rotor is unlikely to increase the mean tangential velocity to the same extent as a closed rotor.

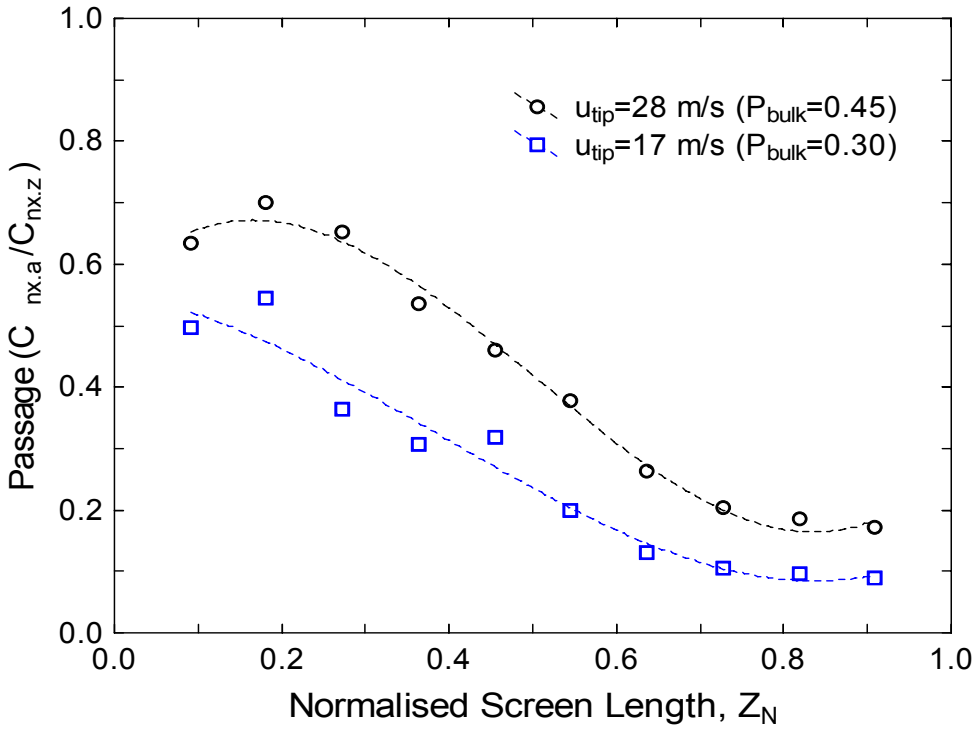

Figure 4-27 Localised passage ratio changes along the screen length for the step rotor at R_v=0.2 for two different rotor speeds ($\bar{u}_s$=0.3 m/s, C_f=0.16 %)

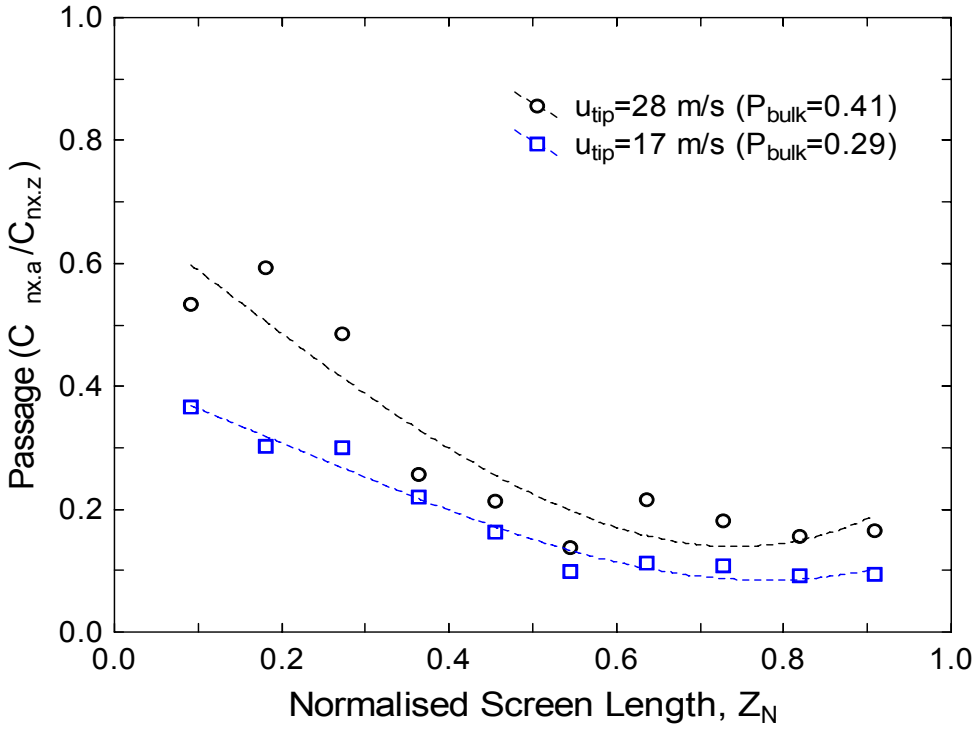

Figure 4-28 Localised passage ratio changes along the screen length for the bump rotor at R_v=0.2 for two different rotor speeds ($\bar{u}_s$=0.3 m/s, C_f=0.12 %)

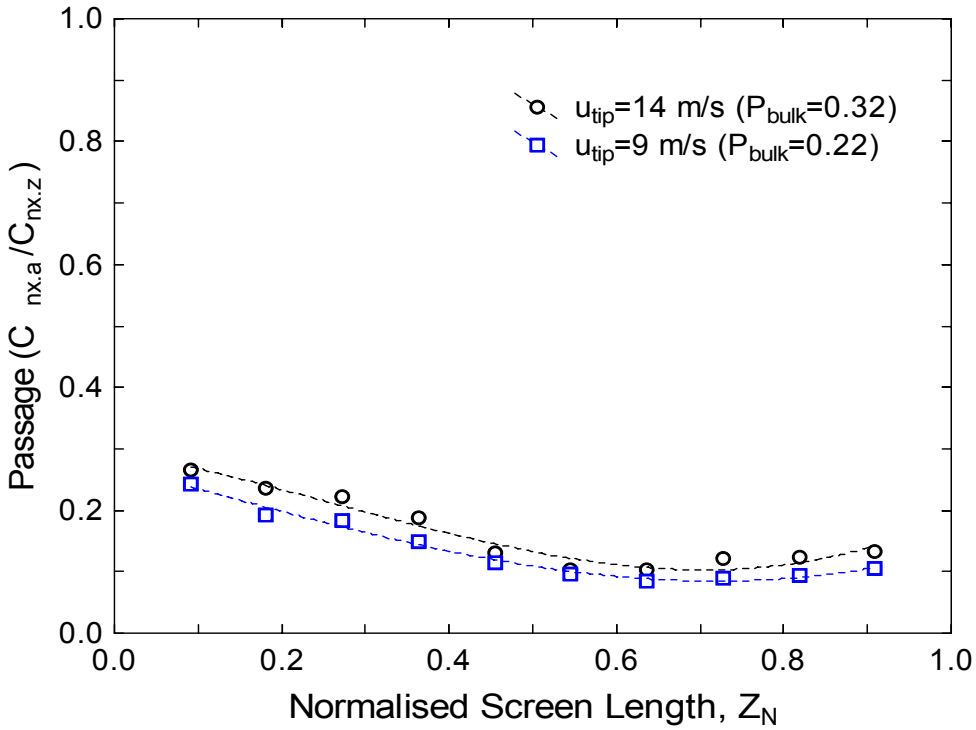

Figure 4-29 Localised passage ratio changes along the screen length for the foil rotor at R_v=0.2 for two different rotor speeds ($\bar{u}_s$=0.3 m/s, C_f=0.12 %)

Weeds (2006) found a complex relationship between feed consistency and passage ratio which was also rotor dependant. It seems reasonable to conclude that the decrease in passage ratio is in part due to the increase in consistency along the screen annulus. An examination of feed consistency versus passage ratio data presented in Figure 2-47 shows that in region 2 for the step or bump rotor, that for a reject thickening factor equal to 2 the decrease in passage ratio due to the thickening of the pulp alone would be approximately 0.048. The measured decrease in passage ratio was substantially greater than this value and therefore implies that the increase in consistency has only a minor influence on the passage ratio along the screen length. Other factors beside increased consistency need to be considered as possible causes of the decrease in passage ratio along the screen length.

The cause of decreasing passage ratio along the screen length is a complex and multifaceted one and it is proposed that a position effect is the cause of the decrease in passage ratio. This position effect is comprised of two factors: a) changes in suspension properties (flocculation and consistency effects), and b) changes in flow conditions (flow and rotor effects). Both of these factors will be discussed in greater detail in Section 4.5. However due to the variable nature of the pressure within the screen it is also reasonable to expect the local accept flow rate to also vary with screen position.

4.3.1 Fibre Length and Passage Ratio

Fibre consistency for each length fraction C_{nx} was expressed as the number of fibres per unit volume of suspension where the subscript n denotes that a number consistency is used and x denotes the desired fraction. This number consistency is used in the calculation of passage ratios of the different length fractions described in Section 3.3.5. The passage ratio for each fibre length fraction P_{nx} was calculated by taking the ratio of the consistency of the fibre length fraction in the accepts $C_{nx.a}$ and the consistency of the fibre length fraction in the feed annulus $C_{nx.z}$ (Equation 4-16).

$$P_{nx} = \frac{C_{nx.a}}{C_{nx.z}} \qquad \textbf{4-16}$$

The passage ratio for each fibre length fraction at different axial positions was calculated (Equation 4-16) and data obtained from fibre length analysis. Typical values are shown in Figure 4-30, Figure 4-31, Figure 4-32, and Figure 4-33 for the step, bump, and foil rotors respectively. The overall fibre length passage ratio curve is also shown in the figures. Usually only the overall fibre length passage ratio curve is reported and given as an indication of fractionation efficiency. The overall passage ratios of the short and long fractions are also indicated on the figures. As is consistent with all previous studies, passage decreased as fibre length increased, but also decreased as the axial position shifted toward the rear of the screen. The decrease in passage along the screen length for each length fraction is also consistent with the trends of decreasing overall passage shown in the previous figures and with the findings of Weeds (2006).

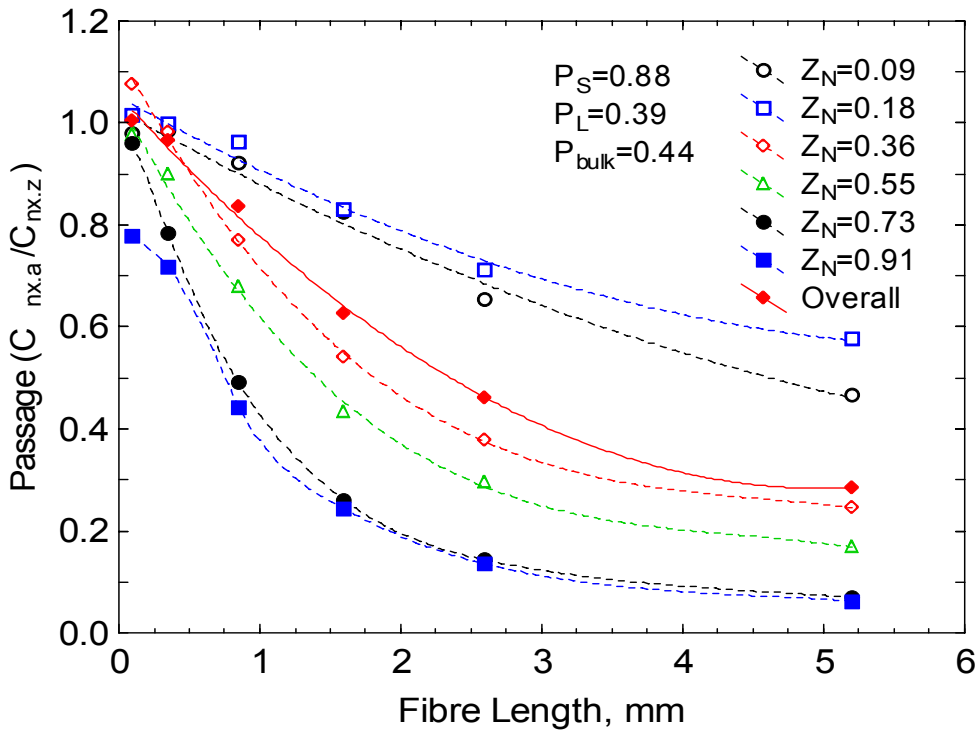

Figure 4-30 Passage ratio of individual fibre length fractions at axial locations along the screen length for the step rotor at R_v=0.2 ($\bar{u}_s$=0.6 m/s, C_f=0.14 %, u_{tip}=28 m/s)

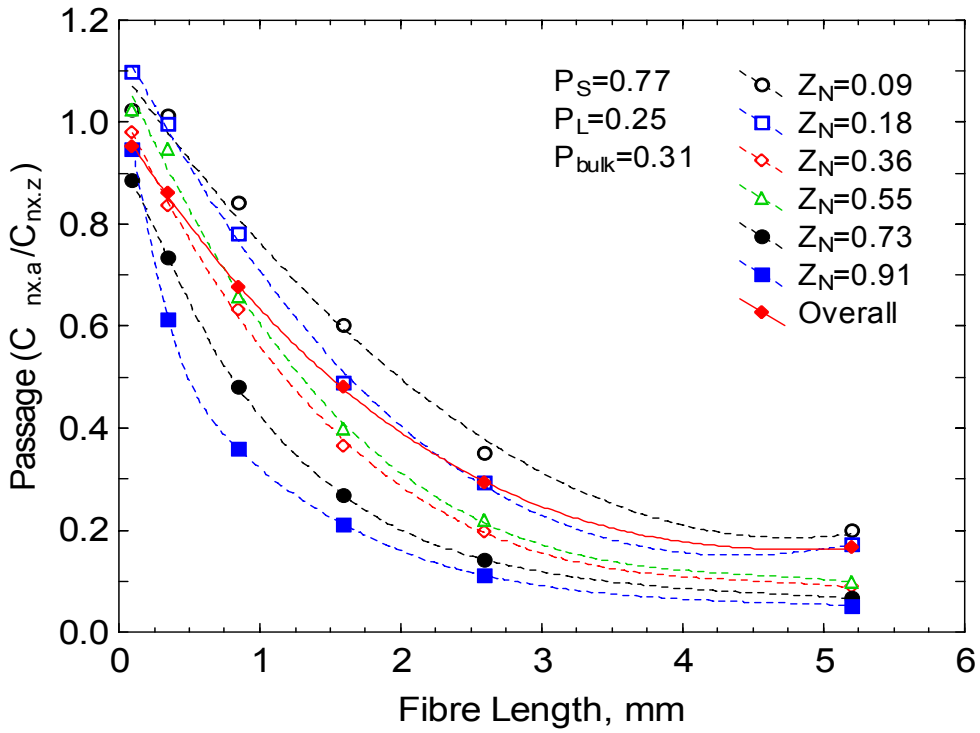

Figure 4-31 Passage ratio of individual fibre length fractions at axial locations along the screen length for the step rotor at R_v=0.3 ($\bar{u}_s$=0.6 m/s, C_f=1.03 %, u_{tip}=28 m/s)

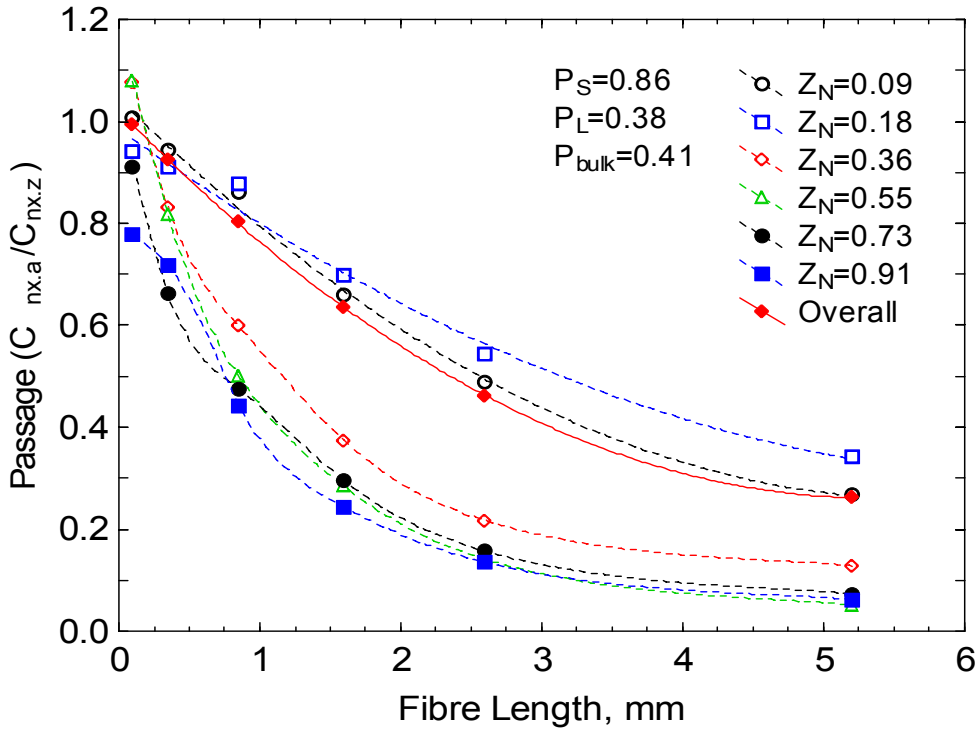

Figure 4-32 Passage ratio of individual fibre length fractions at axial locations along the screen length for the bump rotor at R_v=0.2 ($\bar{u}_s$=0.3 m/s, C_f=0.13 %, u_{tip}=28 m/s)

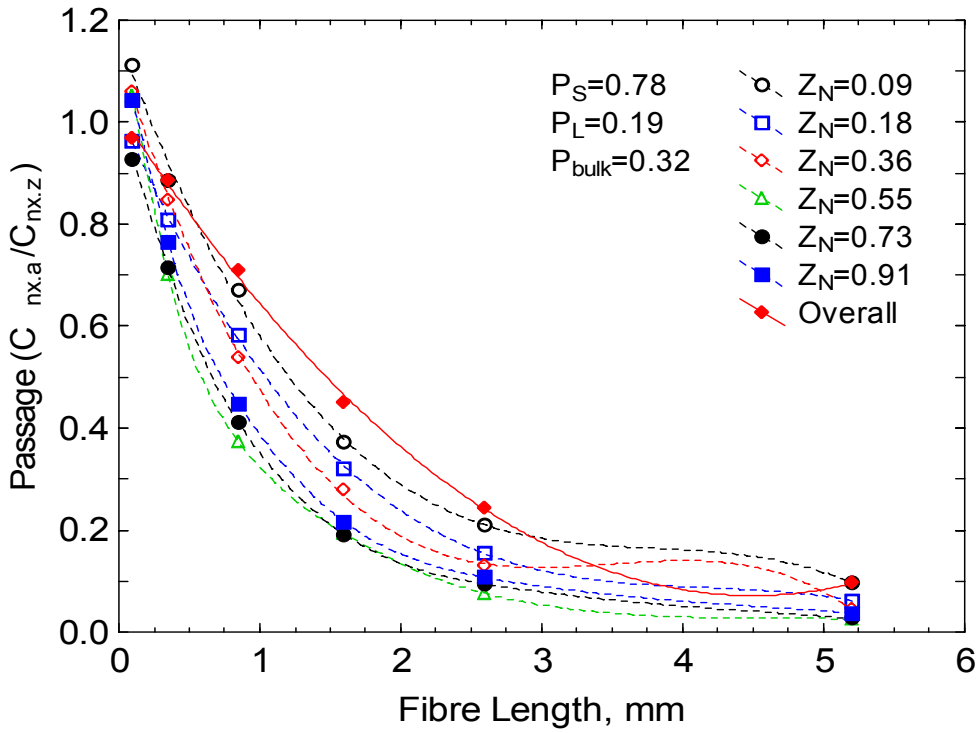

Figure 4-33 Passage ratio of individual fibre length fractions at axial locations along the screen length for the foil rotor at R_v=0.2 ($\bar{u}_s$=0.3 m/s, C_f=0.12 %, u_{tip}=14 m/s)

As can be seen from the previous figures the fines fraction (< 0.2 mm) have a passage approximately equal to one along the entire length of the screen, while the passage of the other length classes is higher at the front of the screen compared to the back. This was expected because the same trend occurred for the localised bulk passage ratio. As fibre length is the dominant fibre property affecting passage, the passage ratio decreases as the fibre length increases (Karnis, 1997; Olson & Kerekes, 1998a; Atkins, 2003; Jokinen, Karjalainen et al., 2007). However as shown in the figures above there is also a position effect which also has a major effect on the passage of different fibre length fractions. The middle fractions from 0.2 to about 2 mm showed the greatest variation in passage with screen length.

The passage ratios of the short and long fibre fractions are useful to illustrate the marked difference in passage between these two fractions. In order to examine the fibre length fractionation efficiency changes along the screen length the passage ratio of the short fibre fraction P_S (Equation 4-17) and long fibre fraction P_L (Equation 4-18) were calculated. The short fibre fraction included all length classes up to 2 mm and the long fibre fraction from 2 to 7.2 mm.

$$P_S = \frac{C_{S.a}}{C_{S.z}} \qquad \textbf{4-17}$$

$$P_L = \frac{C_{L.a}}{C_{L.z}} \qquad \textbf{4-18}$$

The passage ratio of both fractions for the step rotor at both feed consistencies decreased along the screen length as shown in Figure 4-34. As expected the short fibre fraction had a much higher passage ratio than the long fibre fraction. The passage of the short fibre was similar for both feed consistencies while the passage of the long fibre was much higher at the feed lower consistency especially over the front section of the screen. There was much less variation in the passage of the long fibre fraction over the length of the screen and the lower bulk passage ratio at the higher consistency is attributed to the low passage ratio of the long fibre fraction. This indicates that at elevated consistencies flocculation becomes an increasingly important factor in determining the passage of fibre fractions and the overall fibre passage ratio.

The passage of short and long fibre fractions for the bump and foil rotors are shown in Figure 4-35. The bump and step rotor had a similar passage of both short and long fibre (see Figure 4-34) while the foil rotor had a much lower passage of long fibre than the other two rotors. Moreover there was relatively little change in the passage ratio of the long fibre fraction over the length of the screen with the foil rotor.

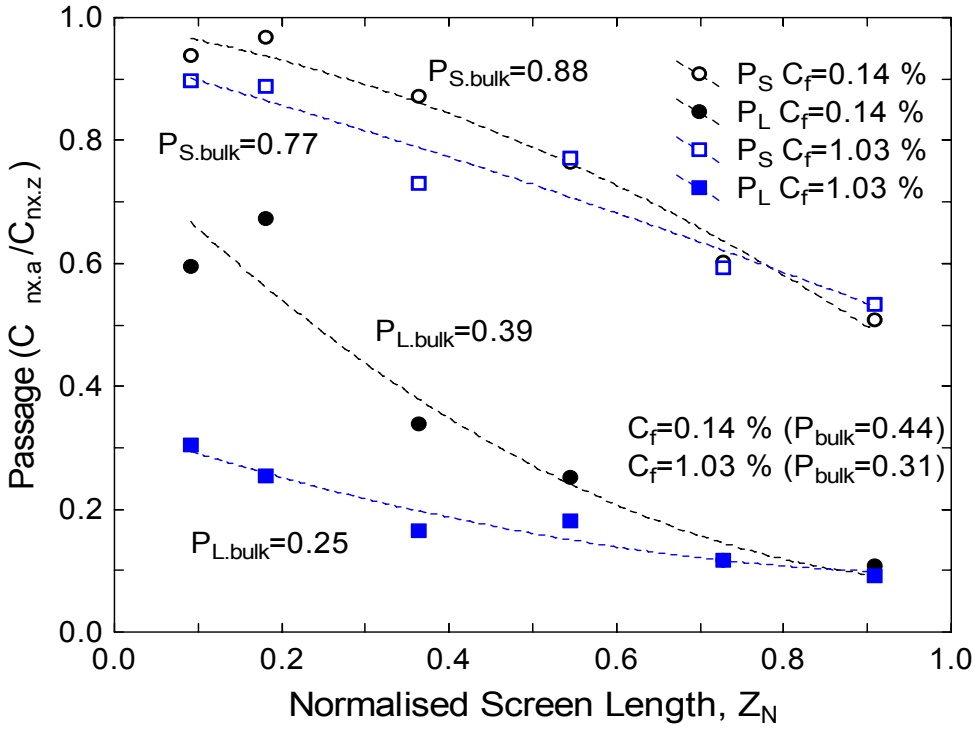

Figure 4-34 Passage ratio for step rotor for the long and short fibre length fractions, C_f=0.14 % at R_v=0.2 and C_f=1.03 % at R_v=0.3 ($\bar{u}_s$=0.6 m/s, u_{tip}=28 m/s)

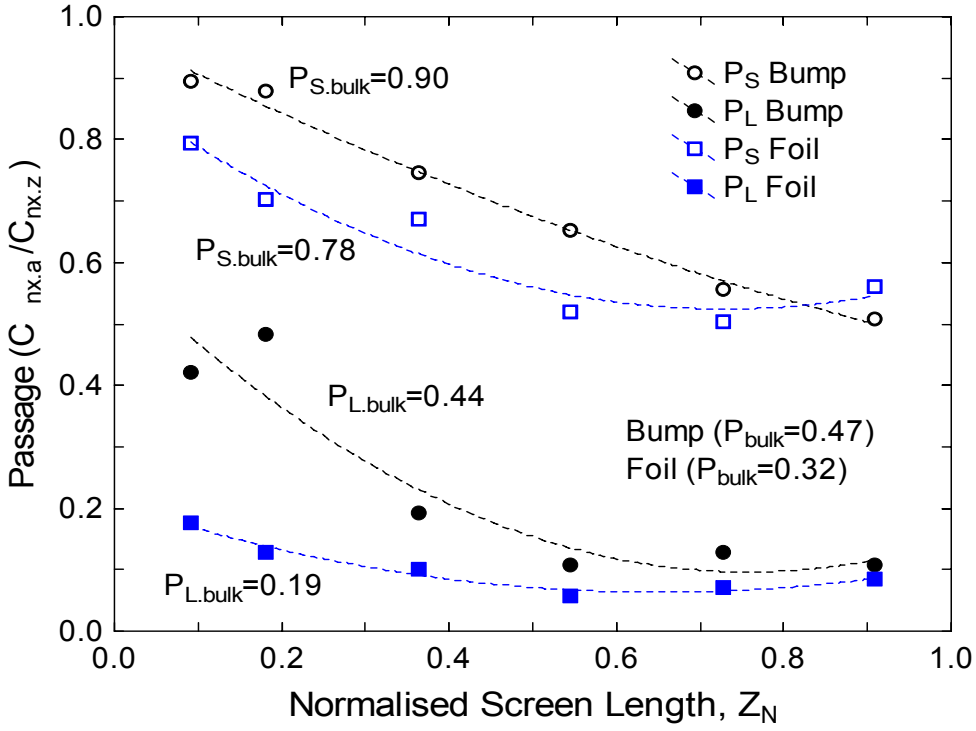

Figure 4-35 Passage ratio for bump and foil rotors for the long and short fibre length fractions (C_f=0.12 %, R_v=0.2, $\bar{u}_s$=0.3 m/s, Bump u_{tip}=28 m/s; Foil u_{tip}=14 m/s)

A decrease in tip speed from 28 to 17 m/s, for the step rotor, affected the passage of the long fraction much more than the short fraction as illustrated in Figure 4-36. The overall passage of the short fraction was unchanged while the long fraction had a large decrease in passage as the tip speed was altered. The passage of both short and long fibre fractions decreased as the rotor speed was decreased for the bump and foil rotors as shown in Figure 4-37 and Figure 4-38 respectively.

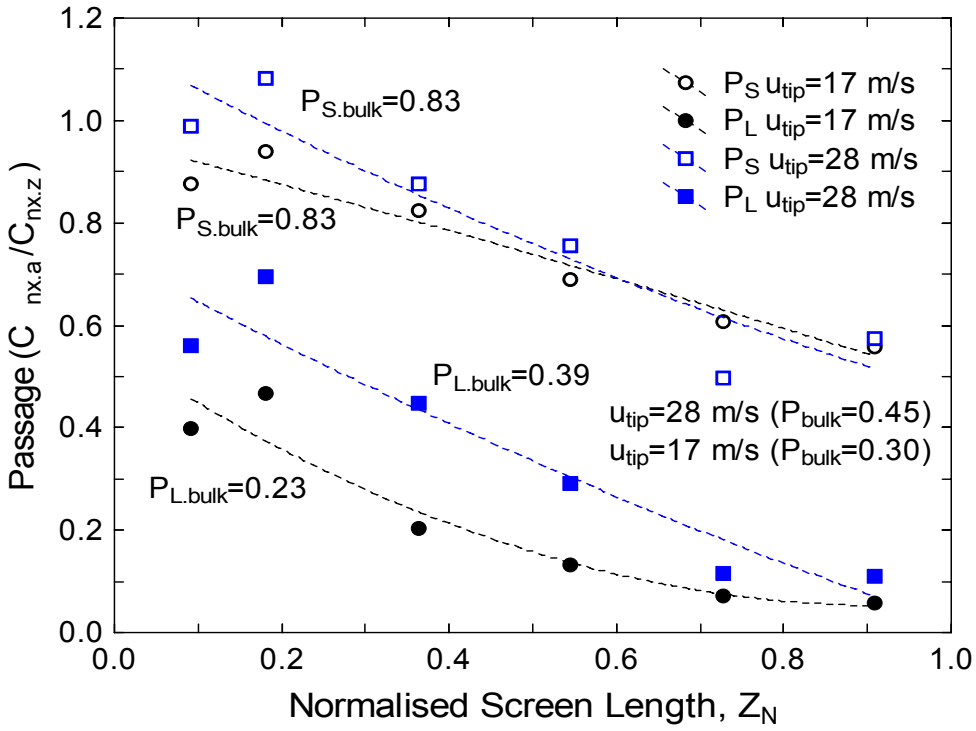

Figure 4-36 Passage ratio for step rotor for the long and short fibre length fractions at two rotor speeds (R_v=0.2, $\bar{u}_s$=0.3 m/s, C_f=0.16 %)

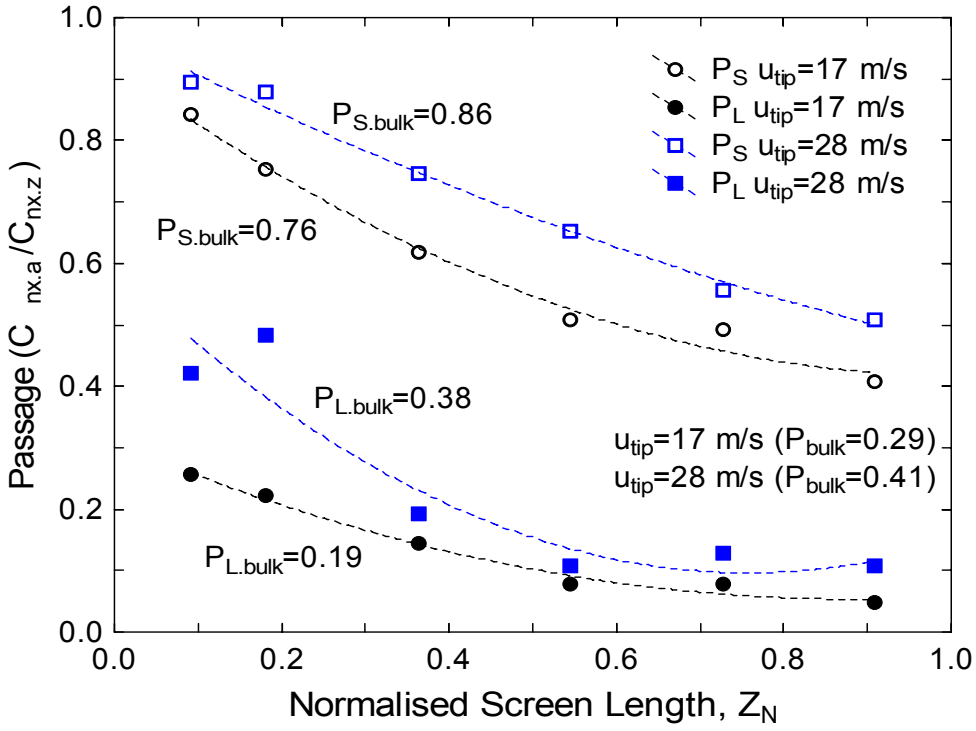

Figure 4-37 Passage ratio for bump rotor for the long and short fibre length fractions at two rotor speeds (R_v=0.2, $\bar{u}_s$=0.3 m/s, C_f=0.12 %)

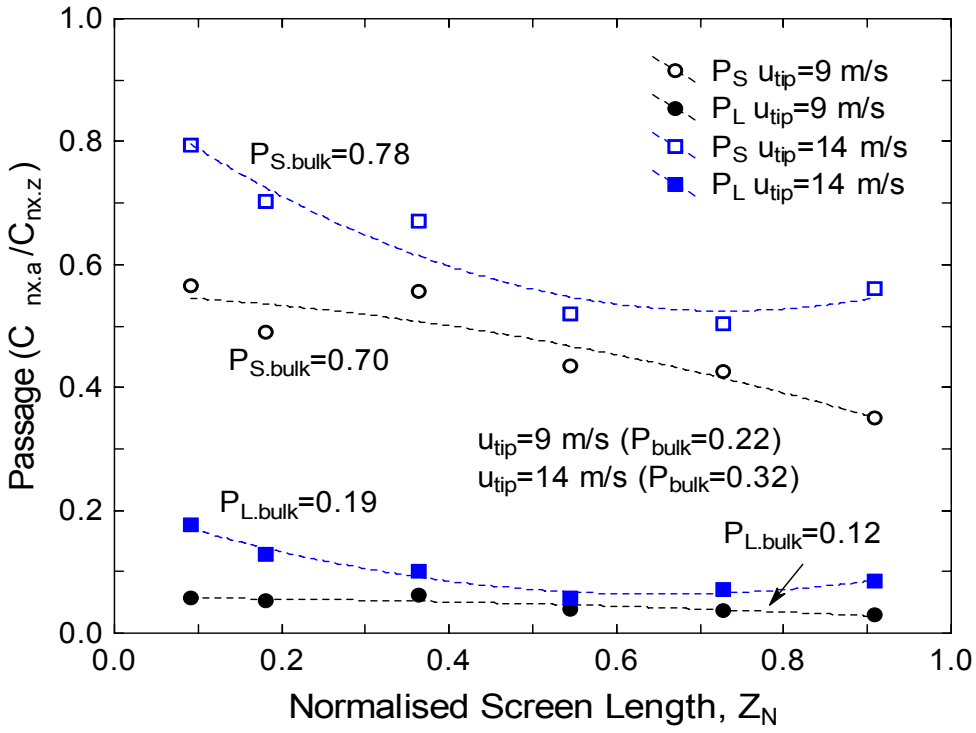

Figure 4-38 Passage ratio for foil rotor for the long and short fibre length fractions at two rotor speeds (R_v=0.2, $\bar{u}_s$=0.3 m/s, C_f=0.12 %)

As a result of the difference in passage ratio of the separate length fractions, long fibre becomes concentrated in the screen annulus as the suspension progresses along the screen. This in turn alters the average fibre length of the suspension. Figure 4-39 shows the localised average fibre length (length weighted average) for the entire screen length of the annulus and accept chamber for the step rotor. The length weighted average fibre length of the bulk accepts at both feed consistencies are shown by a horizontal line. The average length weighted fibre length of the bulk accepts is the value most often reported in the literature for indicating changes in fibre length due to fractionation. As illustrated in Figure 4-39 there is some variation in the local fibre length in the accept chamber. Similar trends of increasing average fibre length in the annulus and variability in the accept chamber were found for the other rotors and flow conditions although data is not presented here for sake of brevity.

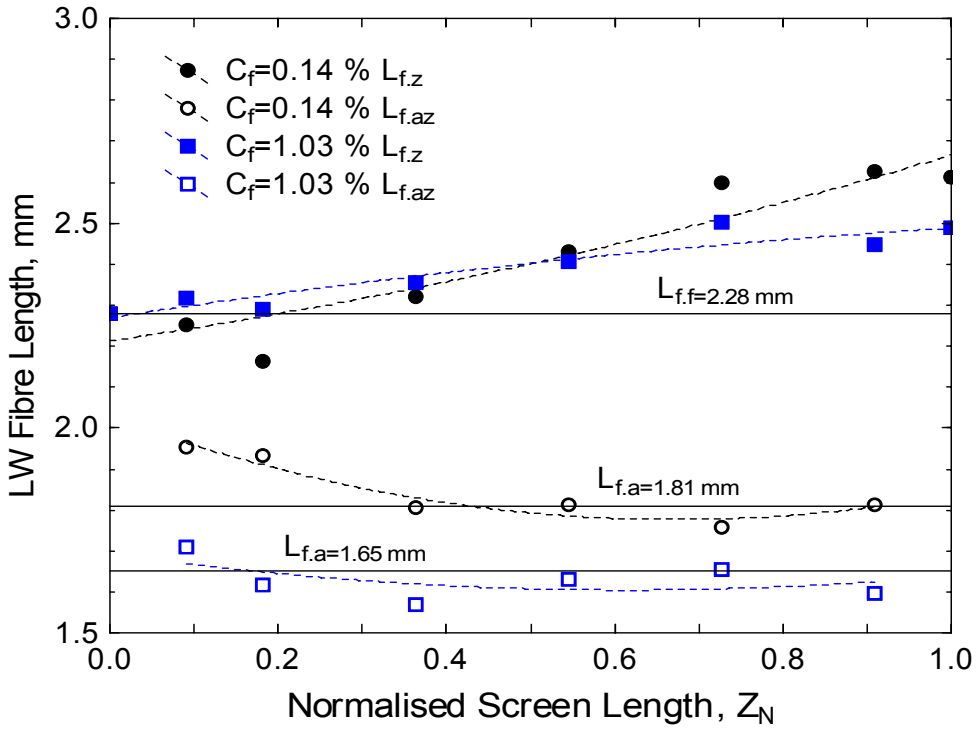

Figure 4-39 Average fibre length changes along the screen length for the step rotor, C_f=0.14 % at R_v=0.2 and C_f=1.03 % at R_v=0.3 ($\bar{u}_s$=0.6 m/s, u_{tip}=28 m/s)

4.4 Fractionation Efficiency

As demonstrated previously in Section 4.3.1 fibre passage decreases as fibre length increases and follows a roughly negative exponential curve. Olson et al. (2000) has modelled this relationship (Equation 4-19) and found that the fitted parameter lambda λ was a useful measure for characterising the relationship between passage ratio and fibre length. The parameter β was found to be equal to 1 for holed screens and 0.5 for slotted screens.

$$P(L_f) = e^{-\left(\frac{L_f}{\lambda}\right)^{\beta}} \qquad \textbf{4-19}$$

The parameter λ was calculated for each of the passage versus fibre length curves shown in Figure 4-30, Figure 4-31, Figure 4-32, and Figure 4-33 and plotted as a function of screen length in Figure 4-40 for the step rotor at both feed consistencies and Figure 4-41 for the bump and foil rotors. In Figure 4-40 it is evident that for the first part of the screen at the lower consistency λ was much greater. This is because the passage of the long fibre was much greater over the initial part of the screen as illustrated in Figure 4-34 which causes the λ value to be greater than it otherwise would be. Decreased rotor speed had the expected effect in that λ decreased over the screen length as illustrated in Figure 4-42. A decrease in λ indicates a decrease the average passage ratio of both the short and long fibre fractions. However the decrease in the average passage ratio of the long fibre fraction is much greater than for the short fraction.

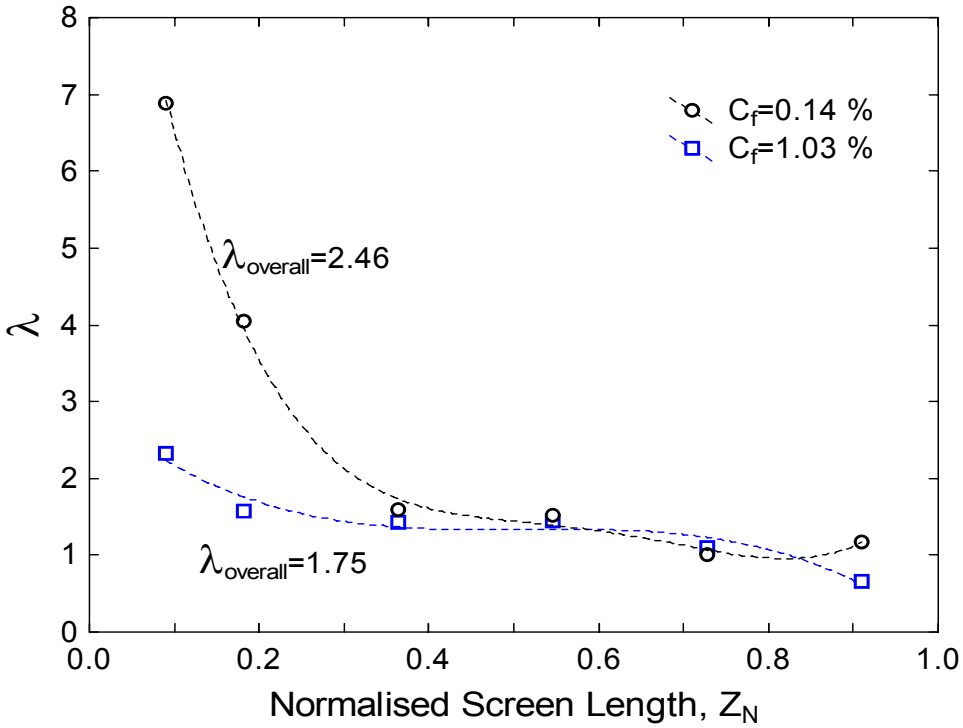

Figure 4-40 Change in parameter λ along the screen length the step rotor, C_f=0.14 % at R_v=0.2 and C_f=1.03 % at R_v=0.3 ($\bar{u}_s$=0.6 m/s, u_{tip}=28 m/s)

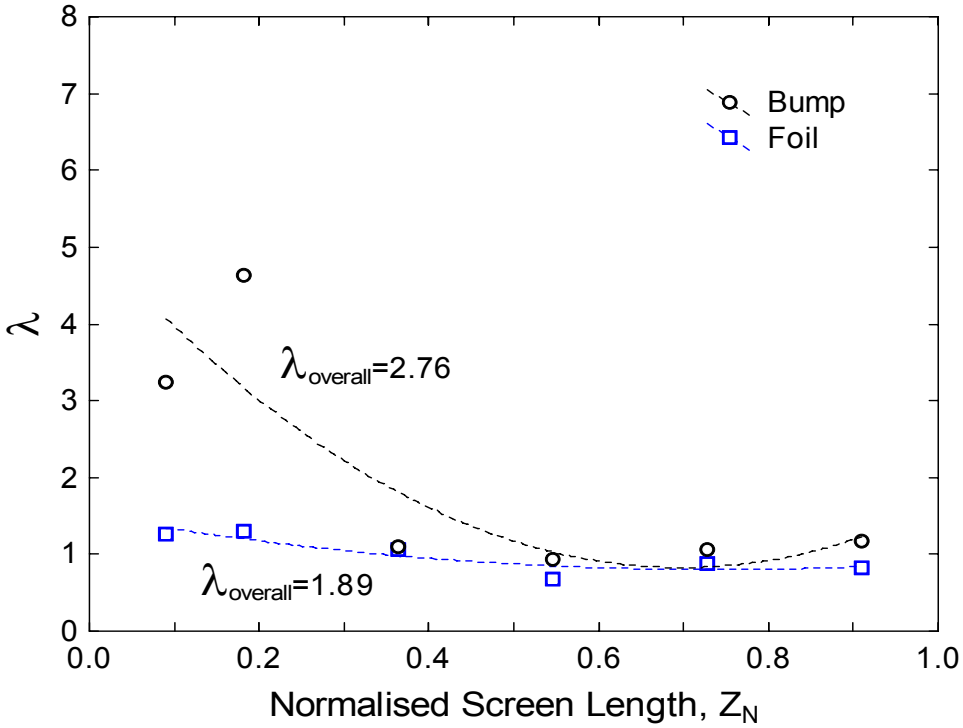

Figure 4-41 Change in parameter λ along the screen length for the bump and foil rotors (C_f=0.12 %, R_v=0.2, $\bar{u}_s$=0.3 m/s, Bump u_{tip}=28 m/s; Foil u_{tip}=14 m/s)

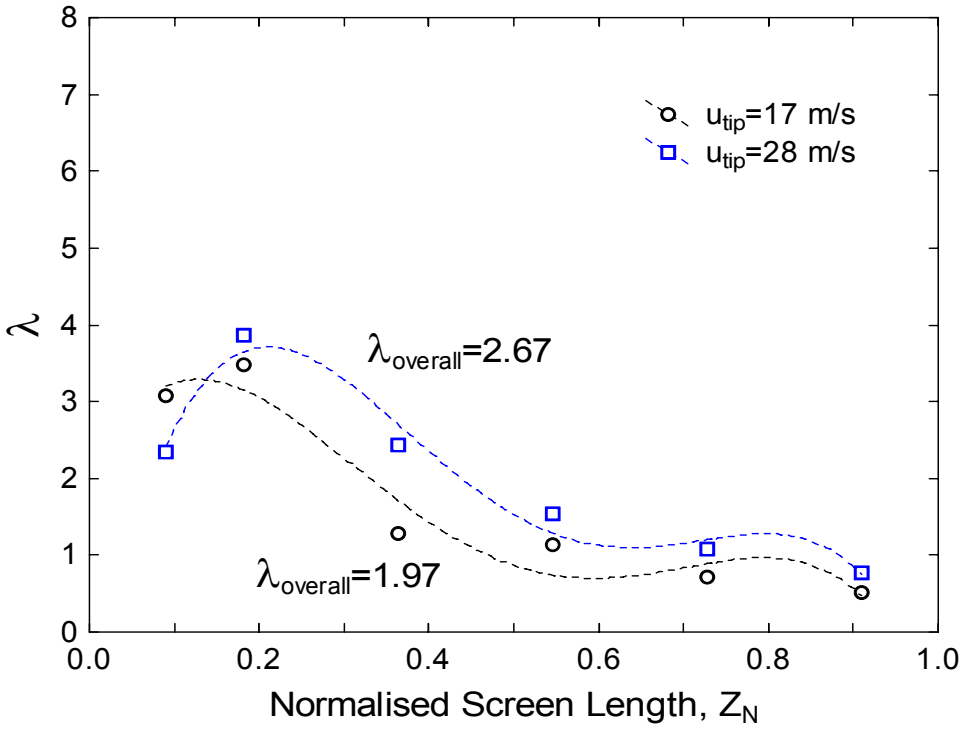

Figure 4-42 Change in parameter λ along the screen length step rotor for two different rotor speeds at R_v=0.2 ($\bar{u}_s$=0.3 m/s, C_f=0.16)

Weeds (2006) extended the work of Olson et al. (2000) and related λ to the fractionation index Φ (Equation 4-20) and demonstrated that for a given volumetric reject rate the fractionation index reached a maximum when λ was approximately equal to one. The maximum value varied slightly with reject rate but when λ was less than one the fractionation index reduced considerably. This reduction is due to the fact that the fractionation index aims to penalise the rejection of short fibre and when λ is less than one the amount of short fibre being rejected increases significantly. Another explanation is that when λ is equal to one, the difference between the passage ratio of short fibre and long fibre fractions is the greatest. The aim in future screen design for length fractionation is to optimise the screen so that at the desired reject rate and the λ over the entire screen length is as close to the optimum value, unity, as possible.

$$\Phi = R_v^{P_L} - R_v^{P_S} \qquad \textbf{4-20}$$

The passage of both long and short fibre fractions were used to calculate the local separation ratio α_z (Equation 4-21), the overall separation ratio α (Equation 4-22), and the overall fractionation index Φ (Equation 4-20). Axial variations in fractionation efficiency were expressed using the separation ratio because other commonly used measures of fractionation efficiency use volumetric reject rate as part of the calculation. The local volumetric reject rate is unknown in the screen annulus and therefore the local fractionation index Φ_z cannot be calculated. The fractionation index is a useful measure as it aims to incorporate the mass flow of short and long fibre to both the accept and reject streams. It penalises the rejection of short fibre to the reject stream and the acceptance of long fibre into the accept stream (Olson, 2001a). Therefore a "perfect" fractionation device would separate all short fibre from the long fibre and would have a fractionation index equal to one.

$$\alpha_z = 1 - \frac{P_{Lz}}{P_{Sz}} \qquad \textbf{4-21}$$

$$\alpha = 1 - \frac{P_L}{P_S} \qquad \textbf{4-22}$$

The separation ratio increased along the length of the screen for the step rotor at both feed consistencies as shown in Figure 4-43. The separation ratio was greater for the higher feed consistency although the variation along the screen length was much less. The overall separation ratio is shown by a horizontal line for each case in addition to the fractionation index which is also indicated in the figure. The separation ratio for the bump and foil rotor is shown in Figure 4-44 and illustrates that the separation ratio was much steadier for the foil rotor than the bump rotor. Moreover the overall separation ratio and fractionation index was higher for the foil rotor than both the step and bump rotors.

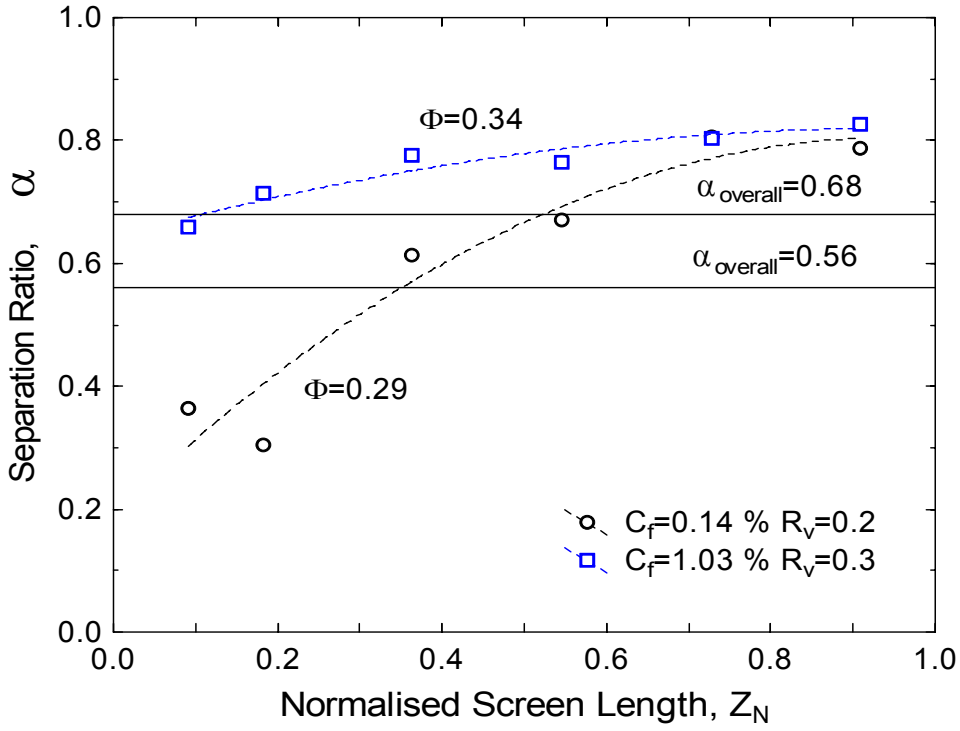

Figure 4-43 Separation ratio changes along the screen length for the step rotor, C_f=0.14 % at R_v=0.2 and C_f=1.03 % at R_v=0.3 ($\bar{u}_s$=0.6 m/s, u_{tip}=28 m/s)

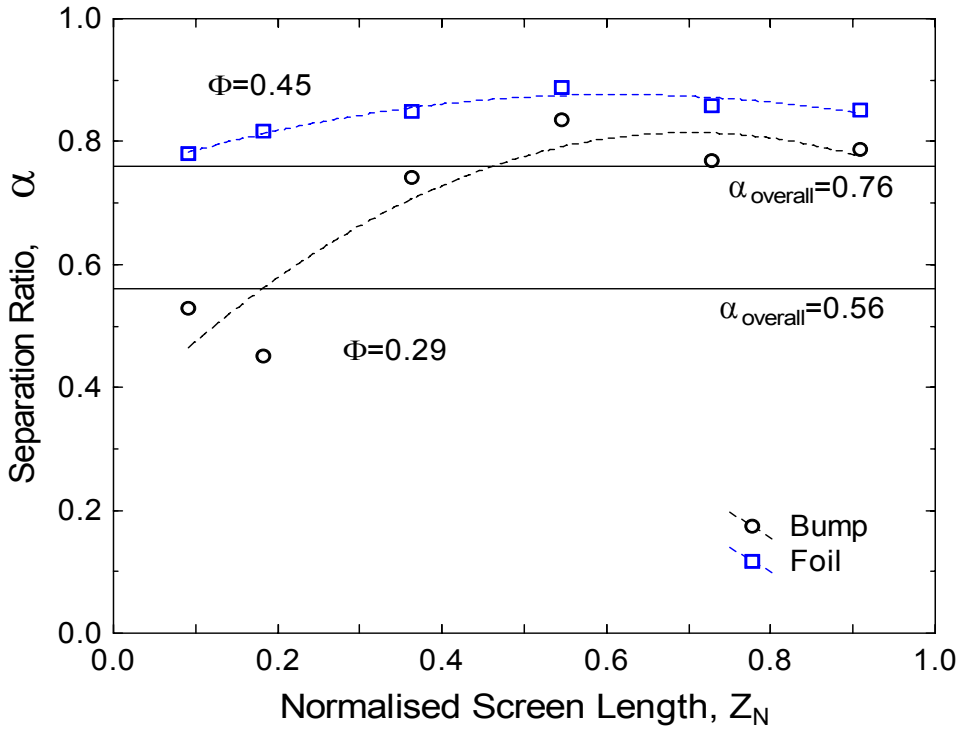

Figure 4-44 Separation ratio changes along the screen length for the bump and foil rotors at R_v=0.2 (C_f=0.12 %, $\bar{u}_s$=0.3 m/s, bump u_{tip}=28 m/s, Foil u_{tip}=14 m/s)

Decreasing the rotor speed caused the separation ratio to increase along the screen length for the step and foil rotors as shown Figure 4-45 and Figure 4-46 respectively. The fractionation index also increased as the rotor speed was decreased with a substantial increase (60 %) for the step rotor. This is a significant increase and it must also be noted that there was only a very small increase in the thickening factor when the rotor speed was decreased. While other researchers have studied to some extent the effect of rotor speed on fractionation efficiency, the fractionation index has only been used by a few. Those that have used fractionation efficiency have not examined the effect of rotor speed making direct comparison not possible. As discussed previously, it seems that there is an optimal rotor speed in order to maximise fractionation efficiency. Other authors have implied that there exists an optimal rotor speed for fractionation although they have not examined fractionation directly (Ämmälä, 2004). Small changes in the rotor speed can maximise the fractionation efficiency and long fibre removal, and minimise energy usage by decreasing rotor power with only a slight change in the reject thickening factor.

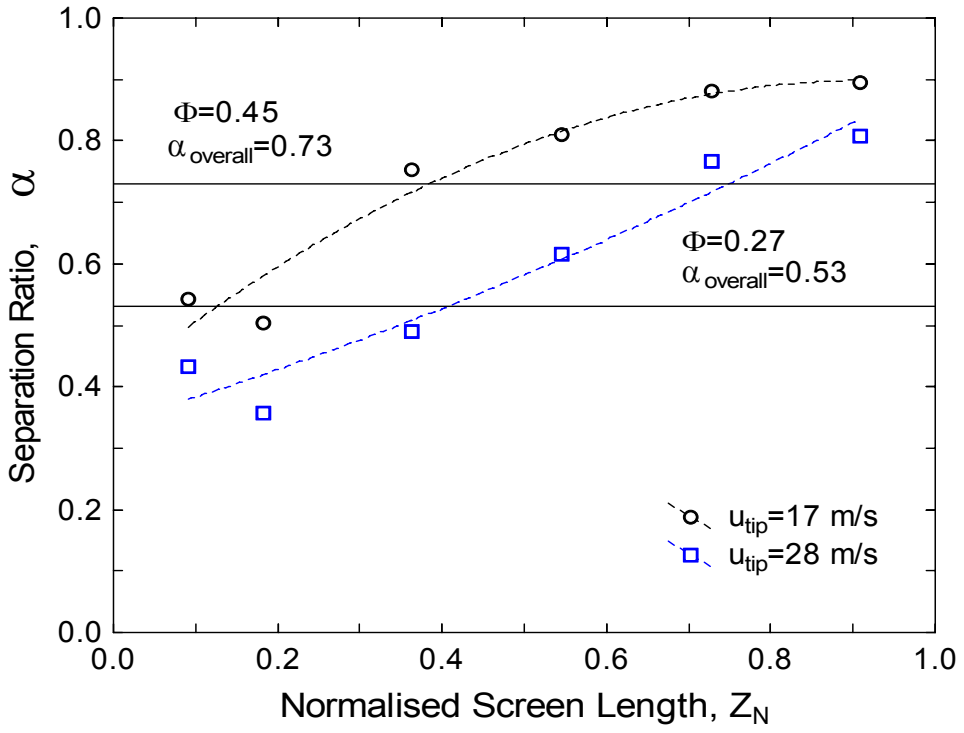

Figure 4-45 Separation ratio changes along the screen length for the step rotor at R_v=0.2 for two different rotor speeds ($\bar{u}_s$=0.3 m/s, C_f=0.16 %)

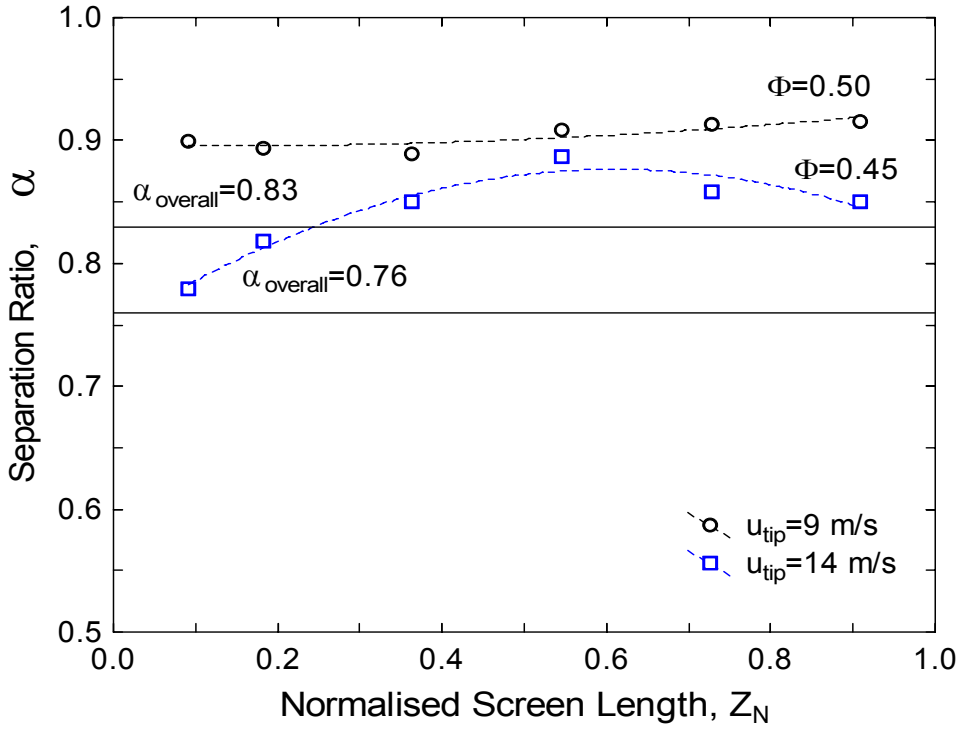

Figure 4-46 Separation ratio changes along the screen length for the foil rotor at R_v=0.2 for two different rotor speeds ($\bar{u}_s$=0.3 m/s, C_f=0.12 %)

Differences in the screening performance along the screen length can be exploited by partitioning the screen or accept chamber into multiple sections. If the efficiency of the sections is known then more efficient use of the fibres can be used. A very clean, short fibre fraction can be taken directly from an accept chamber located toward the rear of the screen due to the very low absolute long fibre passage ratio.

Fractionation efficiency has been shown to increase with reject thickening (Ämmälä, 2001) although the actual mechanism behind this relationship remains unclear. The increase in fractionation efficiency could be due to a number of factors. As demonstrated in this chapter as pulp travels along the annulus the consistency and average fibre length of the pulp in the annulus increases. Fractionation efficiency will increase if the difference in the passage of short and long fibre increases. An important question that remains unanswered is, will an increase in long fibre content (i.e. an increase in average fibre length) for a given consistency increase the fractionation efficiency, or put simply, is fractionation efficiency dependant on long fibre content and consistency?

The passage of a given fibre length fraction is generally assumed to be independent of the fibre length distribution of the furnish. More explicitly the presence of long fibre is not expected to adversely affect the passage of short fibre. There has been no specific experimental research conducted examining the affect of furnish fibre length distribution on fibre passage, although Jokinen, Karjalainen et al. (2007) found that the furnish type affected the passage versus fibre length curves. It would be expected that if the presence of long fibre adversely affected the passage of shorter fibre that furnishes with longer average fibre lengths would have a lower overall passage fibre length curve. Data presented in Jokinen, Karjalainen et al. (2007) of fibre passage versus fibre length for several furnishes was taken and the λ calculated for each furnish and the λ value as a function of the length weighted fibre length of each furnish is presented in Figure 4-47. It is evident that taken as a whole the data suggests a moderate relationship between long fibre content and fibre passage.

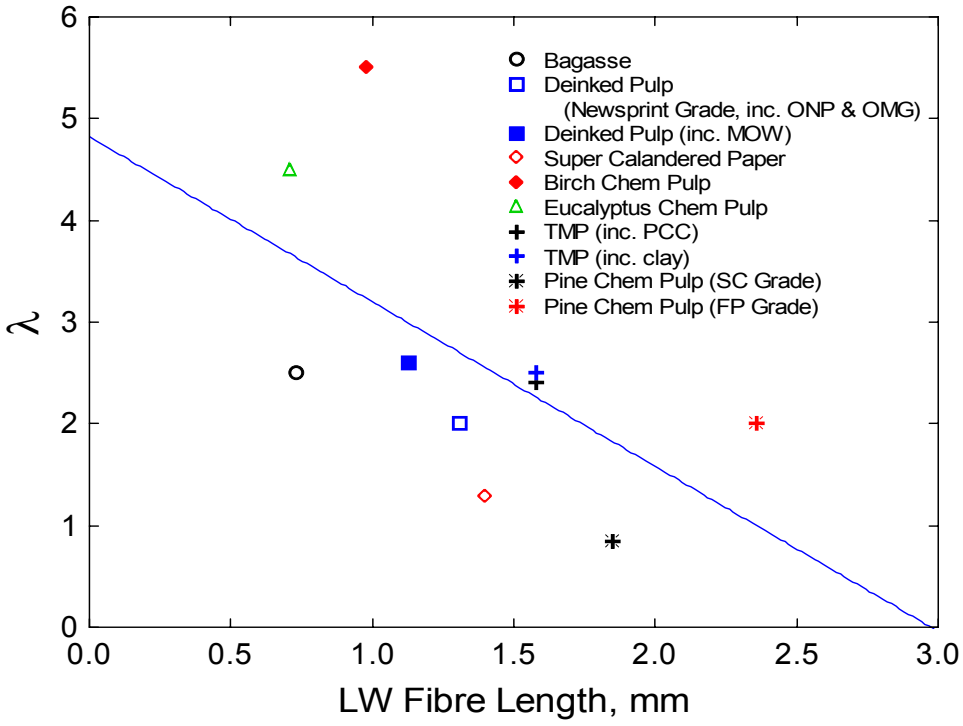

Figure 4-47 λ as a function of length weighted fibre length for several furnishes for reworked data from Jokinen, Karjalainen et al. (2007)

Increased long fibre content will increase the tendency of the furnish to flocculate (Kerekes & Schell, 1992; 1995) and this can be expressed as a crowding number. The crowding number as a function of screen length for the step rotor is shown in

Figure 4-48 for the consistency profiles shown in Figure 4-2 and Figure 4-6 and the average fibre lengths in Figure 4-39. A crowding number of 60 is indicated by the solid horizontal line in the figure and if the crowding number is above this value, fibres are considered to be in constant contact with other fibres. If there is no shear stress on the suspension, a continuous network is considered to be formed at a crowding number of 60.

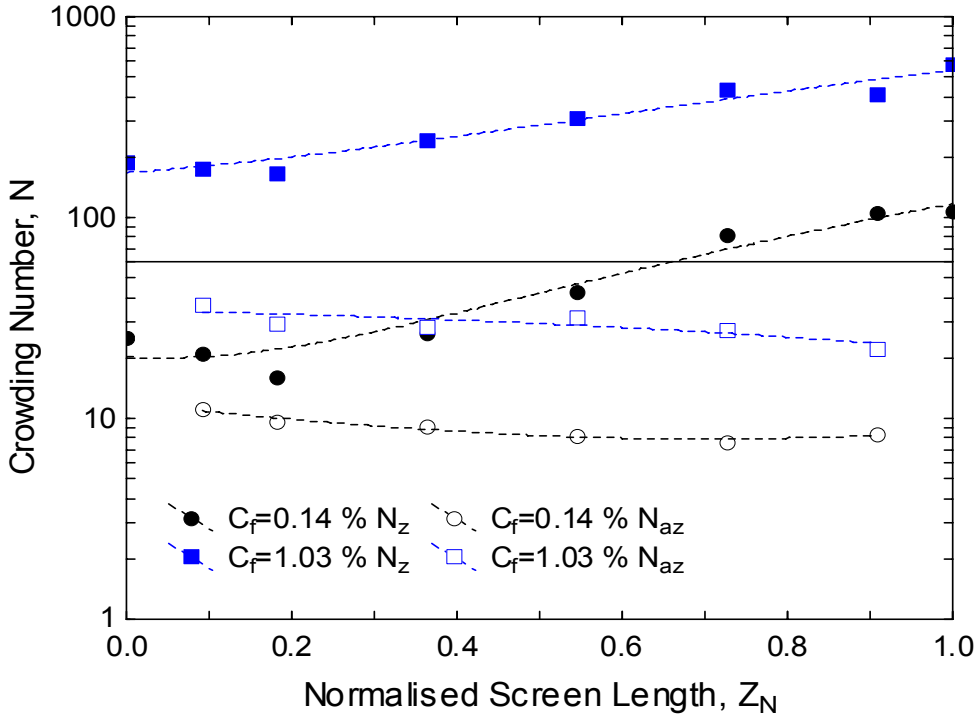

Figure 4-48 Crowding number along the screen length for the step rotor C_f=0.14 % at R_v=0.2 and C_f=1.03 % at R_v=0.3 ($\bar{u}_s$=0.6 m/s, u_{tip}=28 m/s)

The crowding number in the screen annulus was above 60 for the high consistency case and increased from around 200 up to about 600 at the reject end of the screen. The lower consistency case saw the crowding number increase from around 25 at the beginning of the screen up to just over 100 at the rejects. Crowding number on the accept side was less than 60 for both cases and was fairly constant along the screen length indicating little variation in the accept chamber. For the higher feed consistency situation, fibre-fibre interactions are increasingly important toward the rear of the screen and fibres are considered to be in continuous contact with each other for the entire residence time of the suspension in the screen annulus.

Increased long fibre content is expected to increase the tendency of the furnish to flocculate and this should cause more short fibre to become entrapped in a floc and therefore reduce the chances of that short fibre passing through the aperture. If this is correct then an interesting exercise would be to increase the flocculation of the fibre in the annulus to increase to fractionation efficiency. In reality capacity and fractionation efficiency are usually competing factors and an increase in one will lead to a decrease in the other.

4.5 The Position Effect

As previously noted in Section 4.3, the decrease in the passage ratio with screen length is due to a position effect which is comprised of two factors: a) changes in the suspension properties (flocculation effects), and b) changes in the flow conditions (flow & rotor effects). Weeds (2006) has shown using narrow screen sections, that bulk passage of a narrow section decreased as the section was moved toward the rear of the screen. He also discounted a screen specific entry effect as the cause of the reduction by reversing the axial direction through the screen (i.e. made the rejects end the feed end and visa versa). The same decrease in passage along the screen length was found. One of the limitations of using narrow screen sections is that the trends may not generalise to a full-length screen. However in light of the data presented in this section it seems that the trend of decreasing passage with screen length does apply for a full-length screen.

As the suspension travels in the axial direction along the screen, long fibre tends to become more concentrated and the average fibre length in the annulus as well as the crowding number increases. This increase in crowding number will therefore alter the suspension properties and rheology. Properties such as floc size, floc density, rupture strength, and disruptive shear stress would all be expected to increase with increased fibre length (Andersson, 1961; Duffy & Titchener, 1975; Kerekes, 1983b; Kerekes et al., 1985; Beghello & Akademi, 1988; Kerekes & Schell, 1995; Dodson, 1996). Increased flocculation is likely to have an adverse affect on fibre passage (Figure 4-47), although it may have a positive impact on fractionation (Ämmälä, 2001). As fibre length and consistency increase, longer fibre will more likely become

mechanically entangled, less likely to be freed from the peripheral of the floc and therefore more readily rejected.

The state of flocculation of the suspension will not only depend on the suspension properties such as fibre length, consistency, and coarseness, but also on the flow conditions present such as shear stress, velocity, and nature of the turbulence present (Kerekes, 1979; 1983b; Kerekes et al., 1985). The results presented in this chapter show that at 1 % feed consistency, long fibre passage was fairly constant along the length of the screen. The constant low passage ratio for the long fibre fraction with screen length at 1 % implies that ability of long fibre to pass through an aperture is severely restricted by increased fibre-fibre interactions and flocculation.

Even though increased flocculation is expected to decrease fibre passage, this may only occur if the size and properties of the floc inhibit floc extrusion. Photographic and modelling studies have been carried out into the passage of stickies or visco-elastic contaminants found in recycled pulp (Julien Saint Amand et al., 2005). It was shown both experimentally and using CFD and Finite Element Analysis that stickies larger than the slot width could be extruded through the slot if the hydrodynamic forces on the particle were great enough. Although that work dealt exclusively with stickies, it is suggested here that a similar mechanism may also occur with fibre flocs.

As the stock enters the feed chamber it has a mean tangential velocity $\bar{u}_{tan}$ which is much less than the tip speed of the rotor. When the stock contacts the rotor it will accelerate due to the difference in the velocities. The stock will continue to accelerate as it travels along the screen until at some point along the screen it reaches a maximum $\bar{u}_{tan}$. The ratio of $\bar{u}_{tan}$ to u_{tip} is related to a parameter called the slip factor (Equation 4-23). The bulk tangential velocity in the annulus has been estimated to be about 15 % of the tip speed (i.e. γ=0.85) (Gooding, 1986), however this value has yet to be experimentally verified. This value was estimated from the velocity profile in the wake of a cylinder and it was thought that the velocity profile in the wake of a cylinder would be similar to that which occurred for a bump rotor. There has been no validation as to the accuracy of this value for the slip factor. It is also very likely that rotor geometry and the size of the annular gap will affect the slip factor. The velocity

profile in the annulus and along the screen length was modelled using CFD and the results are reported in Chapter 6.

$$\gamma = 1 - \frac{\overline{u}_{tan}}{u_{tip}} \qquad \textbf{4-23}$$

A changing tangential velocity will have a number of effects on the local behaviour of the screen. The level and intensity of the turbulence generated by the rotor will be altered which in turn will affect the flocculation and mixing of the suspension. Flocs readily form in decaying turbulence and can form in an extremely short time (Kerekes, 1983b; Arola et al., 1998). Moreover changes in the tangential velocity will also affect the flow field at individual apertures. It has been demonstrated by the numerous flow channel experiments that the flow field has a great influence on the passage of fibres through an aperture. The next two chapters report a detailed investigation into flow and rotor factors that influence the position or entrance effect.

4.6 Summary

Localised consistency was measured for various screening conditions and rotors. Overall the pulp thickened along the screen length, although it was found that under certain conditions pulp at the front of the screen annulus could become diluted so that the consistency was lower than the feed (annular dilution). A two passage ratio model was developed and established that annular dilution could occur under only one of two situations, localised accept thickening (i.e. $P_z > 1$), or local bulk reverse flow (i.e. $k > 1$). Screening performance parameters, such as fibre passage ratio and fractionation efficiency, were calculated using the consistency and fibre length analysis data and were found to be variable along the axial length of the screen. The overall passage ratio of the pulp and also of the fibre length fractions decreased along the screen length which conflicts the assumption of the plug flow model. The decrease in passage ratio along the screen length was attributed to a position effect which is comprised of two factors: a) changes in the suspension properties (flocculation effects), and b) changes in the flow conditions (flow & rotor effects). The flow and rotor effects are examined in greater detail in the next two chapters.

5 Pressure Pulsation in Pressure Screen

The pressure pulses of various rotors have received attention from numerous researchers, using experimental methods, numerical methods, or both (Javid, 1983; Karvinen & Halonen, 1984; Yu, 1994; Yu, Crossley et al., 1994; Gooding, 1996; Pietilä, 1996; Julien Saint Amand, 1997; Niinimäki, 1998; Wikstrom & Rasmuson, 1998; Julien Saint Amand & Perrin, 1999; Wikström & Fredriksson, 1999; Gonzalez, 2002; Pinon et al., 2003). The foil rotor has received the most interest with detailed experimental and numerical methods being employed in order to understand and optimise the key physical parameters and operating variables. Although this has been fairly successful in some respects, understanding the role the pressure pulse has in determining the reject thickening and fractionation efficiency of the screen has not been adequately examined. Differences in the magnitude and shape of the pressure pulse at different screen positions have been alluded to by early researchers (Yu, 1994; Yu, Crossley et al., 1994) but have not been investigated further. Weeds (2006) showed experimentally that the relationship between fibre passage and feed consistency is dependent on the type of rotor and the position within the screen where screening is occurring. He postulated that the difference in fibre passage behaviour can be explained by consideration of both the forward and reverse flows and fibre passage ratios.

The effect of screen position on the pressure pulse of two rotors, a solid core closed step rotor and an open type foil rotor, was investigated to elucidate the contribution the pulse has on screening performance. In the previous chapter screen fractionation performance was shown to vary along the screen and it was postulated that a difference in pressure pulse magnitude and changes in suspension characteristics were both probable causes. The pressure pulse was measured at two positions along the axial length of the screen using high speed pressure transducers and the affect of operating conditions (e.g. tip speed, reject rate etc) on the pulse was also examined. Pressure loss coefficients for the screen apertures in both the forward and reverse direction have also been determined experimentally. These results have been used with the pressure pulse data to estimate the instantaneous aperture velocities, which are then used to calculate the rotor back-flush ratio k which relates to screen

performance, as demonstrated by the two passage ratio model developed in the previous chapter. This chapter reports the findings of the experimental programme described above.

5.1 Pressure Pulses

The pressure pulse of the step and foil rotors were measured at various flow conditions and rotor speeds. The pulse for the bump rotor was not measured because the pressure transducers could only be mounted in set positions on the screen which unfortunately were not aligned sufficiently well with the bumps of the rotor to make a true measurement of the pulse. A typical pressure pulse of the step and foil rotor at a tip speed of 24 m/s and no accepts flow is shown in Figure 5-1 and Figure 5-2 respectively. The pulses have been rescaled by subtracting the time average pressure of the pulse from the measured pressure pulse data. This method of reporting rotor pulse data has been used by other researchers (Yu, 1994; Yu, Crossley et al., 1994; Gooding, 1996; Gonzalez, 2002; Pinon et al., 2003).

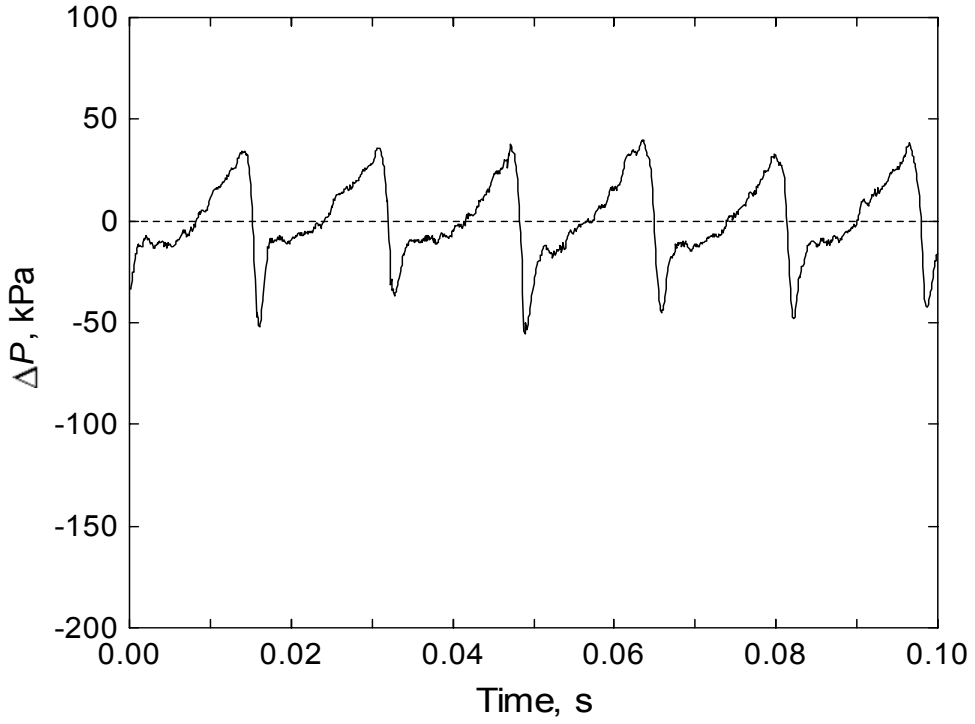

Figure 5-1 Measured pressure pulse for the step rotor at the front of the screen for water (Q_f=1000 L/min, R_v=1, u_{tip}=24 m/s)

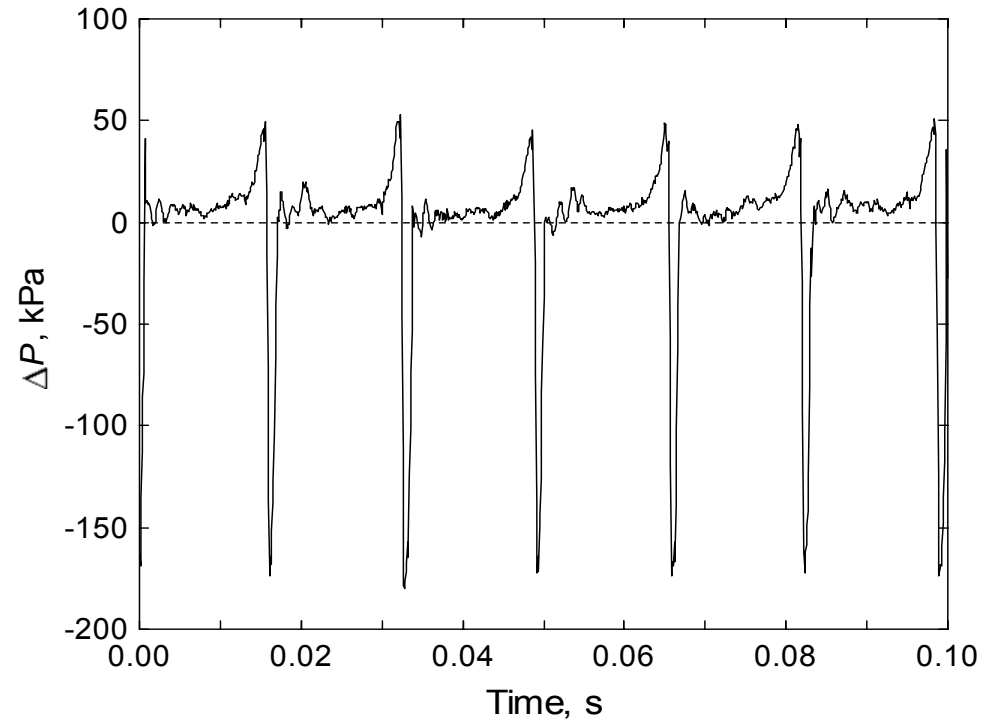

Figure 5-2 Measured pressure pulse for the foil rotor at the front of the screen for water (Q_a=500 L/min, R_v=0.6, u_{tip}=24 m/s)

The pressure decreases as the rotor element passes the aperture due to the reduction or constriction in area between the rotor element and the screen. The reduced area will increase the velocity and reduce the pressure according to the Bernoulli's equation (Karvinen & Halonen, 1984). The increase in velocity and reduction in pressure through a constriction is known as the Venturi effect. The difference in the velocity between the fluid or suspension and the rotor can be termed the relative velocity. The relative velocity (Equation 5-1) can be defined as the difference in the velocity between the tip speed and the mean tangential velocity divided by the tip speed. The relative velocity is equivalent to the slip factor γ.

$$\text{Relative Velocity} = \frac{u_{tip} - \bar{u}_{tan}}{u_{tip}} = \gamma \qquad \textbf{5-1}$$

The pulse of the step rotor exhibits a steady increase in pressure until a maximum before a rapid decrease in pressure to a maximum negative value. Directly after the maximum negative pressure occurs, there is a sharp increase in the pressure followed

by a steady increase once again up to the maximum positive pressure. The sharp increase in pressure directly following the maximum negative pressure has also been observed for the step rotor by Yu and was referred to as the "bounce back" phenomenon (Yu, 1994). The cause of the "bounce back" phenomenon was attributed to flow separation on the surface of the rotor and it was found that as the surface contour of the screen basket was increased the level of "bounce back" was decreased. Yu concludes that the "bounce back" effect has a significant affect on the pressure pulse although does not elaborate on the effect this will have on the performance of the rotor.

The step rotor is similar in concept to a forward-facing step and the flow relative to the step will be moving toward the face of the step and therefore the rotor is a forward-facing rather than a backward-facing step. The basic geometry of the forward-facing step is depicted in Figure 5-3. The flow separates in front of the face and creates a primary recirculation zone of length L_r which reattaches near the top of the face. A smaller separation bubble or secondary recirculation zone is formed on the downstream horizontal wall directly at the top of the step. The primary recirculation zone can be a closed recirculation zone or an open recirculation zone as depicted in (a) and (b) of Figure 5-3 respectively. The closed case only occurs for 2D flows and in reality the open recirculation zone occurs in 3D flow and as a result of continuity the entrained fluid is transported in along the face to the step before being released at some point along the step as in (c) of Figure 5-3.

It is usually assumed that for closed rotors, such as the step rotor, that minimal axial mixing occurs in the screen annulus. The suspension is thought of as travelling through the annulus in a linear fashion, thickening the further it gets toward the reject end of the screen. If the open type 3D separation occurs as illustrated in (c) of Figure 5-3 then there maybe a moderate degree of axial mixing that occurs in the annulus when using a step rotor.

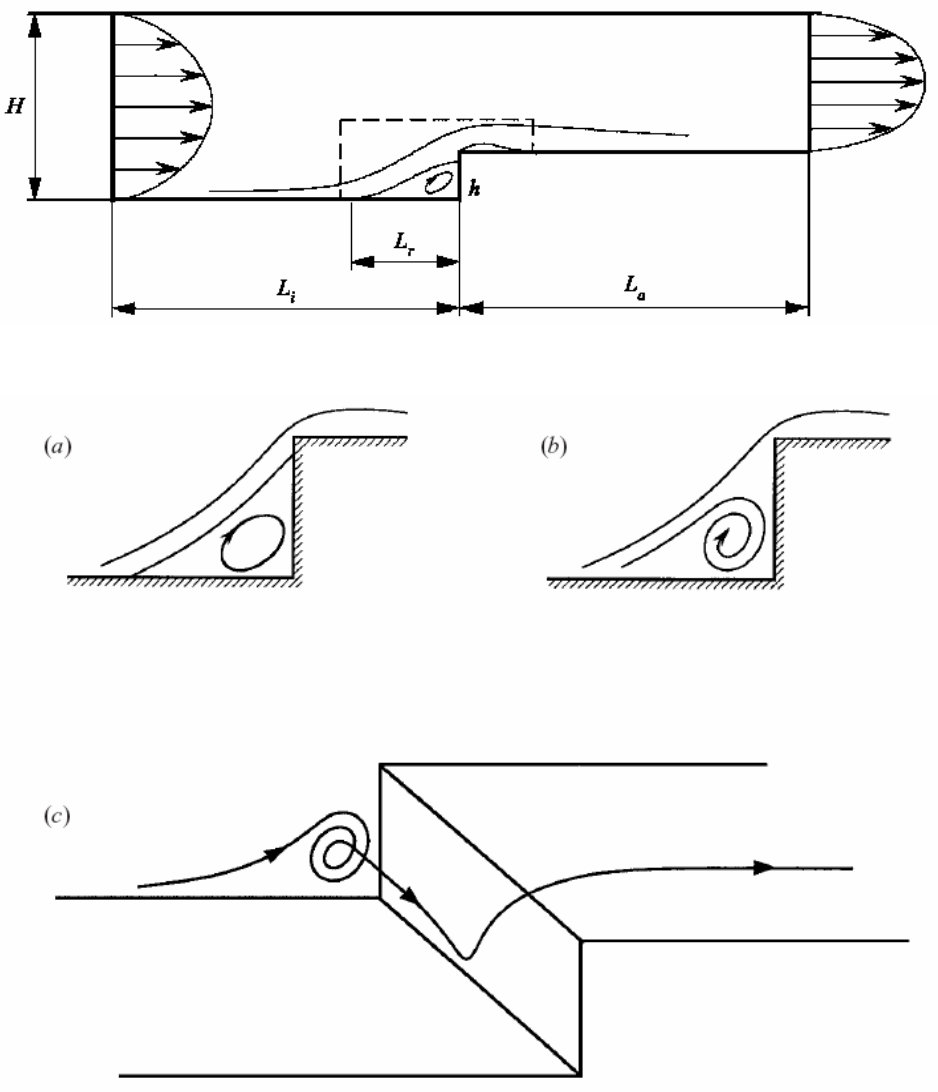

Figure 5-3 Forward-facing step and sketch of the separation region for (a) a closed separation bubble, (b) the side view of an open recirculation zone, and (c) the perspective view of the open recirculation zone (Wilhelm et al., 2003)

Figure 5-4 illustrates a rescaled pressure pulse for the step rotor in Figure 5-1. The maximum and minimum pressures occur at points A and B in the figure respectively. The region between B and C in the figure is the "bounce back" region described by Yu (1994) and it was suggested that this was caused by flow separation. Also shown in the figure is a schematic representation of envisaged typical streamlines around the step rotor. A primary recirculation zone will occur on the face of the step which will begin on the rotor wall at some distance upstream of the step at point A. The flow will then converge through the constriction and a secondary recirculation zone will form on the rotor wall directly downstream of the step face. The velocity at point A

will be the lowest as the distance between the rotor wall and the screen is close to the maximum point and therefore the greatest pressure will occur at this point. A vena contracta will occur at point B which will cause the velocity of the fluid to be the greatest at this point. As a result the pressure will be at the lowest value at this point.

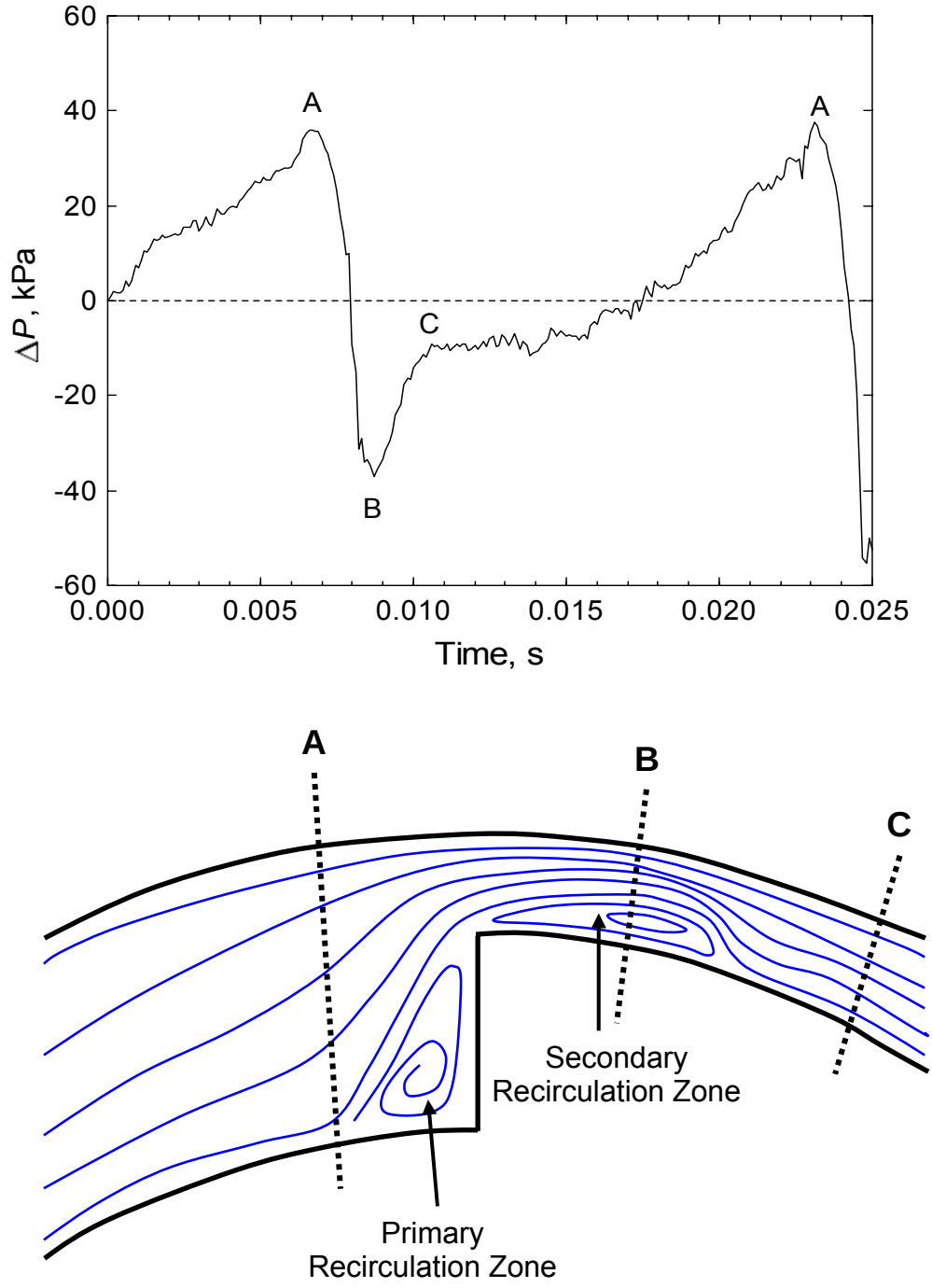

Figure 5-4 Pressure pulse for a step rotor (Q_a=1000 L/min, R_v=1, u_{tip}=24 m/s) and schematic of flow over the step face

An analysis of the time between points A, B, and C for the pulse in Figure 5-4 reveals that at 24 m/s the distance that the decrease in pressure from points A to B occurred over is in the order of 43 mm and the bounce back from points B to C occurred over a distance of approximately 40 mm. These relatively large distances support the hypothesis that the face of the step passes at some point between points A and B.

The step rotor has an extended negative pulse and this rotor has been shown to reduce reject thickening due to this extended pulse (Julien Saint Amand & Perrin, 1998; Weeds, 2006). The reverse flow that occurs during the step rotor is thought to reduce the thickening that occurs although this will depend on the amount of flow that occurs and also the reverse passage ratio. One of the objectives of the research was to calculate the ratio of forward to reverse flow that occurs during the pressure pulse.

The pressure pulse in Figure 5-2 is rescaled and presented in Figure 5-5 along with a schematic diagram of the flow around a foil rotor. The magnitude or strength of the pulse is quite different for the two rotors and the foil rotor in contrast to the step rotor has a very short but strong negative pulse, with a short increase in the positive pulse that occurs immediately before the negative pulse. This brief increase in the positive pressure occurs directly before the foil element passes the transducer and the dramatic decrease in the pressure occurs at the beginning of the foil element proper or point A in the figure. This phenomenon has also been reported by Pinon et al. (2003) and Feng et al. (2005) and the camber of the foil was adjusted by Feng et al. so that the increase in the positive pulse was entirely eliminated. The increase in the positive pulse directly preceding the foil element is thought to increase contaminant passage due to an increase in the instantaneous forward velocity and therefore decrease contaminant removal efficiency (Feng et al., 2005). Deformable contaminants such as stickies may be extruded through the aperture which may be enhanced by this period of higher forward flow and therefore increased hydrodynamic drag on a trapped stickie (Julien Saint Amand et al., 2005).

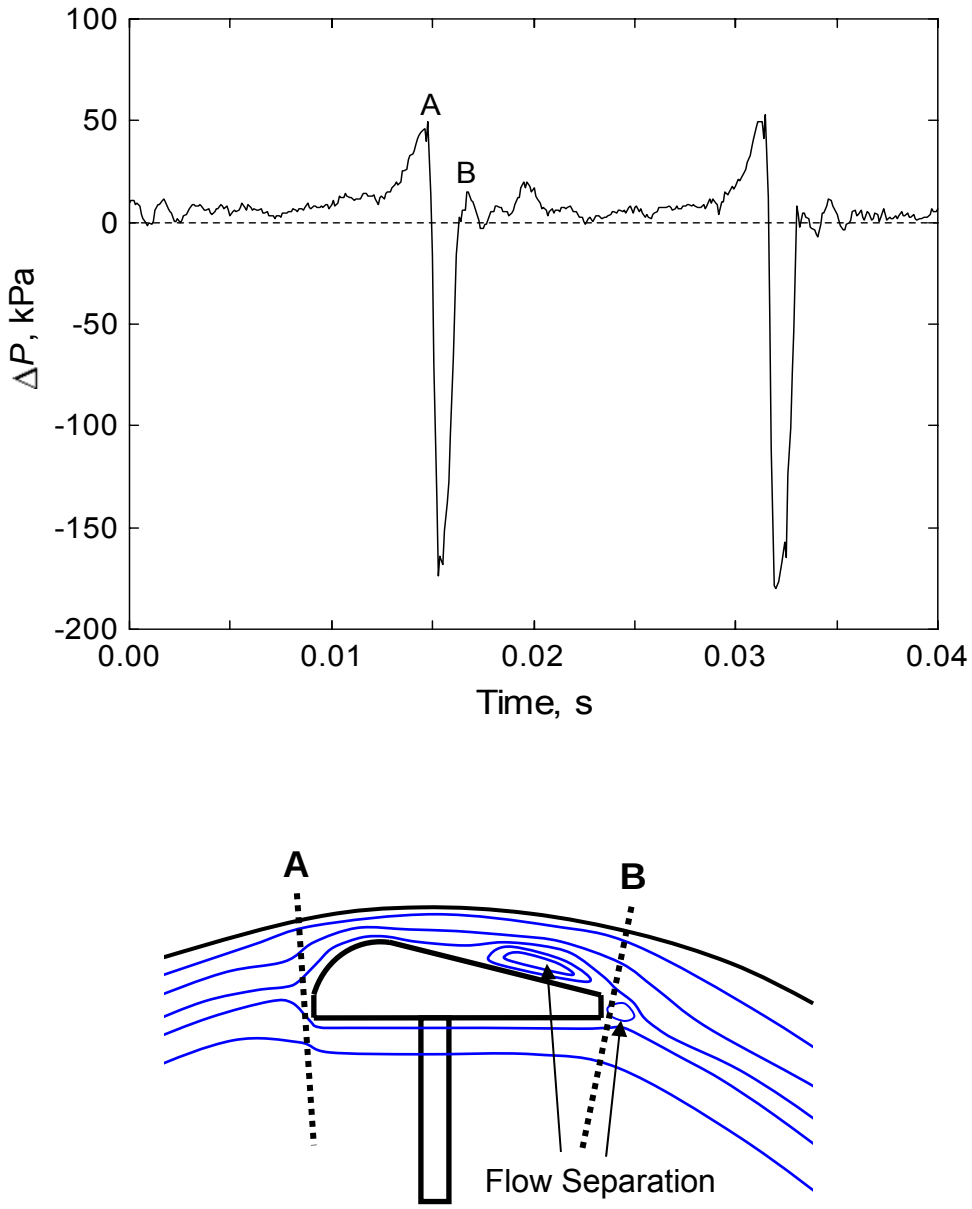

Figure 5-5 Pressure pulse for a foil rotor (Q_a=500 L/min, R_v=0.6, u_{tip}=24 m/s) and schematic of flow over the foil

Feng et al. (2005) modelled a foil rotor and found flow separated from the surface of the foil facing the screen if the angle of attack of the foil was greater than a critical angle. The critical angle at which separation occurred was dependant on the foil shape used and varied from about 5 degrees for a NACA 8312 foil to 15 degrees for a NACA 0012 foil. The difference in the foils was the degree of camber and the flow separation occurs further toward the front of the foil and at a lower angle of attack as the camber is increased. These figures should be treated with caution however as the

turbulence model chosen will greatly affect the prediction of flow separation (Celić & Hirschel, 2006) although they are useful qualitatively. Grégoire et al. (2000) have demonstrated discrepancies in the flow around a foil, with no flow separation predicted using the standard k-ε turbulence model however when using the k-ε RNG turbulence model separation occurred on the top surface of the foil. Extreme caution must be taken when using two-equation eddy-viscosity turbulence models for predicting flow separation (Wikstrom & Rasmuson, 1998; Davidson, 2003; Celić & Hirschel, 2006). Feng et al. demonstrated that for both experimentally and numerically modelled pulses that when separation occurred on the foil rotor it caused a plateau in the pressure pulse during the later stage of the negative pulse.

5.1.1 Pulse Data – Screen Position

The general shape of the pulse has been shown by other researchers and confirmed here to be principally dependant on the geometry of the rotor element. Other factors known to affect the magnitude of a particular type of pulse is the gap between the rotor and the screen plate or basket, the tip speed of the rotor and the surface contour of the screen plate. It is also likely the relative speed of the fluid and the rotor tip will influence the magnitude of the pulse and therefore the magnitude of the pulse at the front of the screen will be greater than at the rear (Karvinen & Halonen, 1984; Weeds, 2006).

Pressure pulses were measured at two positions along the screen for both the step and foil rotor and typical pulses are presented in Figure 5-6 and Figure 5-7 respectively. The pulse at the front was measured 40 mm from the start of the screen and pulse toward the rear of the screen was measured 40 mm from the end of the screen. For both rotors the magnitude of the pulse was lower at rear of the screen compared to the front although the difference was much larger for the step rotor. In this case the magnitude of the pulse at the rear of the screen was in the region of 30 % lower than at the front. By contrast the foil rotor has a very similar positive pulse height but the negative pulse was slightly less toward the rear of the screen. Momentum transfer from the foil rotor to the fluid is expected to be considerably less than the step or a closed type rotor. The reduction in the momentum transfer is because the amount of fluid in the annulus is much greater, and also the ability of the rotor element to

transfer momentum to the fluid is significantly reduced due to the geometry of the foil. The mean tangential velocity is contingent on the degree of momentum transfer from the rotor and if enough momentum is transferred to overcome losses due to the screen profile amongst other factors, the mean tangential velocity should increase as the suspension travels along the axial screen length.

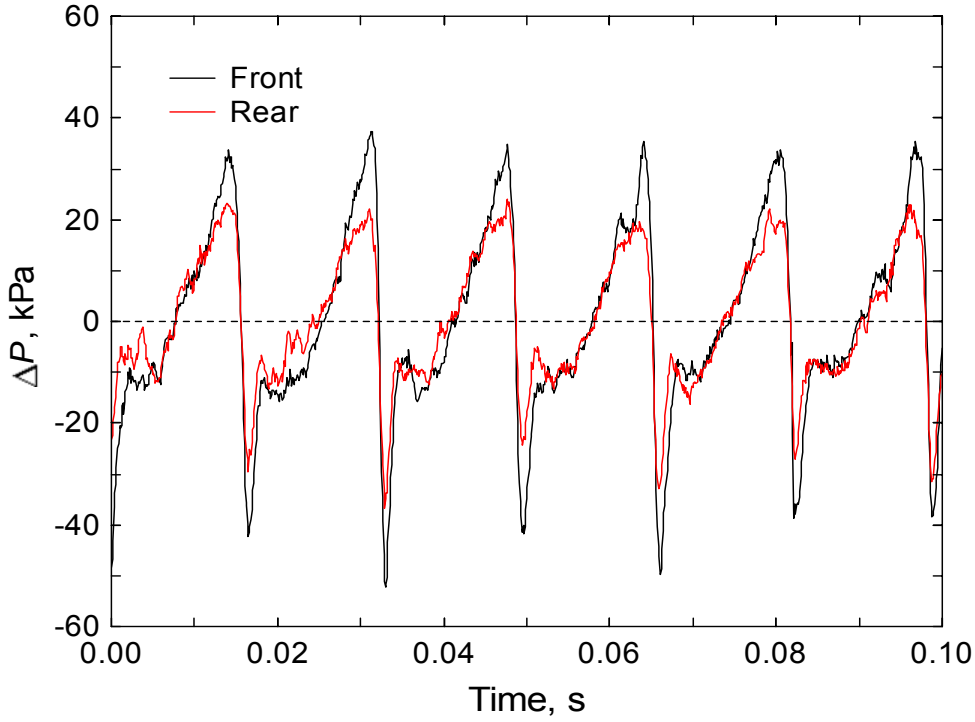

Figure 5-6 Measured pressure pulse for the step rotor at the front and rear of the screen (water, u_{tip}=24 m/s, R_v=0.49, Q_a=660 L/min)

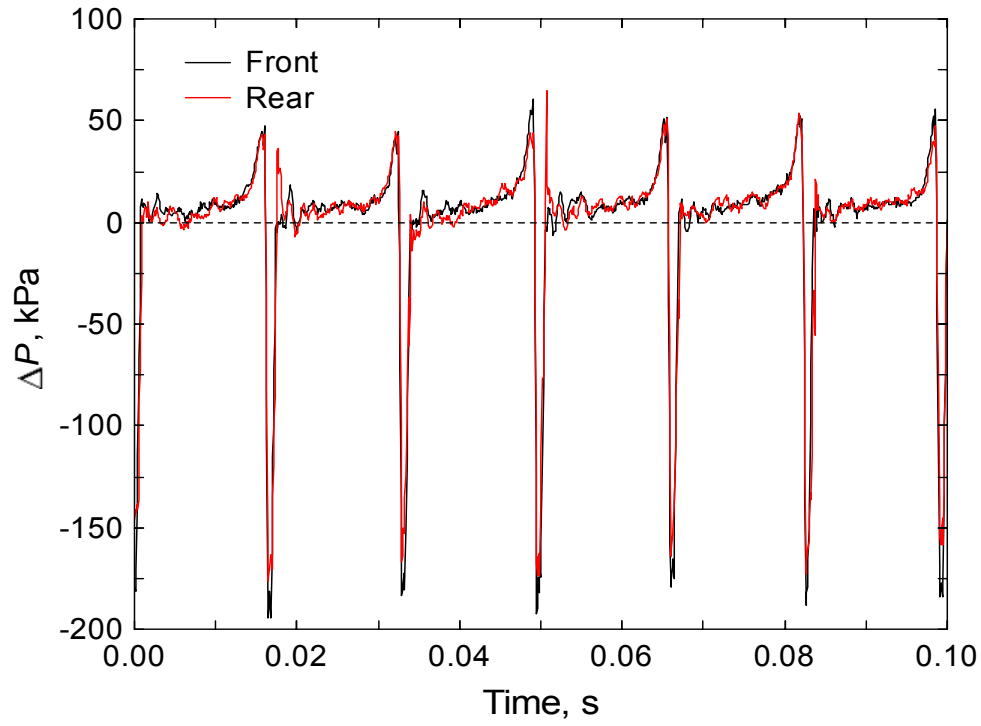

Figure 5-7 Measured pressure pulse for the foil rotor at the front and rear of the screen (water, u_{tip}=24 m/s, R_v=0.45, Q_a=660 L/min)

The rotor speed was varied and pressure pulses were measured at a number of different flow rates with no accept flow through the screen. The pressure pulses at several rotor speeds at the front and rear of the screen are shown in Figure 5-8 for the step rotor and Figure 5-9 for the foil rotor. The frequency and magnitude of the pressure pulse is reduced as the rotor speed was decreased as expected. Furthermore the pulse magnitude at the rear screen position was lower than at the front and the disparity became greater as the rotor speed was increased. The size of the increase in the positive pressure pulse for the foil rotor was increased as the rotor speed increased. The normal practice of calculating the magnitude of a pulse from the average of at least five pulses was used. The size of the positive and negative portions of the pulse was also calculated using the same method.

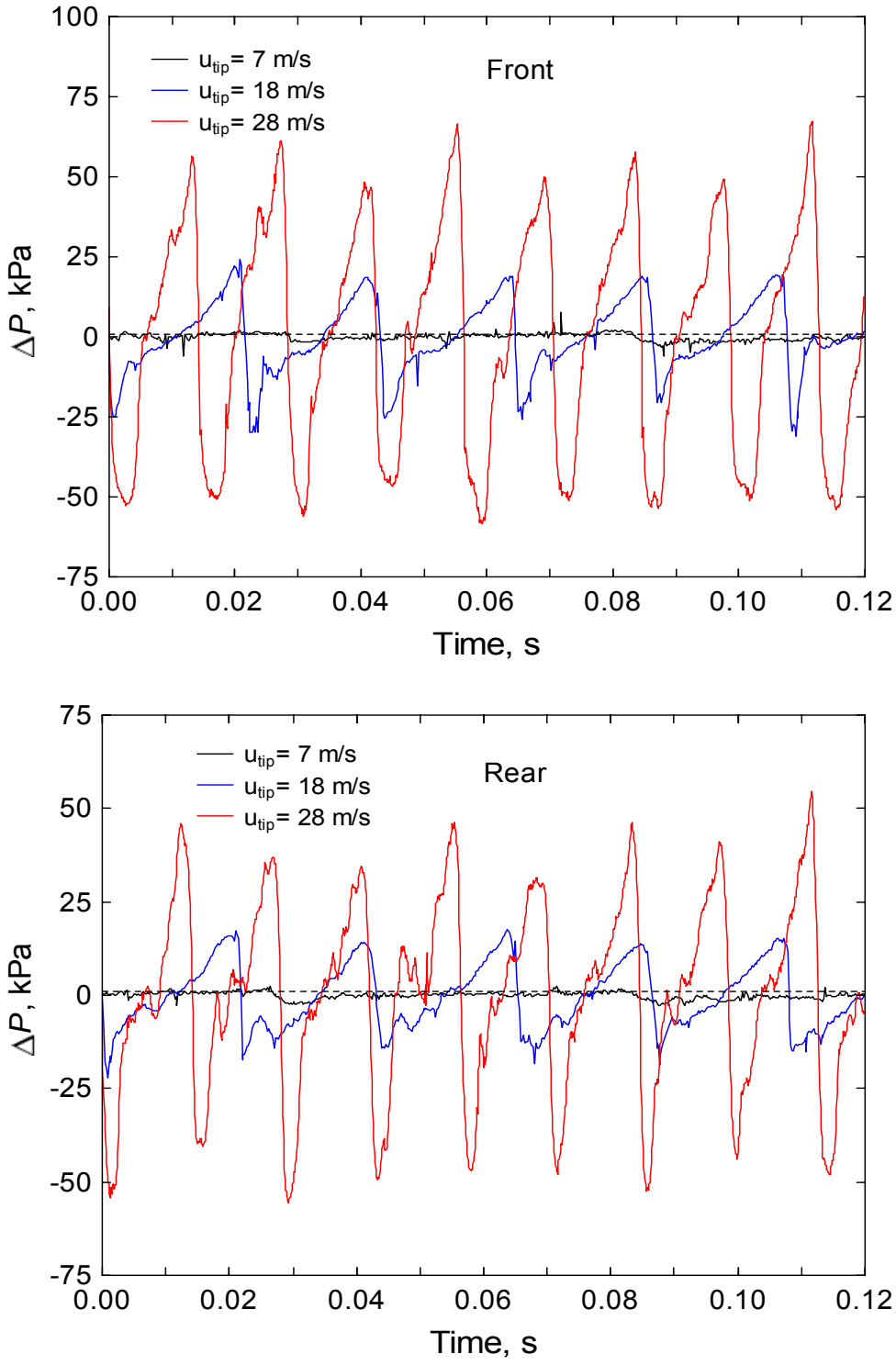

Figure 5-8 Pressure pulse for the step rotor at the front and rear of the screen for several rotor speeds (water, Q_f=500 L/min, R_v=1)

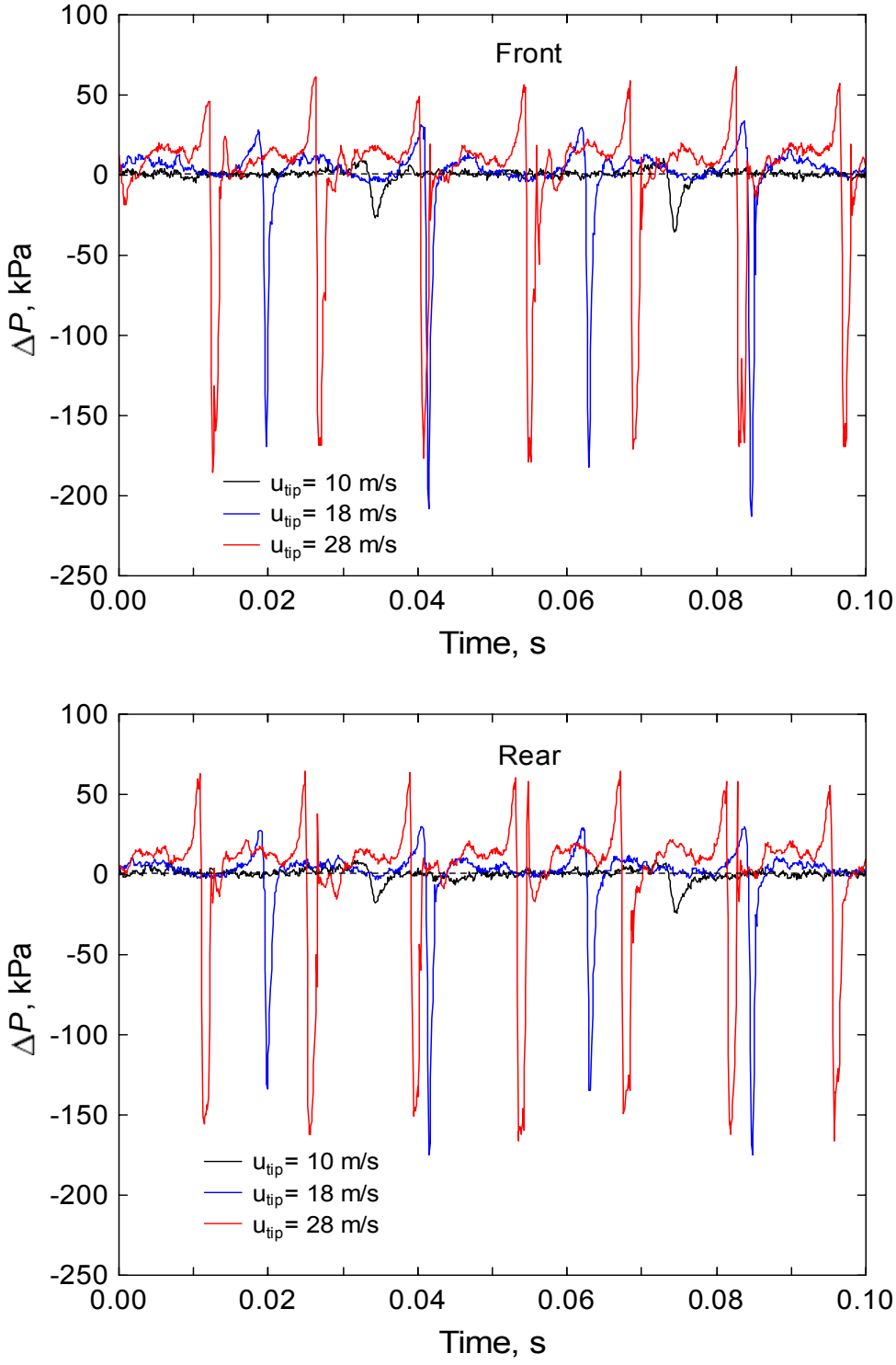

Figure 5-9 Pressure pulse for the foil rotor at the front and rear of the screen for several rotor speeds (water, Q_f=500 L/min, R_v=1)

The pressure pulse magnitude as a function of rotor speed for several feed flow rates is given in Figure 5-10 and Figure 5-11 for the step and foil rotors respectively. Data at the front and rear positions are shown in the figures. For the step rotor the pulse magnitude was roughly proportionate to the square of the tip speed, although as demonstrated in Figure 5-6 and Figure 5-7, the pulse at the rear was considerably less than at the front of the screen. In some cases the magnitude of the pulse at the rear of the screen was up to 40 % lower than at the front. For the foil rotor pulse strength initially increased with the square of velocity and then levelled off above a critical tip speed. Again the disparity between the magnitude of the pulse at the front and rear of the screen became greater as the rotor speed increased, and the difference was greater for the foil rotor compared to the step rotor. The pulse magnitude was not greatly affected by changes in the flow rate through the annulus for the step rotor but was for the foil above the critical tip speed.

The relationship of the pulse magnitude being roughly proportionate to the square of the tip speed has also been found by other researchers for the foil rotor although they do not report a levelling off above a critical tip speed (Gonzalez, 2002; Pinon et al., 2003; Feng et al., 2005). The maximum tip speed measured by these researchers was around 21 m/s and hence may not have exceeded the critical velocity for the particular foil shape that was used. Pulse magnitude has also been reported to be linearly related to rotor speed and unaffected by accept flow rate however only a small range of rotor speeds were tested (Yu, 1994).

The pulse magnitude will have a significant affect on the amount of flow through the screen in both the forward and reverse directions. A detrimental outcome of high pulse magnitude in a pressure screen can occur in an approach flow system to a paper machine and can have adverse effects on the operation of the paper machine. If the pulsation from the rotor is too high or at the incorrect frequency, barring of the paper sheet may occur (Javid, 1983; Bliss, 1992). Barring is a machine wide variation in the basis weight of the paper sheet. Proper screen operation, correct piping of the accept outlet, and suitable rotor selection can all be utilised to prevent or correct this problem.

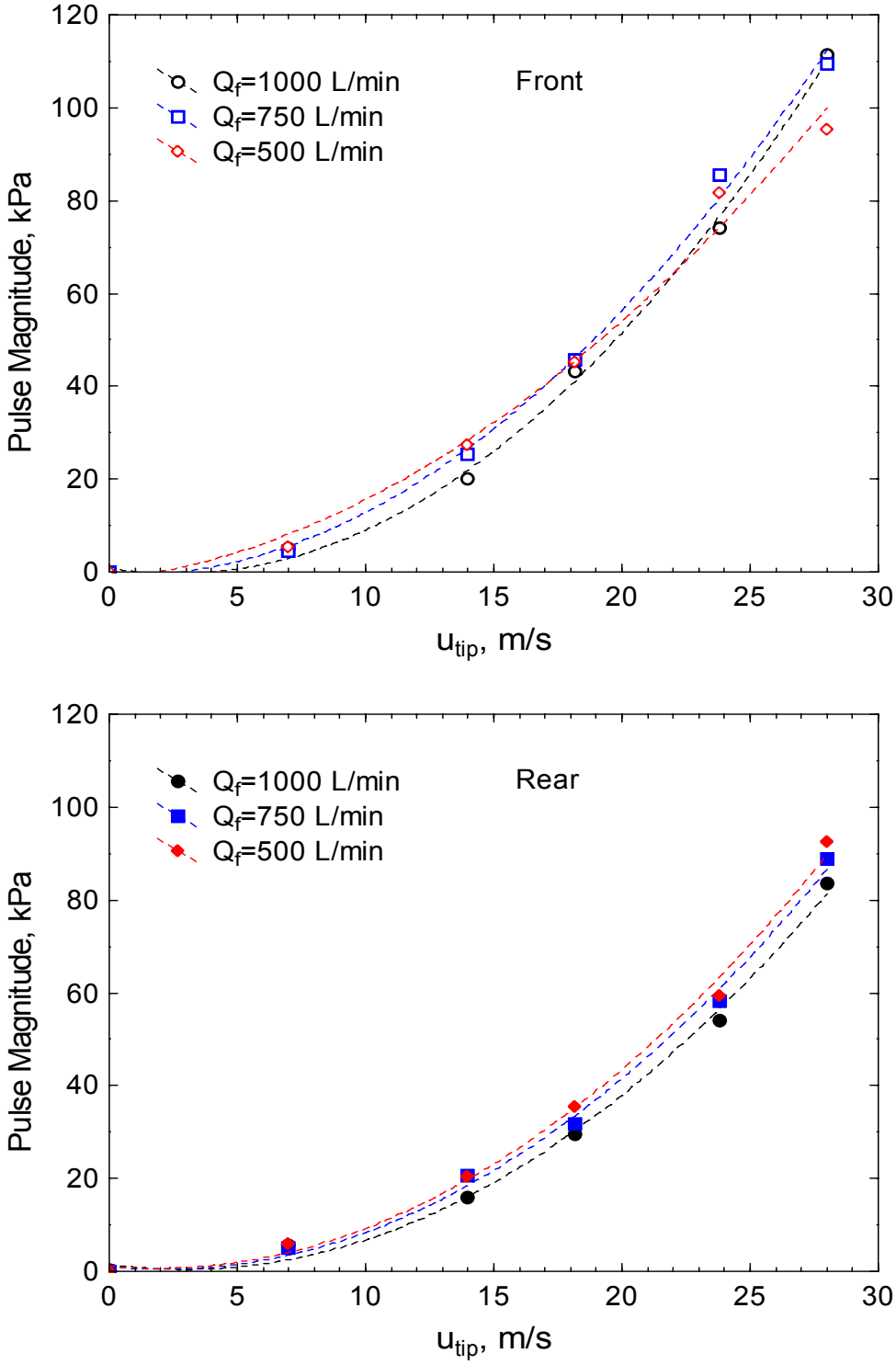

Figure 5-10 Pressure pulse magnitude for the step rotor at several rotor speeds for the front and rear of the screen (water, R_v=1)

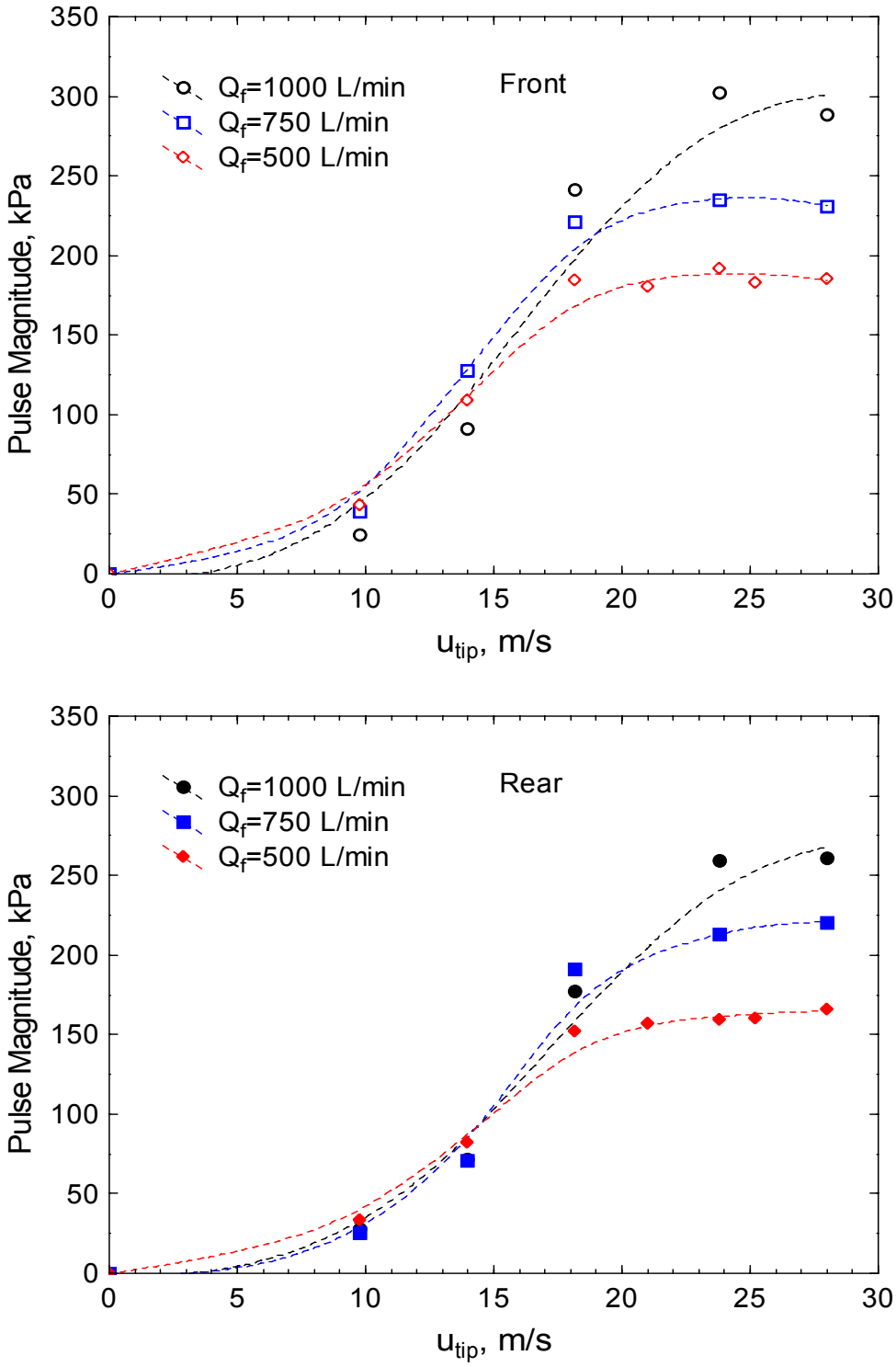

Figure 5-11 Pressure pulse magnitude for the foil rotor for several rotor speeds for the front and rear of the screen (water, R_v=1)

Both sets of results support the proposition that the pulse magnitude is dependant on the relative speed or slip factor γ of the fluid and the rotor. As the rotor speed is increased it is expected that more momentum is transferred to the fluid and the mean tangential velocity of the fluid increases causing the relative velocity between the rotor tip and fluid to decrease. A decrease in the relative velocity in turn causes the pulse magnitude to decrease. The feed flow rate also affected the pulse magnitude for both rotors, especially for the foil rotor above the critical velocity, with a decrease in the size of the pulse occurring as the feed flow rate decreased. The difference between front and back was also more pronounced at the higher feed flow rate which may be due to flow entrance effects taking longer to settle at the high feed rate and hence lower residence time.

It is proposed that the decrease in pulse magnitude is caused by the decrease in the relative speed of the fluid and the rotor in the screen. The rotor transfers momentum to the fluid as it moves along the screen annulus and as a result the mean tangential velocity of the fluid increases along the screen length (Rienecker, 1992). The relative speed between the rotor tip and the fluid consequently decreases toward the rear of the screen and the quantity of momentum transfer from rotor to fluid decreases. With less momentum transfer there is less pressure change in the fluid and the pulse is smaller. Changes in the mean tangential velocity in the annular gap between the rotor and the screen plate have been investigated using numerical techniques and results are reported in the Chapter 6. The numerical work has demonstrated significant increases in the mean tangential velocity along the axial length of the screen for both a smooth rotor and industrial rotors.

A combination of flow separation along the top foil and cavitation is a possible cause of the levelling off of the pulse magnitude above a critical rotor speed. The foil rotor produces a very large negative pressure during the pulse cycle and if the absolute pressure at the lowest part of the pulse is (P_{ann}-P_{neg}) lower than the saturation vapour pressure of the fluid then cavitation will occur. The saturation vapour pressure of water at 20°C is 2.34 kPa and when the critical rotor speed was exceeded the absolute pressures that occur during the extreme parts of the negative pulse are in the order of the saturation vapour pressure of water at 20°C. The temperature of the water used throughout the tests was approximately 20°C. When the absolute pressure is lower

than the saturation vapour pressure then cavitation will occur and this will lead to at decrease in the "efficiency" or pulse magnitude of the rotor. The pressure pulse magnitudes of the foil and step rotor presented previously for the front of the screen are represented and compared in Figure 5-12 with the region that cavitation is thought to occur indicated. The absolute pressures that occur for the step rotor during the negative pulse are not in the region of the saturation vapour pressure. However if the rotor speed was great enough and the absolute pressure low enough during the negative pulse then cavitation is likely to occur. A possible scenario for the step rotor at elevated rotor speeds is offered on the figure.

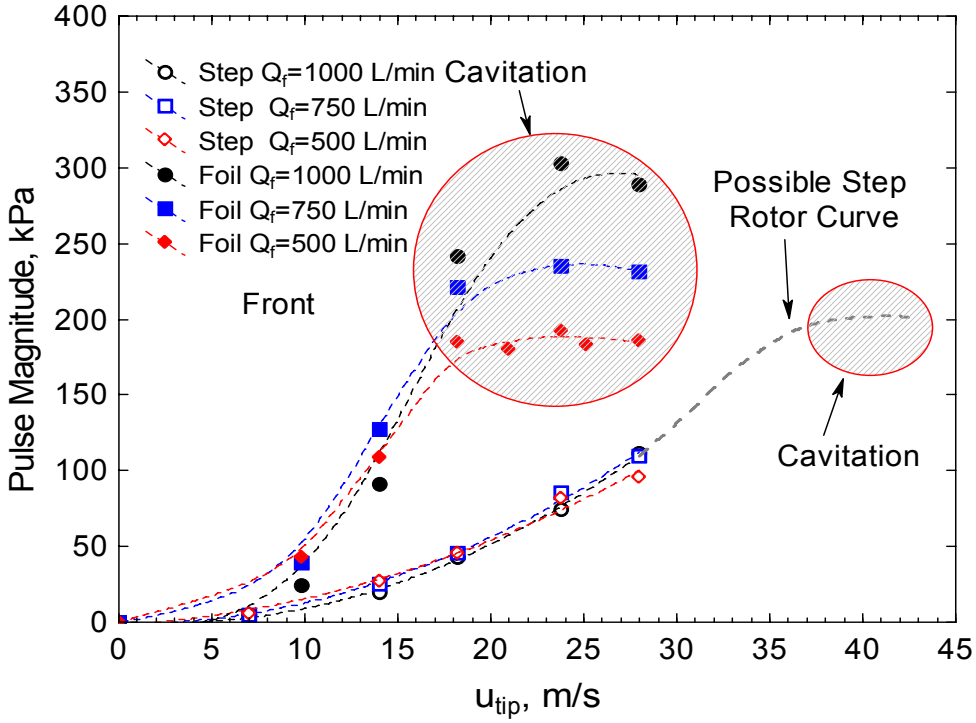

Figure 5-12 Comparison of the pulse magnitude of the step and foil rotors at the front of the screen with the regions of cavitation indicated

The magnitude of the positive and negative pulse was calculated for the two rotors and results for the step rotor are shown in Figure 5-13 and Figure 5-14 and the results for the foil rotor are shown in Figure 5-15 and Figure 5-16. It must be noted that the magnitude of the negative pulse is taken as the deviation from the mean value of the pulse (i.e. zero in the figures) however later the pulse will be considered to be negative when the pressure is below the average accept pressure. As the pressure differential between the averaged pulse pressure and the accept pressure will vary

depending on the accept flow rate, the accept pressure is not used to calculate the magnitude of the positive or negative pulse. This approach has also been used by other researchers to report positive and negative pulse strengths (Gonzalez, 2002; Pinon et al., 2003).

For the foil rotor the positive pulse shows a roughly linear increase with rotor speed for both the front and rear position. The negative pulse reaches a maximum value at around 18 m/s. The negative pulse also increased as the feed flow rate was increased. Levis (1991) suggests that at high rotor speeds the capacity of the screen can be adversely affected due to the elevated levels of reverse flow due to the increased negative pressure pulse. Feng et al. (2005) point out that although the purpose of the negative pulse is to induce reverse flow so that accumulated fibre and contaminants can be dislodged, too much reverse flow can reduce the overall net flow through the aperture and therefore reduce capacity. The data presented here indicates that there is a maximum negative pulse for a foil rotor that occurs at critical rotor speed and any further increases in rotor speed will not increase the negative pulse.

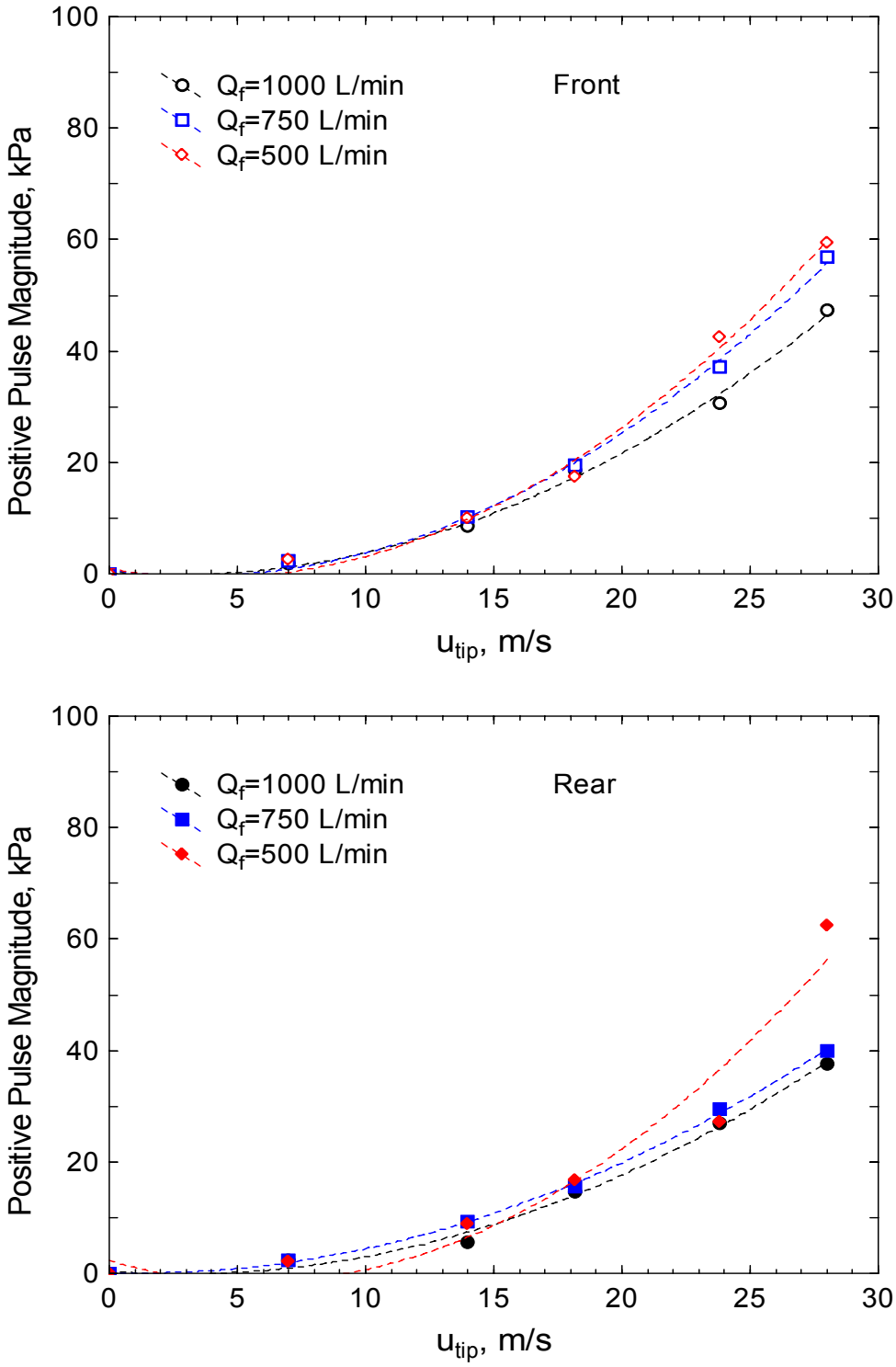

Figure 5-13 Magnitude of the positive pulse for the step rotor at the front and rear of the screen at several rotor speeds (water, R_v=1)

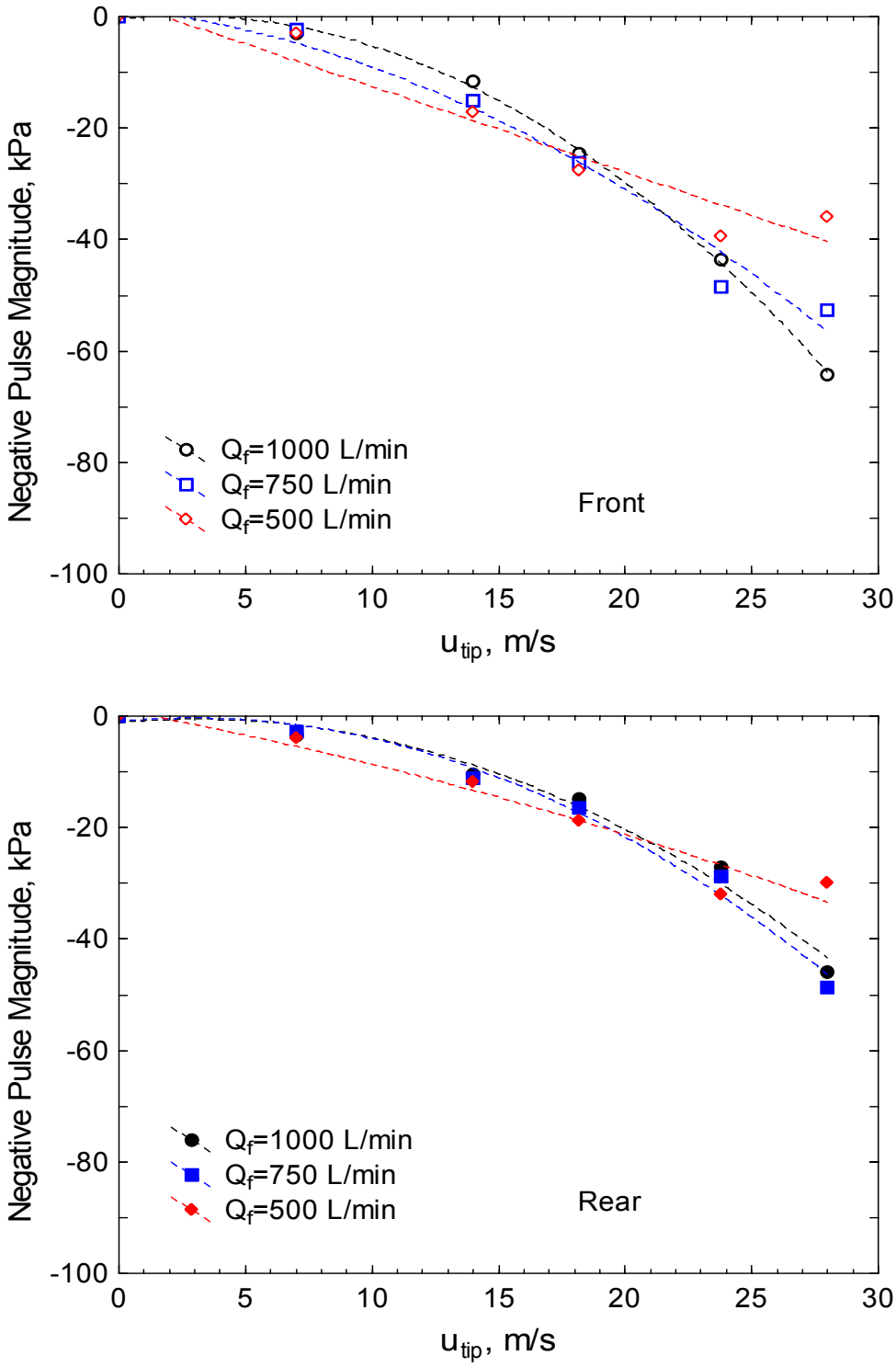

Figure 5-14 Magnitude of the negative pulse for the step rotor front and rear of the screen at several rotor speeds (water, R_v=1)

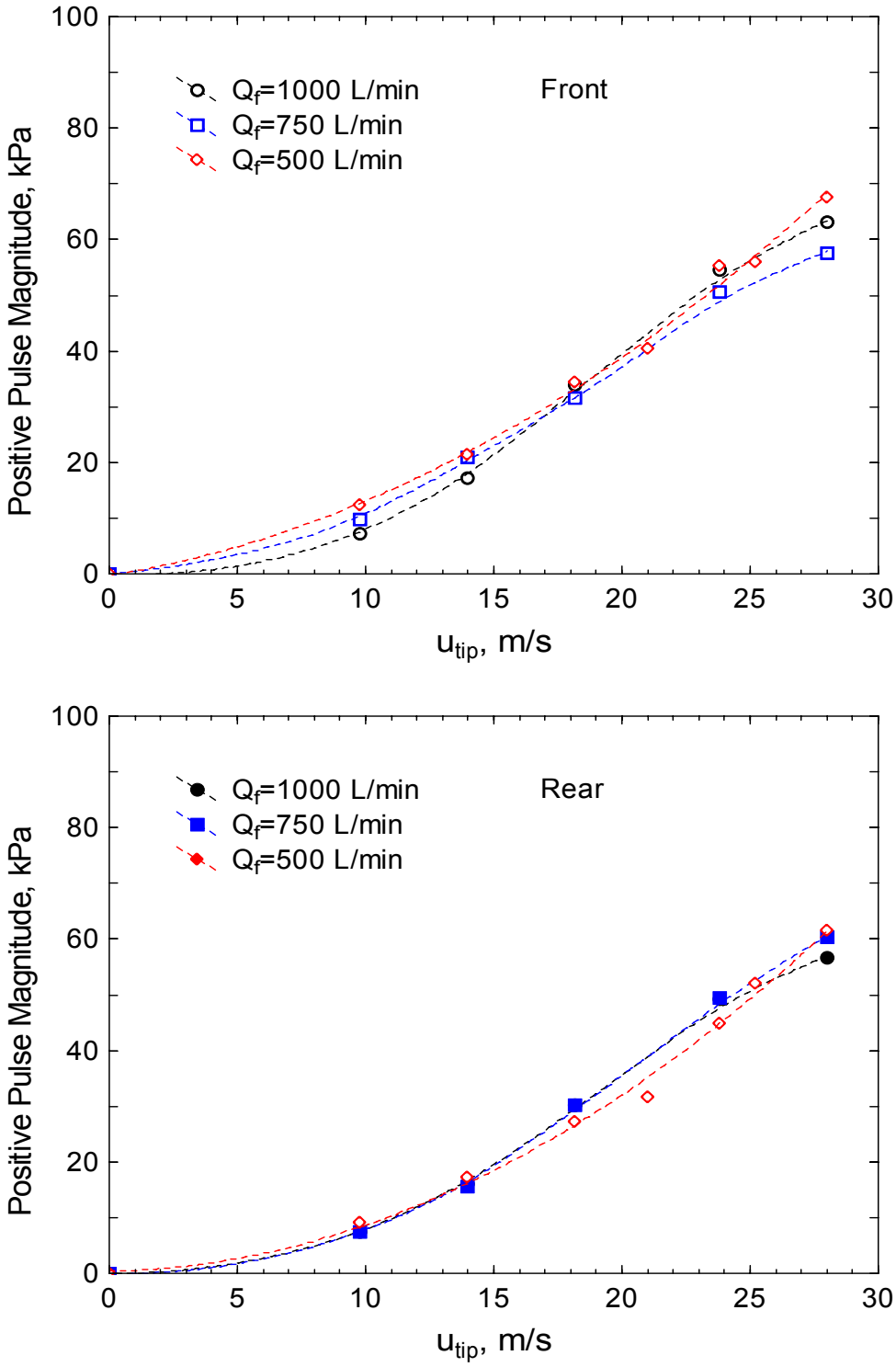

Figure 5-15 Magnitude of the positive pulse for the foil rotor front and rear of the screen at several rotor speeds (water, R_v=1)

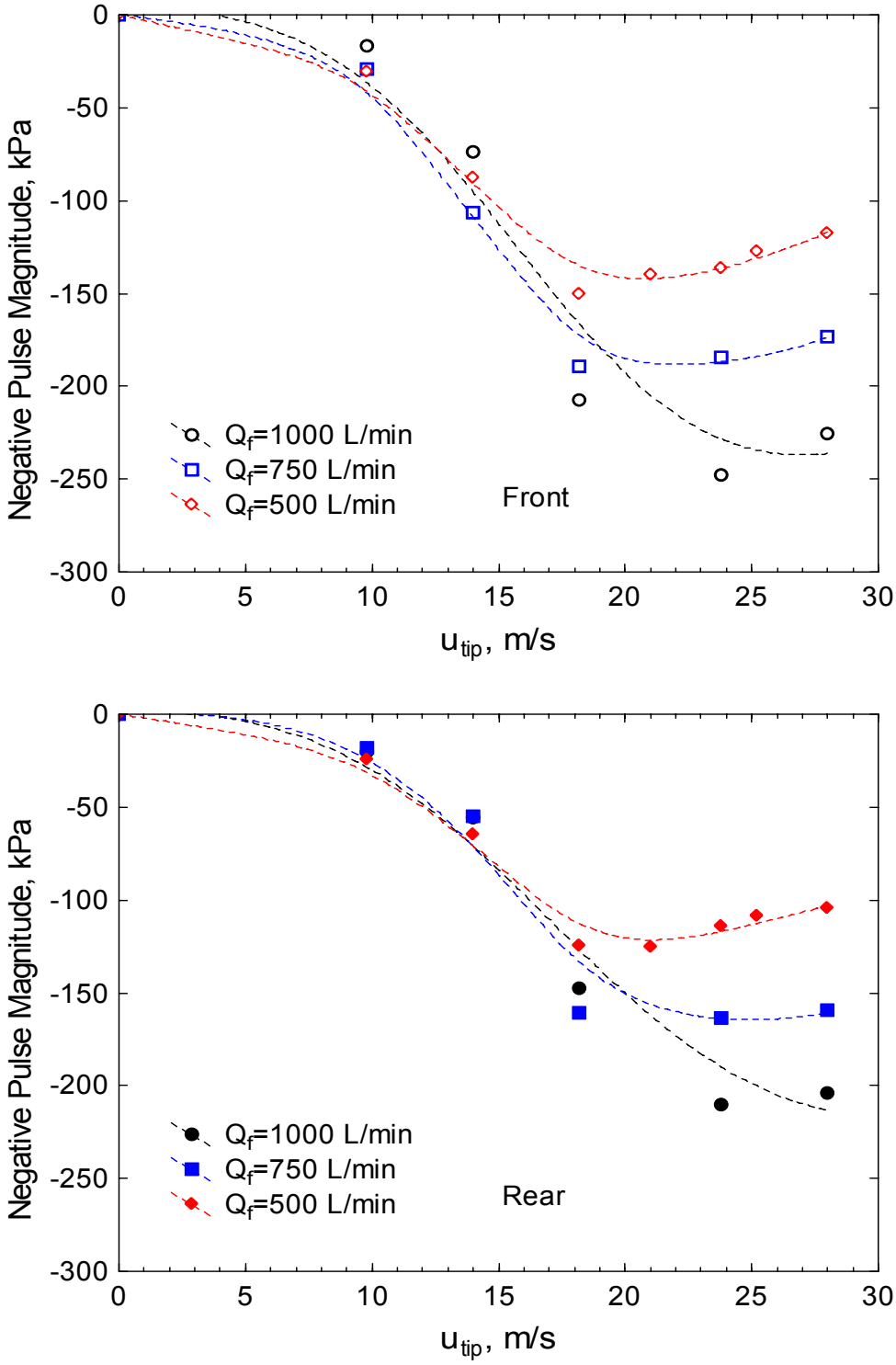

Figure 5-16 Magnitude of the negative pulse for the foil rotor front and rear of the screen at several rotor speeds (water, R_v=1)

The effect of volumetric reject rate and accept flow rate or aperture velocity on the pulse magnitude was also studied. The pulse was measured for a constant accept flow rate while the volumetric reject rate was varied. The pulse magnitudes as a function of reject rate for the step and foil rotors are shown in Figure 5-17 and Figure 5-18 respectively. The pulse magnitude was relatively constant as the volumetric reject rate was changed for the step rotor. The foil rotor was unchanged up to a certain reject rate and then the magnitude increased. The increase occurred at a higher reject rate as the accept flow rate was decreased.

There appears to be a significant difference in pulse strength between the front and rear of the pressure screen. Yu (1994) measured the pressure pulse of a step rotor in a Beloit MR18, a similar design screen to that used in this study except the basket diameter is 18 inches. The pulse was measured at four locations along the screen and it was found that the largest pulse occurred toward the front of the screen. The other sections were reported to have similar pulse magnitudes and the difference in pulse magnitude between the second front section and the others was up to 40 %. No explanation as to the cause of this phenomenon was offered by Yu, but it seems reasonable that if the pulse is caused by a Venturi effect then the relative speed of the rotor and the fluid affects the pulse magnitude (Karvinen & Halonen, 1984). Julien Saint Amand (1997) has reported that the pressure pulse was amplified when contoured screen baskets were used because the contours exert a large breaking force on the suspension. This breaking force will reduce the average tangential velocity of the suspension and therefore magnify the pulse by altering the relative speed of the suspension and rotor. Gooding also speculates that the pulse magnitude will decrease as the relative velocity is decreased (Gooding, 1996).

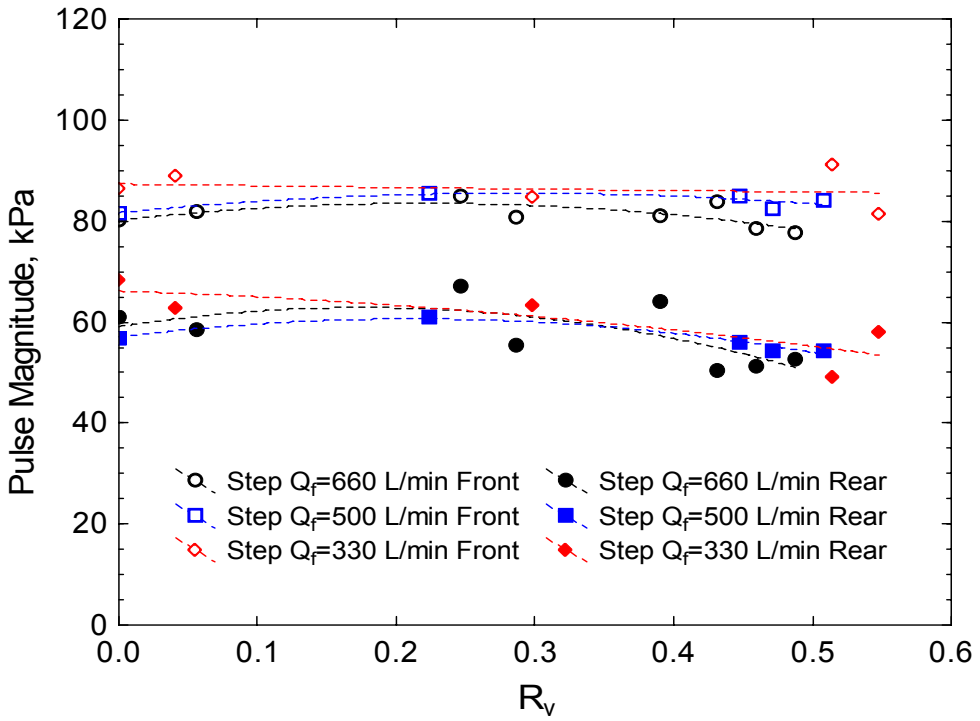

Figure 5-17 Pulse magnitude of the step rotor at different reject rates at the front and rear of the screen (water, u_{tip}=24 m/s)

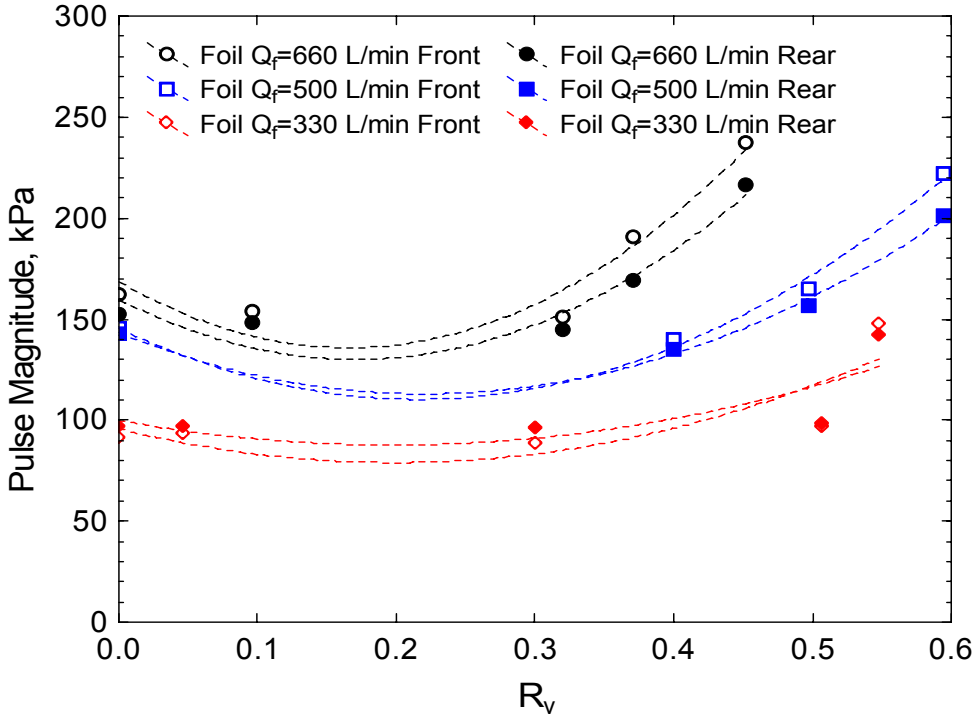

Figure 5-18 Pulse magnitude of the foil rotor at different reject rates at the front and rear of the screen (water, u_{tip}=24 m/s)

5.1.2 Pulse Data – Feed Configuration

It logically follows that if the slip factor at the front of the screen is greater than at the rear, then the feed configuration will also affect the relative speed. An axial feed will cause the velocity difference, and therefore the slip factor, between the fluid and the rotor to be slightly greater than for a tangential feed configuration. This increase in the velocity difference should then give rise to an increase in pulse magnitude. The pulse was measured for both axial and tangential feed configurations at similar flow conditions and typical pulses are shown in Figure 5-19 at the front and Figure 5-20 at the rear. The comparison of axial and tangential feed configurations was only conducted for the step rotor.

It is evident that the pulse for the axial feed configuration is greater than for the tangential at the front of the screen. In this case the pulse magnitude for the axial feed was approximately 45 % greater than the tangential at the front of the screen. However the pulses are of similar strength at the rear of the screen.

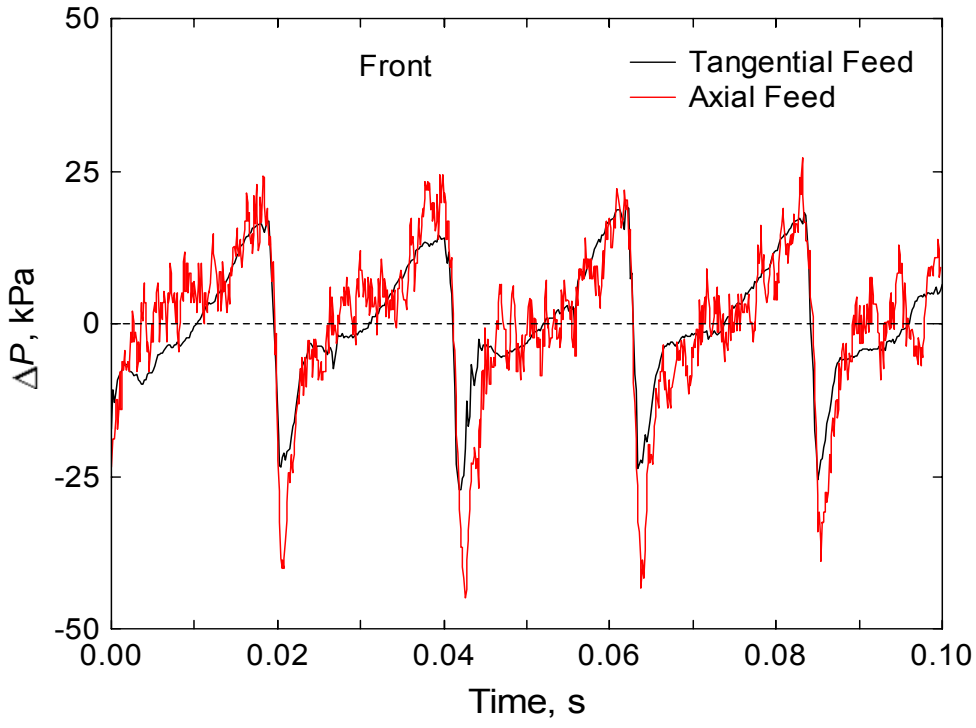

Figure 5-19 Effect of tangential and axial feed configuration on the pressure pulse for the step rotor at the front of the screen (u_{tip}=18 m/s, Q_f=500 L/min)

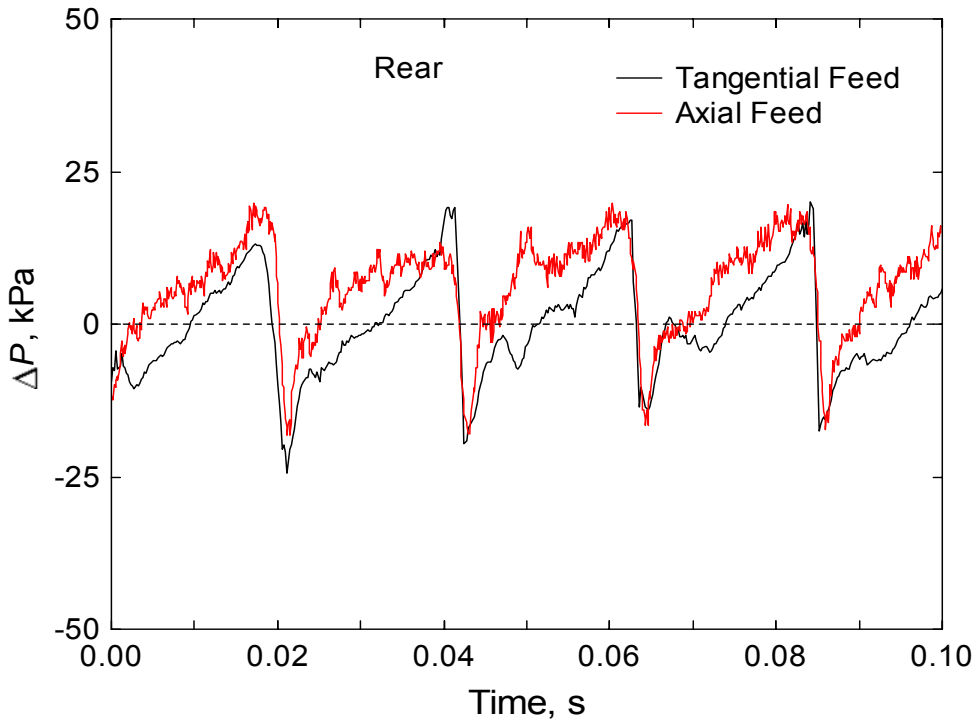

Figure 5-20 Effect of tangential and axial feed configuration on the pressure pulse for the step rotor at the rear of the screen (u_{tip}=18 m/s, Q_f=500 L/min)

It is reasonable to assume that the fluid in the axial feed should not have any initial tangential velocity component as it enters the screen annulus and all of the tangential momentum is gained solely due to momentum transfer from the rotor. The slip factor for this case will be equal to one and will decrease along the screen length. If the screen annulus is long enough, an equilibrium will be established where the rate of momentum transferred from the rotor will equal the braking forces that tend to slow the fluid. These braking forces arise from the wall of the screen basket, viscous forces, friction, etc. When this equilibrium is reached mean tangential velocity will be at the maximum and the slip factor will be minimised. For a tangential feed the same process will occur except the fluid will have an initial tangential velocity component due to the feed configuration. The equilibrium should be reached earlier along the screen length than compared to an axial feed.

The fact that the pulses are of similar magnitude at the rear of the screen suggests that in both the axial and tangential feed cases the maximum tangential velocity and therefore the equilibrium point is reached before the screen position where the pulse is measured at the rear of the screen.

5.1.3 Effect of Consistency

The consistency of the feed was varied in order to ascertain any affects on the magnitude of the pressure pulse. Figure 5-21 shows the pulse magnitude of the step and foil rotors for numerous feed consistencies. The magnitudes of the positive and negative parts of the pulse are presented in Figure 5-22 for the step and foil rotors. All pulse magnitudes were for the pulse measured at the front of the screen and no accepts flow (i.e. R_v=1). The overall, positive, and negative pulse magnitudes were not significantly affected by the presence of fibre even up to a consistency above 2.5 %.

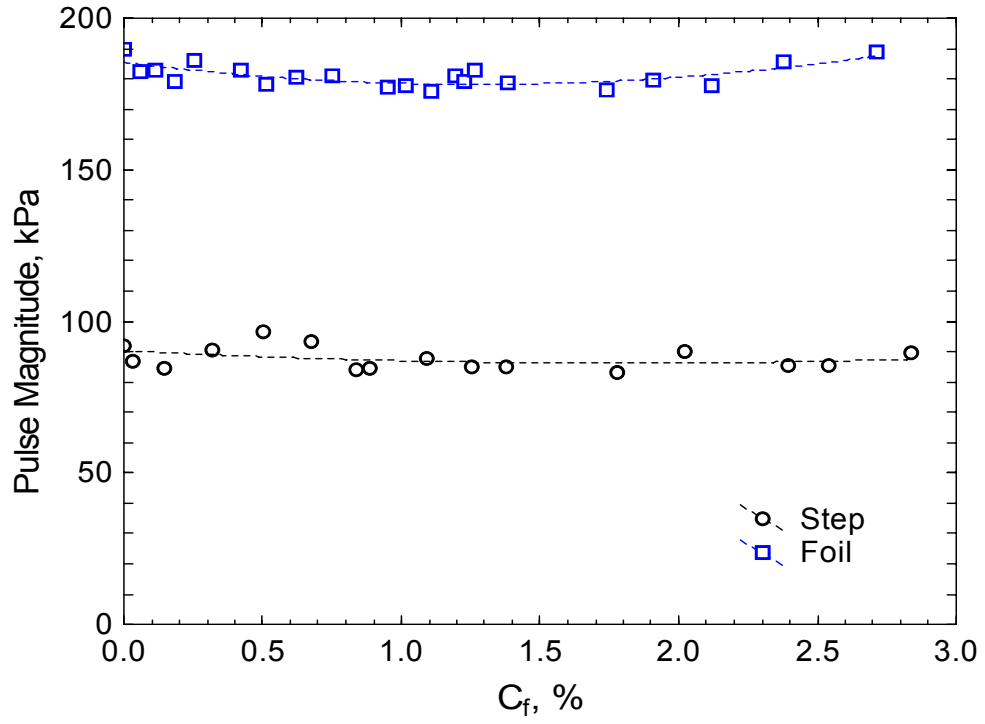

Figure 5-21 Pulse magnitude as a function of feed consistency for the step and foil rotors at the front screen position (u_{tip}=24 m/s, Q_f=500 L/min, R_v=1)

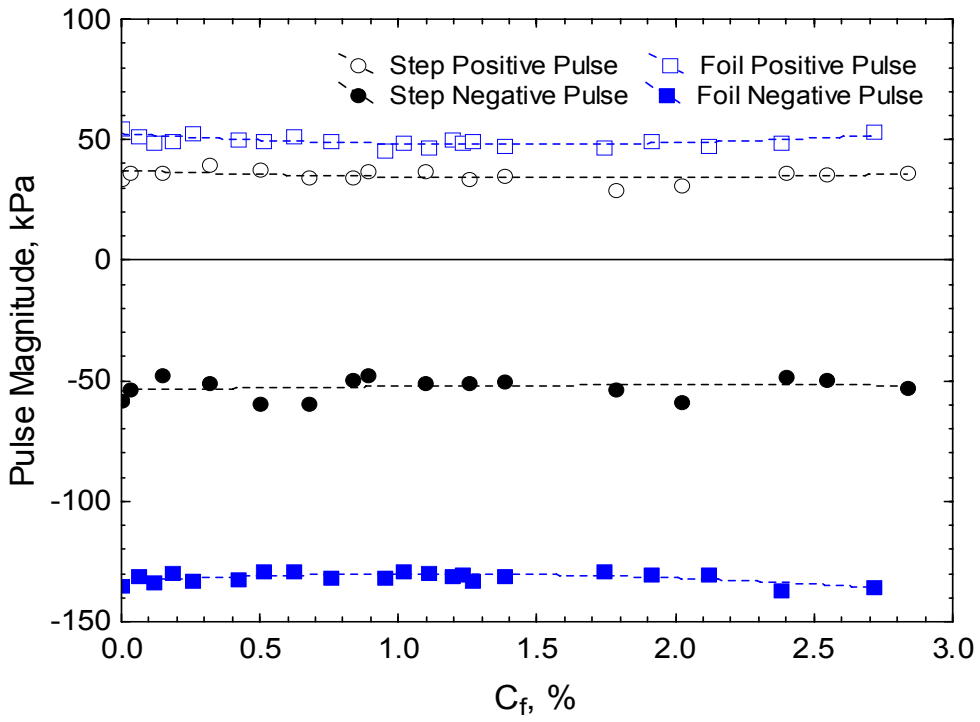

Figure 5-22 Positive and negative pulse magnitude for the step and foil rotors rotor as function of feed consistency at the front screen position (u_{tip}=24 m/s, Q_f=500 L/min, R_v=1)

The rotor speed was varied for several fixed feed consistencies and the overall pulse magnitudes measured at the front and rear of the screen for the step and foil rotors are shown in Figure 5-23 and Figure 5-24 respectively. The pulse magnitudes were once again lower at the rear of the screen compared to the front. There appears to be a slight increase in the pulse magnitude for the step rotor as the consistency is increased up to 2.8 %. The increase was greater at the front of the screen than at the rear. There was no appreciable difference in pulse magnitude with changes in feed consistency for the foil rotor.

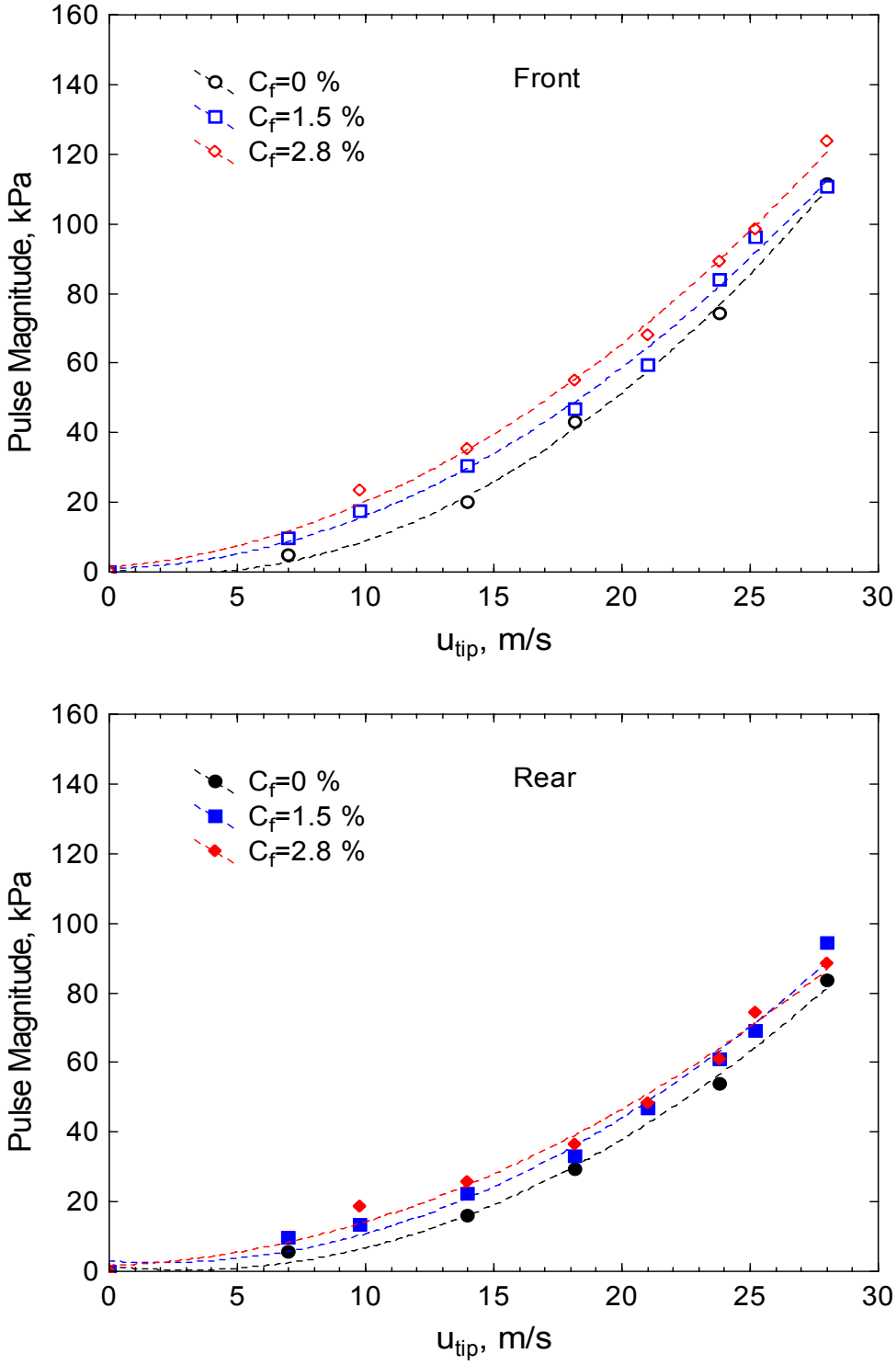

Figure 5-23 Pulse magnitude for the step rotor as function of rotor speed for several feed consistencies (Q_f=500 L/min, R_v=1)

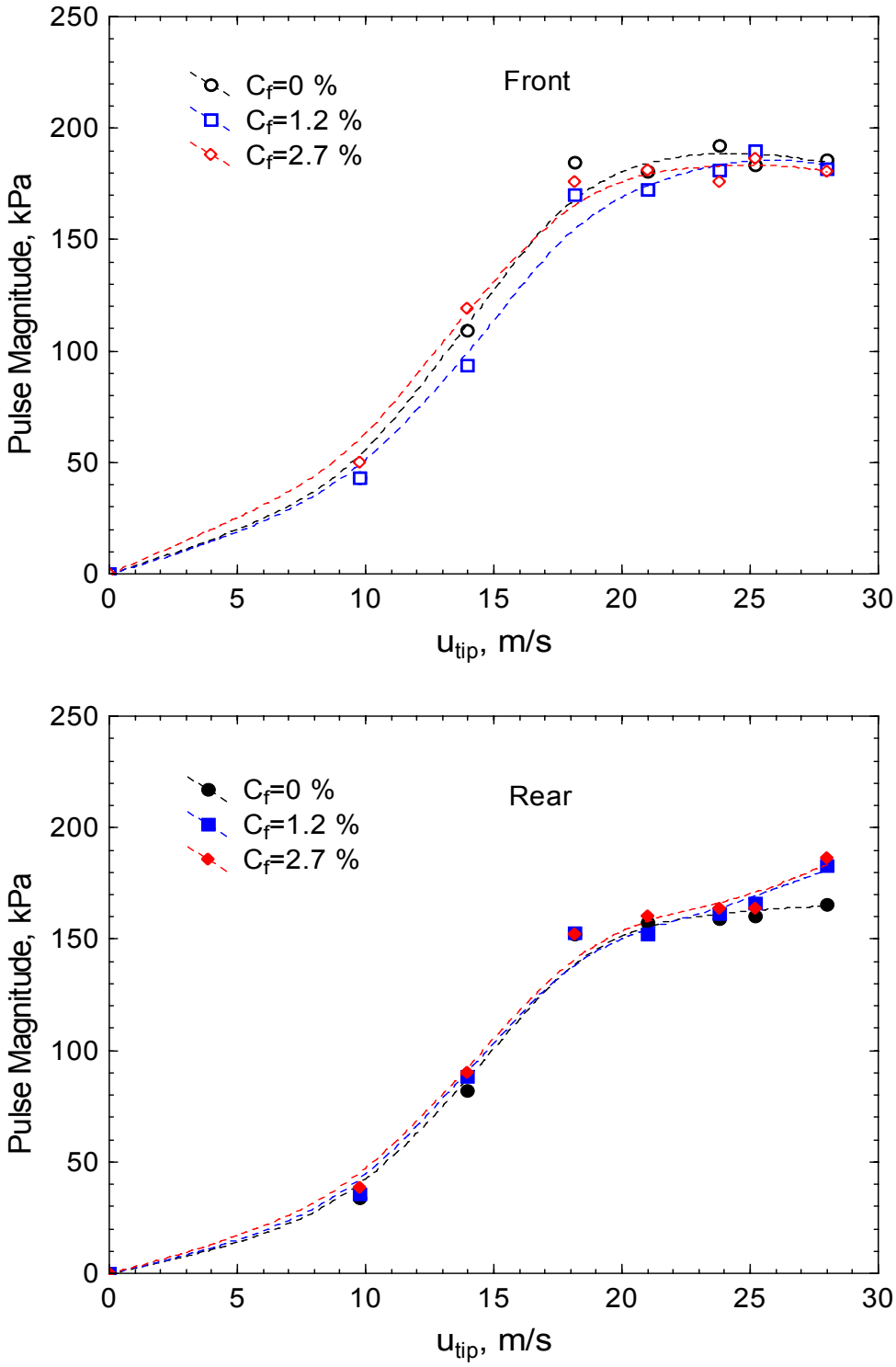

Figure 5-24 Pulse magnitude for the foil rotor as function of rotor speed for several feed consistencies (Q_f=500 L/min, R_v=1)

The shape of the pulse magnitude and tip speed relationship was unaffected by increased consistency and again was roughly proportionate to the square of tip speed for the step rotor. For the foil rotor a critical rotor speed was reached before there was no increase in magnitude and this critical tip speed appeared to be unaffected by consistency also. It is proposed that the addition of pulp did not affect the flow field around the foil rotor.

To determine if the consistency had any affect on the pulse the positive and negative pulse magnitude were calculated for both rotors. The magnitudes of the positive and negative parts of the pulse for the step rotor are shown in Figure 5-25 and Figure 5-26 respectively. Likewise the positive and negative pulse magnitude for the foil rotor for several feed consistencies is shown in Figure 5-27 and Figure 5-28. The positive and negative pulse magnitudes for the step rotor both increased as consistency was increased. Both portions of the pulse were unaffected by changes in consistency for the foil rotor.

The cause of the increase in pulse magnitude at elevated consistency is best explained by consideration of the role that fibre will play in the transfer of pressure or force from the rotor to the screen wall. For pipe flow the pressure drop can be described by a characteristic S shaped curve as discussed in Section 2.3. Several flow regimes can exist depending on the velocity of the suspension, and drag reduction occurs above a critical velocity. The flow of pulp in a rotary shear device on the other hand does not have the same flow regimes that occur in pipe flow. The torque can drop below the water curve under certain conditions but at a consistency of 2 % the torque verse tip speed curve or angular velocity will be slightly greater than for water even at elevated velocities (Gullichsen & Härkönen, 1981; Bennington, 1988). The structure of the suspension at elevated velocities, such as those found in the screen annulus, is likely to be small flocs which are likely to move relatively freely. The fibre dampens turbulence and increases the transfer of force from the rotor to the screen wall where the transducer measures an increased pressure for the same rotor speed. The movement of flocs away from the region of high and low pressure will also be restricted by the presence of other flocs.

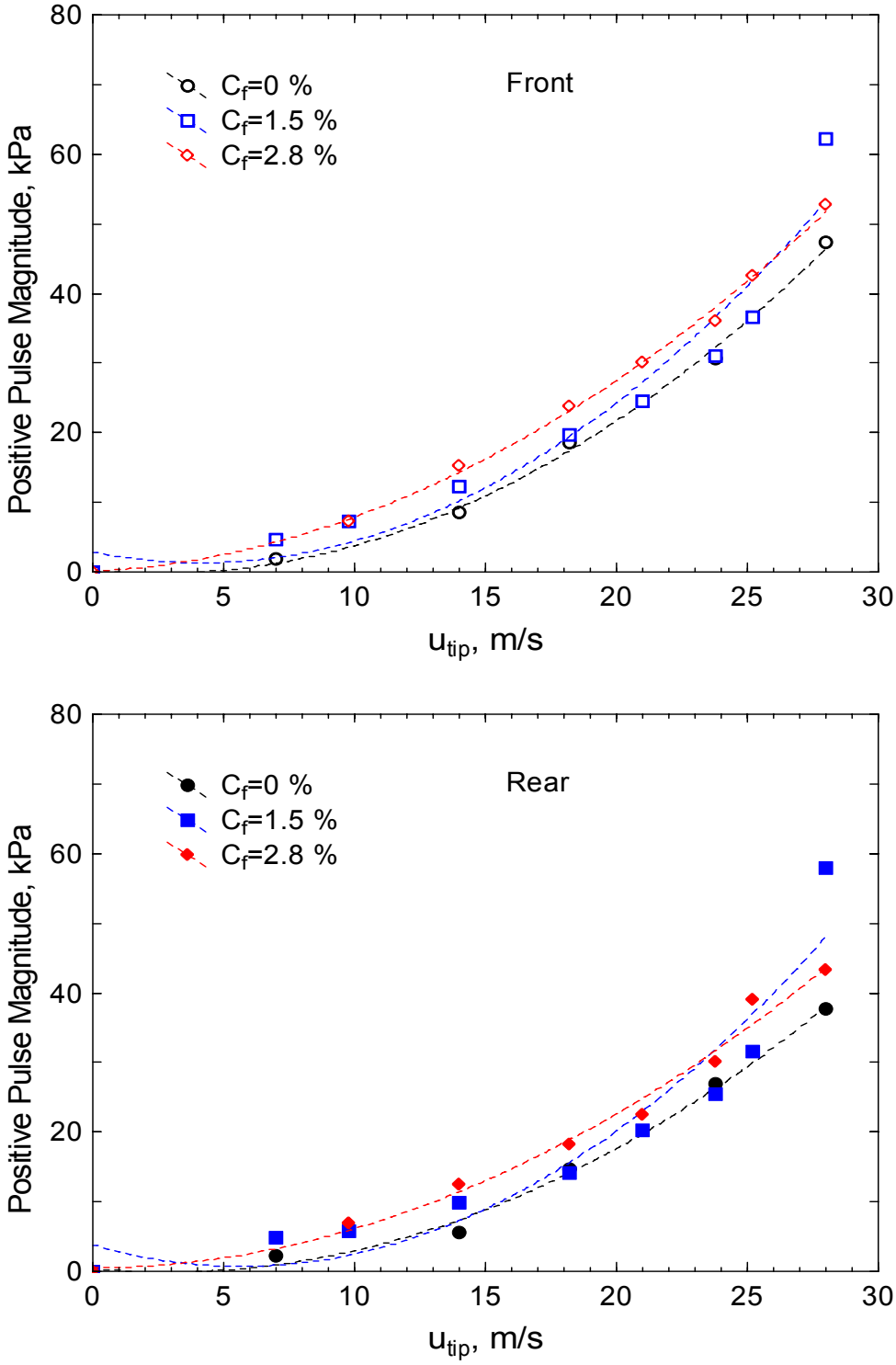

Figure 5-25 Positive pulse magnitude for the step rotor as function of rotor speed for several feed consistencies (Q_f=500 L/min, R_v=1)

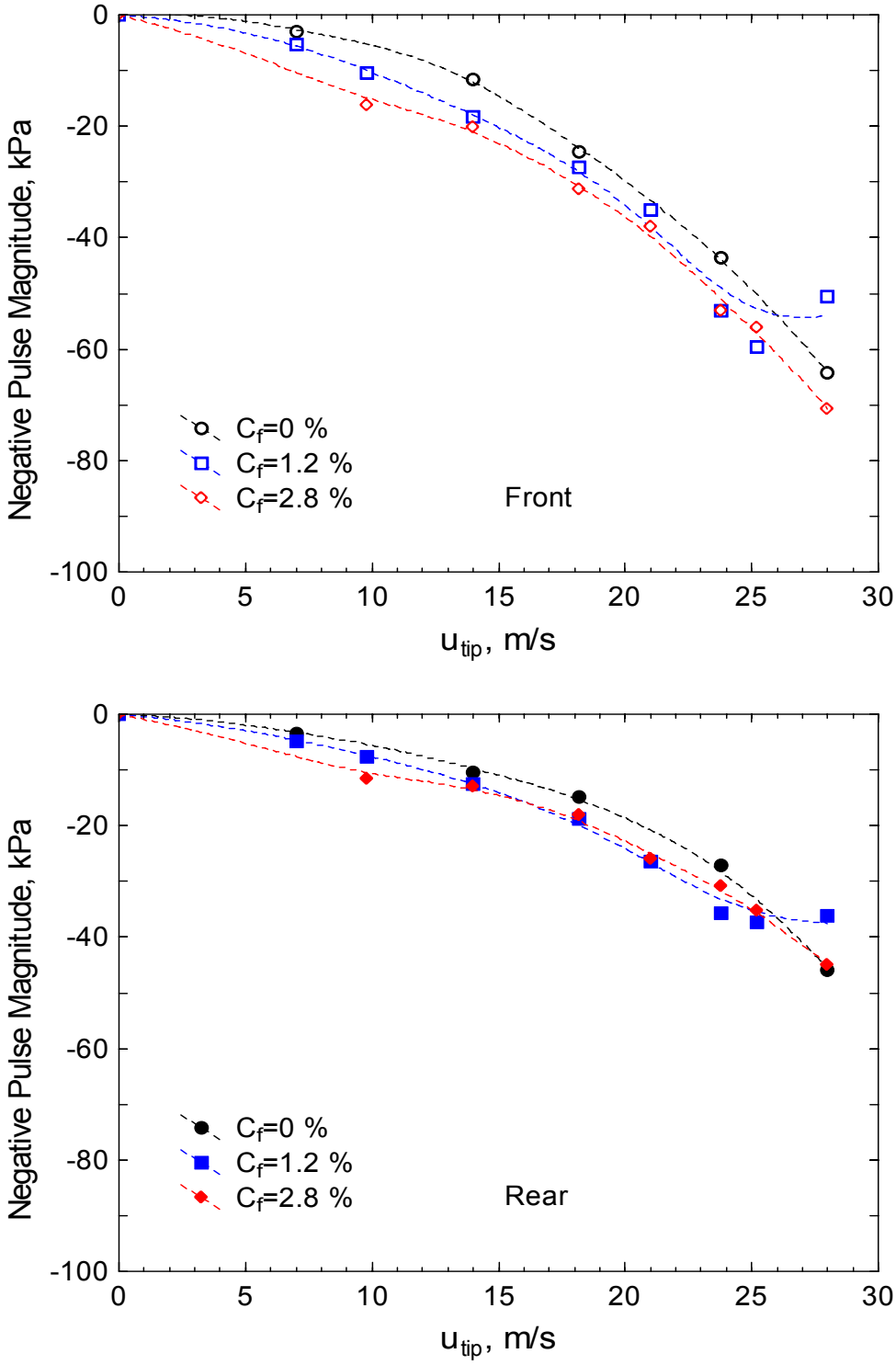

Figure 5-26 Negative pulse magnitude for the step rotor as function of rotor speed for several feed consistencies (Q_f=500 L/min, R_v=1)

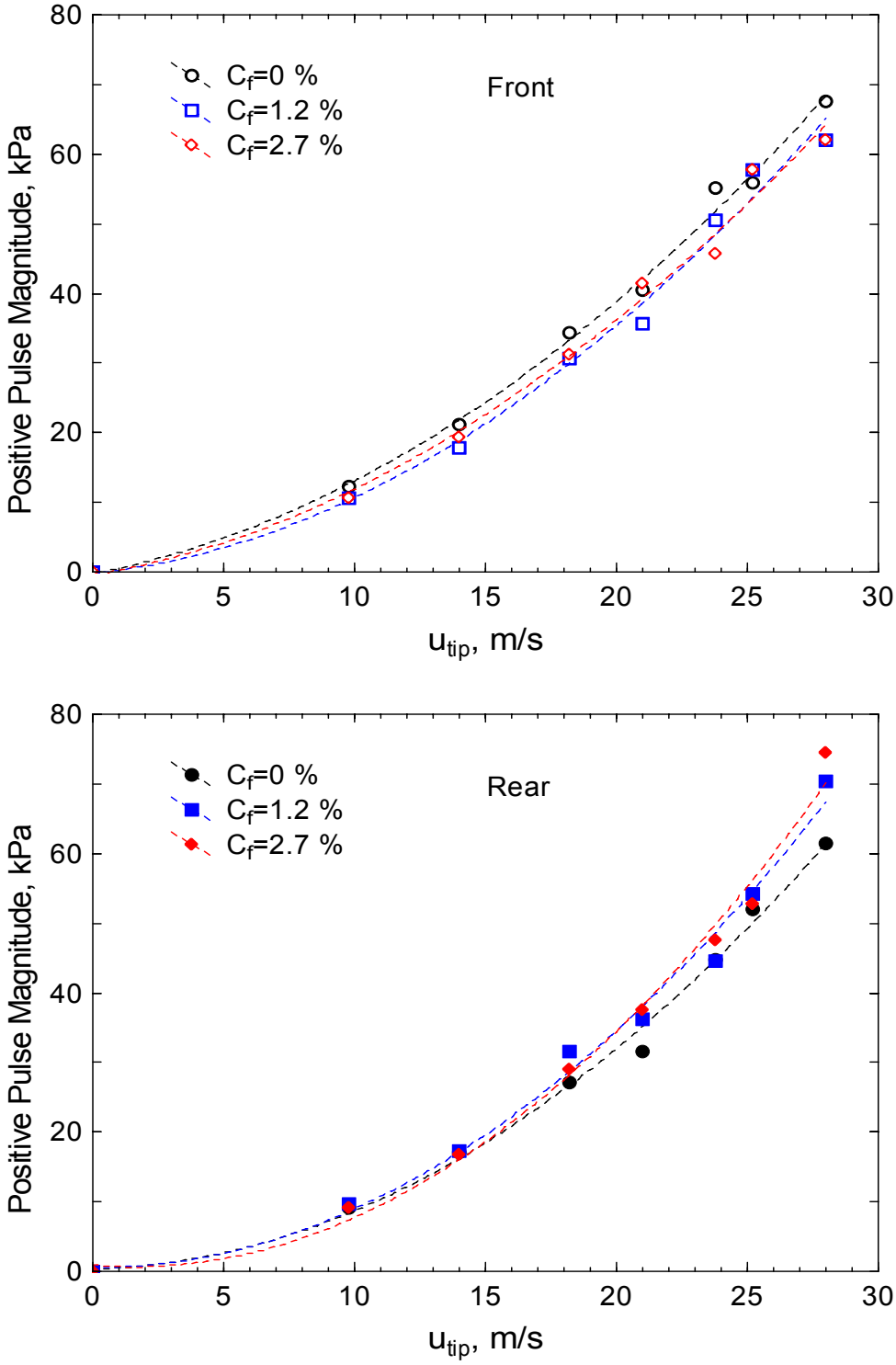

Figure 5-27 Positive pulse magnitude for the foil rotor as function of rotor speed for several feed consistencies (Q_f=500 L/min, R_v=1)

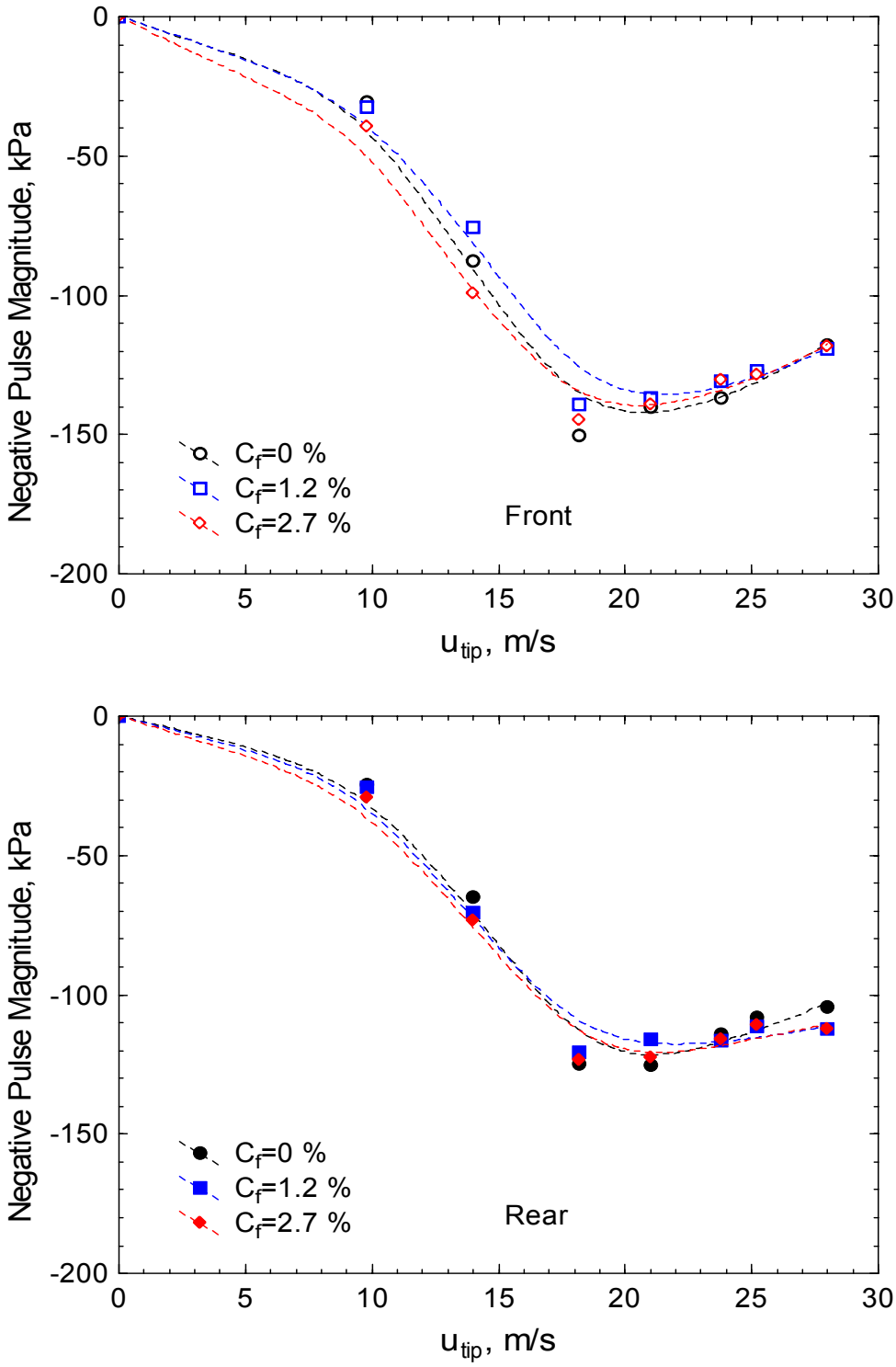

Figure 5-28 Negative pulse magnitude for the foil rotor as function of rotor speed for several feed consistencies (Q_f=500 L/min, R_v=1)

Most researchers that have investigated pressure pulses have also examined the effect of pulp consistency on the pulse shape and magnitude with many reporting a decrease in pulse strength with increased consistency (Gonzalez, 2002; Wikström & Rasmuson, 2002; Pinon et al., 2003) and others reporting no change (Karvinen & Halonen, 1984; Yu, 1994).

Pinon et al. (2003) found that consistency reduced the strength of the negative pulse and the effect of consistency was increased as the rotor speed was increased. The reduction in the magnitude of the negative pressure pulse at 2 % consistency was approximately 45 % at a tip speed of 20 m/s. The presence of fibre also affected the wake of the rotor and this was attributed to instability in the flow or reflocculation. There is evidence that fibres alter the wake of the foil due to reflocculation of the fibre which are thought to increase eddie formation (Gonzalez, 2002). Both Karvinen & Halonen (1984) and Yu (1994) report that the pulse was not affected in any way by the presence of fibre even up to a consistency of 2 %.

The disparity in the reported affect of consistency is difficult to account for. The two studies that have reported no affect with consistency were all conducted on industrial pressure screens while the others, with the exception of Wikström & Rasmuson (2002), were conducted on a small scale laboratory screening apparatus. It may be that the decrease in the negative pulse magnitude is an artefact of the specific screen or apparatus used when measuring the pulse.

5.2 Instantaneous Velocity & Back-Flush Ratio

It has been previously stated that the average aperture velocity is an important variable for screening and that screening conditions are related to this variable (Gooding, 1986; Kumar, 1991; Wakelin et al., 1994; Olson et al., 2000). Others have noted that this superficial velocity is meaningless and the effective passing velocity would be a better indicator of screening conditions (Julien Saint Amand & Perrin, 1998). The average aperture velocity is easily obtained and provides a useful measure for comparison of various results. However actual flow through an aperture is dynamic and as yet no measurements of the instantaneous velocity have been reported, although estimates of effective velocity have been made based on the shape

and magnitude of a pressure pulse (Julien Saint Amand & Perrin, 1998). This section uses measured pressure pulse data to predict the instantaneous and effective aperture velocities of the step and foil rotors and also the back-flush ratio of these two rotors. As part of this approach experimentally derived pressure loss coefficients for the screen apertures were used.

5.2.1 Hydraulic Resistance

The screen aperture velocity or passing velocity at any point in time can be estimated using Equation 5-2, provided the pressure differential P between the feed annulus and the accept chamber and the hydraulic resistance or pressure loss coefficient K_L of the screen plate is known. However, Equation 5-2 will only provide a crude estimate of the instantaneous velocity because the pressure loss coefficient, determined under steady flow conditions, is being applied to a highly unsteady flow situation of variable flow through screen apertures. In the absence of a more accurate method, other than numerical methods, a pseudo steady state method was used.

$$u_s = \sqrt{\frac{2\Delta P}{\rho K_L}} \qquad \textbf{5-2}$$

Gooding (1996) reported that the hydraulic resistance of screen apertures was reduced when using contoured slots, smaller apertures or when the upstream velocity was increased. Hence to apply loss coefficients for the calculation of the forward and reverse flows through the screen, the aperture geometry and the approach flow conditions to the aperture on the feed and accept side of the screen needed to be accounted for. The apertures on the accept side of most holed screens are usually recessed and the approach flow on the accept side is not dominated by a strong tangential flow component. Therefore it is reasonable to expect that the loss coefficient in the reverse direction will be lower than in the forward direction. If both the forward K_{for} and reverse K_{rev} loss coefficients are known the instantaneous aperture velocity in the forward direction $u_{s.for}$ and the reverse direction $u_{s.rev}$ can be estimated using Equations 5-3 and 5-4 respectively where P_{ann} is the pressure in the annulus and P_{acc} is the pressure in the accept chamber.

$$u_{s.for} = \sqrt{\frac{2(P_{ann} - P_{acc})}{\rho K_{for}}} \quad \textbf{5-3}$$

$$u_{s.rev} = \sqrt{\frac{2(P_{acc} - P_{ann})}{\rho K_{rev}}} \quad \textbf{5-4}$$

Once the instantaneous velocity is known the total amount of forward and reverse flow that occurs during the pulse can be calculated and the ratio of these two flows is called the back-flush ratio *k* (Equation 5-5). The back-flush ratio will change depending on the pulse strength, forward and reverse loss coefficients, rotor speed, and rotor type.

$$k = \frac{\int \sqrt{\frac{\Delta P}{K_{rev}}} dt}{\int \sqrt{\frac{\Delta P}{K_{for}}} dt} \quad \textbf{5-5}$$

To determine the forward and reverse loss coefficients a smooth rotor was used to create a steady flow field. The pressure drop across a narrow screen section was measured in the forward direction and in the reverse direction for a range of flow rates (aperture velocities) and rotor speeds. Pressure drops in the forward and reverse directions using the smooth rotor are shown in Figure 5-29 and Figure 5-30 respectively. Screen pressure drops for the case of net forward flow were also measured for the step and foil rotors. Results are shown in Figure 5-31 and Figure 5-32. These data were only measured for the case of net forward flow because the step and foil rotors create flow in both the forward and reverse directions and it is therefore not possible to consider forward or reverse flow only.

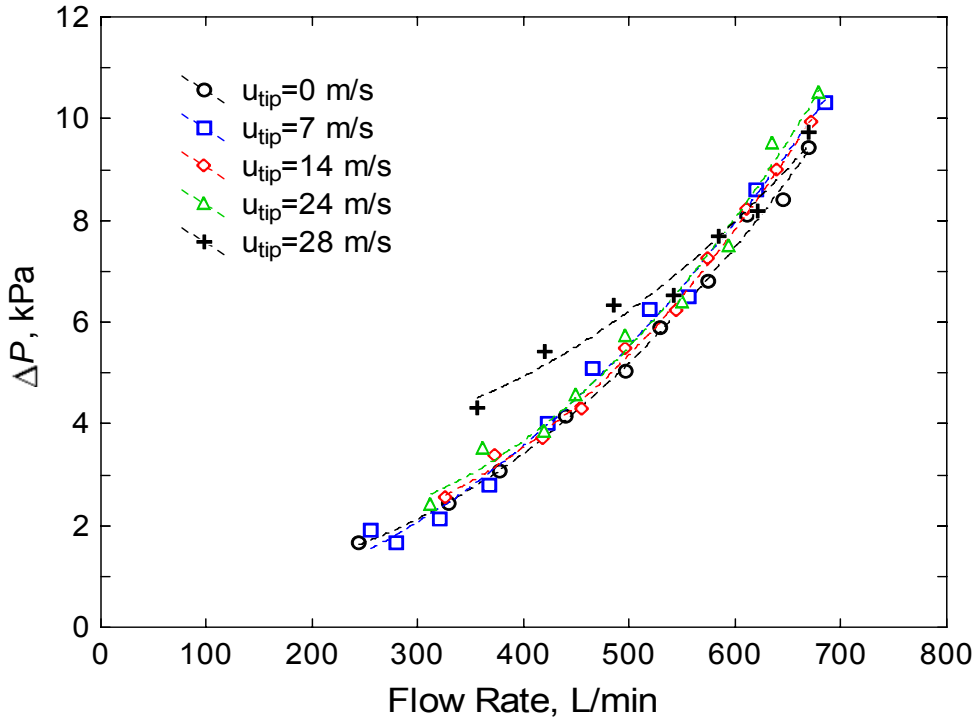

Figure 5-29 Pressure drop across a narrow screen section in the forward direction for the smooth rotor (water, 1 mm holes, R_v=0)

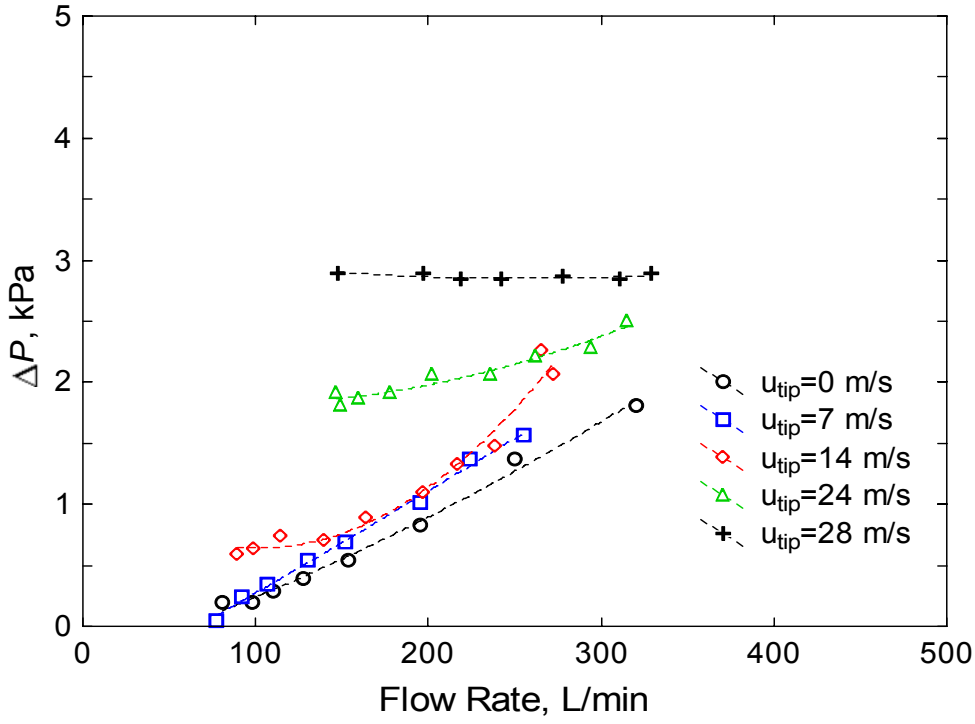

Figure 5-30 Pressure drop across a narrow screen section in the reverse direction for the smooth rotor (water, 1 mm holes, R_v=0)

The pressure drop increased as the flow rate through the screen increased. For the smooth rotor in the forward direction, the pressure drop increased following roughly the square of the flow rate. This relationship was unaffected by rotor speed except for the highest rotor speed where the pressure drop was slightly greater at the lower flow rates. When the flow was reversed for the smooth rotor the rotor speed had a larger affect on the pressure drop. The pressure drop increased as the rotor speed was increased and pressure drop became practically independent of flow rate at the highest rotor speed for the range of flow rates tested. It should be pointed out that the scale on Figure 5-30 for the reverse direction is different than the figure for the forward direction.

An interesting observation when conducting the reverse flow pressure drops with the smooth rotor was that the pump could be turned off completely and reverse flow would still occur with the rotor spinning. This is the reason why the minimum flow rate obtained in the reverse direction was approximately 80 L/min at the lower rotor speeds and approximately 150 L/min at the two highest rotor speeds. The cause of this is thought to be due to the acceleration of the fluid in the annulus due to the rotor. The tangential velocity produced by the rotor will cause the pressure to decrease and therefore a suction affect occurs and causes flow through the screen. It should also be noted that the upper limit of the flow rate that could be measured in the reverse direction was much less than for the forward direction (approximately half). The decreased upper limit was due to the increased resistance in pumping the reverse direction and the maximum head of the pump being reached.

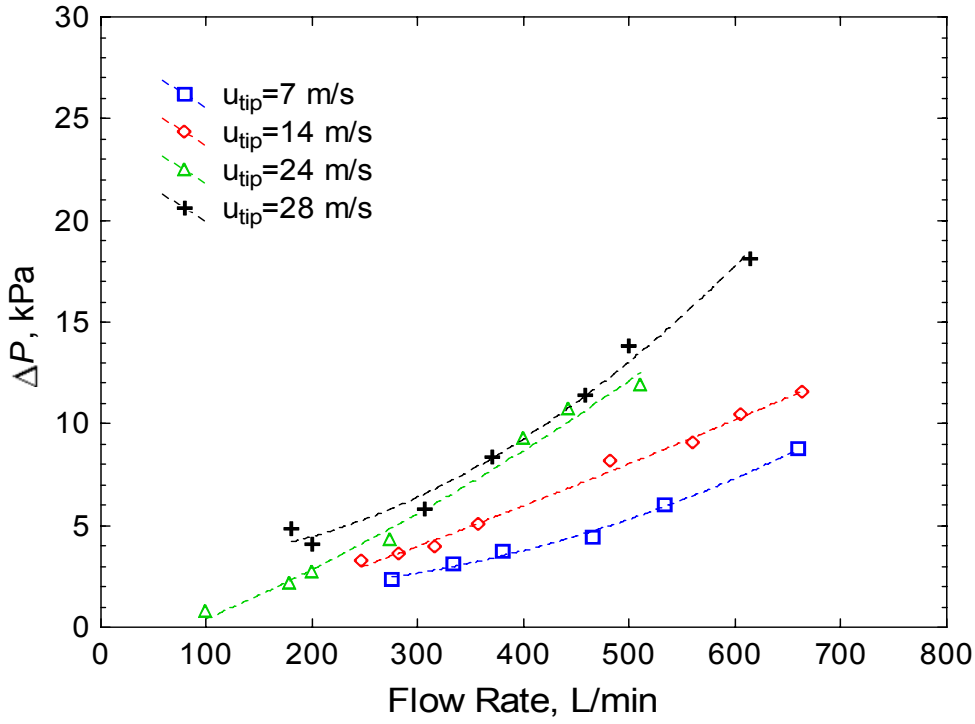

Figure 5-31 Pressure drop across a narrow screen section for the step rotor (water, 1 mm holes, R_v=0)

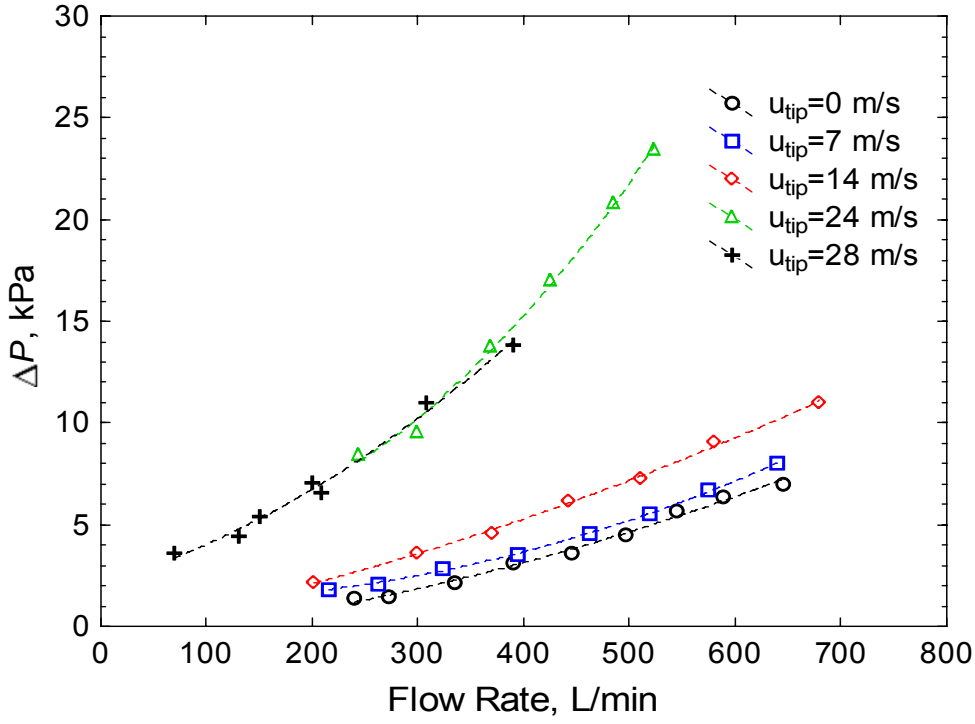

Figure 5-32 Pressure drop across a narrow screen section for the foil rotor (water, 1 mm holes, R_v=0)

The pressure drop for the step rotor increased with flow rate roughly following a squared relationship. Increasing rotor speed shifted the curve up as rotor speed increased. Similar trends as the step rotor were seen for the foil rotor expect that the two curves at the higher rotor speed were almost identical. As discussed previously in Section 5.1.1 this is due to the fact that there is a critical rotor speed where increased rotor speed does not affect the pressure pulse magnitude or negative pulse magnitude for the foil rotor. Therefore above this critical rotor speed there is expected to be no difference in pressure drop due to increased rotor speed.

Pressure drop data was used to calculate the pressure loss coefficients (Equation 5-2) in the forward and reverse directions for the smooth rotor and the apparent loss coefficient for the step and foil rotors. The forward loss coefficients for the smooth rotor as function of aperture velocity for a range of rotor speeds are shown in Figure 5-33 and the reverse loss coefficients are shown in Figure 5-34. The aperture velocity is calculated by dividing the accept flow rate by the open area of the basket. For the step and foil rotors were there is periodic forward and reverse flow across the screen the aperture velocity is the average or superficial aperture velocity $\bar{u}_s$. The loss coefficient significantly increased as the aperture velocity decreased and tended to a common value as aperture velocity increased. Rotor speed tended to increase the loss coefficient at the lower aperture velocities for both the forward and reverse directions. It should be pointed out that due to the inability of measuring the pressure drop at low flow rates the pressure drop curves were extrapolated in order to estimate loss coefficients at low aperture velocities. Hence the disparity in the number of datum between the pressure drop and loss coefficient figures.

Both the forward and reverse loss coefficient data collapse onto a single curve (Figure 5-35 & Figure 5-36) when the aperture velocity is divided by the upstream velocity to give the normalised aperture velocity (Equation 5-6).

$$u_n = \frac{\bar{u}_s}{\bar{u}_u} \qquad \textbf{5-6}$$

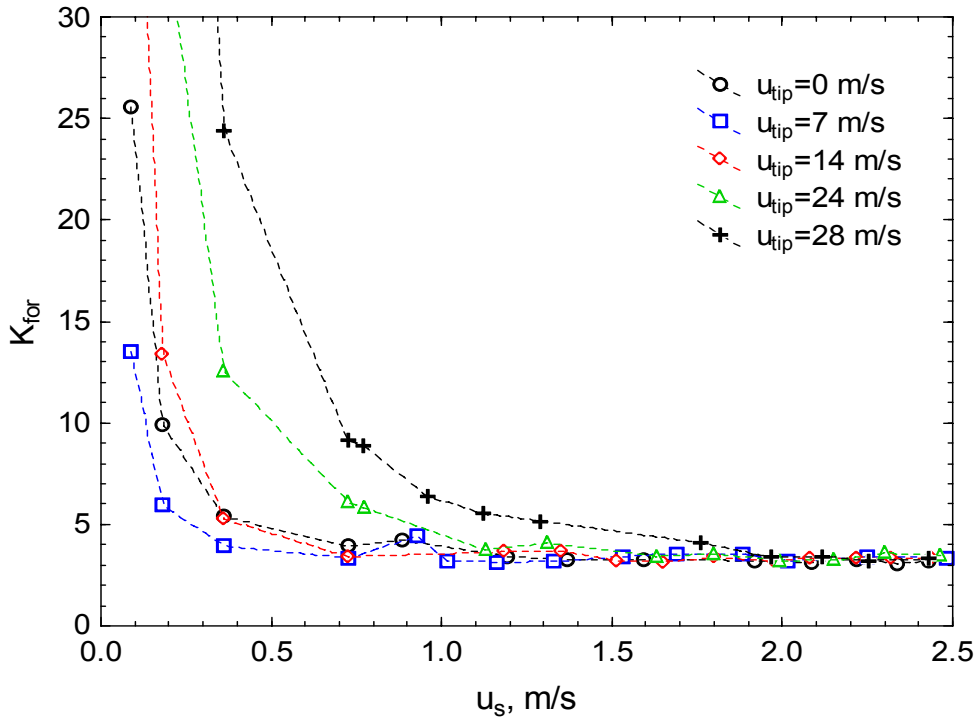

Figure 5-33 Forward pressure loss coefficient for the smooth rotor at a range of rotor speeds (water, 1 mm holes, R_v=0)

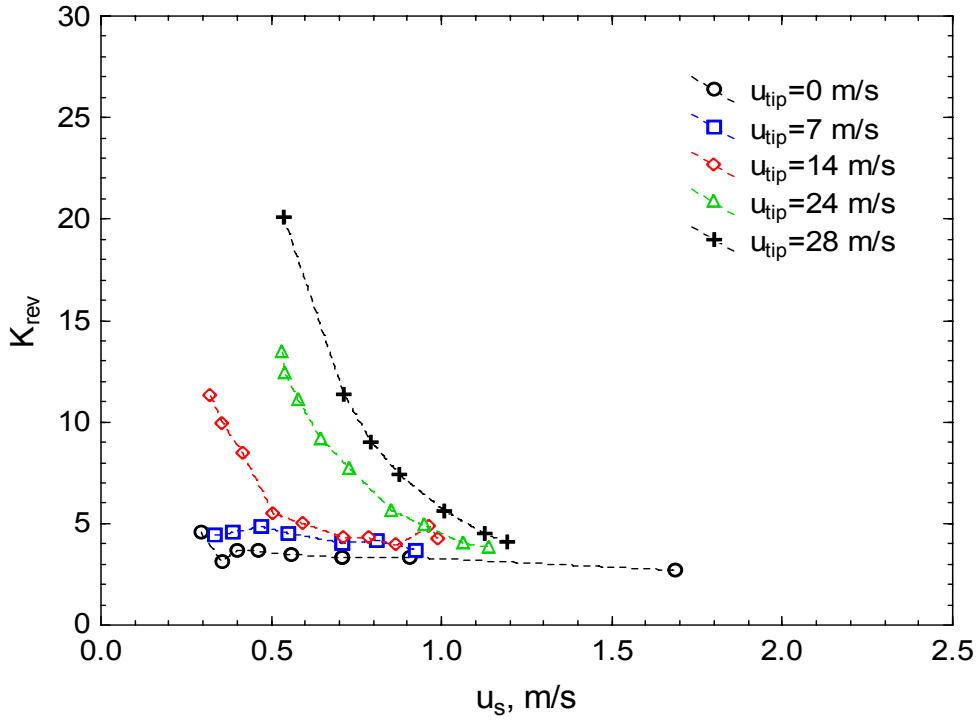

Figure 5-34 Reverse pressure loss coefficient for the smooth rotor at a range of rotor speeds (water, 1 mm holes, R_v=0)

Usually the normalised velocity is used in single aperture flow channel experiments were the upstream velocity is known. The upstream velocity of the flow in a pressure screen annulus is difficult to determine with certainty and will vary along the length of the screen. However an upstream velocity can be estimated for the forward and reverse directions if some simplifying assumptions are made. In the forward direction the fluid will approach the aperture from an angle and not exclusively from the tangential direction. The upstream velocity will be made up of tangential and axial velocity components. The tangential velocity components were estimated by assuming an initial tangential velocity component, which is due to the tangential feed of the screen. The initial tangential velocity component was assumed to be half of the pipe velocity as it enters the feed chamber. The remainder of the tangential velocity component was assumed to be 15 % of the tip speed. A narrow screen section was used and therefore there is no change in the bulk axial velocity along the screen length. The axial velocity was calculated by dividing the feed flow rate by the area of the annulus. The upstream velocity is then calculated using Pythagoras' theorem (Equation 5-7).

$$\overline{u}_u = \sqrt{\overline{u}_{tan}^2 + \overline{u}_{ax}^2} = \sqrt{\left(\frac{Q_a}{2A_{pipe}} + 0.15u_{tip}\right)^2 + \left(\frac{Q_a}{A_{annulus}}\right)^2} \qquad \textbf{5-7}$$

The relative magnitude of the axial and tangential velocity components varies depending on the feed flow rate, reject rate, and the axial position of the screen that is considered. Under most circumstances the tangential velocity component is much greater than the axial component, with the tangential component being in the order of 4 to 20 times greater than the axial component. The axial velocity component is greatest at the front of the screen and decreases along the screen length. As previously discussed the tangential velocity will increase along the screen length due to the action of the rotor.

The upstream velocity in the reverse direction is not meaningful in the same sense as it is in the forward direction case because the flow approaches the aperture from essentially only the radial direction and therefore the upstream velocity will be similar

to the aperture velocity. When the rotor is spinning, however there will be a strong tangential velocity component on the annulus side of the aperture and therefore the aperture velocity is normalised by this downstream velocity (Equation 5-8). In the same way as the forward direction instance the downstream tangential velocity was assumed to be 15 % of the tip speed.

$$\bar{u}_u = 0.15 u_{tip} \qquad \textbf{5-8}$$

The loss coefficient data as a function of normalised aperture velocity in the forward and reverse directions are shown in Figure 5-35 and Figure 5-36 respectively. Data for the situation where there is no rotor running is omitted from the figures. The data collapses onto a single curve for both the forward and reverse directions. The fitted curve for the forward loss coefficient is also presented in Figure 5-36 for comparison. The loss coefficients for both directions increased as the normalised velocity was decreased. The forward and reverse loss coefficients are very similar above a normalised velocity of approximately 0.2 however below this point the reverse loss coefficient is greater than the forward and the difference was enlarged as the normalised velocity approaches zero.

It would appear from the data that K is dependant not only on the flow conditions surrounding the aperture but also on the geometry of the aperture. The geometry in the reverse direction is slightly different to that in the forward direction. It is also well established from the theory that the hydraulic resistance or discharge coefficient is geometry dependant. The hydraulic resistance was found to be greater for narrow slots in the reverse direction largely on the basis of the very different geometry of the accept side of the screen basket (Jokinen, Ämmälä et al., 2007). The same relationship between hydraulic resistance in the forward direction and normalised velocity have been reported although the values of K_{for} were different due to the different apertures and flow conditions that were used (Gooding, 1996; Gooding, Kerekes et al., 2001).

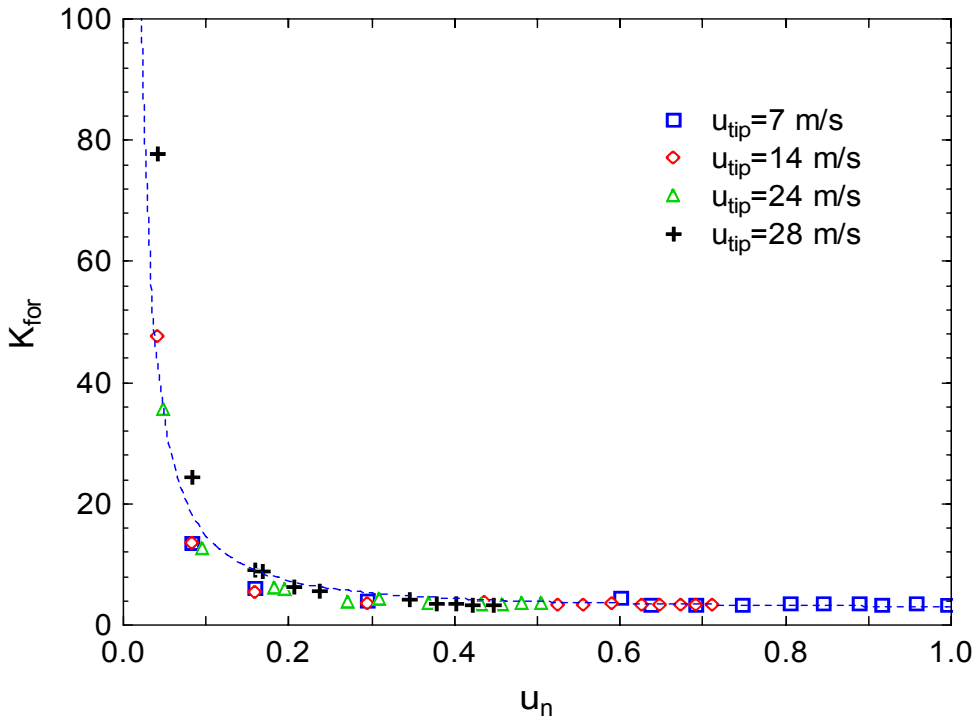

Figure 5-35 Forward pressure loss coefficient for the smooth rotor at a range of rotor speeds as a function of normalised velocity (water, 1 mm holes, R_v=0)

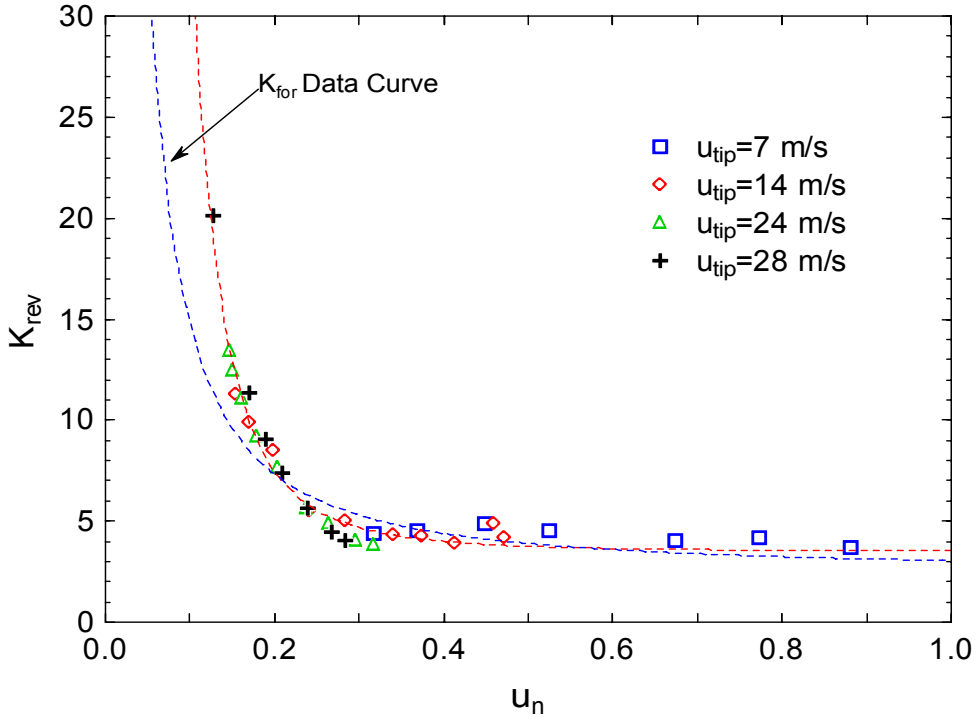

Figure 5-36 Reverse pressure loss coefficient for the smooth rotor at a range of rotor speeds as a function of normalised velocity (water, 1 mm holes, R_v=0)

The loss coefficients are expected to collapse onto a single curve when plotted against normalised velocity because in the forward direction the normalised velocity controls the size of the recirculation zone on the upstream wall of the aperture as illustrated previously in Figure 2-29 (Thomas & Cornelius, 1982; Gooding, 1986; Olson & Kerekes, 1998a). The ratio of the aperture velocity to the upstream velocity is the important factor and the recirculation zone increases in size as the normalised velocity is decreased. The loss coefficient will be increased due to the increased size and restriction on the flow exerted by the recirculation zone. The fraction of the aperture filled by this vortex is therefore an important principal factor that controls the hydraulic resistance of flow through a screen aperture (Gooding, 1996; Gooding, Kerekes et al., 2001).

In the reverse direction, turbulence in the annulus will increase as the tangential velocity in the annulus increases. The flow through the aperture will contact the fluid with a high tangential velocity and the resulting flow is expected to be chaotic and highly turbulent. As the tangential velocity increases the level of turbulence will increase and it will be more difficult for the incoming fluid to enter the annulus therefore increasing the resistance and loss coefficient.

As mentioned previously, there is a presumption that the flow is steady when measuring the loss coefficient. However, when using a typical rotor such as the foil or step rotor the flow is unsteady and pulsating and an apparent pressure loss coefficient K^* can be determined (Gooding, 1996). The apparent loss coefficient is calculated using Equation 5-9 where $\bar{u}_s$ is the superficial aperture velocity and $\overline{\Delta P}$ is the average pressure drop across the screen.

$$K^* = \frac{2\overline{\Delta P}}{\rho \bar{u}_s^{\,2}} \qquad \textbf{5-9}$$

The apparent pressure loss coefficient was measured for the step and foil rotor for a range of mean aperture velocities at several rotor speeds. Data shown in Figure 5-37 and Figure 5-38 is for the step and foil rotors respectively.

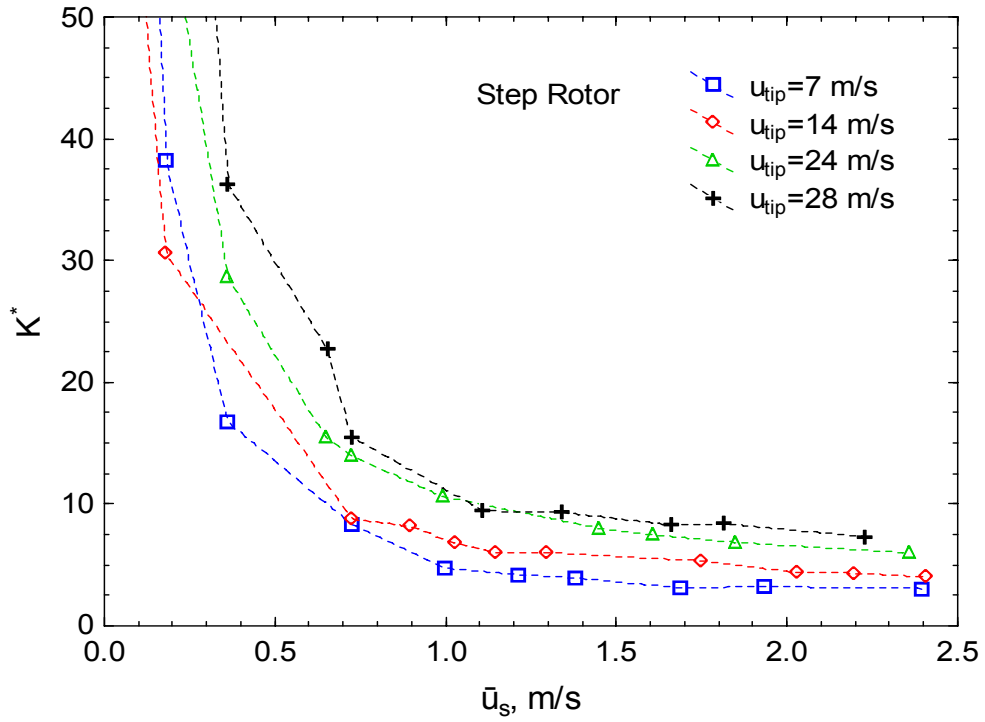

Figure 5-37 Apparent pressure loss coefficient for the step rotor at a range of rotor speeds (water, 1 mm holes, R_v=0)

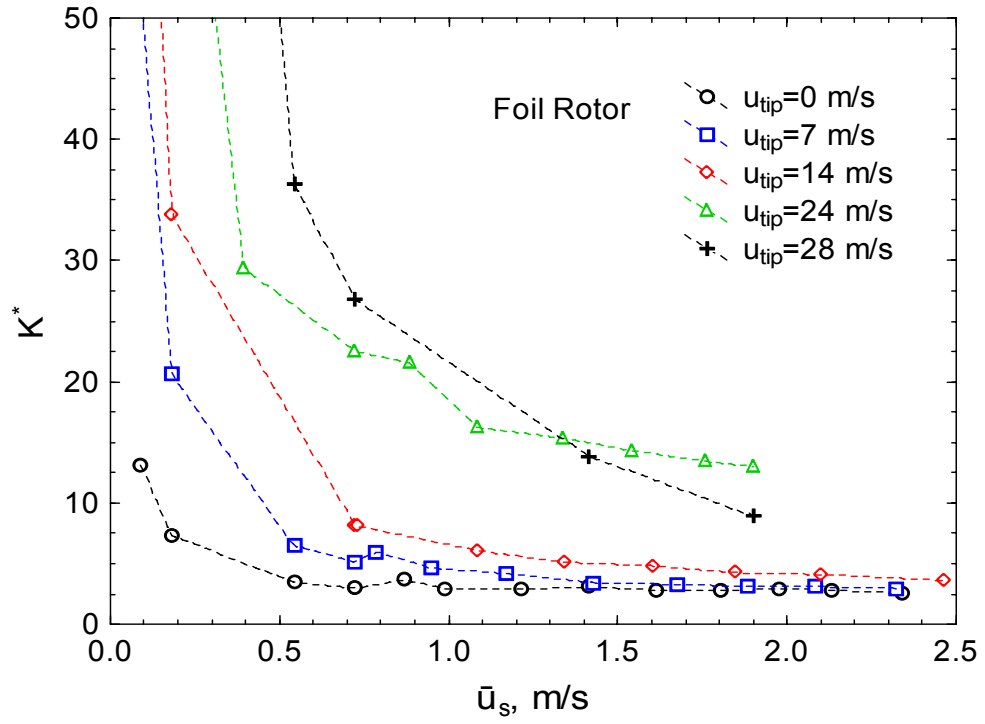

Figure 5-38 Apparent pressure loss coefficient for the foil rotor at a range of rotor speeds (water, 1 mm holes, R_v=0)

Weckroth et al. (2001) note that the holes are much easier to keep clear from fibre accumulations than slots and therefore the pressure pulse can be relatively small than compared to the pulsed needed for slotted screens. Indeed it has been shown that the loss coefficients in both the forward and reverse direction for slots will be higher due to the geometries involved (Jokinen, Ämmälä et al., 2007).

5.2.2 Instantaneous Aperture Velocity

Instantaneous aperture velocities have been calculated for water only using measured pressure pulse data at the rear of the screen and screen aperture loss coefficients. It was assumed that the forward flow rate can be predicted using the positive pressure differential ΔP between the annulus and accept side of the screen and the forward loss coefficient K_{for}. Similarly reverse flow can be predicted using the negative pressure differential ΔP between the annulus and accept side of the screen and the reverse loss coefficient K_{rev}. This approach employs a number of simplifying assumptions which introduce some error. However it is believed that the predicted values give a useful indication of the magnitude of the velocity fluctuations that are occurring.

It is recognised that to accurately derive instantaneous velocities from fluctuating annulus pressures, extensive numerical modelling is required and this is an area of on going work. As a result of the continuously changing pressure differential, the fluid flow rate through the screen and hence the instantaneous aperture velocity also changes continuously and significant amounts of acceleration and deceleration occur in the fluid during each pulse cycle. The approach taken assumes the aperture loss coefficients, derived under steady state conditions or zero acceleration with time conditions, adequately account for fluid momentum changes that occur by incorporating the fluid kinetic energy loss term in the loss coefficient. Fluid momentum changes will also absorb some of the pressure energy which drives the forward and reverse fluid movement. It is estimated using linear momentum theory that for a maximum change in forward and reverse velocity of 17 m/s (5 m/s forward and 12 m/s reverse) in a time period of 0.017 milliseconds, 5 kPa of pressure will be consumed. For the pressure levels present, ignoring linear momentum will introduce an error of not more than 5 % into the instantaneous velocity calculations.

The measured pressure pulse at the rear of the screen and the loss coefficients for the screen apertures were used to predict the instantaneous aperture velocity. A spreadsheet was developed which allowed pulse data to be analysed, an estimate of the instantaneous aperture velocity and back-flush ratio to be made. A typical cycle of six pressure pulses was averaged and this average was assumed to be the mean pressure in the screen annulus. Other researchers have estimated the pressure in the annulus to be the mean of the feed and rejects line pressures (Gooding, 1996; Weeds, 1998) which is a crude estimate because the annulus pressure is changing constantly with time and along screen length due to the action of the rotor and frictional pressure losses. The rear pulse was used for the prediction of instantaneous aperture velocity in order to minimise the influence of any entrance effects at the front of the screen. The rational for using the rear pulse is that the conditions at the centre of the screen, where the pressure drop was measured, will be closer to that of the rear than the conditions at the front.

The pressure drop measured during the loss coefficient studies was used as an initial value for the accept pressure. Forward flow will occur when the instantaneous pressure exceeds the accept pressure while reverse flow occurs when the instantaneous pressure is less than the accept pressure as illustrated in Figure 5-39. The back-flush ratio is the ratio of the total amount of forward and reverse flow that occurs during one pulse.

A function was fitted to forward loss coefficient data presented in Figure 5-35 for the normalised velocity. The loss coefficient is expressed as a function of normalised velocity and is illustrated in Figure 5-40. A second function was fitted to reverse loss coefficient data for a rotor speed of 24 m/s for data presented previously in Figure 5-34. The reverse loss coefficient is expressed as a function of average aperture velocity, and data and the fitted curve are shown in Figure 5-41. Only data for the 24 m/s case was used because that was the tip speed of the pulse used for the instantaneous velocity predictions. The form of the functions used is the same as that used by other researchers to fit data to experimentally measure loss coefficient data (Martinez et al., 1999).

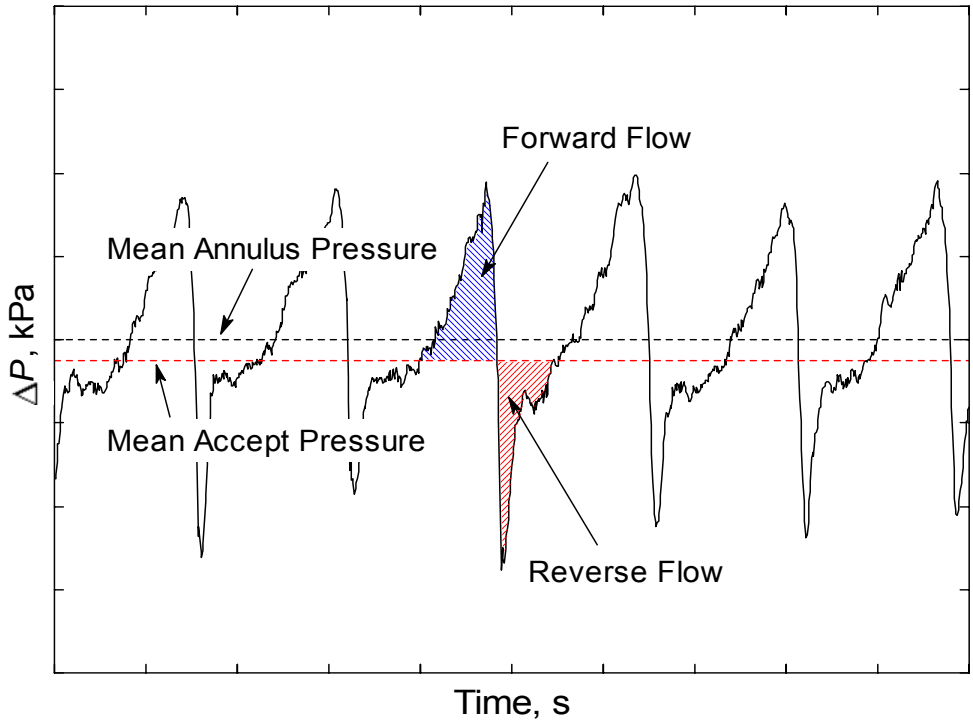

Figure 5-39 Schematic of the pressure pulse with forward and reverse flow sections shown

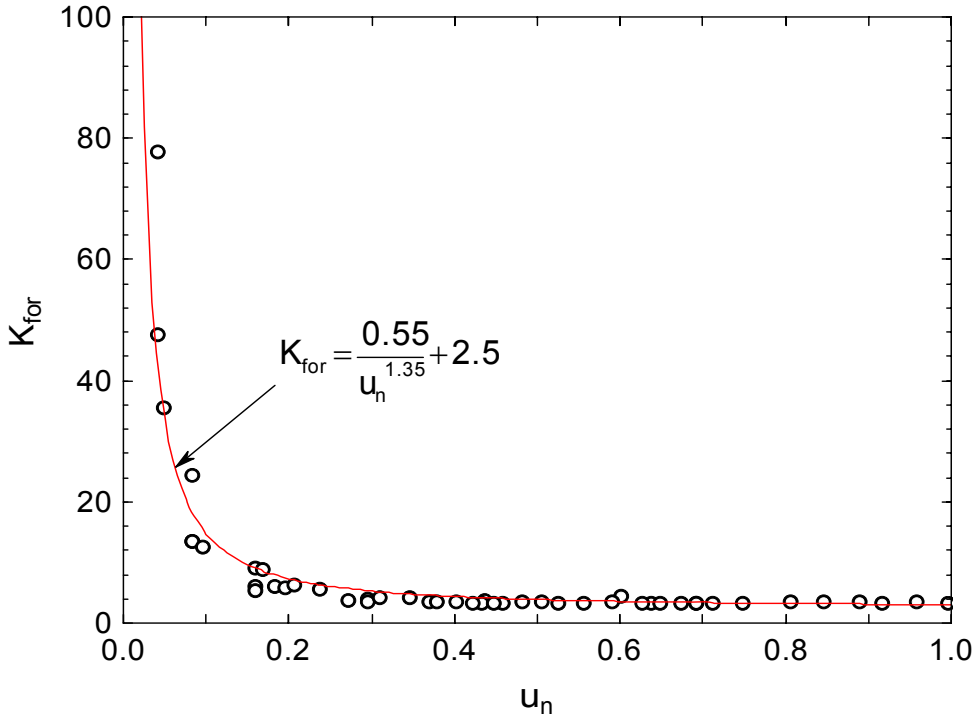

Figure 5-40 Data and fitted equation used in velocity prediction for u_{tip}=24 m/s for the smooth rotor

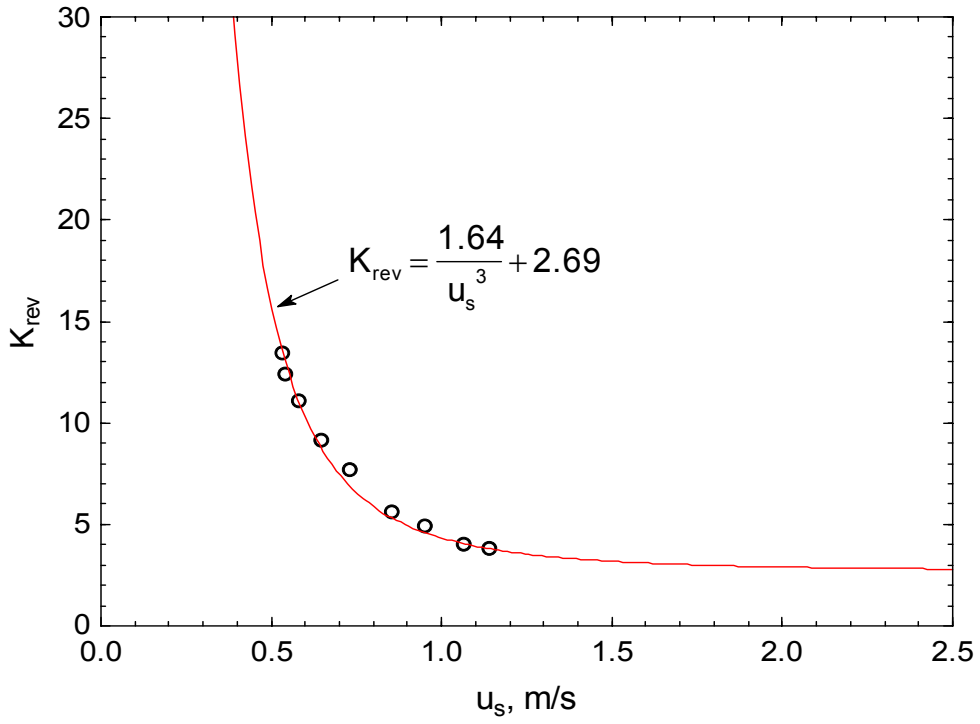

Figure 5-41 Data and fitted equation used in velocity prediction for u_{tip}=24 m/s for the smooth rotor

Values of 2.5 and 2.69 for K_{for} and K_{rev} respectively were used for calculating initial estimate the instantaneous aperture velocities. For this first estimate values of K_{for} and K_{rev} where assumed to remain constant with aperture velocity. From Figure 5-40 and Figure 5-41 this is clearly not the case so on the next iteration the effect of aperture velocity on the loss coefficients is accounted for. This was done by normalising the instantaneous velocities one at a time and determining the new K_{for} for each data point using the fitted function presented in Figure 5-40. The aperture velocity was normalised using the same approach that was used for the forward loss coefficient data discussed previously with the exception that the mean tangential velocity was assumed to be 20 % of the tip speed instead of 15 % as used previously. The greater value was used because the pulse data was measured at the rear of the screen and it is expected that the mean tangential velocity will be slightly greater toward the rear compared to the centre of the screen where the loss coefficients were measured.

At the same time a new K_{rev} was calculated using the function that expressed K_{rev} as a function of aperture velocity as shown in Figure 5-43. These new K_{for} and K_{rev} varied

with changes in u_s and a number of iterations were carried out, calculating a new u_s and then recalculating new values of K_{for}, K_{rev} and u_s until there was little change in their values. This iterative approach allowed the loss coefficients to change as u_s varied.

The total amounts of flow in the forward and reverse directions were calculated using the estimated instantaneous velocities. The difference between the forward and reverse flow values was then the total forward flow or accept flow through the screen. It was found that there was a moderate mass balance error between the predicted amount of total forward flow and that predicted from the accept flow rate and the time over which the pulse occurred. In order to correct this mass balance error, the total amount of flow was set as the target value and then a back calculation was performed and the accept pressure adjusted to correct the mass balance error. The adjustment had only a minor affect on the instantaneous velocities and was usually within the experimental error of the pressure drop measurement. The adjustment was made because the actual local pressure drop was not measured during the pulse measurement and it was found that the local annulus pressure was not well represented by the pressure measured in the reject or feed pipe.

The predicted instantaneous aperture velocity for the step and foil rotor at a given reject rate is shown in Figure 5-42 and Figure 5-43 respectively. As can be seen in both the figures the instantaneous velocity deviates greatly from the superficial velocity which is indicated by the dashed horizontal line in the figure. The average or effective forward $\bar{u}_{s.for}$ and reverse $\bar{u}_{s.rev}$ aperture velocities are also indicated on the figures. A comparison of the two rotors shows that the average forward velocity is moderately higher for the step rotor but the foil rotor has a much higher average reverse aperture velocity. The peak forward velocity is also similar for the two rotors. The total amount of fluid passed in the forward and reverse directions in one pulse was similar for the two rotors although it occurred over different time spans. This is seen in the difference in the average forward and reverse velocities. The duration of the reverse flow is also much more, approximately five to six times longer, for the step rotor than for the foil. The instantaneous velocity followed the general shape of pressure pulses of each rotor.

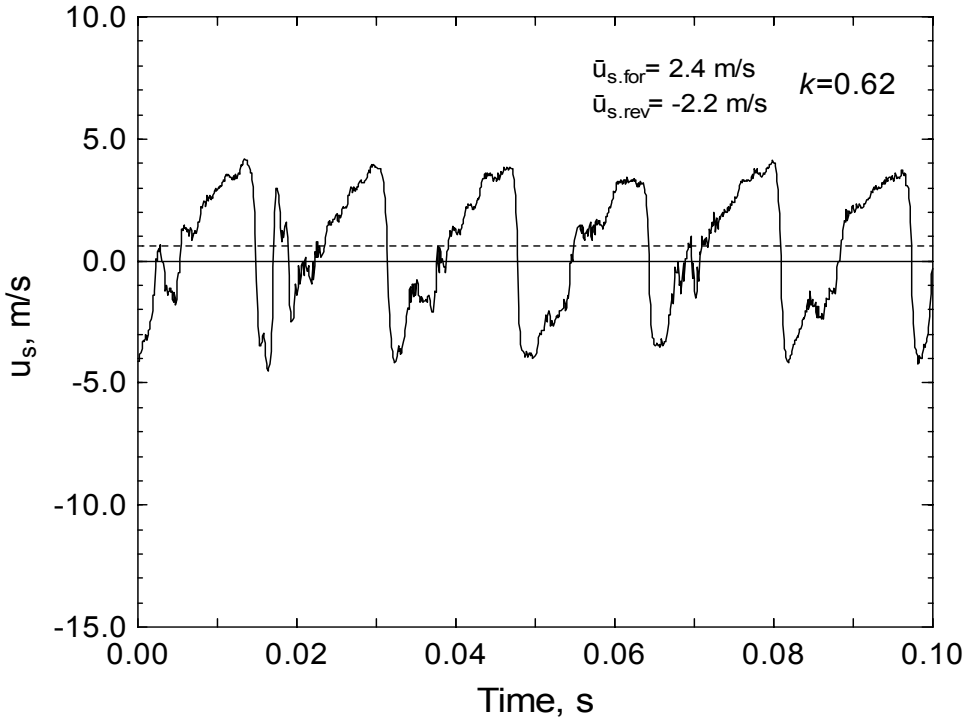

Figure 5-42 Predicted instantaneous aperture velocity for the step rotor (Q_a=660 L/min, $\bar{u}_s$=0.6 m/s, R_v=0.43, u_{tip}=24 m/s)

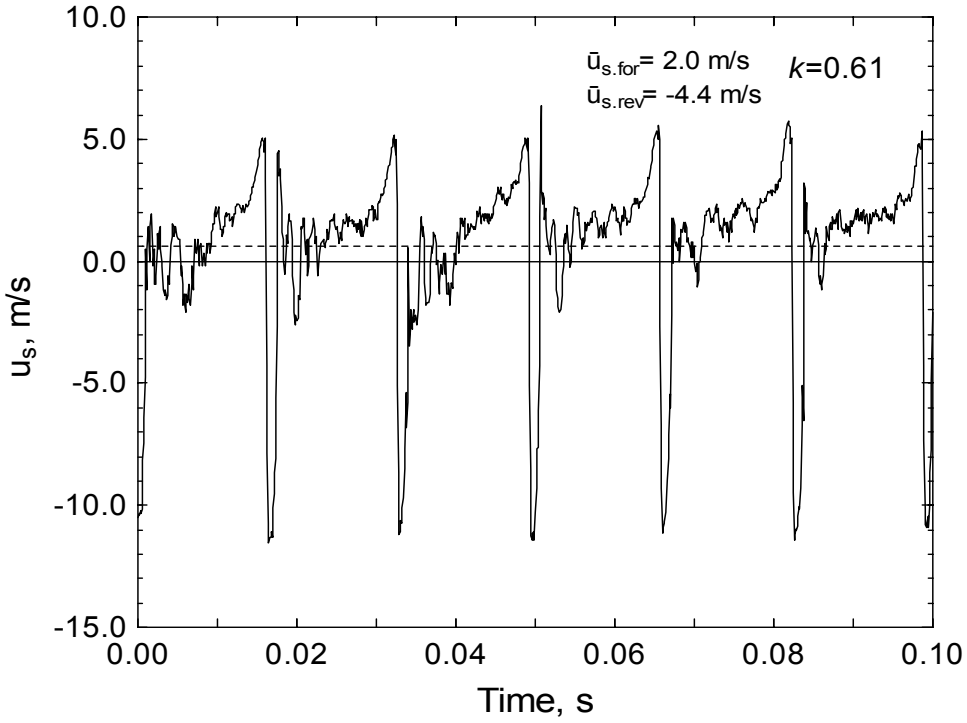

Figure 5-43 Predicted instantaneous aperture velocity for the foil rotor (Q_a=660 L/min, $\bar{u}_s$=0.6 m/s, R_v=0.45, u_{tip}=24 m/s)

Fundamental studies examining the passage of fibres through single apertures in steady flow have unanimously found that passage increases as the aperture velocity increases (Gooding, 1986; Kumar, 1991; Olson, 1996; Atkins, 2003). Based on these studies it may seem reasonable to conclude that the passage of fibre may also increase as the instantaneous velocity increases. However, all of these fundamental studies were conducted under steady flow conditions and at very low consistencies. At elevated consistencies fibre will accumulate at the aperture at some rate and this will adversely affect fibre passage and fluid passage. This will actually cause the fibre passage and the fluid passage to decrease during the forward portion of the pulse. Furthermore there is evidence that fibre passage and aperture obstructions will involve flocs and contaminants and an extrusion mechanism and not just individual fibres (Yu & DeFoe, 1994; Julien Saint Amand et al., 2005). It has also been noted that for a fixed upstream velocity fibre stapling only occurs below a critical aperture velocity and this critical aperture velocity increased as the upstream velocity was increased (Atkins, 2003). It was estimated that the critical normalised velocity for stapling to occur was between approximately 0.75 to 1.2 depending on the feed consistency, aperture type and upstream velocity.

The effect of fibre accumulations on screening performance and also on the passage of fibre though an aperture is poorly understood. Gooding (1996) monitored the pressure drop across a single aperture as fibre accumulated at the aperture and found the pressure drop increased and aperture velocity decreased as fibre accumulated. The pressure loss coefficient increased as fibre accumulated, although the initial aperture velocity affected the final value. At low aperture velocities the loss coefficient increased by about 30 % whereas at higher velocities it can triple when the aperture is partially obstructed with pulp.

It is reasonable to assume that accumulated fibre will have an adverse affect on the instantaneous velocity especially in the forward direction. For slotted apertures a fibre mat or fibre accumulations could also form on the accept side of the screen under certain conditions and the accept side profile of modern slots would seem to minimise reverse fibre passage. The accumulation of fibre on the accept side of the screen plate could have a significant affect of the reverse loss coefficient and therefore reduce substantially the reverse flow. If the reverse pulse is not strong

enough this reduced reverse flow could have a detrimental affect on the ability of the rotor to clear the apertures.

The instantaneous velocities calculated here should only be seen as tentative values and due to the simplifying assumptions are likely to over estimate the velocities. The presence of fibre and contaminants will negatively affect the flow through the screen by increasing the hydraulic resistance and lowering the flows in both directions. However the method of calculating the velocities and the velocity estimates are still instructive as these have not been reported before.

5.2.3 Back-Flush Ratio

The back-flush ratio (Equation 5-5) was calculated for each case and the back-flush ratio as a function of volumetric reject at three superficial aperture velocities for the step and foil rotors are shown in Figure 5-44 and Figure 5-45 respectively. There was only slight variation in back-flush ratio with reject rate although back-flush ratio increased as the superficial aperture velocity was decreased for both rotors.

As the superficial aperture velocity is decreased there is less bulk forward flow across the screen and therefore the back-flush ratio approaches one as the superficial aperture velocity tends to zero as illustrated in Figure 5-46 for a volumetric reject rate of 0.5. The back-flush ratio was very similar for both rotors.

The calculated back-flush ratio is somewhat sensitive to the value of the accept pressure used in the calculation of the instantaneous velocity. A ±10 % change in the accept pressure caused approximately a ±7 % change in the back-flush ratio for the step rotor and a ±3 % change for the foil rotor. A ±10 % change in the accept pressure had only a marginal affect on the magnitude of the maximum and minimum instantaneous velocities and also the average forward and reverse aperture velocities for both rotors. Once again however these values are only tenative values and are likely to over predict the velocities and back-flush ratios due to the absence of fibre.

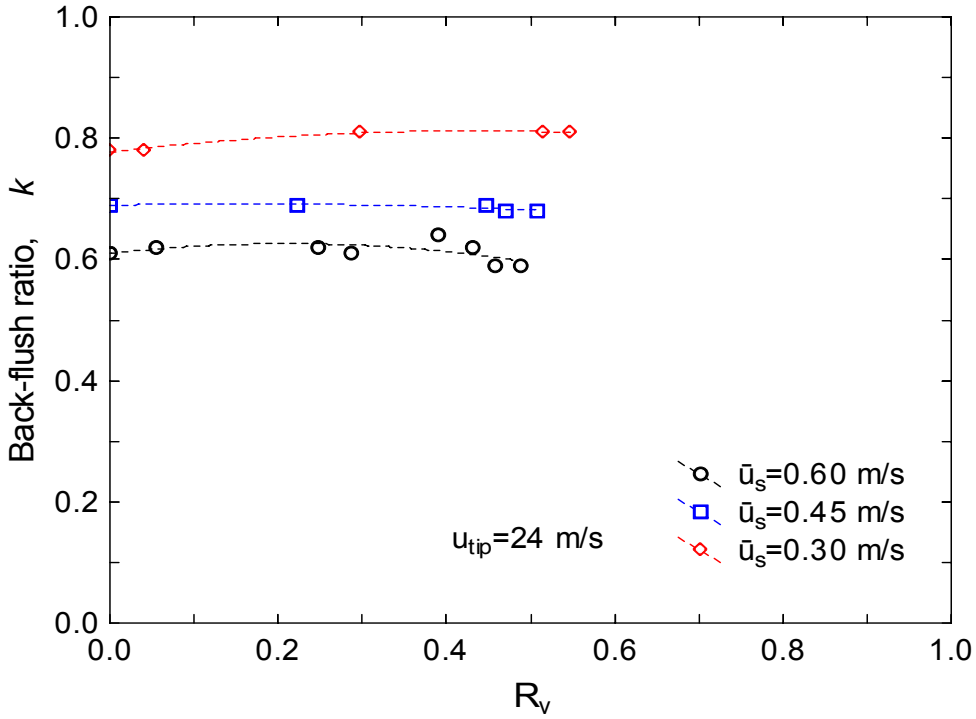

Figure 5-44 Back-flush ratio for the step rotor as a function of volumetric reject rate for a range of superficial aperture velocities (u_{tip}=24 m/s)

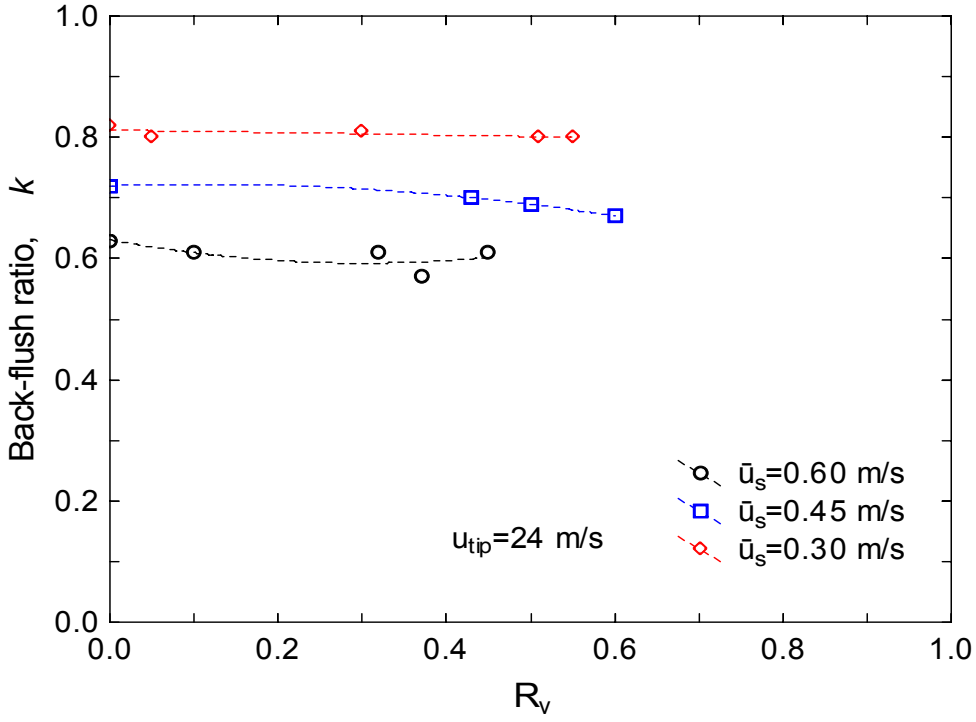

Figure 5-45 Back-flush ratio for the foil rotor as a function of volumetric reject rate for a range of superficial aperture velocities (u_{tip}=24 m/s)

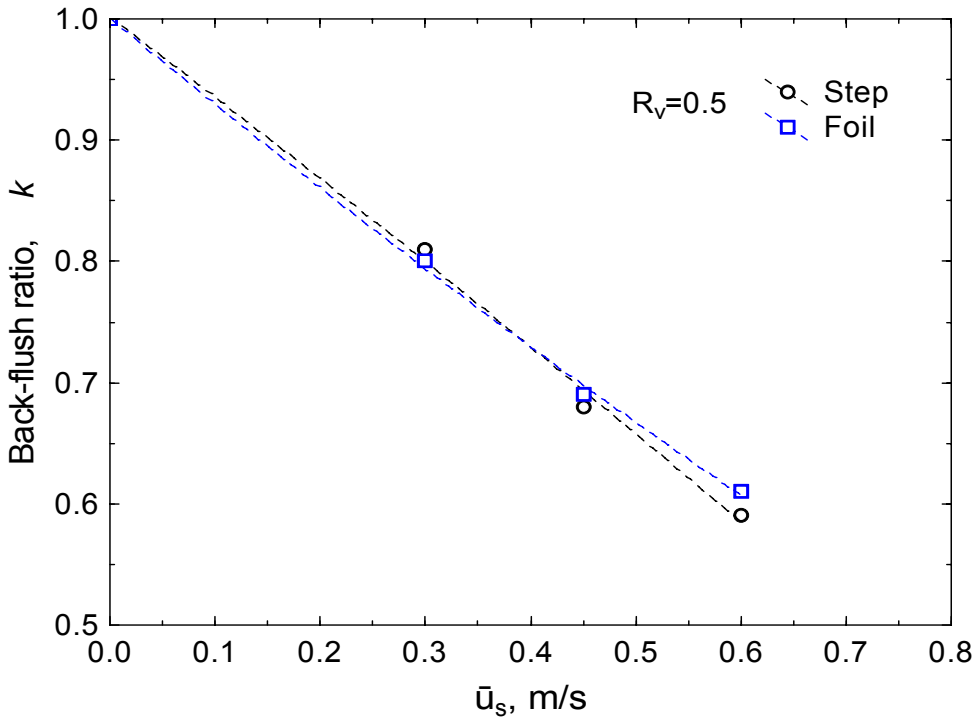

Figure 5-46 Back-flush ratio for the step and foil rotors as a function of superficial aperture velocity for a tip speed of 24 m/s

The average aperture velocity is often used in the literature and various performance parameters have been shown to be dependant on this average velocity. However, it is acknowledged that the instantaneous aperture velocity will be much higher and occur in both the forward and reverse direction. Julien Saint Amand & Perrin (1998) suggest that the effective aperture velocity or average forward aperture velocity is more important for characterising the screening conditions than the superficial aperture velocity. Although this may be the case in theory, the effective aperture velocity is difficult to measure and has not been experimentally estimated until now.

The average forward or effective aperture velocity as a function of volumetric reject rate for the step and foil rotor is shown in Figure 5-47. The step rotor generally had a higher average forward velocity than the foil rotor for the range of superficial aperture velocities tested. This is reasonable as the positive pressure pulse was much greater for the step than for the foil rotor. There was only minor variability in the effective aperture velocity with changes in reject rate. The effective aperture velocity was much higher in all cases than the average aperture velocity. It has been suggested that

the effective aperture velocity is more appropriate for characterising the screening conditions than the superficial aperture velocity (Julien Saint Amand & Perrin, 1998).

The average aperture velocity in the reverse direction as a function of volumetric reject rate for the step and foil rotor is shown in Figure 5-48. The foil rotor had a much greater average reverse aperture velocity than the step rotor. Once again there was not much change with volumetric reject rate.

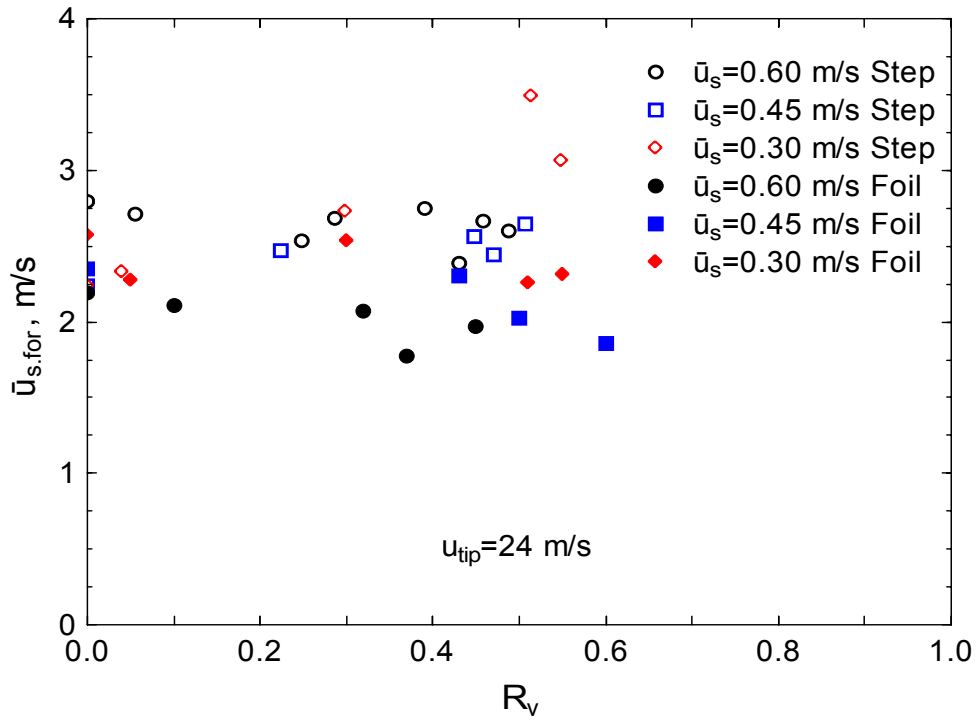

Figure 5-47 Average forward or effective aperture velocity for the step and foil rotors as a function of volumetric reject rate for a range of superficial aperture velocities (u_{tip}=24 m/s)

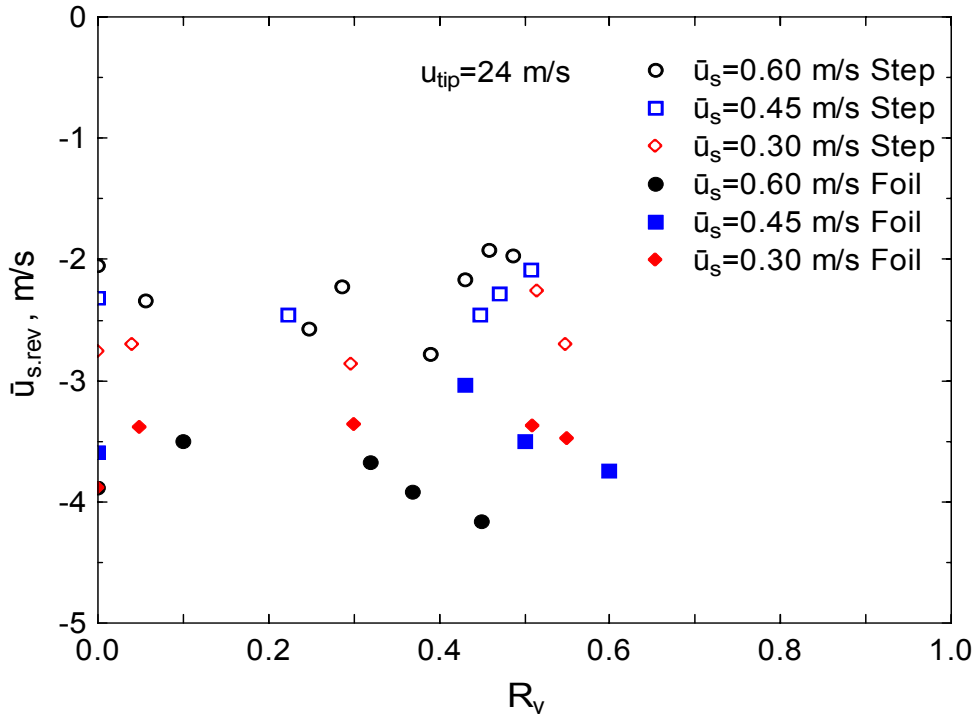

Figure 5-48 Average reverse aperture velocity for the step rotor as a function of volumetric reject rate for a range of superficial aperture velocities (u_{tip}=24 m/s)

In practise screens usually block from the rear to the front because the thickening factor is too high and the negative pulse is insufficient to clear the apertures of accumulated pulp and contaminants. One possible way to overcome this is to deliberately change the geometry of the rotor or the gap between the rotor tip and the screen so that the pulse magnitude is increased. This may increase the operability of the screen, increase the capacity, or allow a lower reject rate to be used.

5.3 Summary

Pressure pulses of the step and foil rotors were measured at the front and rear of the pressure screen at various consistencies, screening conditions and rotor speeds. Although both rotors had unique pressure pulse signatures, the pulse magnitude was significantly lower at the rear of the screen by up to 40 %, even when using only water. Furthermore the pulse magnitude was increased further still at the front of the screen when an axial feed configuration was used. It was concluded that the relative speed of the suspension in the annulus and the rotor speed will change as the suspension travels along the screen length and this change is the cause of the decrease

in pulse magnitude from front to rear. The change in mean tangential velocity along the screen length will be investigated further in the next chapter using Computational Fluid Dynamics. The pulse magnitude of the step rotor was increased moderately with the addition of pulp up to about 2.8 % consistency while the pulse for the foil rotor was unaffected by changes in consistency.

Pulse data was used to predict the instantaneous aperture velocity, the back-flush ratio, and effective aperture velocity. The pressure loss coefficients in the forward and reverse direction under steady flow conditions were experimentally measured in order to calculate the instantaneous aperture velocities. It was found that the instantaneous aperture velocities varied greatly from the superficial aperture velocity which is often used as a measure of the screening conditions.

6 Numerical Modelling of Screen Annuli

The flow field generated within the screen plays an important role in determining the efficiency, capacity, and specific energy consumption of the screen. It has been established in the two previous chapters that there are significant variations in suspension properties such as fibre length and consistency along the length of the screen. Furthermore, the pressure pulse generated by the rotor also varies along the screen length and it was argued that the variability in pulse magnitude was due to the change in mean tangential velocity. Determination of velocity profiles between the screen plate and the rotor for the full length of the screen using modern flow visualisation tools such as Particle Image Velocimetry (PIV) or Computational Fluid Dynamics (CFD) modelling tools has not been achieved previously even for simplified screen geometries with no accept flow. To address this deficiency in understanding an idealised CFD model of a pressure screen annulus with no accept flow was developed and used to determine indicative screen gap velocity profiles.

This chapter will give a brief explanation of the principles and methodology of CFD and then present results from two broad CFD studies that were conducted: a) fundamental study of flow through a concentric annulus with a smooth rotating rotor, and b) flow through a screen annulus with two rotating industrial rotors, the step and bump rotors.

6.1 Computational Fluid Dynamics – Theory

CFD is becoming increasingly popular for use in complex engineering modelling due to the availability of robust commercial codes and relatively inexpensive computer processing power and memory that are needed to conduct this type of numerical simulation. It can be employed for any process that involves mass, heat transfer, combustion etc. There are several different discretisation methods used for CFD modelling however only the finite volume method will be discussed here. For a general overview of CFD principles and methodology see Roache (1998a) or Chung (2002). For a general introduction of the finite volume method see Versteeg & Malalasekera (2007). A brief explanation of the principles and methodology of CFD is presented here as background.

6.1.1 Model Equations

The CFD code solves the conservation equations for mass, momentum, and several additional equations depending on the turbulence model selected and whether heat transfer, species mixing or reactions, or combustion is involved. The continuity equation for an incompressible fluid (i.e. constant ρ) is given for three dimensions in Equation 6-1.

$$\frac{\partial u}{\partial x}+\frac{\partial v}{\partial y}+\frac{\partial w}{\partial z}=0 \qquad \textbf{6-1}$$

If Newton's Second Law is applied then the rate of change of the momentum of a particle of fluid will equal the sum of the forces on the particle. The momentum conservation equations in three dimensions are given in Equations 6-2, 6-3, and 6-4, where S is the source terms which include contributions due to body forces.

$$\rho\frac{Du}{Dt}=\frac{\partial(-p+\tau_{xx})}{\partial x}+\frac{\partial\tau_{yx}}{\partial y}+\frac{\partial\tau_{zx}}{\partial z}+S_{Mx} \qquad \textbf{6-2}$$

$$\rho\frac{Dv}{Dt}=\frac{\partial\tau_{xy}}{\partial x}+\frac{\partial(-p+\tau_{yy})}{\partial y}+\frac{\partial\tau_{zy}}{\partial z}+S_{My} \qquad \textbf{6-3}$$

$$\rho\frac{Dw}{Dt}=\frac{\partial\tau_{xz}}{\partial x}+\frac{\partial\tau_{yz}}{\partial y}+\frac{\partial(-p+\tau_{zz})}{\partial z}+S_{Mz} \qquad \textbf{6-4}$$

For problems which involve heat transfer there is also conservation of energy. In this study there were no cases that involved heat transfer and therefore the energy conservation equations are not presented here. For the solver to include heat transfer the energy equation must also be resolved, however this increases the model complexity and the resulting computational time and expense.

6.1.2 Methodology

The methodology used for CFD modelling will vary depending on the problem and flow domain of interest, however some general steps can be described. Firstly the problem or flow domain of interest is defined and simplified to aid in the computational time and expense of reaching an acceptable solution. Geometry and conditions may be simplified, however there are trade offs between simplification and accuracy or relevancy. Secondly the geometry is drawn and discretised using an appropriate mesh. The generation of the mesh is an important step as it sub-divides the domain into cells on which the flow variables are calculated. A high quality mesh is important as it will directly affect the accuracy of the solution. After the mesh or grid has been generated, appropriate boundary conditions and model parameters must be selected. Inappropriate boundary conditions and model parameters will lead to poor quality solutions and increased computational time.

The next step involves computationally solving the relevant equations using an iterative process. Solution times will depend on the mesh and domain size, model complexity, required accuracy, and computational resources. Once the solution is reached the next step is the post-processing stage where a large range of tools exist for extracting and presenting the desired data. The final step involves verification and validation of the model and the results. Verification is ensuring that the model has been correctly implemented and the solution is converged and is independent of the boundary conditions, the mesh used, and the time step used for unsteady flow calculations. Validation is the process of determining if the solution is an accurate representation of the real world and may involve comparison with experimental data. Verification is concerned mainly with mathematical issues or correctly solving the equations, while validation is concerned with physical issues or solving the right equations (Roache, 1998b; Oberkampf & Trucano, 2002).

6.1.3 Modelling Turbulence

Most flows found in engineering applications, and almost all unit operations in the pulp and paper industry, involve turbulent flow and therefore any CFD solver needs to be able to incorporate a method to resolve turbulent flow structures. Current

computing power is unable to directly solve the time-dependant solutions of the Navier-Stokes equations for high Reynolds numbers that are needed to gain a solution for the smallest scales of turbulence. In order to overcome this problem there are numerous turbulence models available which solve the Reynolds-averaged Navier-Stokes equations. These models are known as Reynolds Averaged Navier Stokes models (RANS) with the most widely known model being the k-ε model and its several variants that have found widespread use. Several of these RANS models take slightly different approaches of dealing with turbulence but it must be remembered that all are approximations and the turbulence model chosen will affect the accuracy of the final solution. Turbulence modelling is a complex and highly technical field and selecting an appropriate turbulence model is non-trivial and dependant on a number of factors including required accuracy, application, established practice, and computational resources and time. A detailed assessment of the current state of turbulence modelling is beyond the scope of this study. For a detailed study and examination of the current state of turbulence modelling see Wilcox (1998).

6.2 3D Annulus Cases

6.2.1 Model Parameters

The 3D smooth rotor annuli models were solved with the commercial code FLUENT 6.2 using the 3D double precision segregated solver. The 3D step and bump rotor annuli were solved with FLUENT 6.3 using the 3D double precision coupled solver. A first order upwind discretisation scheme was used for all variables with the exception of pressure where the PRESTO scheme was used. The SIMPLEC algorithm was used for the pressure-velocity coupling. The solution was considered to be converged when the residuals for continuity, x, y, z velocities, turbulent kinetic energy k, and specific dissipation rate ω were less than $1x10^{-5}$. Furthermore, as an additional indication of convergence the mass balance error was checked and the solution was considered converged if the error was less than 0.2 % of the net flow through the domain.

Although pressure screens process pulp at a range of different consistencies, the modelling of fibre suspensions using CFD can be problematic and suspension

rheology changes significantly with fibre consistency. As the consistency in a screen is constantly changing it is not possible to use the few available flow models for pulp suspensions (Hammarström, 2004). Therefore throughout this work water is the fluid modelled. Results can be interpreted in light of pulp rheological considerations. Implications to real screening applications can then be inferred from the results and a good understanding of pulp rheology.

6.2.2 Mesh Properties

The screen annulus was modelled using a simplified geometry as a concentric annulus with a smooth rotor. The domain geometry for the standard and large diameter annuli is shown in Figure 6-1. Three annular gaps δ were modelled for the smooth rotor: 5, 10, and 15 mm, each under similar boundary conditions. The geometry for the step and bump rotors are illustrated in Figure 6-2. A structured mesh was used for the smooth rotors and an unstructured tetrahedral mesh was used for the bump and step rotor meshes. The number of cells for each domain is shown in Table 6-1.

The annuli used for the smooth rotor were only 300 mm and 180 mm for the standard and large smooth rotors respectively and were not longer due to computational resource limitations and mesh resolution reasons. Ideally the annular length should have been long enough for a fully developed profile to be established however as only entrance effects are of interest here a shorter annular length was used. The resolution of the boundary layers adjacent to the walls was also an area of consideration. Mesh independence studies were conducted and the bulk velocity in the centre region was relatively unaffected by increases in mesh resolution as illustrated in Figure 6-4 for the 10 mm annulus. Increasing the number of cells in the boundary layer improved the resolution of the velocity profile near the walls, but did not significantly affect the resolution of the bulk velocity. The number of cells in the coarse, refined, and extra refined meshes was 1,080,000, 2,160,000, and 3,240,000 respectively for the 10 mm annulus. In light of the results it was decided that the refined mesh would be used as it represented a compromise between a good resolution near the wall area and computational time. Samples of the cross section of the mesh for the 10 mm annulus, step rotor, and bump rotor are shown in Figure 6-5, Figure 6-6, and Figure 6-7 respectively.

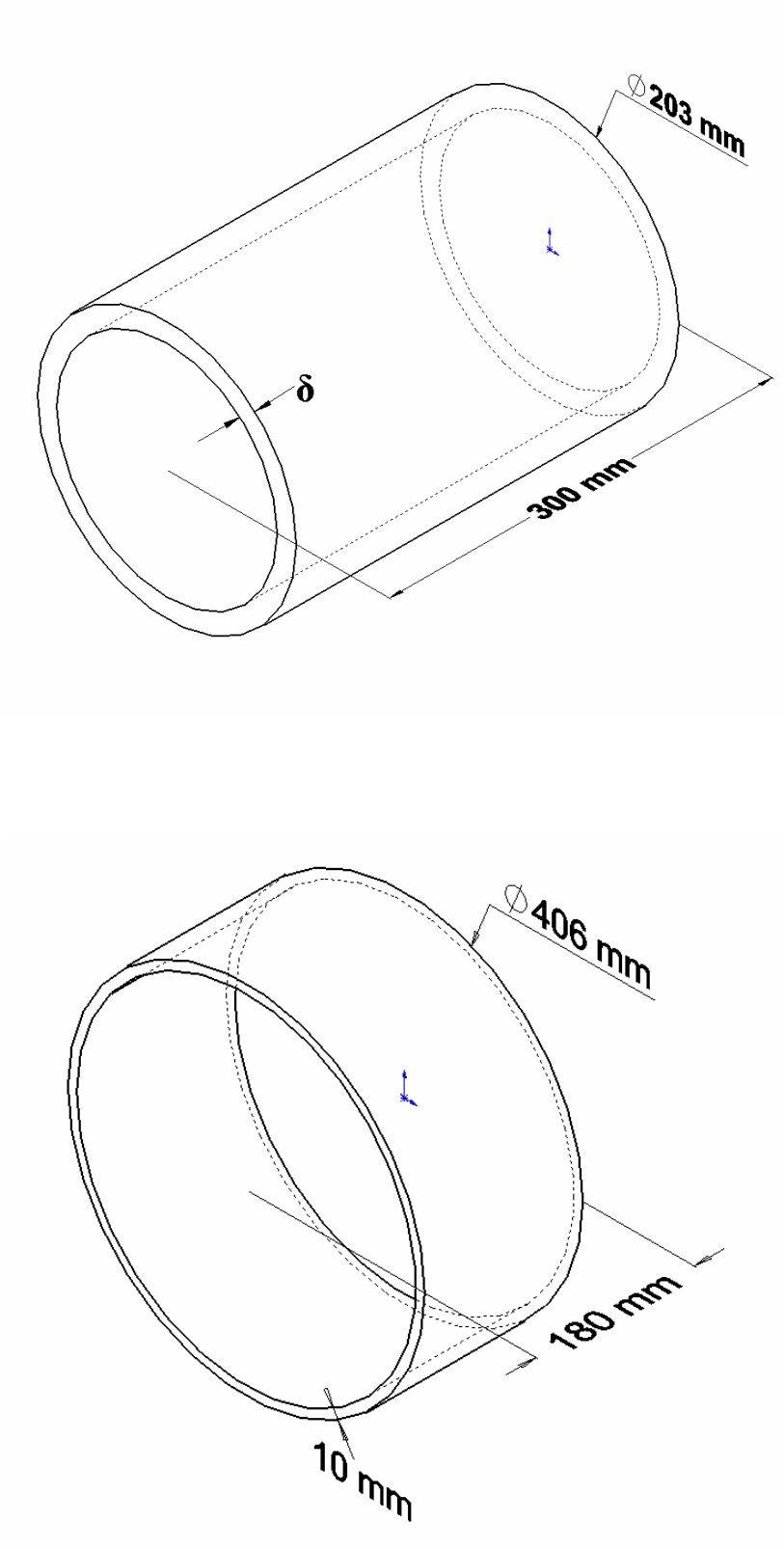

Figure 6-1 Smooth rotor domain geometry and dimensions for the standard and large diameter annuli

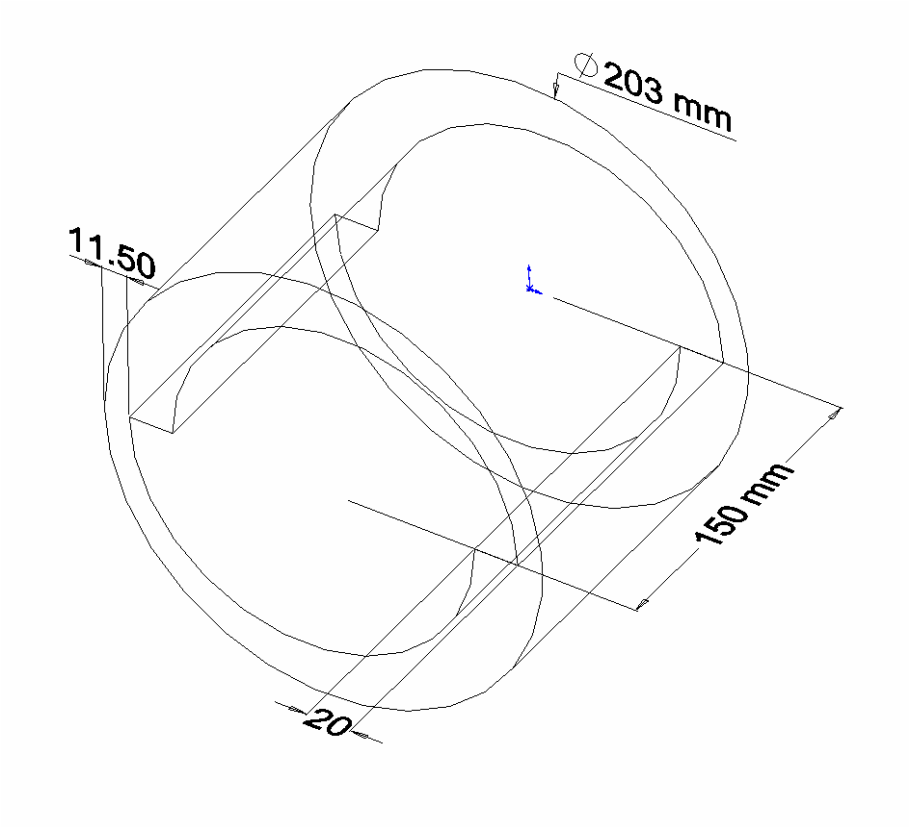

Figure 6-2 Step rotor domain geometry and dimensions

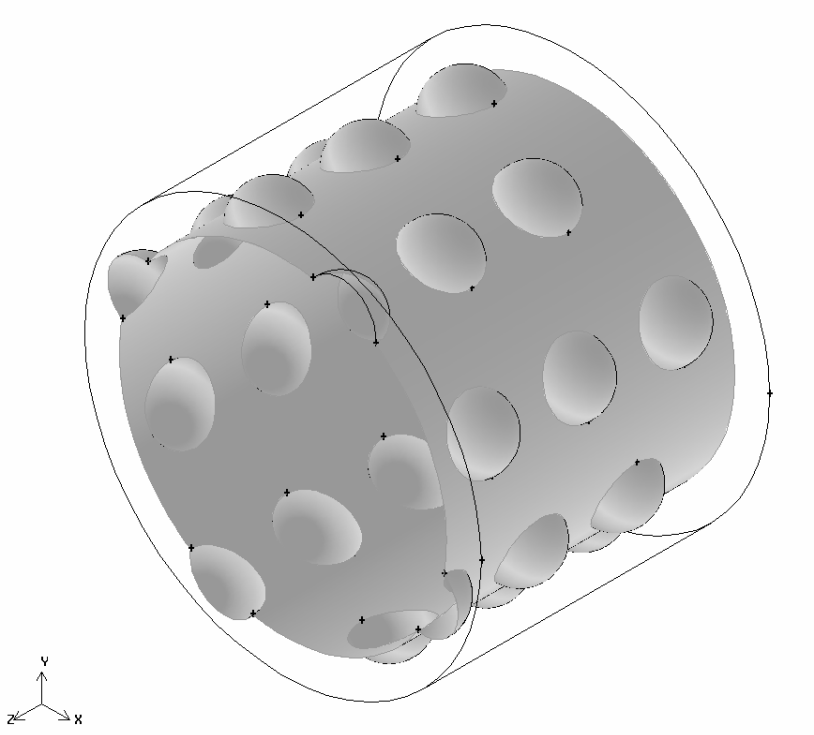

Figure 6-3 Bump rotor domain geometry

Table 6-1 Mesh sizes for the computational domains

Domain	Cell Count	Annular Length (mm)
Smooth δ=5 mm	1,548,000	300
Smooth δ=10 mm	2,160,000	300
Smooth δ=15 mm	3,240,000	300
Smooth Large δ=10 mm	3,240,000	180
Step	2,283,577	150
Bump	3,499,415	150

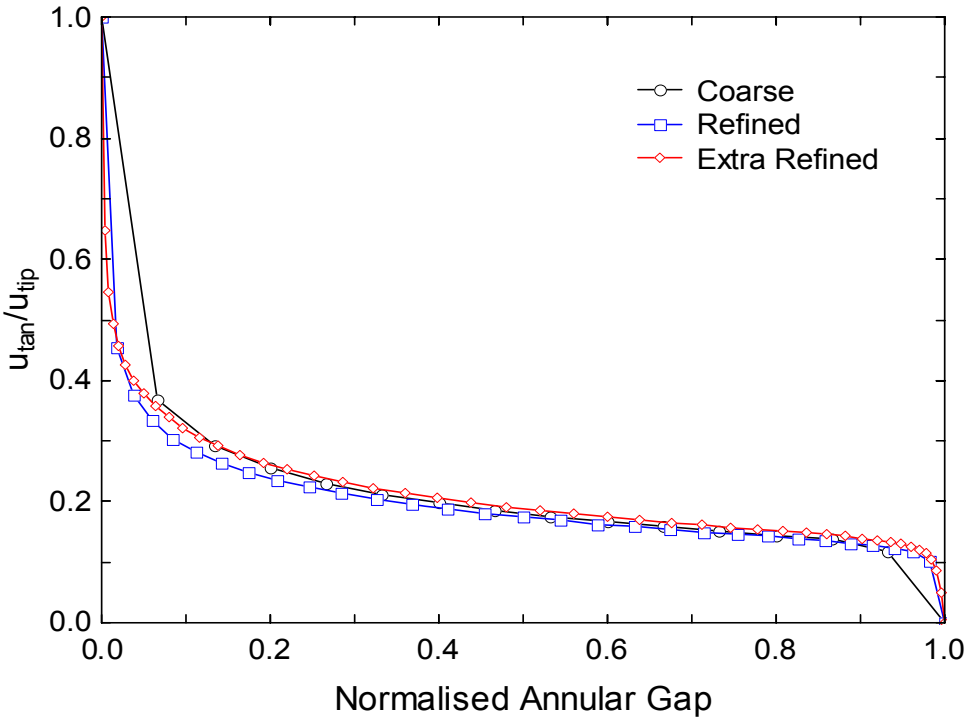

Figure 6-4 Tangential velocity profiles in the radial direction for the δ=10 mm at u_{tip}=20 m/s for the three different mesh resolutions tested midway along the annulus

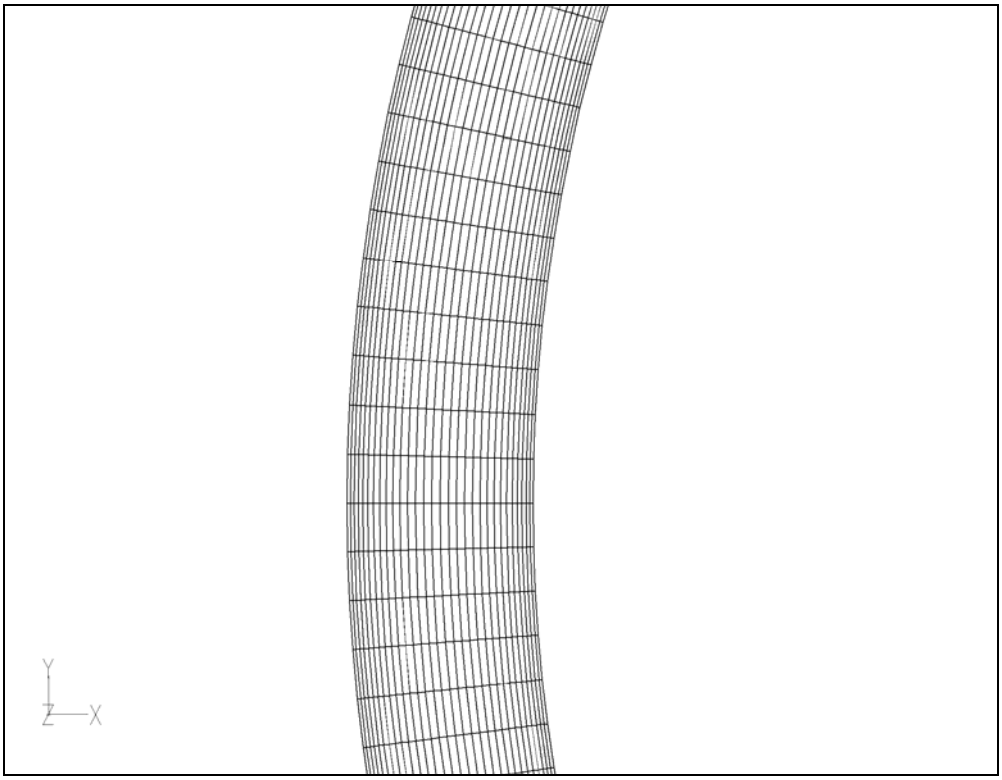

Figure 6-5 Sample of the cross section of the mesh for the 10 mm annulus

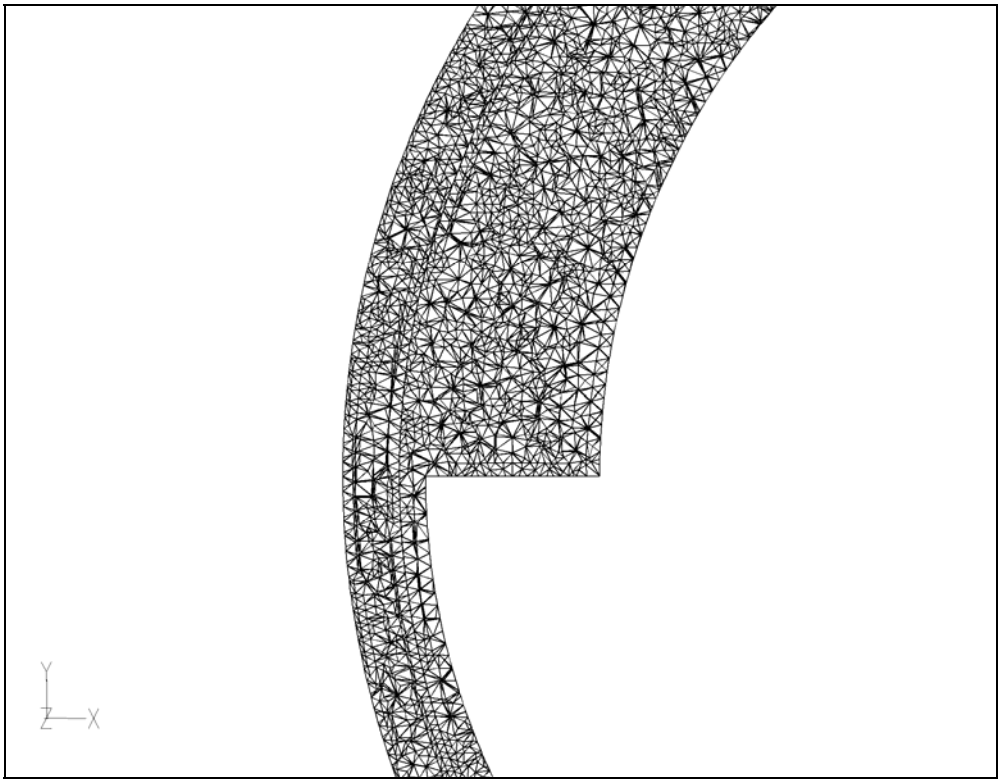

Figure 6-6 Sample of the cross section of the mesh for the step rotor midway along the screen length

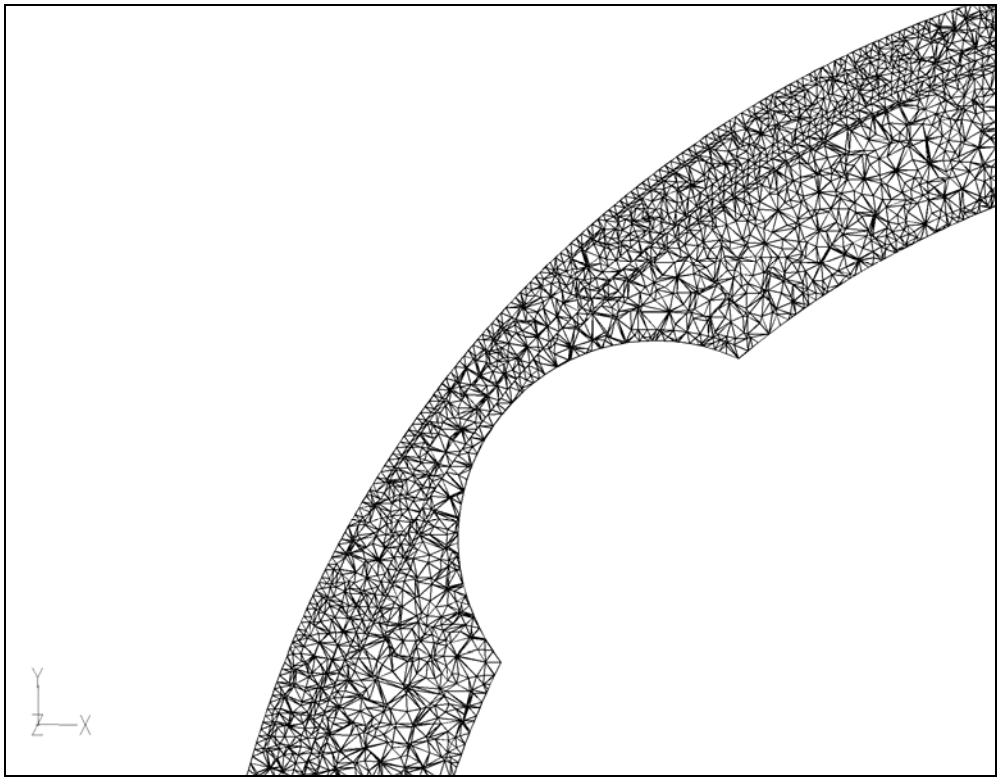

Figure 6-7 Sample of the cross section of the mesh for the bump rotor midway along the screen length

6.2.3 Selection of a Turbulence Model

The k-ω shear stress transport (SST) model (Menter, 1994) was selected as the turbulence model in the present study. The k-ω SST model is a modification of the standard k- ω model developed by Wilcox (1993). It uses the standard k-ω approach close to the wall and the k-ε model for the bulk flow. A blending function is used to smooth the transition between the two models. This near wall treatment overcomes the foremost deficiencies of the k-ε model. In the low Reynolds number region close to the wall, the k-ε model (as with other two-equation models) employs damping functions whereas the k-ω model does not. The k-ω model has also been shown to be superior in the logarithmic region of the boundary layer for adverse pressure gradients than the more popular k-ε models (Wilcox, 1993; Menter, 1994; Wilcox, 1998).

The SST model was chosen over the more common k-ε turbulence model and its several variants because, as has been previous noted, the k-ε model has difficulty in replicating the complex turbulence associated with rotating flows and centre-body rotation, and ad hoc modifications are needed for realistic predictions (Naser, 1997; Wilcox, 1998; Versteeg & Malalasekera, 2007). Furthermore, it has been shown that the k-ε model does not respond well to curvature effects, either from a wall or from streamline curvature (Chambers & Wilcox, 1977; Davidson, 2003). The k-ω SST model has been successfully used for flows with moderate to adverse pressure gradients where the k-ε models have difficulty (Menter, 1992; 1994).

6.2.4 Boundary Conditions

A stationary reference frame was used for the smooth rotors rather than a rotating reference frame as computational time is significantly reduced and the difference in the solutions between the two methods for the smooth rotor is negligible (R^2=0.999). The inlet and outlet boundary conditions were set as a mass flow inlet and pressure outlet respectively. The rotor and screen were both set as walls and the no slip condition selected. The rotor was also set as a rotating wall and the desired rotational velocity specified. Most of the cases were axially fed models which were used over the tangential feed arrangement it simplifies the geometry and isolates the entrance effect from that caused by any artefacts of a feed chamber. Moreover the tangential velocity component will be dependant on the feed chamber geometry and the feed flow rate. The addition of a tangential feed chamber to the domain would have increased the domain size and therefore computational time considerably. For comparison some selected cases incorporated an initial tangential velocity component, as part of the initial inlet boundary conditions. All the trends that were found using an axial feed could also be extended to a tangential feed except the tangential feed case would have an initial tangential velocity component to consider.

A sliding mesh was used for the step and bump rotors. A sliding mesh involves one fluid zone sliding over another which allows the inner wall or rotor to rotate with time thus simulating a real rotor. The downside to this approach is that the solution is solved in an unsteady solver and therefore significantly greater amounts of computational time are needed for a solution. Both rotors were run long enough for

two complete revolutions to occur. The case is first run using a steady state solver to give the initial conditions and then the case is solved using the unsteady solver. The time step used for the step and bump rotor cases were 0.0001 and 0.0005 seconds respectively. The bump rotor was solved with a longer time step because a trial was done using the step rotor mesh and it was found that there was no significant increase in accuracy of the pressure pulse when the longer time step was used. Therefore to save computational time the longer time step was used for the bump rotor. Solving these two cases proved problematic and numerous issues arose however these will be discussed with the results.

6.2.5 Computational Time

Computational time varied depending on the complexitiy of the model and whether the steady or unsteady solver was used. For the smooth annuli, which were solved using a steady solver, computational time was approximately 80 hours for the 5 mm annulus cases, 100 hours for the 10 mm annulus cases, and 150 hours for the 15 mm annulus cases. The step and bump rotors were solved using a sliding mesh and an unsteady solver. For two revolutions of the rotors to occur the computational time was around 2500 hours and 2700 hours for the step and bump rotors respectively.

6.3 Tangential Velocity Profiles

The results of several 3D smooth rotor cases are presented in the following section. A number of different factors are examined and velocity profiles are presented in dimensionless or normalised velocity and distance in order to aid in comparison of results at different boundary conditions.

6.3.1 Theoretical Considerations

The velocity profile in the radial direction is important because the degree of flocculation of the suspension has been shown to be affected by the shear stress applied on the network by the fluid (Bennington, 1988). The velocity profile is also thought to affect the passage of fibre in a number of ways. Flow channel experiments have demonstrated that the passage of a fibre is dependant on the trajectory of a fibre

and the trajectory will be directly influenced by the velocity profile or flow field adjacent to the aperture (Gooding, 1986; Oosthuizen et al., 1992). The structure of the suspension or degree of "fluidisation" in the boundary layer or exit layer above the screen will also affect the passage. A high tangential velocity will require a single fibre to make the 90 degree turn more quickly to be accepted. Higher velocities may also cause high density contaminants to slip over apertures due to their greater momentum therefore increasing contaminant removal efficiency (Julien Saint Amand, 1997; Julien Saint Amand et al., 2005).

There is experimental evidence that the mean tangential velocity $\bar{u}_{tan}$ of the suspension in the annulus is an important variable in fibre passage through the screen (Gooding, 1986; 1996; Olson, 1996; Weeds, 2006). As yet there has been no experimental measurement of the tangential velocity in an industrial pressure screen. Flow conditions have been inferred from consistency data and other indirect experimental observations, however a detailed picture of the internal flows that occur in a screen is still lacking. Gooding (1986) evaluated the velocity profile in the wake of a cylinder and then applied the analysis to that of a bump rotor in a pressure screen. Based on this analysis he estimated that the mean tangential velocity in the annulus was 15 % that of the rotor. Others have suggested that this figure will change as more tangential momentum is transferred from the rotor to the suspension as the suspension moves along the annulus (Rienecker, 1992; Niinimäki et al., 1996a; Niinimäki, 1998; Weeds, 2006).

It is accepted that the mean tangential velocity will increase along the length of the screen due to the interaction between the suspension and the rotor. Fundamental studies into the tangential flow development in an annulus with a rotating inner cylinder have shown that there is an entrance effect where the tangential velocity is developed (Martin & Payne, 1972). For a pressure screen this will mean that the stock will accelerate as it enters the screen and will continue to accelerate as it moves along the screen until some point when it will reach a maximum. The rotor geometry, speed, and annular gap should determine this maximum velocity.

There has been little published work regarding velocity profiles in the screen annulus specifically examining pressure screening. However a large amount work has been carried out investigating velocity profiles in the radial, axial and tangential directions with a smooth rotating inner (centre body rotation) both with and without axial through flow. For laminar flow the velocity profile across the annulus is predicted by Equation 6-5 (White, 2003) where Ω_i is the annular velocity of the inner cylinder and r_x is the radial position.

$$u_{tan} = \Omega_i r_i \frac{r_o/r_x - r_x/r_o}{r_o/r_i - r_i/r_o} \qquad \textbf{6-5}$$

The predicted profile in dimensionless velocity and annular gap is presented in Figure 6-8.

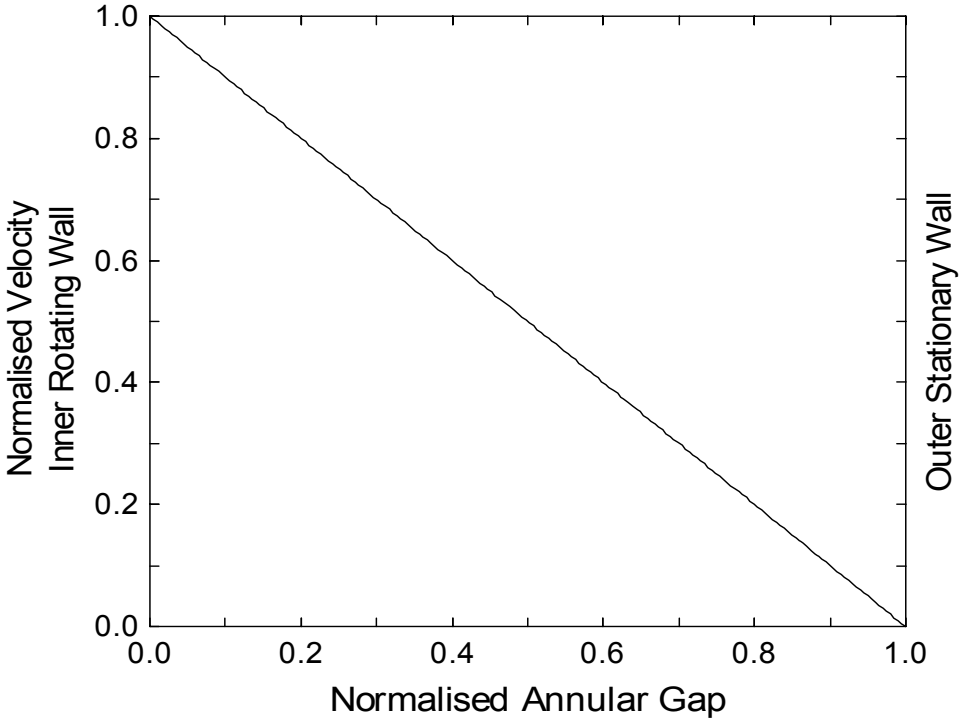

Figure 6-8 Predicted velocity profile using Equation 6-5 for laminar flow

Taylor (1935) measured the radial velocity profile between concentric rotating cylinders and reported that a tri-layer structure existed as shown in Figure 6-9. The structure consisted of: a) a thin layer adjacent to the inner wall where the tangential

velocity rapidly increases to that of the rotating wall, b) a large region of fairly constant velocity that was much less than that of the inner rotating wall, and c) a thin layer adjacent to the outer wall surface where the tangential velocity decreases to zero. Numerous other researchers have also reported the tri-layer structure for a number of similar situations (Astill, 1964; Nelson, 1981; Nouri & Whitelaw, 1994; Antunes et al., 1996; Naser, 1997). Taylor postulated a dramatic change in the turbulence structure which resulted in the tri-layer structure. Moreover he concluded that the momentum transport theory could explain the velocity profile close to the solid walls (layers a & c) but not the profile in the centre region (layer b). The vorticity transport theory on the other hand could account for the velocity profile in the centre region but not the regions close to the walls.

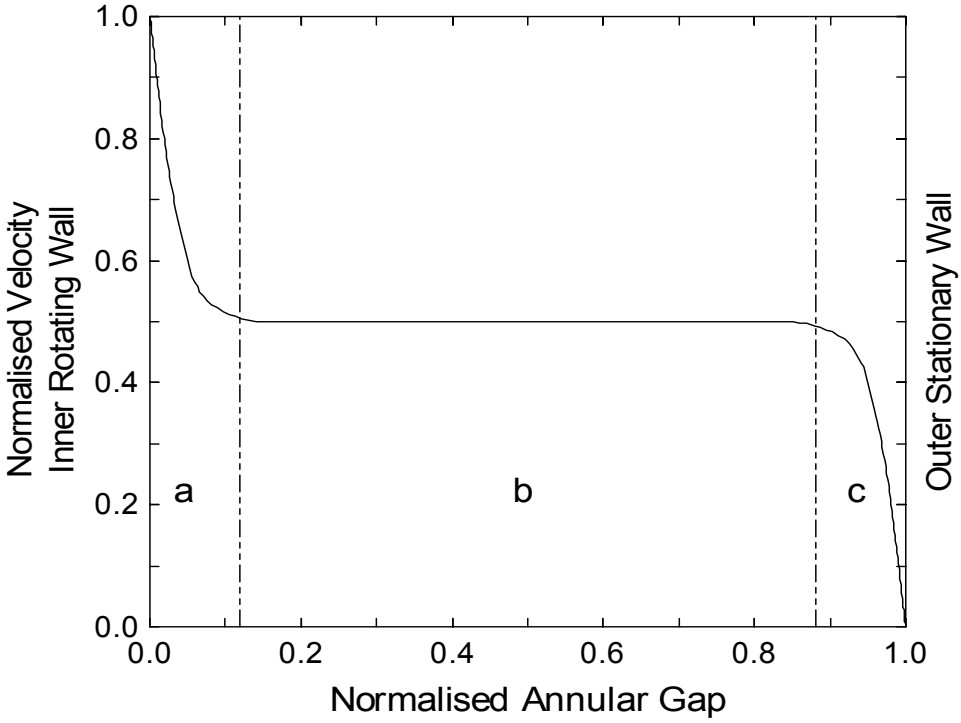

Figure 6-9 Schematic of the velocity profile in an annulus with a smooth rotating inner - adapted from Taylor (1935)

Numerical modelling of non-Newtonian flow by Naser (1997) has shown a linear velocity profile at low Reynolds numbers corresponding to Equation 6-5. However comparison with experimental data from Escudier & Gouldson (1995) for the same conditions showed that even at low Reynolds numbers a tri-layer structure existed. Taylor postulated a dramatic change in turbulence structure which resulted in the

tri-layer structure. Naser argued that turbulence is present in the experimental measurements for laminar flow and that turbulence is suppressed near the inner rotating wall. Furthermore the eddy viscosity concept is not applicable for flow between two concentric cylinders with a rotating inner. The discrepancy between the calculated and measured profiles is attributed to the fact that the k-ε turbulence model is based on the eddy viscosity concept.

6.3.2 Radial Velocity Profile

A vector plot of tangential velocity derived from the 3D CFD model of the standard size screen is shown in Figure 6-10. The vector plot is of the 10 mm annulus for a section halfway along the length of the annulus for a rotor speed of 20 m/s. As can be seen the velocity close to the outer wall is close to zero and this increases as closer to the inner rotating wall.

As the suspension travels along the annulus, momentum will be transferred from the rotor to the fluid. The velocity profile will develop along the annulus and the profile development for 10 mm annulus and u_{tip}=20 m/s is shown in Figure 6-11. The velocity was normalised by dividing the local tangential velocity u_{tan} by the velocity of the rotor. This normalised velocity is plotted against a non-dimensional radial location ξ (Equation 6-6). The axial position is expressed in terms of a non-dimensional axial length ζ (Equation 6-7) which is essentially the number of annular lengths, where z is the axial position along the annulus.

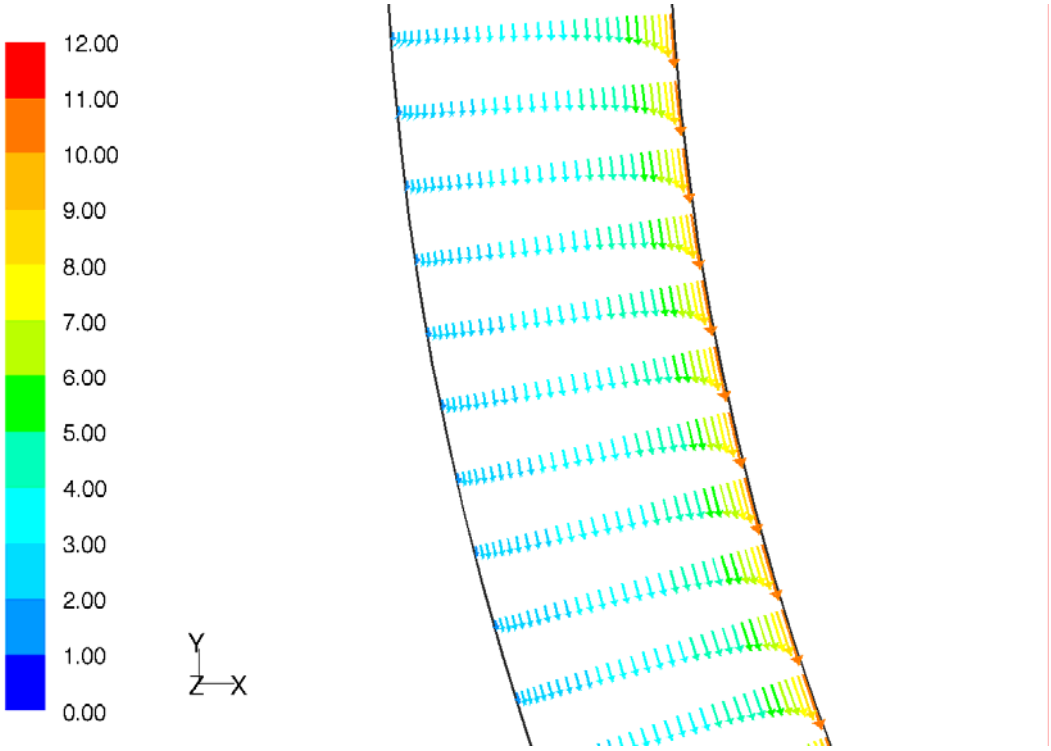

Figure 6-10 Vector plot of tangential velocity of a section of the δ=10 mm annulus midway along the annulus (ζ=15, u_{tip}=20 m/s)

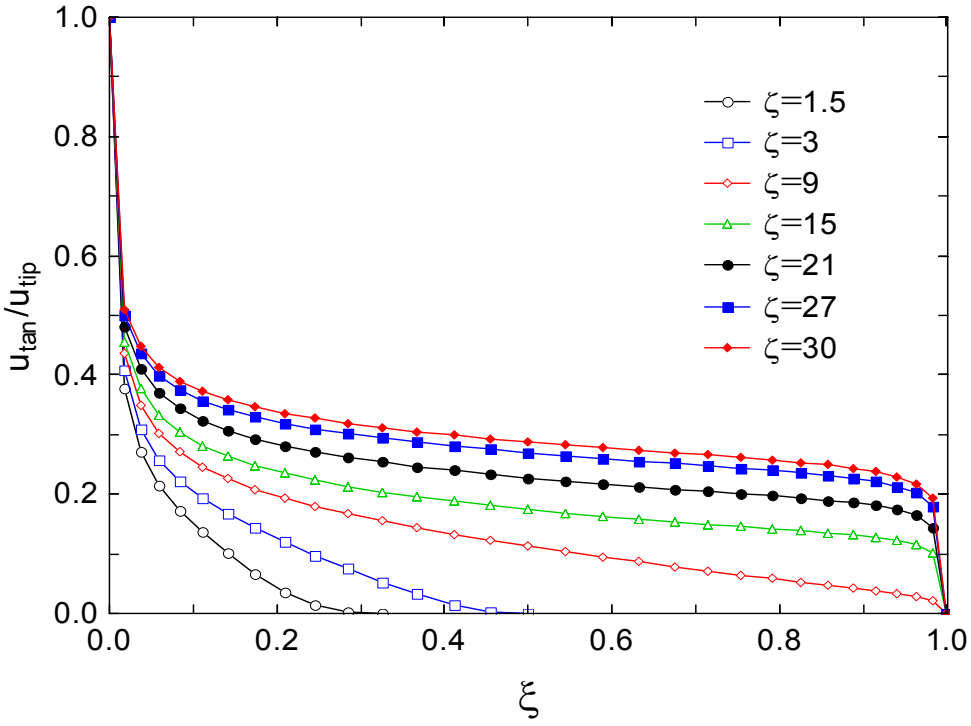

Figure 6-11 Tangential velocity profile in the radial direction for the δ=10 mm at u_{tip}=20 m/s at different annular lengths in the axial direction

$$\xi = \frac{r_x - r_i}{\delta} \qquad \textbf{6-6}$$

$$\zeta = \frac{z}{\delta} \qquad \textbf{6-7}$$

The tri-layer structure is not immediately formed and comes into existence at about 9 annular lengths in the axial direction. Similar development of the velocity profile has been reported for axial flow (Astill, 1964). Martin & Payne (1972) note that at the beginning of the annulus only the fluid which is in contact with the rotating wall will acquire any tangential velocity. The rest of the fluid will continue to travel in the axial direction of the annulus before this fluid has an opportunity to gain any tangential momentum.

It should be pointed out that even at ζ=30 (the length of the annulus in the model) the velocity profiles are still not fully developed. The average velocity of the centre region approaches 50 % of the rotor (Taylor, 1935). As noted earlier, an ideal model would have been longer to allow the velocity profile to develop fully, however mesh resolution and computational time considerations made this not possible.

The fluid in the annulus will have both tangential and axial velocity components and therefore the fluid will follow a helical path around the annulus. Pathlines are shown in Figure 6-12 for the 10 mm annulus at a rotor speed of 20 m/s. A helical path is evident and the total path travelled is longer for a fluid element closer to the rotor (the blue pathline) than for one closer to the screen (the red pathline).

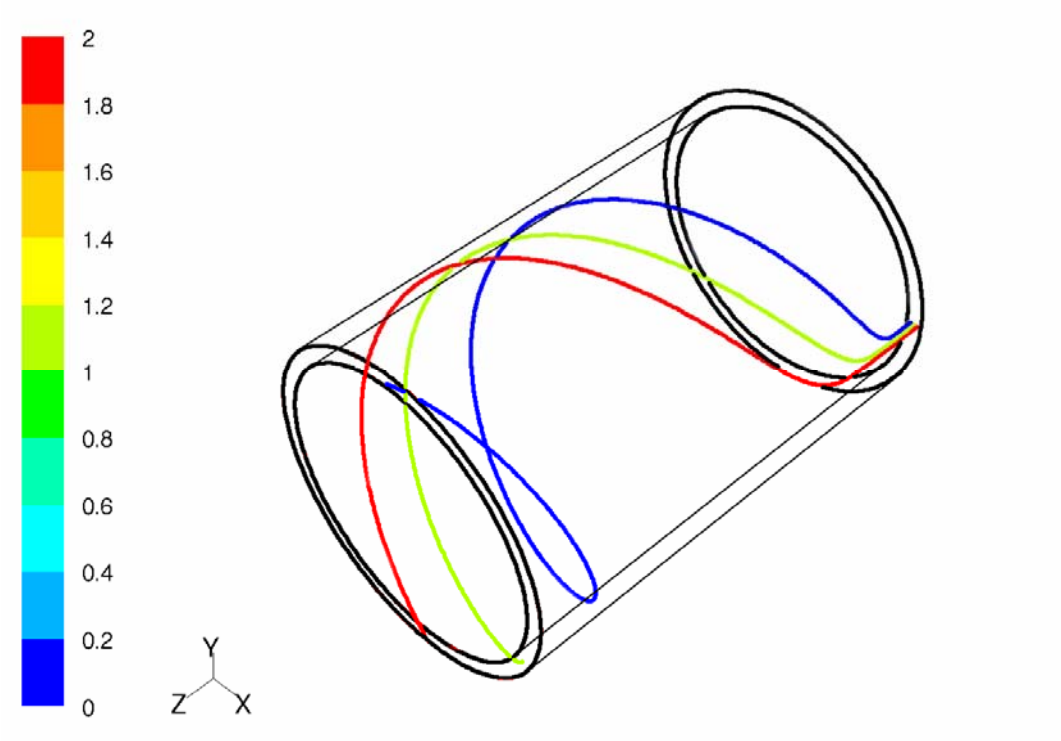

Figure 6-12 Pathlines for δ=10 mm and u_{tip}=20 m/s

6.3.3 Rotor Speed

The effect of rotor speed on the tangential velocity profile in the radial direction for the 10 mm annulus is shown in Figure 6-13. The tri-layer structure is clearly evident with the thin layer adjacent to the screen (ξ=1) where there is a rapid increase in the tangential velocity from zero to between about 10 – 25 % of the rotor speed depending on the rotor speed. As the rotor speed increased the large region of bulk flow increases in velocity from about 20 % of the rotor speed at u_{tip}=10 m/s to about 35 % at u_{tip}=30 m/s.

The fairly even profile across approximately 80 % of the annulus has implications on the structure of the suspension in the annulus. It is possible that for a fibre suspension at typical screening consistencies (> 1 %) that the network would be subject to a high degree of shear in the regions adjacent to both the rotor and the screen. However, mechanisms that apply for suspension flow in pipes should not be directly applied to other situations such as this. Care needs to be taken as the velocity profiles and flow fields are quite different (Duffy, 1995).

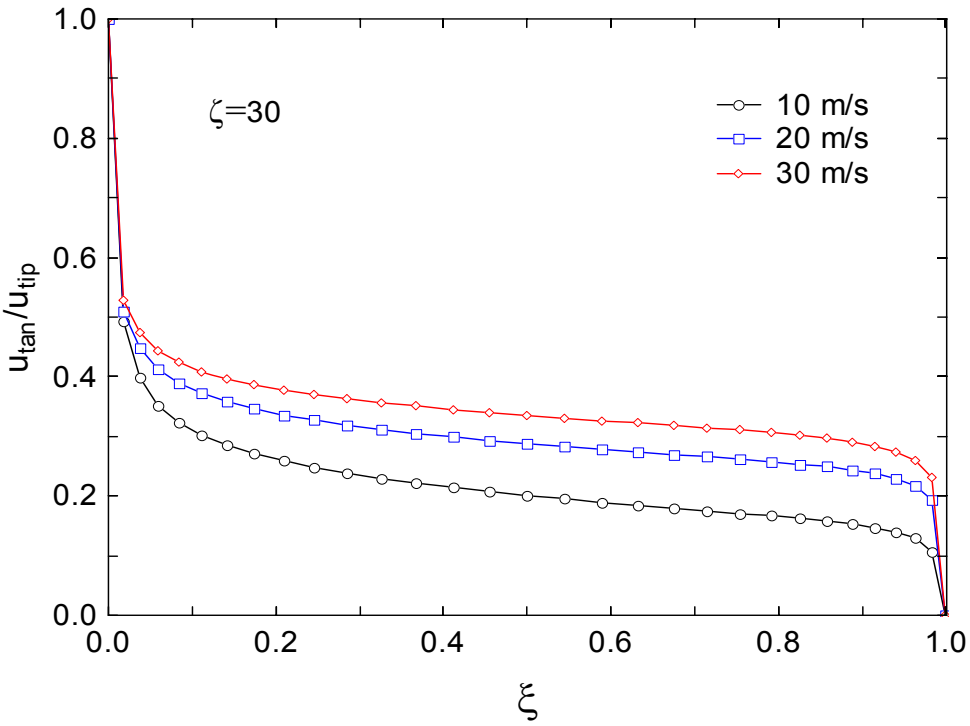

Figure 6-13 Tangential velocity profile in the radial direction for the δ=10 mm and ζ=30 for several different tip speeds

The high degree of shear adjacent to the rotor and the screen will promote the disruption of flocs. Although it is doubtful that the suspension next to the screen will be completely free of flocs, the flocs will be much smaller than compared to the bulk flow. This may allow flocs to be extruded through the apertures along with individual fibres in the free fibre fraction. Experimental studies using rotary shear devices have observed that even at very high rotational speeds flocs still exist in the flow (Norman et al., 1986; Bennington, 1988). A recent investigation by Julien Saint Amand et al. (2005) utilising experimental techniques, CFD and finite element analysis has demonstrated that stickies larger than the aperture often pass through the screen aperture via an extrusion mechanism. It is logical that a similar mechanism may also occur in which flocs are extrude through screen apertures.

The mean tangential velocity $\bar{u}_{tan}$ was calculated by taking the faceted average of radial lines at certain points along the annulus. Once again under fully developed flow conditions for an infinitely long annulus the mean tangential velocity should approach 50 % of the rotor speed. Figure 6-14 shows the mean tangential velocity of the 10 mm annulus for three different tip speeds. The mean velocity increases from

zero at the start of the annulus and the rate of change increases as rotor speed increased. Once again the higher tip speed gave increased momentum transfer between the rotor and the suspension.

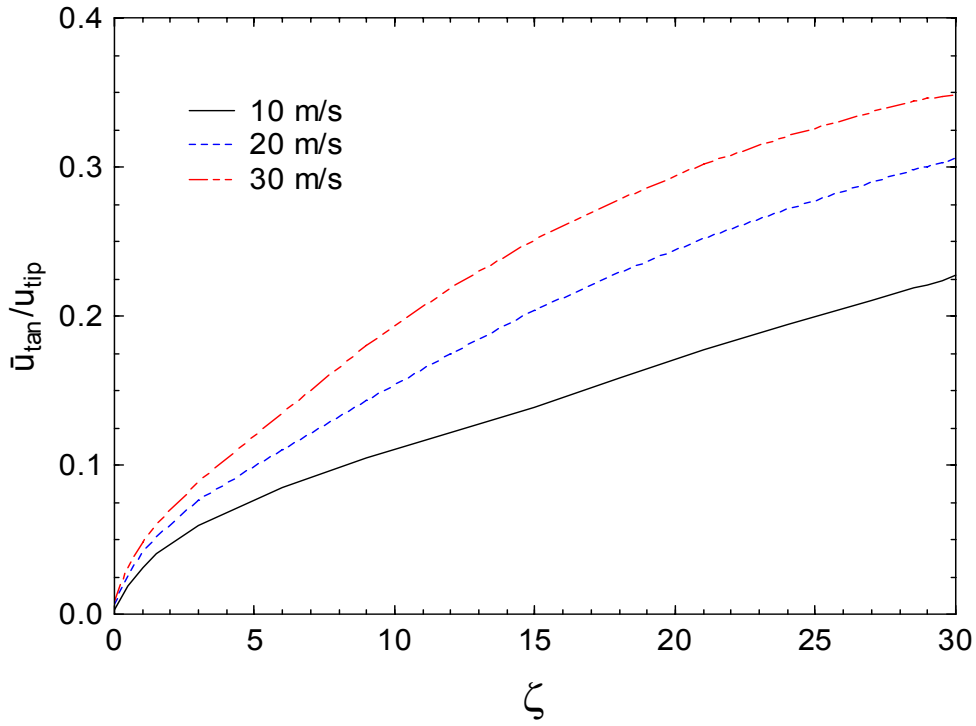

Figure 6-14 Normalised mean tangential velocity for the smooth rotor for δ=10 mm and $\bar{u}_{ax}$=1.65 m/s and a range of rotor speeds

6.3.4 Axial Velocity

The axial flow rate through the annulus or mean axial velocity $\bar{u}_{ax}$ also affected the tangential velocity in the radial direction. The radial tangential velocity profiles for the 10 mm annulus and a rotor speed of 20 m/s at two mean different axial velocities or axial feed flow rates are shown in Figure 6-15. An increased axial velocity decreased the tangential velocity across the annulus which was more apparent in the central region of the annulus. Nouri & Whitelaw (1994) also found a decrease in the velocity of the centre region with increased bulk axial flow. The explanation of the decrease in tangential velocity with increased axial velocity is associated with the residence time of the fluid in the annulus and the opportunity for momentum transfer between the rotor and the fluid. An increased residence time increases the momentum transfer and increases the tangential velocity. The axial velocity is governed

primarily by the flow rate through the annulus in the axial direction or the pressure differential between the inlet and outlet of the annulus. The cross sectional area of the annulus will also affect the axial velocity. The velocity profile of the $\bar{u}_{ax}$=1.65 m/s at a position of ζ=15 was approximately equal to that of the $\bar{u}_{ax}$=3.30 m/s at an axial position of ζ=30.

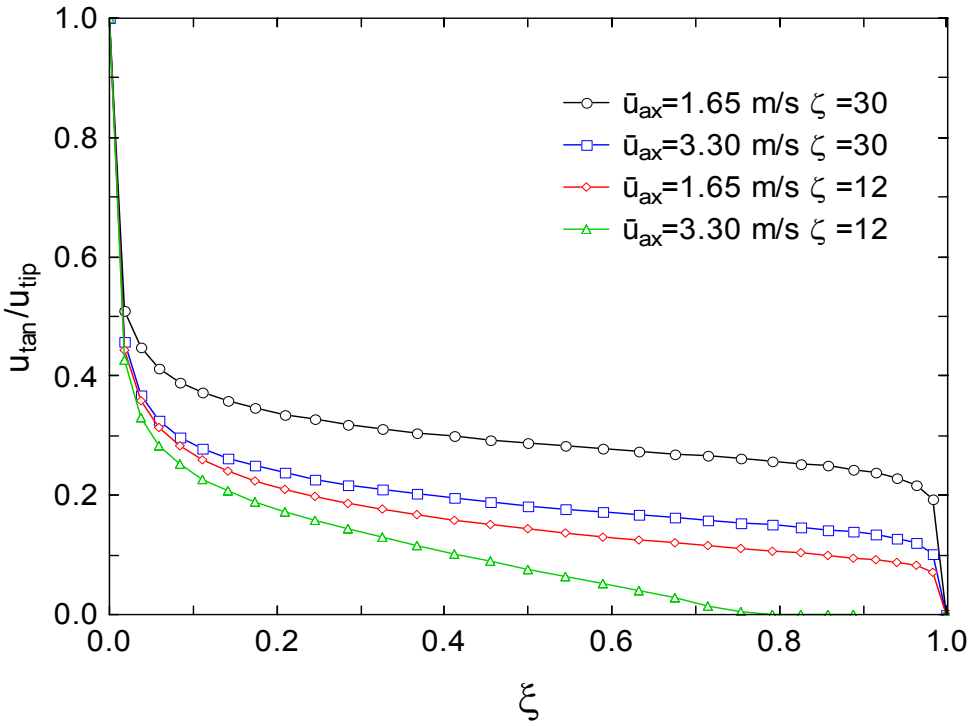

Figure 6-15 Tangential velocity profile in the radial direction for the δ=10 mm at u_{tip}=20 m/s for two different axial velocities at two positions along the annulus

The mean tangential velocity for the 10 mm annulus at a rotor speed of 20 m/s and a range of bulk axial velocities is shown in Figure 6-16. As the axial velocity is increased the mean tangential velocity and the rate of change decreased. It is also reasonable to suppose that the addition of a rotor element will be more effective at momentum transfer than a smooth cylinder. Different rotor elements will also be more effective at transferring momentum than others, for example the step rotor with the large face is expected to transfer more momentum than the bump rotor. These rotors were modelled and the results are reported in Section 6.5.

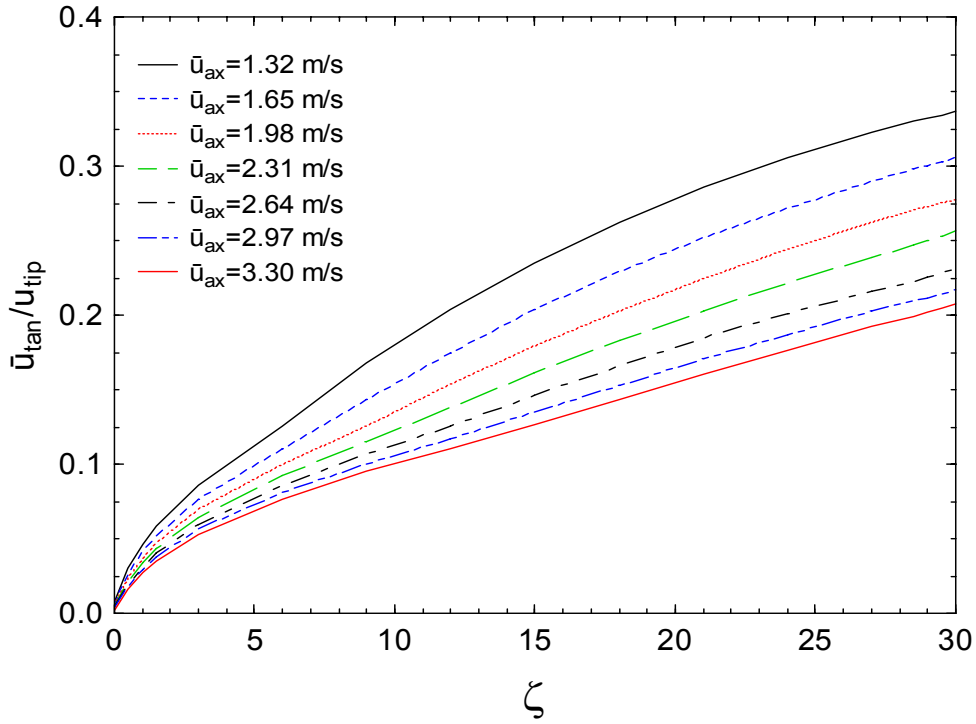

Figure 6-16 Normalised mean tangential velocity for δ=10 mm and u_{tip}=20 m/s and a range of axial velocities

In a real pressure screen the axial velocity decreases along the length of the annulus as fluid is removed due to accept flow through the screen. Accept flow rate is usually assumed to be constant along the screen length and therefore the decrease in axial velocity along the screen length will be linear. If the mean tangential velocity is assumed to be dependant on the bulk axial velocity and follow the curves shown in Figure 6-16, the mean tangential velocity profile along a screen, with accept flow, can be predicted using the calculated curves. The predicted tangential velocity profile and slip factor for several different volumetric reject rates, assuming a constant accept flow rate along the screen length, is shown in Figure 6-17. The average velocity profiles show a steady increase along the screen length for all the reject rates with a higher mean tangential velocity at the lower reject rate. There is a constant decrease in the slip factor from the front of the screen to the rear of the screen.

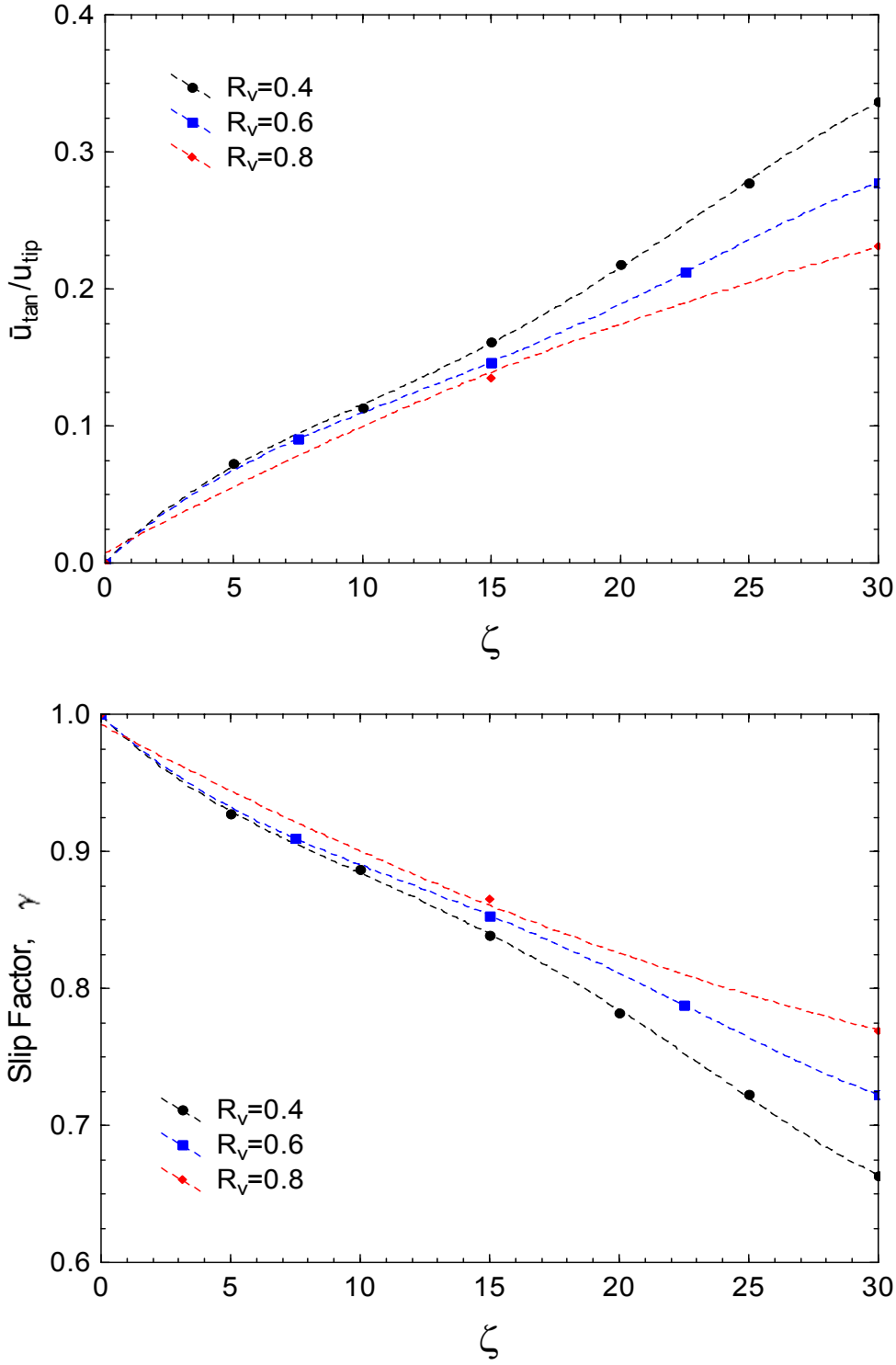

Figure 6-17 Normalised mean tangential velocity and slip factor prediction with constant accept flow rate for δ=10 mm and u_{tip}=20 m/s and a range of volumetric reject ratios

It was demonstrated in the previous chapter that there was a difference in the pressure pulse magnitude between the pulse at the front and the rear of the screen. The disparity was attributed to a decrease in the slip factor along the screen. Pulse magnitude at the front of the screen was found to be virtually unaffected by changes in volumetric reject rate however there was a small decrease in pulse magnitude at the rear of the screen as reject rate was increased. As demonstrated in Figure 6-17 the slip factor at the front of the screen was very similar for the three reject rates but toward the rear of the annulus the difference became greater. The pressure pulse magnitude at the rear of the screen is expected to decrease as the reject rate is increased.

6.3.5 Tangential Fed Screen

Many screens are tangential fed and as a result the suspension will have an initial tangential velocity component $u_{tan.ini}$ as it enters the annulus. This can be included in the boundary conditions of the case and several initial tangential velocities were used as boundary conditions. The tangential velocity profile in the radial direction at different axial position with an initial tangential velocity of $u_{tan.ini}$=3.4 m/s is shown in Figure 6-18 for the 10 mm annulus. The initial axial velocity is the same as the previous cases (see Figure 6-11). The initial tangential velocity creates a flat profile at the start of the annulus and then the tri-layer structure is produced almost immediately. This is caused because the fluid adjacent to the outer wall (ξ=1) slows down and approaches zero at the outer wall and similarly the fluid adjacent to the rotor (ξ=0) speeds up to and approaches the rotor speed at the rotor.

The mean tangential velocity profiles along the length of the annulus for several initial tangential velocities are illustrated in Figure 6-19 for the 10 mm annulus and a tip speed of 20 m/s. The initial tangential velocity had a large effect on the normalised velocity along the annulus. As the initial tangential velocity was increased the normalised velocity profile flattened. At the highest initial tangential velocity the velocity profile was virtually unchanged along the length of the annulus. The maximum normalised velocity that was reached was just over 0.4 which was less than the value of 0.5 that was expected from theory.

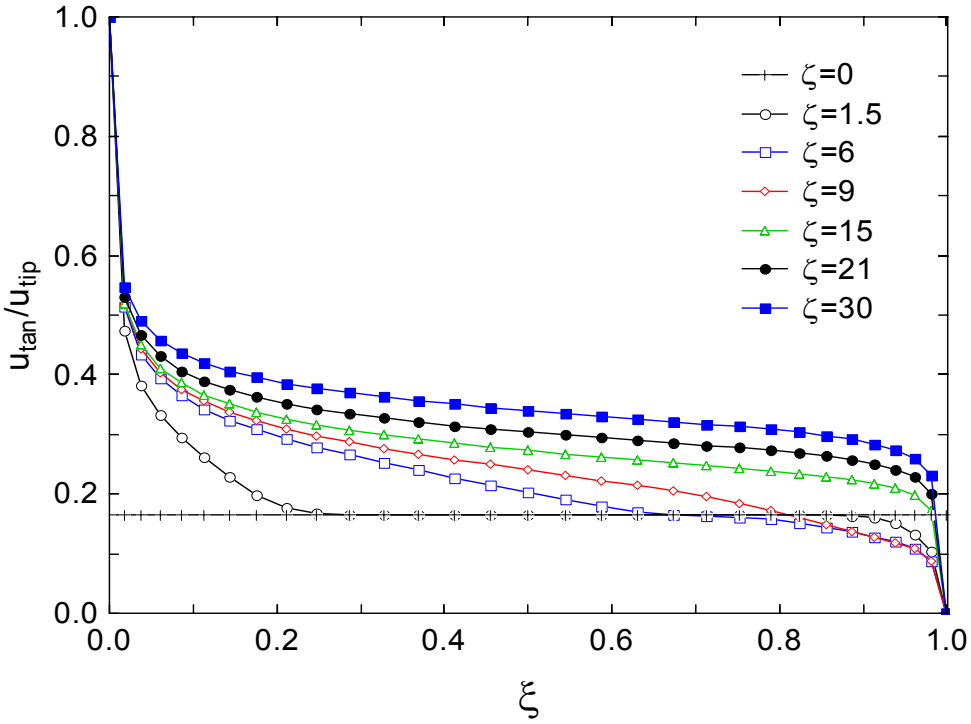

Figure 6-18 Tangential velocity profile in the radial direction for the δ=10 mm at u_{tip}=20 m/s at different annular lengths in the axial direction with initial tangential velocity $u_{tan.ini}$=3.4 m/s

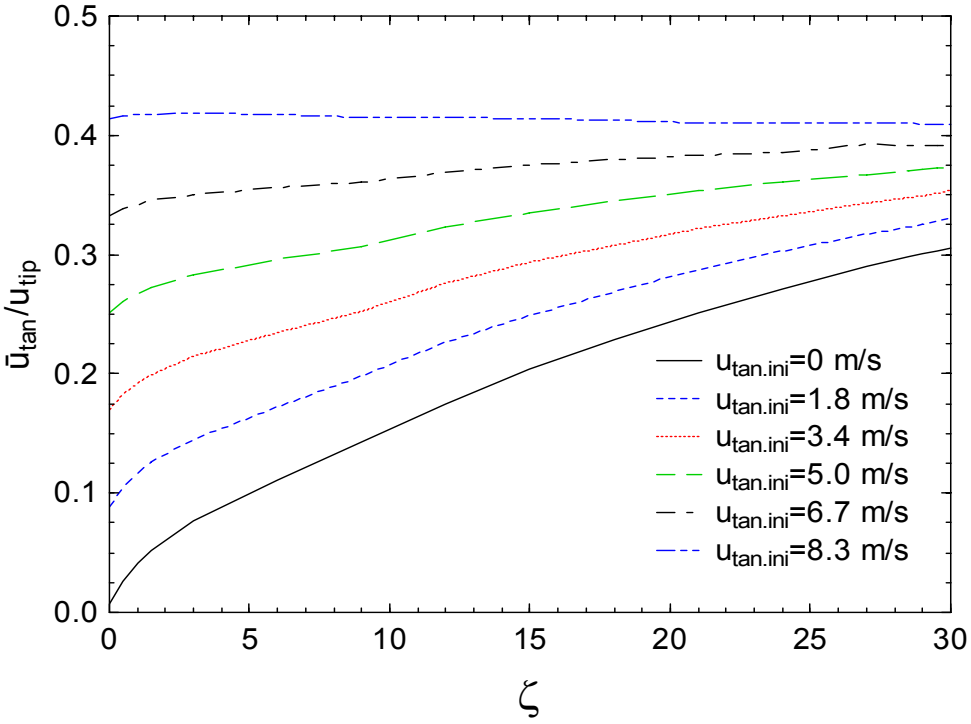

Figure 6-19 Normalised mean tangential velocity for δ=10 mm and u_{tip}=20 m/s at several different initial tangential velocities

A tangential feed will reduce any entrance effects because the acceleration of the suspension is reduced at the front of the annulus. Niinimäki et al. (1996a) have demonstrated that the feed configuration of a screen will have a slight effect on the shive removal efficiency of the screen and postulated a back flow mechanism of fluid into the feed chamber from the front of the annulus. It is expected that the flow structure of the fluid entering the screen annulus will be substantially different for an axially fed over a tangential fed screen. For an axially fed screen much greater turbulence will be created as the fluid contacts the rotor at the start of the annulus as the relative velocity between the two will be substantial. The turbulence scale and intensity will have implications on the state of the suspension in the annulus. It is well established that floc and fibre network disruption and dispersion occurs as a result of sustained turbulence and reflocculating will occur extremely quickly in the presence of decaying turbulence. There will be greater turbulence in the region of greater fluid acceleration and this will occur at the beginning of the screen and will cause deflocculation and increase the number of transient flocs which in turn will aid fibre passage.

6.3.6 Annular Gap

The effect of annular gap was also studied. Previous studies have shown that the pressure pulse magnitude is dependant on the clearance or gap between the rotor element and the screen (Gonzalez, 2002; Pinon et al., 2003). The annular gap is often changing when closed rotors are being used and the average gap will vary from rotor to rotor. In practice average annular gaps for closed rotors are seldom less than 10 mm and the gap between the foil and the screen is usually less than 5 mm. The tangential velocity profile at Z_N=1 and u_{tip}=20 m/s is shown in Figure 6-20. The average velocity in the centre region increased from approximately 25 % to 30 % of the rotor speed as the annular gap decreased from 15 mm to 5 mm. The variation in the velocity of the centre region was greater for the smaller annulus indicating a greater velocity gradient. Figure 6-21 shows that the normalised mean tangential velocity increased as the annular gap decreased and it increased at a greater rate at the start of the screen for the smaller annuli. When the annular gap is reduced there is more efficient momentum transfer from the rotor to the fluid.

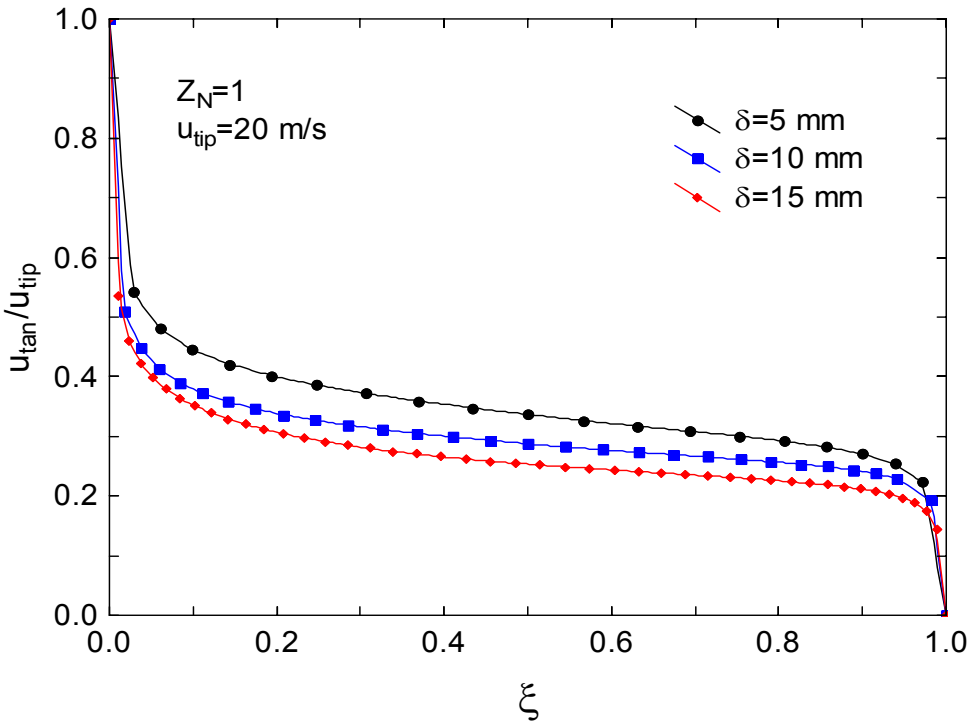

Figure 6-20 Tangential velocity profile in the radial direction for u_{tip}=20 m/s and Z_N=1 for axially feed annuli

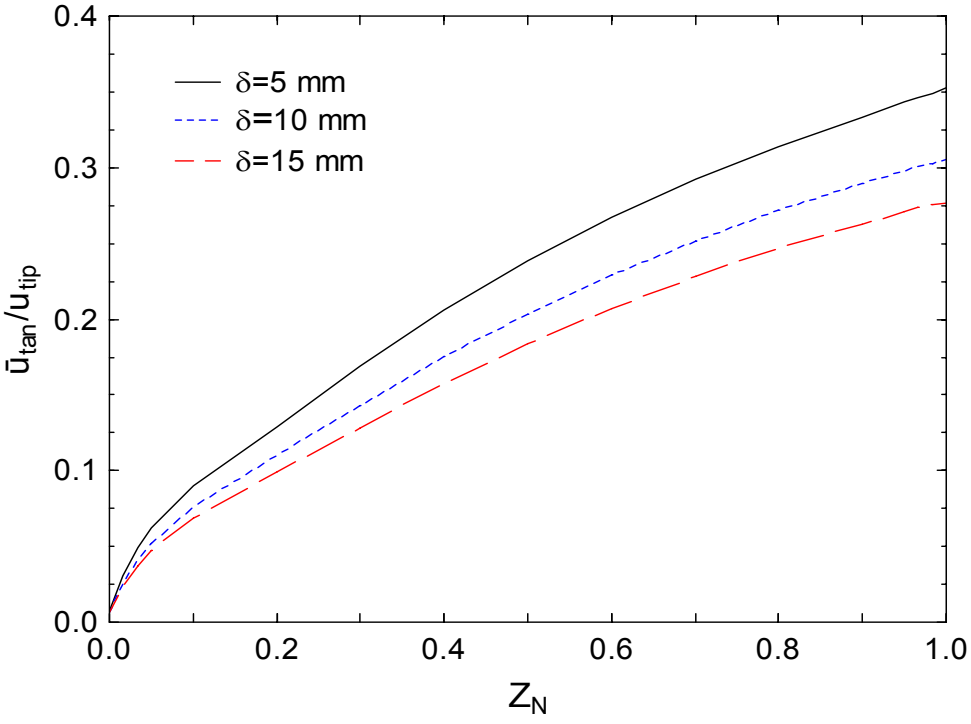

Figure 6-21 Normalised mean tangential velocity for the smooth rotor for u_{tip}=20 m/s and a range annular gaps

6.4 Larger Diameter Screen

A larger diameter screen and rotor with the same annular gap (δ=10 mm) was also used for selected cases in order to examine the affect of screen radius on the change in tangential velocity profile development. The diameter of the large screen was 406 mm as opposed to the smaller diameter of 203 mm however the overall length was only 180 mm as opposed to 300 mm. The length of the screen was reduced to keep the same absolute mesh scale in the radial and axial directions. The diameter of pressure screen baskets varies considerably, with the smaller diameter screens being in the order of 200 mm and larger ones in the order of 2 – 3 m. The tangential velocity profiles in the radial direction of the two size screens are illustrated in Figure 6-22. The tri-layer velocity profile is once again present but only after a sufficient number of annular lengths for it to develop. However the velocity profile develops quicker for the large diameter screen than for the smaller diameter screen. It must be noted here that the flow rate through the annulus was held constant and therefore the axial velocity will be lower for the large annulus.

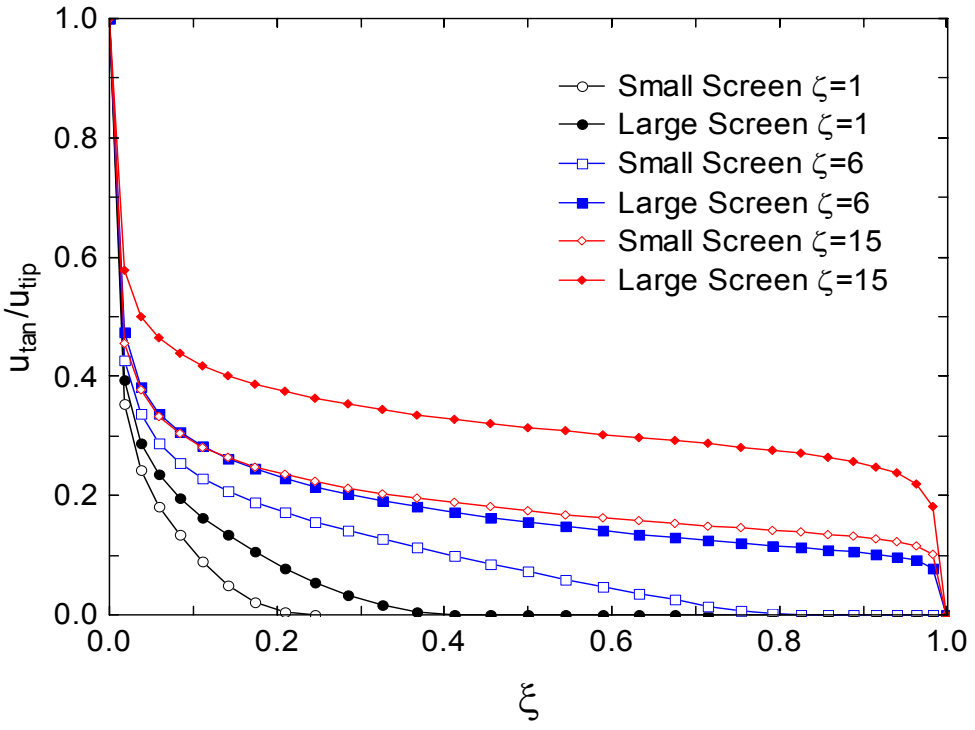

Figure 6-22 Tangential velocity profiles in the radial direction for the two different diameter screens for δ=10 mm and u_{tip}=20 m/s, Q_f=10 L/s

The normalised mean tangential velocity of the two screens at two different rotor speeds is illustrated in Figure 6-23. The flow rate through the annulus is held constant for both cases and therefore the axial velocity will be lower for the larger annulus cases. The tangential velocity increases at a much greater rate for the larger diameter screen. The increased velocity is due to the increase in momentum transfer from the rotor to the fluid due to the lower axial velocity. This increases the residence time of the fluid and as a result there is more time for momentum transfer. When the axial velocity is held constant there is very little difference in the tangential profiles of the two rotors with the tangential velocity of the larger annulus being slightly larger as demonstrated in Figure 6-24.

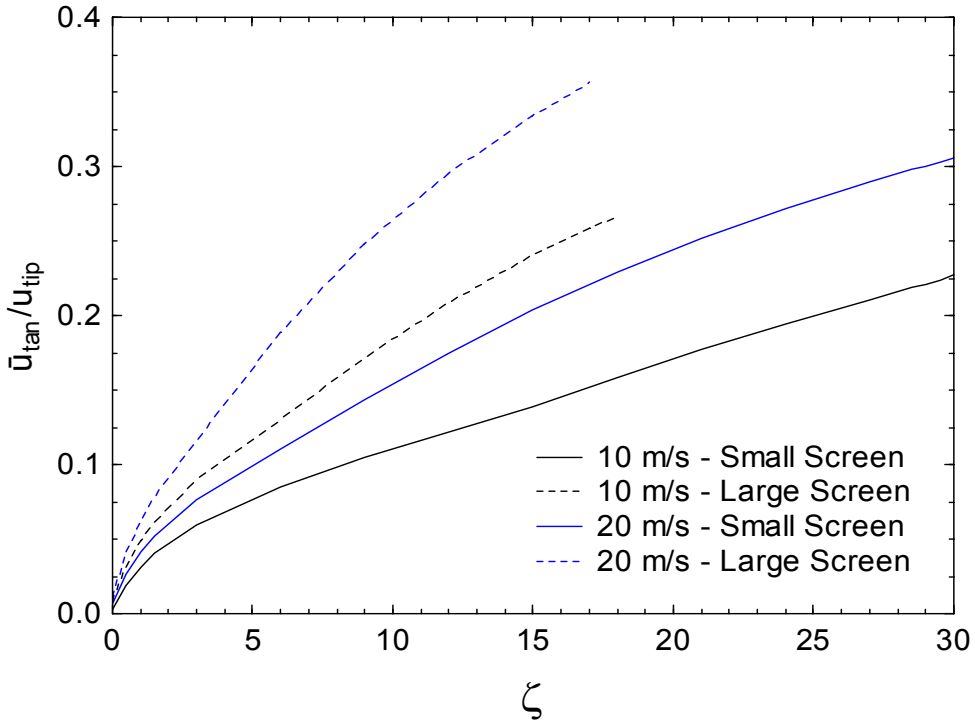

Figure 6-23 Normalised mean tangential velocity for the two different diameter screens at the same annular flow rate (δ=10 mm, Q_f=10 L/s)

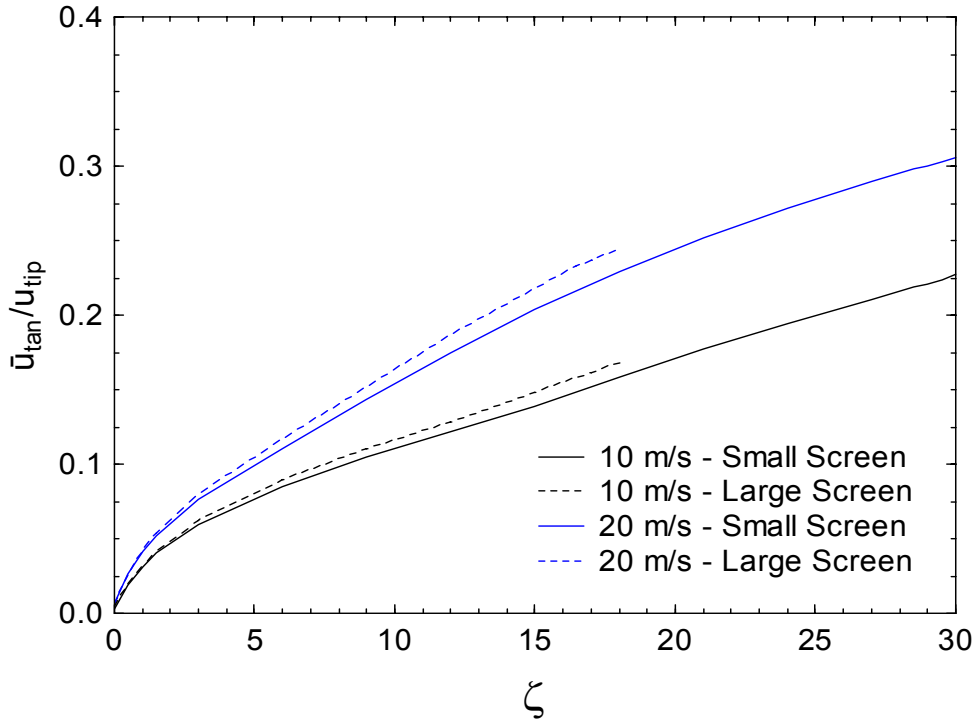

Figure 6-24 Normalised mean tangential velocity for the two different diameter screens at the same bulk axial velocity (δ=10 mm, $\bar{u}_{ax}$=1.65 m/s)

It is also useful to express the mean tangential velocity against the aspect ratio A (Equation 6-8) where D_s is the diameter of the screen. The aspect ratio is convenient for comparing screens of different dimensions and therefore the mean tangential velocity is presented in terms of aspect ratio in Figure 6-25 and Figure 6-26 for a constant annular flow rate and bulk axial velocity respectively.

$$A = \frac{z}{D_s} \qquad \textbf{6-8}$$

At the same flow rate the increase in tangential velocity is much greater for the large diameter screen. The entry effect occurs over a shorter distance and the rate of increase in tangential velocity is much greater. This suggests that for the same flow rate that entry effects would occur over less of the screen for larger diameter screens. If constant axial velocity is considered, tangential velocity still increases faster for the larger screen however the rate of increase is lower. Both data implies that for larger diameter screens entrance effects maybe less of a concern than for smaller screens.

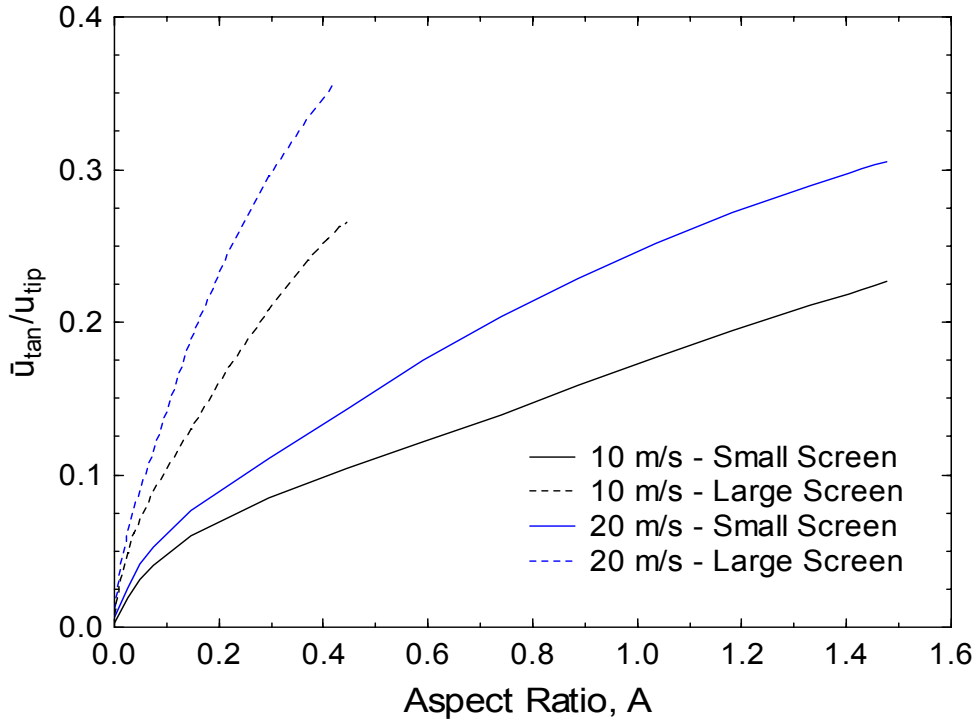

Figure 6-25 Normalised mean tangential velocity for the two different diameter screens as a function of aspect ratio at the same annular flow rate (δ=10 mm, Q_f=10 L/s)

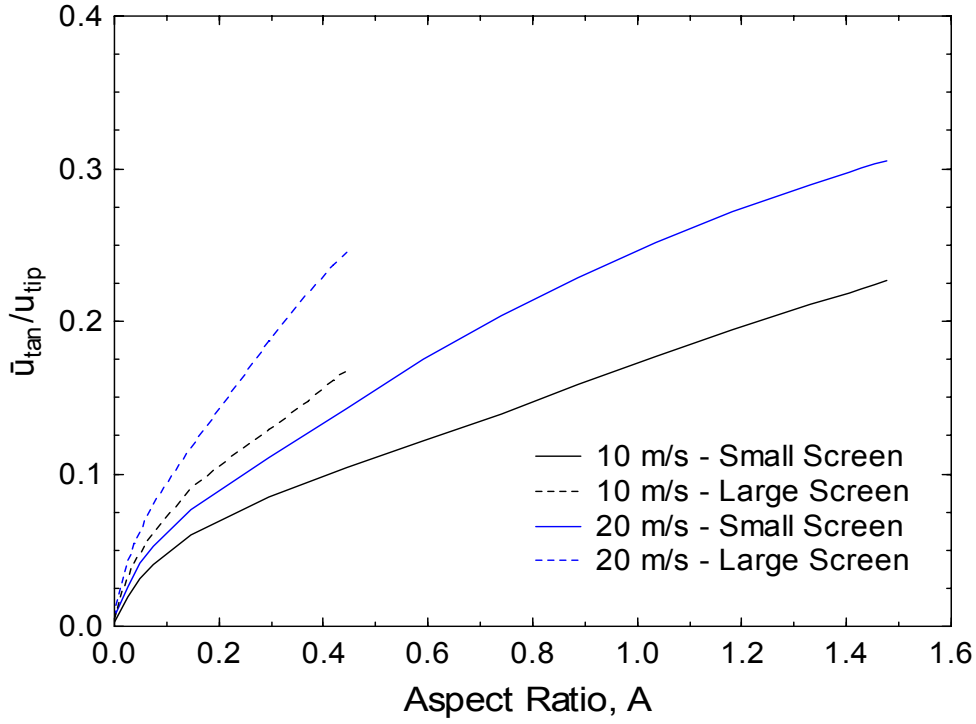

Figure 6-26 Normalised mean tangential velocity for the two different diameter screens as a function of aspect ratio at the same bulk axial velocity (δ=10 mm, $\bar{u}_{ax}$=1.65 m/s)

It is evident that not only the aspect ratio of the screen but also the diameter of the screen will affect the length of any entrance effects caused by the increase in tangential velocity. Reject thickening is likely to increase when the suspension is more flocculated which will decrease the passage of fibre through the screen. When the acceleration due to the rotor is reduced the turbulence is likely to decrease or decay and therefore flocs are likely to become larger and restrict fibre passage and promote reject thickening. The effect of aspect ratio or screen length has been investigated by Weeds (2006) and the length of the screen was found to affect the reject thickening behaviour. The plug flow model accurately described the behaviour of long screens although screens with an aspect ratio of around 0.6 have been reported to exhibit plug flow behaviour (Wakelin, 1997; Wakelin & Corson, 1997; Sloane, 2000). Plug flow conditions usually are thought to occur in tubular reactors of aspect ratios in the order of 100 (Metcalfe, 1997). It is clear that given the aspect ratio of most screens, which are in the order of 0.5 – 2, that plug flow conditions would not occur. However, when the helical nature of the flow is considered the path length is greatly increased compared to the case with no spinning rotor. The rotor will introduce a certain amount of mixing in the annulus and therefore the flow will deviate from pure plug flow. Weeds (2006) proposed a tanks-in-series flow model which could vary between mixed and plug flow models depending on the number of tanks used. As the number of tanks used in the model increased the prediction of reject thickening got closer to that of the plug flow model. More work is needed in quantifying the flow conditions in various screen annuli with different rotors to ascertain the flow regime (i.e. plug flow, mixed flow, dispersed plug flow, etc) exits with various rotors.

6.5 Industrial Screen Rotors -Step & Bump Rotors

Two industrial screen rotors, a step and bump rotor, were also modelled to examine the effect of rotor type on the velocity and pressure pulse changes in the annulus. It is expected that the addition of a rotor element would increase the efficiency of the momentum transfer from the rotor to the suspension. The face of the step rotor will push the fluid around the annulus and the tangential velocity will be much greater than that of the smooth rotor. The bumps represent an intermediate case between the two extremes of a step and a smooth rotor.

The normalised mean tangential velocity and slip factor are illustrated in Figure 6-27 for the step, bump and smooth rotors for a tip speed of 20 m/s and almost similar flow conditions. Only data for the first half of the smooth rotor is used so that the screen lengths are the same for all three rotors. The mean tangential velocity increased rapidly at the front of the annulus for the bump and step rotors although the increase was much greater for the step. For the step rotor the greatest increase occurred over the first 10 % of the screen and reached a maximum value of about 0.7 at just over a quarter a way along the screen annulus. The velocity slowly decreased to about 0.6 over the next 50 % of the screen before dropping rapidly to a final normalised velocity of just over 0.2. The normalised mean tangential velocity for the bump rotor increased following a roughly logarithmic relationship until the maximum velocity of just under 0.6 was reached at about 80 % along the screen length. The velocity then rapidly decreased in the same manner as the step rotor to a final value of just over 0.2. The smooth rotor shows a steady increase in mean tangential velocity along the entire annulus up to a maximum of slightly under 0.2 at the end of the annulus.

Also illustrated in the figure is the slip factor along the annular length for the three rotors. The slip factor for the step rotor rapidly decreases as the tangential velocity increases and reaches a minimum slip factor of approximately of 0.3 at around about a quarter along the annulus. The slip factor then increases slowly to a value of around 0.4 before a sharp increase toward the rear of the annulus. The bump rotor decreases following a negative logarithmic curve until a minimum slip factor about 0.4 is reached before a rapid increase in slip factor near the end of the annulus. In contrast the slip factor of the smooth rotor decreases progressively along the annulus to reach a minimum slip factor of just over 0.2.

The decrease in tangential velocity and the increase in slip factor toward the rear of the screen for both the step and bump rotors was unexpected and problematic. It was expected that the tangential velocity would continue to increase, reach a maximum value at some point along the screen, and then settle at or near the maximum value over the remainder of the annulus. Similarly it was anticipated that the slip factor would decrease and reach a minimum value at some point along the screen length and then stay at or near this value over the remainder of the screen.

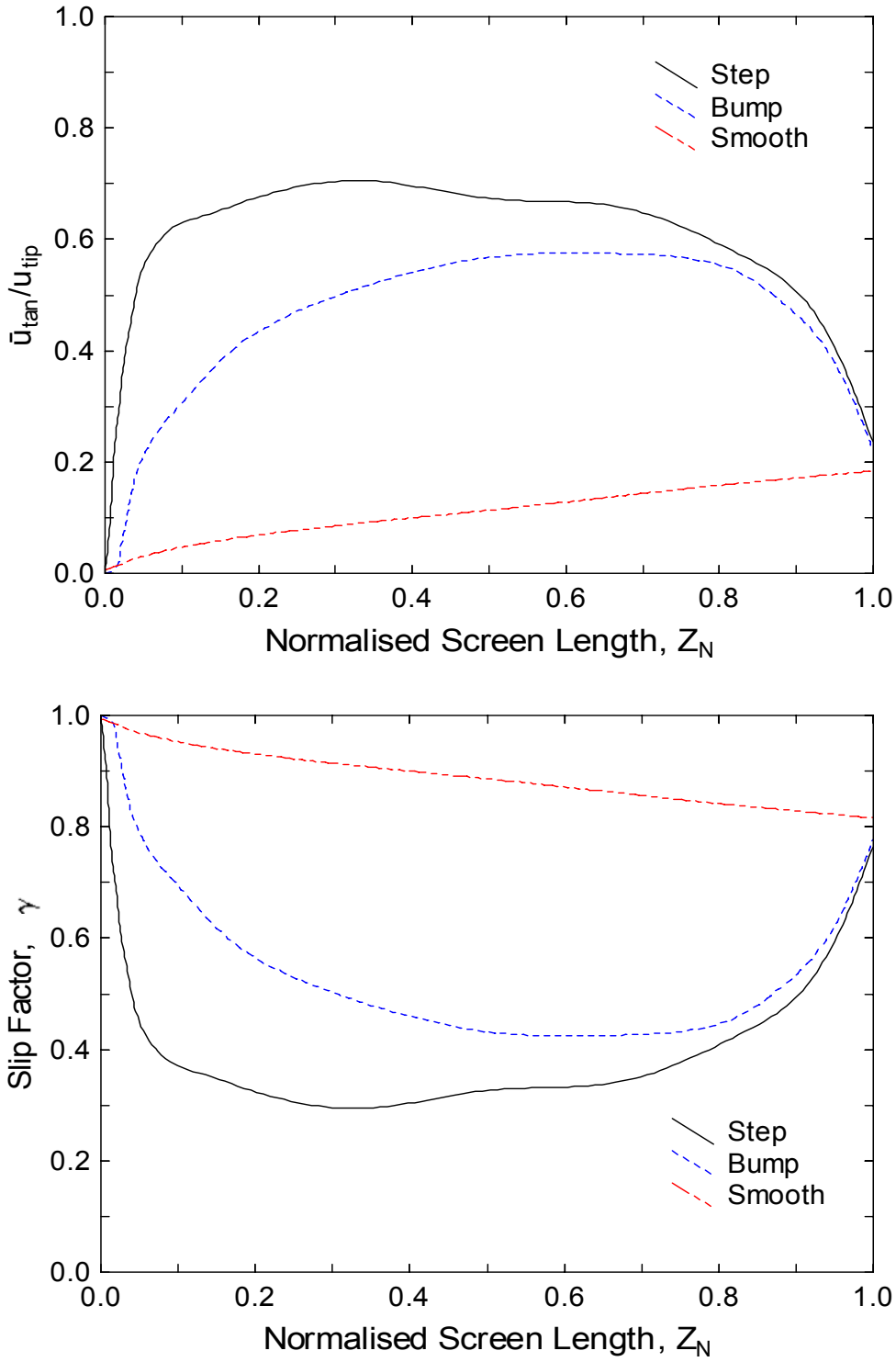

Figure 6-27 Normalised mean tangential velocity for the step, bump and smooth rotors u_{tip}=20 m/s, R_v=1 (step – Q_f=672 L/min, bump – Q_f=690 L/min, smooth – δ=10 mm, Q_f=600 Lmin)

The unexpected velocity profiles can be explained by the occurrence of back-flow which caused a bulk flow into the flow domain through one of the pressure outlets of the domain. Back-flow occurred for both the step and bump rotor solutions and is schematically illustrated in Figure 6-28. Due to the sliding mesh there were two fluid zones in the domain which then form a zone interface or sliding interface. The inner zone adjacent to the rotor rotates in time with the rotor while the outer zone adjacent to the outer wall remains stationary. This technique of using a sliding mesh eliminates the need for a deforming mesh which would otherwise add an enormous amount of computational time and expense. As a result of the sliding mesh approach, two separate inlets and outlets are needed. The inlets were set as pressure inlets and the outlets as pressure outlets. The outlet pressure is the reference pressure and in this case was set to zero gauge pressure. Due to these simplifications and assumptions the final numerical solution for the step and bump rotors are not boundary condition independent.

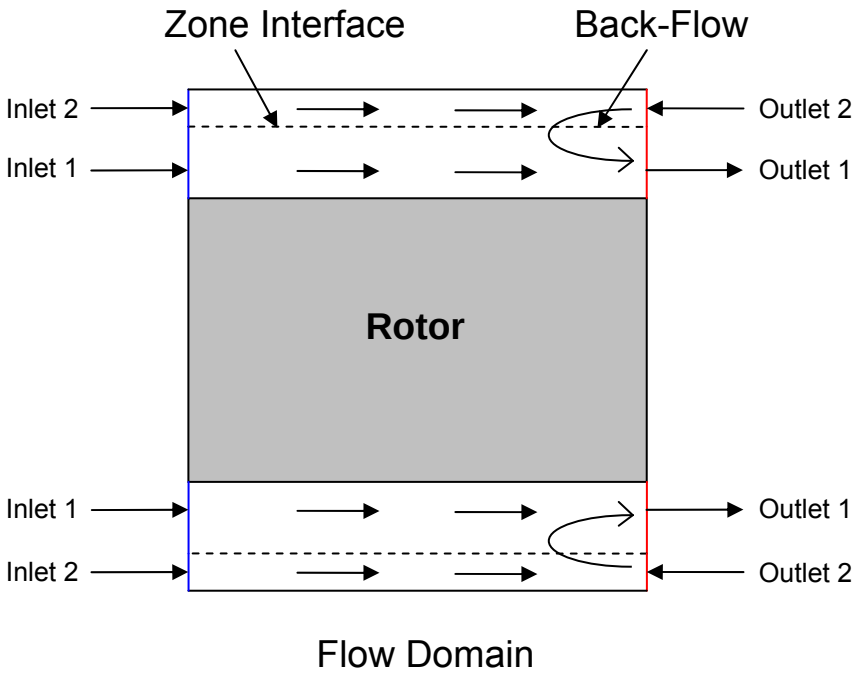

Figure 6-28 Schematic of back flow in to the domain

Back-flow occurred due the negative pressure created by the rotor near some sections of the domain boundary. As no reject chamber was included in the domain the arrangement of the two outlets attempt to create an "artificial" boundary condition

where the sum of the flow out of both outlets is equal to the sum of the flows in the inlets. The mass flux through all the boundaries was conserved but only by increasing the flow out of outlet 1 to compensate for the net flow into the domain via outlet 2. The effect this back-flow had on the mean tangential velocity profile and the slip factor is readily explained by considering the approach which the CFD code would use for any back-flow into the domain. If no back-flow occurred it would be expected that the tangential velocity of the fluid exiting the screen would have a significant tangential velocity component and this would be close to the maximum value. The flow into the domain via the outlet (in this case outlet 2) would have no tangential velocity component as it enters the screen. The fluid from the outlet would mix with the fluid already in the annulus and decrease the tangential velocity in the region of back-flow.

Tangential velocity profiles could be more accurately or realistically modelled if a reject chamber is included in the domain. This would reduce the amount of back-flow that may occur to more realistic amounts and provide a more accurate representation of the envisaged flow patterns toward the end of a screen annulus. However the addition of a reject chamber on the end of the model would increase the complexity and computational time and expense even further.

Although these results should be treated with caution they are nonetheless instructive and tentative conclusions can be drawn. Firstly, the rotor type should have a major effect on the tangential velocity of the suspension in the annulus and some rotor designs will increase the tangential velocity at a greater rate and extent than others. This was the case with the three rotors illustrated here. The step rotor gave the highest mean tangential velocity and also the greatest rate of momentum transfer due the step face forcing the fluid around. At the other extreme the smooth rotor gave the lowest tangential velocity and the lowest rate of change in velocity. The bump rotor was also relatively efficient in causing the tangential velocity to increase although not to the same extent and rate as the step rotor.

Secondly, it is possible that back-flow would occur in a real pressure screen toward the reject end of the screen. If the step rotor is considered, a localised zone of low pressure will occur close to the constriction directly after the face of the step. This

low pressure zone will cause fluid to flow back into the annulus from the reject chamber in the case of a real screen or from outside the flow domain in the case of the CFD model. This concept is illustrated schematically in Figure 6-29. Back-flow of thick reject pulp back into the annulus toward the rear of the screen would most likely increase the propensity for the screen to block in that region. The phenomenon of back-flow requires further investigation using both experimental and modelling techniques.

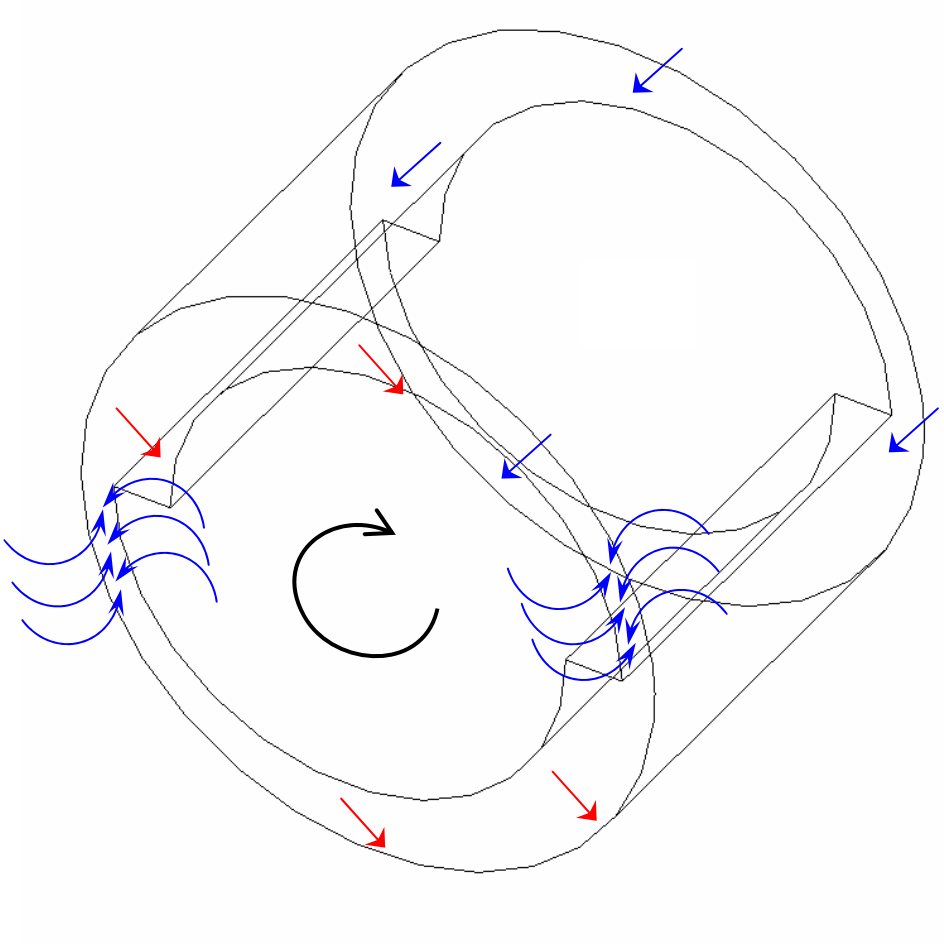

Figure 6-29 Back-flow mechanism for the step rotor

It should also be noted that it may be possible for flow from the front of the annulus to flow back into the feed chamber at the start of the annulus. Open recirculation zones which form directly upstream of the step face will cause three-dimensional vortices as described in the previous chapter. These vortices transport fluid away from the face in the axial direction of the screen. At the front of the screen this may occur and cause a moderate amount of back-flow into the feed chamber. It is most likely that

this back-flow into the feed chamber would only be of any significance for the step rotor. Ämmälä et al. (1999a; 1999b) speculated that a back-flow mechanism occurred at the front of the screen for a foil rotor and an axially fed screen. This mechanism was used to explain a dramatic increase in the consistency at the front of the screen annulus. It was hypothesised that the cause of the back-flow was the formation of a fibre mat at the front of the screen. This assumption is questionable and has been discussed previously. It is unlikely that the mechanisms of back-flow suggested by the CFD model and the flow around a forward facing step would occur for a foil rotor due to the open annulus created by this rotor.

The pressure was monitored at three positions along the annulus. The step rotor positions that pressure was monitored at were 25, 75, and 125 mm and the total length of the annulus was 150 mm. The bump rotor positions corresponded with the top of the face of the bump at 25, 75, 125 mm. The pulse was first rescaled by subtracting the time average pressure of the pulse from the calculated pressure. A non-dimensional pressure coefficient C_p (Equation 6-9) was used so that the calculated pulse could be compared with experimentally measured pressure pulse data. The non-dimensional pressure coefficient allows pulses for different conditions to be compared. This approach has been used both other researchers (Gooding, 1996; Gonzalez, 2002; Pinon et al., 2003; Feng et al., 2005). The time was normalised by the period of the pulse as the rotor speed of the pulses was slightly different.

$$C_p = \frac{\Delta P}{\frac{1}{2}\rho u_{tip}^{\ 2}} \qquad \textbf{6-9}$$

The calculated pressure pulse for the step rotor is compared to an experimentally measured pulse in Figure 6-30. The experimental data is presented slightly offset for easy of comparison. The calculated pulse was of a similar shape to that of the experimental pulse although the magnitude was somewhat greater. The bounce back phenomenon was not seen for the simulated pulse. This will likely be due to the limitations of the mesh and turbulence model that was used.

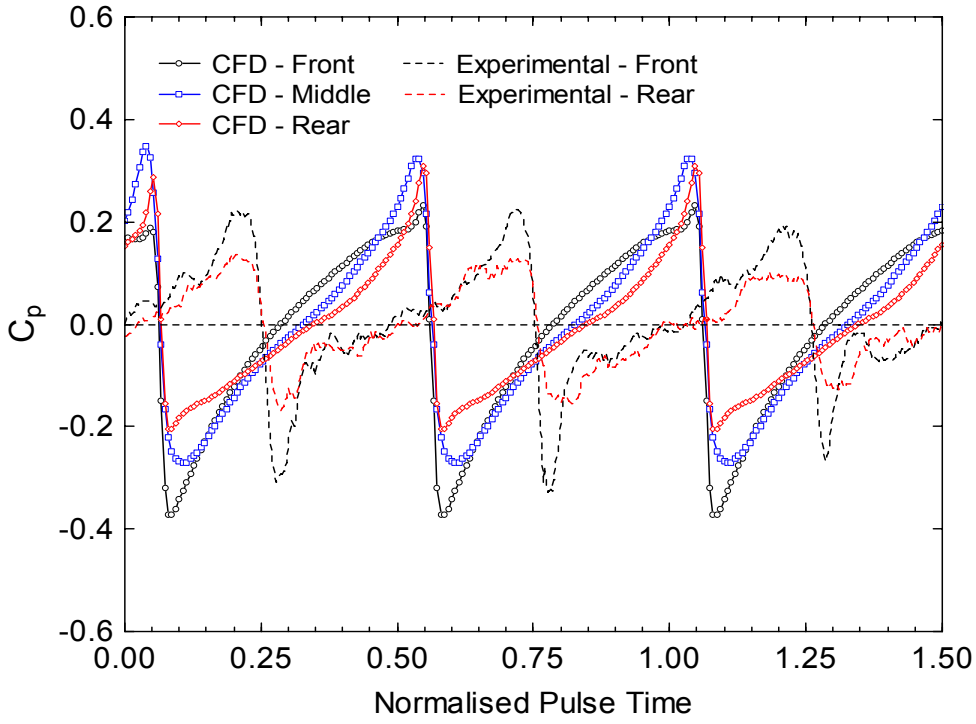

Figure 6-30 Measured pressure pulse for the step rotor at the front, middle, and front of the screen annulus (R_v=1, CFD – u_{tip}=20 m/s, Q_f=672 L/min, Exp - u_{tip}=18 m/s, Q_f=660 L/min)

The calculated and experimentally measured pressure pulses for the bump rotor are shown in Figure 6-31. The experimental data is taken from Yu (1992) and was measured on a Beloit MR18 pressure screen a similar model to the one used throughout this research except the MR18 has an 18 inch screen basket instead of a 8 inch basket. The bump rotor would be similar in arrangement to the one used in this study expect that more bumps would be around the circumference of the rotor. To compensate for this the period of the rotor was taken as four bumps. The major negative pulse occurs as the face of the bump passes the monitoring point and a minor negative pulse occurs slightly after. This minor negative pulse is caused by the next bump which is offset to the bump for which the pulse was measured.

Once again these data should be treated with caution due the shortcomings of the model and solution however there is comparatively good agreement in the shape of the pressure pulse for both rotors. The amplitude of the pulse for both rotors was over predicted.

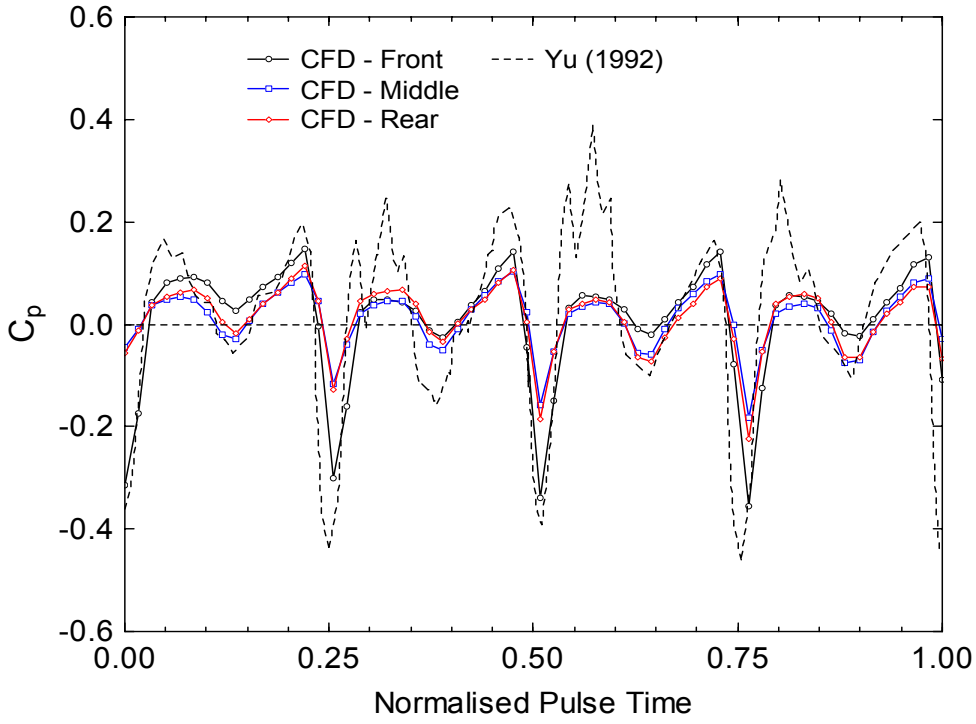

Figure 6-31 Measured pressure pulse for the bump rotor at the front, middle, and front of the screen annulus (R_v=1, CFD – u_{tip}=20 m/s, Q_f=690 L/min, Exp - u_{tip}=22.2 m/s, Q_f=unknown)

Although these results for the step and bump rotor should be treated cautiously due to the need of further model verification and experimental validation they provide a framework on which to build. CFD can be a useful tool for the design and evaluation of pressure screen rotors. The shape of the pressure pulse will directly affect the forward and reverse flow of fibre and fluid through the screen. As yet CFD has only been utilised occasionally for the design and optimisation of pressure screen foil rotors but with very promising results (Feng et al., 2005). It has been noted that there exists no strict engineering definition of an "ideal" pressure pulse (Pinon et al., 2003) although it is likely that the screening application will prescribe certain characteristics the pulse must have. If the issues of the sliding mesh approach used here can be resolved this methodology could be use for the evaluation, design, and optimisation of closed rotors for specific applications. There is significant scope for additional modelling and experimental study of the macro flows within a screen using CFD and advanced experimental techniques such as Particle Image Velocimetry (PIV). PIV especially holds potential for increased understanding with regards to the role the rotor plays in determining the flow field and fibre passage.

6.6 Summary

While the geometry modelled in this paper is a simplification of the actual screening situation (no feed chamber and no accept flow) the results are nevertheless instructive and of interest. It has clearly been shown that for a smooth rotor that the longer the screen the greater the tangential velocity toward the rear of the screen. It is well established from flow channel studies that the upstream or tangential velocity is an important factor in the passage of fibre through the screen. As has been demonstrated the mean tangential velocity may change considerably as the suspension travels along the screen length. This occurs both with and without accept flow. This increase in tangential velocity has a number of implications on the phenomena that occur in the screen, including effects on the state of the fibre suspension and the pressure pulse strength.

The step and bump rotors were also modelled using a sliding mesh approach but not to an acceptable degree of accuracy. A back-flow phenomenon occurred in the model which caused the mean tangential velocity toward to the rear of the screen to decrease significantly. The shape of the pressure pulse was well predicted using the sliding mesh approach. The results from the step and bump rotor cases are instructive but should be treated with caution.

7 Conclusions

Several conclusions can be drawn from the three major areas of investigation reported in this work. These conclusions are set forth in this chapter.

1. Passage ratio and fractionation efficiency vary with screen position

Passage ratio generally decreases along the screen length while fractionation efficiency increases. The passage of different fibre length fractions also decreased along the axial length of the screen. Fractionation efficiency generally increased along the screen length due to the disparity in the passage ratio of the long and short fibre fractions.

2. A position effect occurs along the screen which affects screen performance

The variability of performance parameters such as the fibre passage ratio and fractionation efficiency is due to a position effect that consists of two factors: a) changes in the suspension properties or flocculation effects, and b) changes in the flow conditions or rotor and flow effects.

3. The pressure pulse magnitude is dependant on the slip factor

The pressure pulse magnitude is dependant on the relative velocity of the fluid and the rotor or slip factor. As a consequence the pressure pulse at the rear of the screen is significantly lower, up to 40 % in some cases, than at the front of the screen. The slip factor generally decreases along the length of the screen and this change in slip factor accounts for the disparity in pulse magnitude with axial screen length. The feed configuration can also affect the slip factor toward the front of the screen and therefore influence the pulse magnitude.

4. Instantaneous aperture velocity varies greatly with time and deviates significantly from the superficial aperture velocity

Indicative instantaneous aperture velocities can be calculated using pulse data and pressure loss coefficients for the screen apertures for flow in the forward and reverse directions. The instantaneous aperture velocity deviated by an order of magnitude from the superficial aperture velocity. The back-flush ratio can also be estimated

from the instantaneous aperture velocity. A two passage ratio model has been developed to show the relationship between back-flush ratio, forward and reverse passage ratios and reject thickening.

5. **Computational Fluid Dynamics can be useful tool for modelling simplified screen annuli**

Computational Fluid Dynamics (CFD) can be a useful engineering tool for modelling changes in velocity through simplified screen annuli with the presence of a rotor. Although accept flow through the screen is missing, indicative trends of tangential velocity profiles are able to be predicted. In the absence of experimental data of internal velocity changes, CFD provides a simple and economic method for examining bulk flows within a pressure screen. Although there are limitations with unsteady modelling of pressure screen rotors, the general shape of the pressure pulse can be predicted reasonably well using CFD. A sliding mesh approach is well suited to this problem, however model verification is still an issue. The model will only give indicative forms of the pressure pulse at this stage.

6. **The step rotor gives a higher mean tangential velocity than the bump or smooth rotors**

The maximum mean tangential velocity reached in the annulus and the rate of acceleration, is dependant on the rotor geometry. For example a step rotor pushes or forces the fluid around the annulus to a much greater extent than a bump or smooth rotor.

7. **A possible back-flow mechanism was identified which affects the slip factor toward the reject end of the screen**

The unsteady CFD model of industrial screen rotors indicate that a back-flow mechanism may occur where fluid from the reject chamber is “sucked” back into the screen annulus. This back-flow mechanism is caused by the low pressure zone of the rotor and possibly includes a contribution from three-dimensional vortices at the step rotor face.

8 Recommendations - Future Work

Several areas for future work have been identified that may yield valuable insight into the screening mechanisms that occur within industrial pressure screens. These recommendations are outlined in this chapter.

1. Internal macro-flow studies

There is significant scope for additional modelling and experimental study of the macro flows within a screen using CFD and advanced experimental techniques such as Particle Image Velocimetry (PIV). PIV especially holds potential for increased understanding with regards to the role the rotor plays in determining the flow field and fibre passage.

2. Rotor mixing studies

Residence time studies would be useful in determining the mixing characteristics of various rotors and to what extent they exhibit mixed or plug flow behaviour. This could lead to more accurate predictive models for reject thickening etc.

3. Fibre length distribution effects on passage ratio

The effect the long fibre content of a furnish has on the passage ratio of shorter fibre should be investigated to determine if fractionation efficiency can be enhanced by increasing the long fibre content. This should also help elucidate if long and short fibre separation is solely a function of reject thickening or if flocculation effects are also relevant.

4. Visual studies of fibre passage through screen apertures at typical screening consistencies

High speed cinematography of the suspension near screen apertures under typical screening conditions would clarify to what degree of fluidisation occurs near the screen apertures. The process of aperture blocking and possibly floc extrusion could be productively studied using this approach.

5. CFD modelling of macro and micro flows within a pressure screen

There is enormous potential for the use of computational fluid dynamics to elucidate both macro-flow patterns in the screen annulus and accept chamber and micro-flows through multiple apertures in both the forward and reverse direction. The effect of difference pressure pulses on forward and reverse flow through various screen apertures can be assessed.

References

Alexander, S. O., Marton, R., & McGovern, S. D. (1968) Effect of Beating and Wet Pressing on Fibre and Sheet Properties. *Tappi 51*(6), 277-283.

Ämmälä, A. (2001) *Fractionation of Thermomechanical Pulp in Pressure Screening.* PhD Thesis, Department of Process and Environmental Engineering, University of Oulu, Oulu, Finland.

Ämmälä, A. (2004) Dual Effect of the Foil Tip Speed on Reject Thickening in Pressure Screening. *Appita 57*(2), 128-131.

Ämmälä, A., Dahl, O., Kuopanportti, H., & Niinimäki, J. (1999a) Pressure Screening: Changes in Pulp Properties in the Screen Basket. *Tappi 82*(10), 99-104.

Ämmälä, A., Dahl, O., Kuopanportti, H., & Niinimäki, J. (1999b) The Role of Back Flow in an Axially Fed Pressure Screen. *Paperi ja Puu 81*(3), 210-215.

Anagnost, S. E., Mark, R. E., & Hana, R. B. (2002) Variation of Microfibril Angle within Individual Tracheids. *Wood and Fibre Science 24*(2), 337-349.

Andersson, O. (1961) Flocculation at Sedimentation - Part 5: Factors Influencing Flocculation Tendency. *Svensk Papperstidning 64*(11), 417-426.

Andersson, O. (1966) Some Observations on Fibre Suspensions in Turbulent Motion. *Svensk Papperstidning 69*(2), 23-31.

Antunes, J., Axisa, F., & Grunenwald, T. (1996) Dynamics of Rotors Immersed in Eccentric Annular Flow Part 1 - Theory. *Journal of Fluids and Structures 10*(8), 893-918.

Arola, D. F., Powell, R. L., McCarthy, M. J., Li, T., & Odberg, L. (1998) NMR Imaging of Pulp Suspension Flowing Through an Abrupt Pipe Expansion. *American Institute of Chemical Engineers Journal 44*(12), 2597-2606.

Astill, K. N. (1964) Studies of the Developing Flow Between Concentric Cylinders with the Inner Cylinder Rotating. *ASME Journal of Heat Transfer 86*, 383.

Atkins, M. J. (2003) *Screening Behaviour of Earlywood and Latewood Pinus Radiata Kraft Pulps.* Masters of Science Thesis, Department of Materials and Process Engineering, University of Waikato, Hamilton, New Zealand.

Beaulieu, S., Karnis, A., Wild, D. J., & Wood, J. R. (1977) Domtar Installs TMP at Donnacona Newsprint Mill. *Pulp & Paper Canada 78*(3), 59-65.

Beghello, L., & Akademi, A. (1988) Some Factors that Influence Fibre Flocculation. *Nordic Pulp and Paper Research Journal 13*(4), 274-279.

Bennington, C. P. J. (1988) *Mixing Pulp Suspensions.* PhD Thesis, Department of Chemical Engineering, University of British Columbia.

Bennington, C. P. J., Kerekes, R. J., & Grace, J. R. (1989) *Journal of Pulp and Paper Science 15*(5), 186.

Bennington, C. P. J., Kerekes, R. J., & Grace, J. R. (1991) Motion of Pulp Fibre Suspensions in Rotary Devices. *The Canadian Journal of Chemical Engineering 69*(Feb), 251-258.

Bennington, C. P. J., & Mmbaga, J. P. (2001) *Liquid-Phase Turbulence in Pulp Fibre Suspensions.* 12th Fundamental Research Symposium, Oxford, UK, 255-286.

Björkman, U. (2005) Floc Dynamics in Flowing Fibre Suspensions. *Nordic Pulp and Paper Research Journal 20*(2), 247-252.

Bliss, T. (1990) *Screening in the Stock Preparation System.* Stock Preparation Short Course, Atlanta, GA, USA, 59-75.

Bliss, T. (1992) Screening. In *Pulp and Paper Manufacture* (pp. 229-247). Atlanta: Tappi.

Bonano, E. J. (1984) A Study of Floc Breakup and Formation in Flowing Concentrated Fibre Suspensions. *International Journal of Multiphase Flow 10*(5), 623-633.

Braaten, K. R., & Wakelin, R. F. (1999) Fiber Length Fractionation of TMP Using Pressure Screens. *Tappi Journal 82*(6), 129-135.

Celić, A., & Hirschel, E. H. (2006) Comparison of eddy-viscosity turbulence models in flows with adverse pressure gradient. *Aiaa Journal 44*(10), 2156-2169.

Chambers, T. L., & Wilcox, D. C. (1977) Critical Examination of Two-Equation Turbulence Closure Models for Boundary Layers. *Aiaa Journal 15*(6), 821-828.

Chung, T. J. (2002) *Computational Fluid Dynamics*. Cambridge, UK: Cambridge University Press.

Clark, J. (1985) *Pulp Technology and Treatment for Paper*. San Francisco, CA, USA: Miller Freeman Publications.

Claudio-da-silva, E. (1983) *The Flexibility of Pulp Fibres - A Structural Approach.* International Paper Physics Conference, 13-25.

Cowan, W. F. (1969) The Screening of Groundwood Pulp - A Reappraisal. *Pulp and Paper Canada 65*(Jan).

Cown, D. J. (1975) Variation in Trachied Dimensions in the Stem of a 26 Year Old Radiata Pine Tree. *Appita 28*(4), 237-245.

d'Incau, S. (1983). Taapi Engineering Conference, 583.

Davidson, L. (2003) *An Introduction to Turbulence Models*. Götenborg, Sweden: Chalmers University of Technology.

Davidson, P. A. (2004) *Turbulence - An Introduction for Scientists and Engineers*. Oxford, UK: Oxford University Press.

Dinwoodie, J. M. (1965) The Relationship Between Fibre Morphology and Paper Properties: A Literature Review. *Tappi 48*(8), 440-447.

Dodson, C. T. J. (1996) Fibre Crowding, Fibre Contacts, and Fibre Flocculation. *Tappi 79*(9), 211-215.

Duffy, G. G. (1976a) High-Consistency Flow of Pulp Suspensions in Pipes. *Tappi 61*(8), 85-88.

Duffy, G. G. (1976b) A Review and Evaluation of Design Methods for Calculating Friction Loss in Stock Piping Systems. *Tappi 59*(8), 124-127.

Duffy, G. G. (1979) *Flow Models and Pipeline Design Equations for Fibre Suspension Flow.* First National Conference on Rheology, Melbourne, Australia, 61-65.

Duffy, G. G. (1995) Flow of Medium Consistency Wood Pulp Fibre Suspensions. *Appita 48*(1), 51-55.

Duffy, G. G. (1999) *Increasing Profit Through Selective Fibre Treatment.* 53rd Appita Conference, Rotorua, NZ, 205-209.

Duffy, G. G., & Abdullah, L. (2002) *Flow of Fibre Suspensions in Small Diameter Pipes.* 56th Appita Annual Conference, Rotorua, New Zealand, 127-133.

Duffy, G. G., & Abdullah, L. (2003) Fibre Suspension Flow in Small Diameter Pipes. *Appita 56*(4), 290-295.

Duffy, G. G., & Lee, P. F. W. (1978) Drag Reduction in the Turbulent Flow of Wood Pulp Suspensions. *Appita 31*(4), 280-286.

Duffy, G. G., Moller, K., Lee, P. F. W., & Milne, S. W. A. (1974) *Design Correlations for Groundwood Pulps and the Effects of Minor Variables on Pulp Suspension Flow.* 27th Appita Annual Conference, Rotorua, New Zealand, 327-333.

Duffy, G. G., & Titchener, A. L. (1975) The Disruptive Shear Stress of Pulp Networks. *Svensk Papperstidning 75*(13), 474-479.

Duffy, G. G., Titchener, A. L., Lee, P. F. W., & Moller, K. (1976) The Mechanisms of Flow of Pulp Suspensions in Pipes. *Appita 29*(5), 363-370.

Elson, T. P. (1979) Velocity Profiles of Concentric Flow Between Coaxial, Rotating Cylinders with a Stationary Lower Boundary. *Chemical Engineering Science 34*, 373-377.

Escudier, M. P., & Gouldson, I. W. (1995) Concentric Annular Flow with Centerbody Rotation of a Newtonian and a Shear-thinning Liquid. *International Journal of Heat and Fluid Flow 16*(3), 156-162.

Feng, M., Ollivier-Gooch, C., Gooding, R. W., & Olson, J. A. (2005) Numerical Simulation and Experimental Measurement of Pressure Pluses Produced by a Pulp Screen Foil Rotor. *Journal of Fluids Engineering 127*(2), 347-357.

Forgacs, O. L., & Mason, S. G. (1958) The Flexibility of Wood Pulps. *Tappi 41*(11), 695-704.

Franko, A. (1987) Centri-Cleaning. In *Pulp and Paper Manufacture Vol. 2 Mechanical Pulping* (pp. 204-209). Atlantia: Tappi.

Goldenberg, P. H. (1987) *Pressure Screen Improvements with New Rotor Design.* 73rd Annula Meeting of Technical Section of Canadian Pulp and Paper Association, Montreal, Canada, B275-B277.

Gonzalez, J. A. (2002) *Characterization of Design Parameters for a Free Foil Rotor in a Pressure Screen.* Masters Thesis, Department of Mechanical Engineering, University of British Columbia, Vancouver, Canada.

Gooding, R. W. (1986) *The Passage of Fibres through Slots in Pressure Screening.* Masters Thesis, Department of Chemical Engineering, University of British Columbia, Vancouver, Canada.

Gooding, R. W. (1996) *Flow Resistance of Screen Plate Apertures.* PhD Thesis, Department of Chemical Engineering, University of British Columbia, Vancouver, Canada.

Gooding, R. W., & Craig, D. F. (1992) The Effect of Slot Spacing on Pulp Screen Capacity. *Tappi Journal 71*(2), 71-75.

Gooding, R. W., & Kerekes, R. J. (1989) Derivation of Performance Equations for Solid-Solid Screens. *The Canadian Journal of Chemical Engineering 67*(10), 801-805.

Gooding, R. W., & Kerekes, R. J. (1992) Consistency Changes Caused by Pulp Screening. *Tappi Journal 75*(11), 109-118.

Gooding, R. W., Kerekes, R. J., & Salcudean, M. (2001) *The Flow Resistance of Slotted Apertures in Pulp Screens.* Fundamental Research Symposium, Oxford, England,

Gooding, R. W., Olson, J. A., & Roberts, N. (2001) *Parameters for Assessing Fibre Fractionation and Their Application to Screen Rotor Effects.* International Mechanical Pulping Conference, Helsinki,

Grégoire, G., Favre-Marinet, M., & Julien Saint Amand, F. (2000) *Numerical Simulation of the Flow in a Pressure Screen* COST Action E7 Final Conference "Multi-phase Flows in Papermaking", Manchester, UK,

Grégoire, G., Favre-Marinet, M., Julien Saint Amand, F., Serres, A., & Fernandez de Grado, A. (1998) *Modelling of the Producitve and Reverse Flow at the Screen Surface.* COST Workshop" Recent Research in Multi-Phase Flows in Paper Making", Paris, France,

Grundström, K. J., Norman, B., & Wahren, D. (1973) High Consistency Forming of Paper. *Tappi 56*(7), 81-84.

Gullichsen, J., & Härkönen, E. (1981) Medium Consistency Technology 1: Fundamental Data. *Tappi 64*(6), 69-72.

Hammarström, D. (2004) *A Model for Simulation of Fiber Suspension Flow*. Stockholm, Sweden: Royal Institute of Technology.

Hautala, J., Hourula, I., Jussila, T., & Pitkänen, M. (1999) Screening and Cleaning. In J. Sundholm (Ed.), *Mechanical Pulping*. Jyväskylä, Finland: Fapet Oy.

Hooper, A. W. (1987) Screening of Mechanical Pulp - Effect of Control Parameters and Screen Operation on Pulp Quality. In *Pulp and Paper Manufacture Vol. 2 Mechanical Pulping* (pp. 181-195). Atlanta: Tappi.

Hooper, A. W. (1989) Speck Dirt Removal with Slotted Screens. *Pulp & Paper Canada 90*(5), 47-54.

Hubley, C. E., Robertson, A. A., & Mason, S. G. (1950) *Candian Research Journal 28*(8), 770-787.

Hunter, D. (1947) *Papermaking - The History and Technique of an Ancient Craft*. New York, NY, USA: Dover.

James, D. F., Yogachandran, N., Loewen, M. R., Liu, H., & Davis, A. M. J. (2003) Floc Rupture in Extensional Flow. *Journal of Pulp and Paper Science 29*(11), 377-382.

Javid, S. R. (1983) Pressure Screen Design, Application is Key to Headbox Pulsation Control. *Pulp & Paper 57*(3), 182-186.

Jokinen, H., Ämmälä, A., Virtanen, J. A., Lindroos, K., & Niinimaki, J. (2007) Pressure Screen Capacity - Current Findings on the Role of Wire Width and Height. *Tappi Journal 6*(1), 3-10.

Jokinen, H., Karjalainen, M., Niinimäki, J., & Ämmälä, A. (2007) Effect of Furnish Quality on Pressure Screen Performance. *Appita 60*(1), 35-40.

Jokinen, O., & Ebeling, K. (1985) Flocculation Tendency of Papermaking Fibres. *Paperi ja Puu 1985*(5), 317-325.

Julien Saint Amand, F. (1997) *Principles and Technology of Screening* (No. 16). Grenoble: Centre Technique du Papier.

Julien Saint Amand, F. (2001) *Screening: State of the Art and Future: To Understand Mechanisms and Innovations Better in Order to Improve Quality and Increase Productivity.* 54th ATIP Annual meeting "Water, energy, waste: issues of the paper industry", Grenoble, France,

Julien Saint Amand, F., Gooding, R. W., Huovinen, A., Heederik, P., Pahl, A., Haar, W., et al. (2005) *Optimisation of Screening and Cleaning Technology to Control Deinking Pulp Cleanliness*.

Julien Saint Amand, F., & Perrin, B. (1998) *Screening: Experimental Approach and Modelling.* Tappi Pulping Conference, 1019-1031.

Julien Saint Amand, F., & Perrin, B. (1999) *Fundamentals of Screening: Effect of Rotor Design and Fibre Properties.* Tappi Pulping Conference, Orlando, USA, 941-955.

Kallmes, O. (1977) Flocculation of Pulp Suspensions. *Paper Trade Journal 161*(44).

Karnis, A. (1997) Pulp Fractionation by Fibre Characteristics. *Paperi ja Puu 79*(7), 480-488.

Karvinen, R., & Halonen, L. (1984) The Effect of Various Factors on Pressure Pulsation of a Screen. *Paperi ja Puu 66*(7), 80-83.

Kelly, E. G., & Spottiswood, D. J. (1982) *Introduction to Mineral Processing*. New York, NY, USA: Wiley.

Kerekes, R. J. (1979) High Turbulence for Headboxes Questioned. *Pulp And Paper Canada 80*(9), 31-32.

Kerekes, R. J. (1983a) Pulp Floc Behaviour in Entry Flow to Constrictions. *Tappi 66*(1), 88-91.

Kerekes, R. J. (1983b) Pulp Flocculation in Decaying Turbulence: A Literature Review. *Journal of Pulp and Paper Science 9*(3), 86-91.

Kerekes, R. J. (2006) Rheology of Fibre Suspensions in Papermaking: An Overview of Recent Research. *Nordic Pulp and Paper Research Journal 21*(5), 598-612.

Kerekes, R. J., & Schell, C. J. (1992) Characterization of Fibre Flocculation Regimes by a Crowding Factor. *Journal of Pulp and Paper Science 18*(1), 32-38.

Kerekes, R. J., & Schell, C. J. (1995) Effects of Fiber Length and Coarseness on Pulp Flocculation. *Tappi 78*(2), 133-139.

Kerekes, R. J., Soszynski, R. M., & Tam Doo, P. A. (1985) *The Flocculation of Pulp Fibres.* Transactions of the Fundamental Research Symposium, 265-309.

Kibblewhite, R. P. (1973) Effects of Beating and Wood Quality on Radiata Pine Kraft Paper Qualities. *New Zealand Journal of Forestry Science 3*(2), 220-239.

Kibblewhite, R. P., & Bailey, D. G. (1988) Measurement of Fibre Cross-section Dimensions Using Image Processing. *Appita 41*(4), 297.

Kropholler, H. W., & Sampson, W. W. (2001) The Effect of Fibre Length Distribution on Suspension Crowding. *Journal of Pulp and Paper Science 27*(9), 301-305.

Kubát, J. (1956a) Experimental Evidence of the Validity of the Statistical Screening Theory - Theory of Screening 7. *Svensk Papperstidning 59*, 251-256.

Kubát, J. (1956b) Screening Processes Involving Particle Interaction - Theory of Screening 6. *Svensk Papperstidning 59*, 175-178.

Kubát, J., & Steenberg, B. (1955) Screening at Low Particle Concentrations - Theory of Screening 3. *Svensk Papperstidning 58*(9), 319-324.

Kuhn, D. C. S., Oosthuizen, P. H., & Whiting, P. (1990) *A Single Slot Screen for Fibre Flexibility Measurements.* 76th Annual Meeting, CPPA Techincal Section, 275-280.

Kumar, A. (1991) *Passage of Fibres Through Screen Apertures.* PhD Thesis, Department of Chemical Engineering, University of British Columbia, Vancouver, Canada.

Kumar, A., Gooding, R. W., & Kerekes, R. J. (1996) *Passage of Fibre Through Single Slots at Dilute Consistency* (No. PPR 1246): Pulp and Paper Research Institute of Canada.

Lawryshyn, Y. A., & Kuhn, D. C. S. (1996) Large Deflection Analysis of Wet Fibre Flexibility Measurement Techniques. *Journal of Pulp and Paper Science 22*(11), 423.

Lawryshyn, Y. A., & Kuhn, D. C. S. (1998) Simulation of Flexible Fibre Motion Through Screen Apertures. *Journal of Pulp and Paper Science 24*(12), 404-411.

LeBlanc, P. E. (1986) *A Breakthrough in Pressure Screening.* Tappi Pulping Conference, Atlanta, GA, USA, 75-77.

Lee, P. F. W., & Duffy, G. G. (1976a) Relationships Between Velocity Profiles and Drag Reduction in Turbulent Fibre Suspension Flow. *AIChE 22*(4), 750-753.

Lee, P. F. W., & Duffy, G. G. (1976b) Velocity Profiles in the Drag Reducing Regime of Pulp Suspension Flow. *Appita 30*(3), 219-226.

Levenspiel, O. (1999) *Chemical Reaction Engineering*. New York, NY, USA: Wiley.

Levis, S. H. (1991) Screening of Secondary Fibers. *Progress in Paper Recycling 5*(1), 31-45.

Lundell, F., Söderberg, D., Storey, S., & Holm, R. (2005) *The Effect of Fibres on Laminar-Turbulent Transition and Scales in Turbulent Decay.* 13th Fundamental Research Symposium, Cambridge, UK, 19-34.

Martin, B. W., & Payne, A. (1972) Tangential Flow Development for Laminar Axial Flow in an Annulus with a Rotating Inner Cylinder. *Proceedings of the Royal Society of London. Series A, Mathematical and Physical Sciences 328*, 123-141.

Martinez, D. M., Gooding, R. W., & Roberts, N. (1999) A Force Balance Model of Pulp Sceen Capacity. *Tappi Journal 82*(4), 181-187.

Mason, S. G. (1948) *Pulp and Paper Magazine Canada 49*(13), 99-104.

Mason, S. G. (1950) The Motion of Fibres in Flowing Liquids. *Pulp And Paper Magazine of Canada 51*(5), 94-98.

Mason, S. G. (1954) Fibre Motions and Flocculation. *Tappi 37*(11), 494-501.

McCarthy, C. (1988) Various Factors Affect Pressure Screen Operation and Capacity. *Pulp & Paper 62*(9), 233-237.

Menter, F. R. (1992) Performance of Popular Turbulence Models for Attached and Separated Adverse Pressure Gradient Flows. *Aiaa Journal 30*(8), 2066-2072.

Menter, F. R. (1994) 2-Equation Eddy-Viscosity Turbulence Models for Engineering Applications. *Aiaa Journal 32*(8), 1598-1605.

Metcalfe, I. S. (1997) *Chemical Engineering - A First Course*. New York, NY, USA: Oxford University Press.

Meyer, R., & Wahren, D. (1964) On the Elastic Properties of Three-Dimensional Fibre Networks. *Svensk Papperstidning 67*(10), 432-436.

Naser, J. A. (1997) *Prediction of Newtonian & non-Newtonian Flow Through Concentric Annulus with Centerbody Rotation.* International Conference on CFD in Mineral & Metal Processing and Power Generation, CSIRO, Melbourne, Australia, 273-278.

Nelson, G. L. (1981) The Screening Quotient: A Better Index for Screening Performance. *Tappi Journal 64*(5), 133-134.

Niinimäki, J. (1998) *On the Fundamentals of Pressure Screening.* PhD Thesis, Department of Process Engineering, University of Oulu.

Niinimäki, J., Dahl, O., Hautala, J., Tirri, T., & Kuopanportti, H. (1996a) Effect of Feed Construction on the Efficiency of Pressure Screening. *Tappi Journal 79*(11), 119-123.

Niinimäki, J., Dahl, O., Hautala, J., Tirri, T., & Kuopanportti, H. (1996b) *Effect of Operating Parameters and Rotor Body Shape on Flow Conditions and the Performance of a Pressure Screen.* Tappi Pulping Conference, 761-765.

Norman, B., Moller, K., & Duffy, G. G. (1977) *Hydrodynamics of Papermaking Fibres in Water Suspension.* Transactions of the Fundamental Research Symposium, Oxford, UK, 195-249.

Norman, B., Wedin, P. O., Grundstrom, K., & Hagen, N. (1986) *Visualization of Flow in a High Consistency Screen.* Tappi Engineering Conference, 585-587.

Nouri, J. M., & Whitelaw, J. H. (1994) Flow of Newtonian and Non-Newtonian Fluids in a Concentric Annulus with Rotation of the Inner Cylinder. *Journal of Fluids Engineering-Transactions of the Asme 116*(4), 821-827.

Oberkampf, W. L., & Trucano, T. G. (2002) *Verification and Validation in Computational Fluid Dynamics*. Albuquerque, NM, USA: Sandia National Laboratories

Olson, J. A. (1996) *The Effect of Fibre Length on Passage Through Narrow Apertures.* PhD Thesis, Department of Chemical Engineering, University of British Columbia, Vancouver, Canada.

Olson, J. A. (2001a) Fibre Length Fractionation Caused by Pulp Screening, Slotted Screen Plates. *Journal of Pulp and Paper Science 27*(8), 255-261.

Olson, J. A. (2001b) The Motion of Fibres in Turbulent Flow, Stochastic Simulation of Isotropic Homogeneous Turbulence. *International Journal of Multiphase Flow 27*(2001), 2083-2103.

Olson, J. A., Allison, B. J., & Roberts, N. (2000) Fibre Length Fractionation Caused by Pulp Screening, Smooth-Hole Screen Plates. *Journal of Pulp and Paper Science 26*(1), 12-16.

Olson, J. A., & Kerekes, R. J. (1998a) Fibre Passage Through a Single Screen Aperture. *Appita 51*(2), 122-126.

Olson, J. A., & Kerekes, R. J. (1998b) The Motion of Fibres in Turbulent Flow. *Journal of Fluid Mechanics 337*, 1-18.

Olson, J. A., & Wherrett, G. (1998) A Model of Fibre Fractionation by Slotted Screen Apertures. *Journal of Pulp and Paper Science 24*(12), 398-403.

Oosthuizen, P. H., Kuhn, D. C. S., & Whiting, P. (1992) *Fluid and Fibre Flow Near a Wall Slot in a Channel.* 78th Annual Meeting, CPPA Technical Section, 49-52.

Paavilainen, L. (1993) Conformability, Flexibility, and Collapsibility of Sulphate Pulp Fibres. *Paperi ja Puu 75*(9), 689-702.

Parker, J. D. (1961) Recent Theoretical Work in the Area of Sheet Formation. *Tappi 44*(4), 162-167.

Paul, S. T. (1999) *Fibre Suspension Processing in Viscous Media.* PhD Thesis, University of Auckland, Auckland, NZ.

Pietilä, M. (1996) *Computational Study of Fluid Dynamics of a Pressure Screen Foil Rotor.* Masters Thesis, Aeronautical Engineering, Helsinki University of Technology, Helsinki, Finland.

Pimley, J. J., & Rees, B. (1998) *Replacing Dispersion with Screeing for the Elimination of Sitckes.* 58th Appita Conference, Brisbane, Australia, 267-270.

Pinon, V., Gooding, R. W., & Olson, J. A. (2003) Measurements of Pressure Pulses From a Solid Core Screen Rotor. *Tappi Journal 2*(10), 9-12.

Repo, K., & Sundholm, J. (1996) The Effect of Rotor Speed on the Separation of Coarse Fibres in Pressure Screening with Narrow Slots. *Pulp & Paper Canada 97*(7), 67-71.

Richardson, J. D., Waller, A., & Jenson, A. A. C. (1999) Developing Pressurized Refiner Mechanical Pulping for the Tasman Pulp and Paper Mill. *Appita 52*(1), 23-29.

Rienecker, R. (1992) *Spectro Screen D - A New Concept for Effective Screening Within the Stock Consistency Range of Approx. 3%*: Voith Paper.

Rienecker, R. (1997) *Screening of Recovered Paper Stock for the Production of Graphic Papers*: Voith Paper.

Riese, J. W., Spiegelberg, H. L., & Kellenberger, S. R. (1969) Mechanism of Screening: Dilute Suspensions of Stiff Fibers at Normal Incidence. *Tappi Journal 52*(5), 895-903.

Ringner, J. (1995) *The Influence of Fibre Length Distributions on the Network Strength of Fibre Suspensions.* Masters Thesis, Department of Chemical Engineering, Chalmers University of Technology, Goteborg, Sweden.

Roache, P. J. (1998a) *Fundamentals of Computational Fluid Dynamics*. Albuquerque, NM, USA: Hermosa Publishers.

Roache, P. J. (1998b) *Verification and Validation in Computational Science and Engineering*. Albuquerque, NM, USA: Hermosa Publishers.

Salmela, J., & Kataja, M. (2005) *Floc Rupture and Re-Flocculation in Turbulent Shear Flow.* 13th Fundamental Research Symposium, Cambridge, UK, 35-50.

Samuelsson, L. G. (1963) Measurement of the Stiffness of Fibres. *Svensk Papperstidning 66*(15), 541-546.

Samuelsson, L. G. (1964) Stiffness of Pulp Fibres Part 1: Comparison of the Stiffness of Unbeaten Sulphite and Sulphate Pulp Fibres of Spruce. *Svensk Papperstidning 67*(22), 905-910.

Sastry, C. B. R., & Wellwood, R. W. (1972) Coarseness of Some Coniferous Wood Pulps: A New Approach. *Tappi 55*(6), 901-903.

Schlichting, H. (1960) *Boundary-Layer Theory* (J. Kestin, Trans. Fourth ed.). New York, NY, USA: McGraw-Hill.

Schniewind, A. P., Ifju, G., & Brink, D. L. (1966) Effect of Drying on the Flecural Rigidity of Single Fibres. In F. Bolam (Ed.), *Consolidation of the Paper Web* (Vol. 2, pp. 538-543): British Paper and Board Makers' Association.

Schweiss, P. (2000) *Application of the Finite Volume Method and Design Example for a Multi-Screen*: Voith Paper.

Serres, A., & Rees, B. (2002) "ID2" Brings a New Leap for the Screening Process. *Appita 55*(4), 267-271.

Siewert, W. M., Selder, H., & Flynn, P. J. (1989) *Customizing Fractionation Performances.* Tappi Engineering Conference, Orlando, FL, USA, 429-438.

Sloane, M. C. (1993) *Separation Techniques for Coarse Fibre Removal to Improve Pulp and Paper Quality.* M. Phil Thesis, University of Auckland, Auckland, NZ.

Sloane, M. C. (1998) *Wastepaper Quality Development for Packaging Papers - Fractionation or Whole Stock Refining?* Tappi Recycling Symposium, New Orleans, LA., 395-405.

Sloane, M. C. (2000) Kraft Pulp Processing - Pressure Screen Fractionation. *Appita 53*(3), 220-226.

Smook, G. A. (1992) *Handbook for Pulp & Paper Technologists* (Second ed.). Vancouver, Canada: Angus Wilde Publications.

Steenberg, B. (1953) Principles of Screening System Design - Studies in Screening Theory 1. *Svensk Papperstidning 56*(20), 771-778.

Takeuchi, N., Senda, S., Namba, K., & Kauwabara, G. (1983) Pulp Suspension Reflocculation Times. *Appita 37*, 223.

Tam Doo, P. A., & Kerekes, R. J. (1981) A Method to Measure Wet Fibre Flexibility. *Tappi 64*(3), 113-116.

Tangsaghasaksri, W., & Göttsching, L. (1994) Effect of Contoured Slots on Fiber Passage - Investigations by Means of a Model Screen. *Das Papier 48*(4), 172-179.

Tangsaghasaksri, W., Steuernagel, M., & Göttsching, L. (1994) Modelling of Fiber Passage Through Slotted Screens. *Das Papier 48*(10), 635-638.

Taylor, G. I. (1935) Distribution of Velocity and Temperature between Concentric Rotating Cylinders. *Proceedings of the Royal Society of London. Series A, Mathematical and Physical Sciences 151*(874), 494-512.

Thalen, N., & Warhen, D. (1964) Shear Modulus and Ultimate Shear Strength of Some Paper Pulp Fibre Networks. *Svensk Papperstidning 67*(7), 259-264.

Thomas, A. S. W., & Cornelius, K. C. (1982) Investigation of a Laminar Boundary-Layer Suction Slot. *AIAA Journal 20*(6), 790-796.

Versteeg, H. K., & Malalasekera, W. (2007) *An Introduction to Computational Fluid Dynamics - The Finite Volume Method* (2 ed.). Harlow, Essex, England: Pearson Education Ltd.

Wahlström, B. (1981) *Svensk Papperstidning 84*(18), 32-39.

Wakelin, R. F. (1997) *Objectives and Constraints for Pressure Screen Fractionation.* International Mechanical Pulping Conference, Stockholm, Sweden,

Wakelin, R. F. (1998) Reject Thickening Behaviour of TMP Screening. *Pulp & Paper Canada 99*(1), 27-30.

Wakelin, R. F., Blackwell, B. G., & Corson, S. R. (1994) *The Influence of Equipment and Process Variables on Mechancial Pulp Fractionation in Pressure Screens.* 48th Appita Annual Conference, Melbourne, Australia, 611-619.

Wakelin, R. F., & Corson, S. R. (1997) TMP Long Fibre Fractionation with Pressure Screens. *Pulp & Paper Canada 98*(12), 179-182.

Wakelin, R. F., Dahlqvist, G. K., & Isaken, J. E. (1999) *Balancing the Roles of Refiners, Screens and Hydrocyclones in the Production of High Quality Mechanical Pulps.* 53rd Appita Conference, Rotorua, New Zealand, 509-517.

Wakelin, R. F., & Paul, T. (2001) Effects of Some Process Variables on Screen Fractionator Performance. *Appita 51*(4), 357-363.

Walmsley, M., & Atkins, M. J. (2003) *Comparing Fibre Length Fractionation of a Laboratory Flow Channel to an Industrial Pressure Screen.* 57th Appita Annual Conference, Melbourne, Australia, 369-376.

Walmsley, M., Hodgson, K. T., O'Reilly, T., Kibblewhite, R. P., Lloyd, J., & Richardson, J. (2005) *Physical and Chemical Properties of Earlywood and Latewood Radiata Pine and Douglas Fir Kraft Fibres.* 58th Appita Conference, Auckland, New Zealand,

Walmsley, M., & Weeds, Z. (1998) *Flow Characteristic of Eucalyptus Pulp Suspensions in a Pressure Screen with 1 mm Holes.* 52nd Appita Annual Conference, 271-278.

Walmsley, M., & Weeds, Z. (2002) *Flow and Consistency Variations in Pressure Screen.* 56th Appita Annual Conference, Rotorua, New Zealand, 475-482.

Walmsley, M., & Weeds, Z. (2004) Plug Flow versus Mixed Flow Modelling of a Pressure Screen. *Appita 57*(2), 121-127.

Walmsley, M., & Weeds, Z. (2007) Feed Consistency and Rotor Effects on Pulp Screening Mechanisms and Reject Thickening. *Appita 60*(2), 136-143.

Watson, A. J., & Dadswell, H. E. (1961) Influence of Fibre Morphology on Paper Properities: Part 1 - Fibre Length. *Appita 14*(5), 168-176.

Weckroth, R., Tuomela, P., Rintamäki, J., & Gooding, R. W. (2001) Recent Developments in Papermachine Headbox Screening. *Paperi ja Puu 83*, 462.

Weeds, Z. (1998) *The Flow Behaviour of an Industrial Pressure Screen.* Masters Thesis, University of Waikato, Hamilton, NZ.

Weeds, Z. (2006) *Pressure Screening Studies with Wood Pulp.* PhD Thesis, Department of Engineering, University of Waikato, Hamilton.

White, F. M. (2003) *Fluid Mechanics* (Fifth ed.). New York, NY, USA: McGraw-Hill

Wikström, T., & Fredriksson, B. (1999) *Hydrodynamics in a Pressure Screen - Consequences on the Separation Process.* 5th Research Forum Recycling, PAPTAC, Ottawa, Canada, 197-202.

Wikstrom, T., & Rasmuson, A. (1998) Yield Stress of Pulp Suspensions: The Influence of Fibre Properties and Processing Conditions. *Nordic Pulp and Paper Research Journal 13*(3), 243-250.

Wikström, T., & Rasmuson, A. (2002) Transition Modelling of Pulp Suspensions Applied to a Pressure Screen. *Journal of Pulp and Paper Science 28*(11), 374-378.

Wilcox, D. C. (1993) Comparison of 2-Equation Turbulence Models for Boundary-Layers with Pressure-Gradient. *Aiaa Journal 31*(8), 1414-1421.

Wilcox, D. C. (1998) *Turbulence Modelling for CFD* (Second ed.). California, USA: DWC Industries Inc.

Wilhelm, D., Härtel, C., & Kleiser, L. (2003) Computational Analysis of the Two-Dimensional-Three-Dimensional Transition in Forward-Facing Step Flow. *Journal of Fluid Mechanics 489*, 1-27.

Yan, H., & Norman, B. (2006) A Flow Loop System for Study of Fibre Suspension Flocculation. *Nordic Pulp and Paper Research Journal 21*(1), 19-23.

Yu, C. J. (1992) *Beloit Technical Report*: Beloit.

Yu, C. J. (1994) *Pulsation Measurement in a Screen Part 1: Pulse Signature and Magnitude of S-Shape Rotor.* Tappi Engineering Conference, 767-782.

Yu, C. J., Crossley, B. R., & Silveri, L. (1994) Fundamental Study of Screening Hydraulics Part 3: Model for Calculating Effective Open Area. *Tappi Journal 77*(9), 125-131.

Yu, C. J., & DeFoe, R. J. (1994) Fundamental Study of Screening Hydraulics Part 1: Flow Patterns at the Feed-Side Surface of Screen Baskets; Mechanisms of Fiber-Mat Formation and Remixing. *Tappi Journal 77*(8), 219-226.

Yu, C. J., DeFoe, R. J., & Crossley, B. R. (1994) *Fractionation Technology and its Applications.* Tappi Pulping Conference, 451-463.